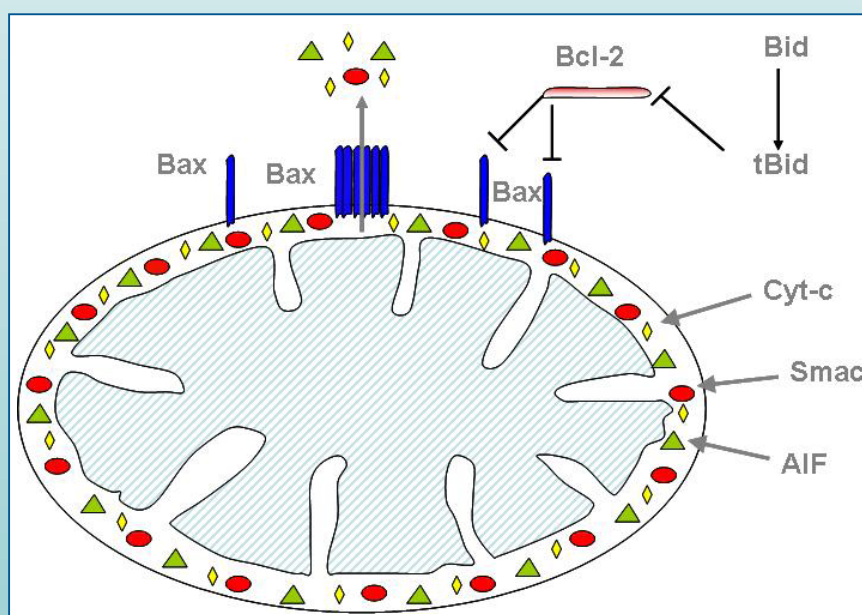


Drug Discoveries & Therapeutics

ISSN 1881-7831 Online ISSN 1881-784X

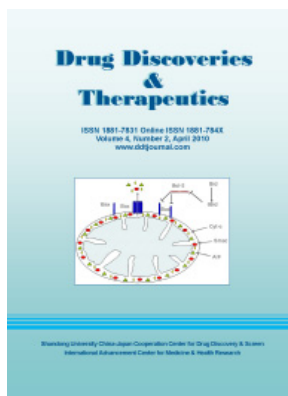
Volume 4, Number 2, April 2010

www.ddtjournal.com



Shandong University China-Japan Cooperation Center for Drug Discovery & Screen
International Advancement Center for Medicine & Health Research

Drug Discoveries & Therapeutics



Editor-in-Chief:

Kazuhisa SEKIMIZU
(The University of Tokyo, Tokyo, Japan)

Associate Editor:

Norihiro KOKUDO
(The University of Tokyo, Tokyo, Japan)

Drug Discoveries & Therapeutics is a peer-reviewed international journal published bimonthly by *Shandong University China-Japan Cooperation Center for Drug Discovery & Screen (SDU-DDSC)* and *International Advancement Center for Medicine & Health Research Co., Ltd. (IACMHR Co., Ltd.)*.

Drug Discoveries & Therapeutics mainly publishes articles related to basic and clinical pharmaceutical research such as pharmaceutical and therapeutical chemistry, pharmacology, pharmacy, pharmacokinetics, industrial pharmacy, pharmaceutical manufacturing, pharmaceutical technology, drug delivery, toxicology, and traditional herb medicine. Studies on drug-related fields such as biology, biochemistry, physiology, microbiology, and immunology are also within the scope of this journal.

Subject Coverage: Basic and clinical pharmaceutical research including Pharmaceutical and therapeutical chemistry, Pharmacology, Pharmacy, Pharmacokinetics, Industrial pharmacy, Pharmaceutical manufacturing, Pharmaceutical technology, Drug delivery, Toxicology, and Traditional herb medicine.

Language: English

Issues/Year: 6

Published by: IACMHR and SDU-DDSC

ISSN: 1881-7831 (Online ISSN 1881-784X)

CODEN: DDTRBX

Editorial and Head Office

Wei TANG, MD PhD
Executive Editor
Drug Discoveries & Therapeutics

TSUIN-IKIZAKA 410,
2-17-5 Hongo, Bunkyo-ku,
Tokyo 113-0033, Japan.

Tel: 03-5840-9697

Fax: 03-5840-9698

E-mail: office@ddtjournal.com

URL: www.ddtjournal.com



Drug Discoveries & Therapeutics

Editorial Board

Editor-in-Chief:

Kazuhisa SEKIMIZU (*The University of Tokyo, Tokyo, Japan*)

Associate Editor:

Norihiro KOKUDO (*The University of Tokyo, Tokyo, Japan*)

Executive Editor:

Wei TANG (*The University of Tokyo, Tokyo, Japan*)

Managing Editor:

Munehiro NAKATA (*Tokai University, Kanagawa, Japan*)

Web Editor:

Yu CHEN (*The University of Tokyo, Tokyo, Japan*)

English Editors:

Curtis BENTLEY (*Roswell, GA, USA*)

Thomas R. LEBON (*Los Angeles Trade Technical College, Los Angeles, CA, USA*)

China Office:

Wenfang XU (*Shandong University, Shandong, China*)

Editorial Board Members:

Yoshihiro ARAKAWA (<i>Tokyo, Japan</i>)	Yuxiu LIU (<i>Nanjing, China</i>)
Santad CHANPRAPAPH (<i>Bangkok, Thailand</i>)	Hongxiang LOU (<i>Jinan, China</i>)
Fen-Er CHEN (<i>Shanghai, China</i>)	Ken-ichi MAFUNE (<i>Tokyo, Japan</i>)
Zhe-Sheng CHEN (<i>Queens, NY, USA</i>)	Norio MATSUKI (<i>Tokyo, Japan</i>)
Zilin CHEN (<i>Wuhan, China</i>)	Tohru MIZUSHIMA (<i>Kumamoto, Japan</i>)
Guanhua DU (<i>Beijing, China</i>)	Abdulla M. MOLOKHIA (<i>Alexandria, Egypt</i>)
Chandradhar DWIVEDI (<i>Brookings, SD, USA</i>)	Masahiro MURAKAMI (<i>Osaka, Japan</i>)
Mohamed F. EL-MILIGI (<i>Cairo, Egypt</i>)	Yoshinobu NAKANISHI (<i>Ishikawa, Japan</i>)
Harald HAMACHER (<i>Tuebingen, Germany</i>)	Yutaka ORIHARA (<i>Tokyo, Japan</i>)
Hiroshi HAMAMOTO (<i>Tokyo, Japan</i>)	Xiao-Ming OU (<i>Jackson, MS, USA</i>)
Xiaojiang HAO (<i>Kunming, China</i>)	Weisan PAN (<i>Shenyang, China</i>)
Waseem HASSAN (<i>Santa Maria, RS, Brazil</i>)	Rakesh P. PATEL (<i>Gujarat, India</i>)
Langchong HE (<i>Xi'an, China</i>)	Shafiqur RAHMAN (<i>Brookings, SD, USA</i>)
David A. HORNE (<i>Duarte, CA, USA</i>)	Shivanand P. PUTHLI (<i>Mumbai, India</i>)
Yongzhou HU (<i>Hangzhou, China</i>)	Adel SAKR (<i>Cincinnati, OH, USA</i>)
Wei HUANG (<i>Shanghai, China</i>)	Abdel Aziz M. SALEH (<i>Cairo, Egypt</i>)
Yu HUANG (<i>Hong Kong, China</i>)	Tomofumi SANTA (<i>Tokyo, Japan</i>)
Hans E. JUNGINGER (<i>Phitsanulok, Thailand</i>)	Yasufumi SAWADA (<i>Tokyo, Japan</i>)
Amrit B. KARMARKAR (<i>Mumbai, India</i>)	Brahma N. SINGH (<i>Commack, NY, USA</i>)
Toshiaki KATADA (<i>Tokyo, Japan</i>)	Hongbin SUN (<i>Nanjing, China</i>)
Gagan KAUSHAL (<i>Charleston, WV, USA</i>)	Benny K. H. TAN (<i>Singapore, Singapore</i>)
Ibrahim S. KHATTAB (<i>Safat, Kuwait</i>)	Renxiang TAN (<i>Nanjing, China</i>)
Hiromichi KIMURA (<i>Tokyo, Japan</i>)	Chandan M. THOMAS (<i>Bradenton, FL, USA</i>)
Shiroh KISHIOKA (<i>Wakayama, Japan</i>)	Murat TURKOGLU (<i>Istanbul, Turkey</i>)
Kam Ming KO (<i>Hong Kong, China</i>)	Zhengtao WANG (<i>Shanghai, China</i>)
Nobuyuki KOBAYASHI (<i>Nagasaki, Japan</i>)	Stephen G. WARD (<i>Bath, UK</i>)
Toshiro KONISHI (<i>Tokyo, Japan</i>)	Takako YOKOZAWA (<i>Toyama, Japan</i>)
Masahiro KUROYANAGI (<i>Hiroshima, Japan</i>)	Liangren ZHANG (<i>Beijing, China</i>)
Chun Guang LI (<i>Victoria, Australia</i>)	Jianping ZUO (<i>Shanghai, China</i>)
Hongmin LIU (<i>Zhengzhou, China</i>)	
Jikai LIU (<i>Kunming, China</i>)	

(as of April 20, 2010)

Reviews

- 54 - 61 **Development of mitochondrial permeability transition inhibitory agents: a novel drug target.**
Eva E. Hellebrand, Gabor Varbiro
- 62 - 69 **Uses of single-particle tracking in living cells.**
Xuan Zhou, Lei Wang

Original Articles

- 70 - 76 **Proton magnetic resonance (¹HNMR) spectroscopy and physicochemical studies of zaleplon-hydroxypropyl-β-cyclodextrin inclusion compounds.**
Manali R. Shah, Pankajkumar P. Sancheti, Vikrant M. Vyas, Poonam S. Karekar, Yogesh V. Pore
- 77 - 84 **Enhancement of the dissolution profile of allopurinol by a solid dispersion technique.**
Ahmed M. Samy, Maha A. Marzouk, Amal A. Ammar, Maha K. Ahmed
- 85 - 92 **Formulation and bioavailability of controlled release salbutamol sulphate tablets using natural additives.**
Ahmed T. Nouh, Abd El-Gawad H. Abd El-Gawad, Tawhida K. Guda
- 93 - 99 **Stability, bioavailability, and ulcerative activity of diclofenac sodium-mastic controlled release tablets.**
Ahmed T. Nouh, Abd El-Gawad H. Abd El-Gawad, Tawhida K. Guda
- 100 - 108 **Biopharmaceutical evaluation of formulated metformin/rosiglitazone tablets.**
Howida K. Ibrahim, Ahmed M. Attia, Mahmoud M. Ghorab
- 109 - 122 **Calcium alginate cross-linked polymeric microbeads for oral sustained drug delivery in arthritis.**
K. M. Manjanna, T. M. Pramod Kumar, B. Shivakumar

CONTENTS

(Continued)

- 123 - 128 **Effects of lubricants on binary direct compression mixtures.**
Timuçin Uğurlu, Mekin Doğa Halaçoğlu, Murat Türkoğlu
- 129 - 134 **Effects of the herbal medicine Hachimi-jio-gan (Ba-Wei-Di-Huang-Wan) on insulin secretion and glucose tolerance in type 2 diabetic Goto-Kakizaki rats.**
Yoshihiko Hirotani, Kenji Ikeda, Michiaki Myotoku
- 135 - 143 **Phagocytosis plays a dual role in activating dendritic cells; digestive production of active Toll-like receptor ligands and cooperation with Toll-like receptor signaling.**
Masanori Miyauchi, Masashi Murata, Keiko Shibuya, Erina Koga-Yamakawa, Yoshiki Yanagawa, Ichiro Azuma, Yasuo Kashiwazaki

Guide for Authors

Copyright

Cover figure: provided by Dr. *Gabor Varbiro*.

Review

Development of mitochondrial permeability transition inhibitory agents: a novel drug target

Eva E. Hellebrand¹, Gabor Varbiro^{2,*}

¹ Department of Biochemistry and Medicinal Chemistry, Faculty of Medicine, University of Pecs, Hungary;

² Institute of Science and Technology in Medicine, School of Pharmacy, Keele University, UK.

ABSTRACT: Apoptosis is a genetically conserved mechanism that eliminates unnecessary or surplus cells and is also involved in the pathomechanism of a wide variety of diseases. The intrinsic pathway of apoptosis includes the mitochondria where numerous pro-apoptotic proteins are sequestered and their release marks the point-of-no-return, indicating the ultimate commitment to cell death. The *mitochondrial permeability transition* (mPT) is a mechanism enabling the release of Cytochrome-c (Cyt-c), AIF and other pro-apoptotic proteins, and is characterized by an alteration in the permeability of the organelle's membrane. This is due to reactive oxygen species or Ca²⁺ triggered dynamic assemble of a trans bi-membrane channel from various protein components including the voltage dependent anion channel, the adenine nucleotide translocase, the cyclophyllin D that enables solutes up to 1.5 kDa to pass through. The resultant influx of water into the mitochondrial matrix leads to mitochondrial swelling and the rupture of the membranes. Numerous agents can inhibit mPT including amiodarone, a widely used antiarrhythmic agent. Modification of this benzofuran derivate with nitroxides or their secondary amine derivatives that exhibits antioxidant properties leads to the enhancement of mPT inhibitory effect of the original compound. Furthermore this hybrid compound is also capable of influencing the necrotic cell death pathway. This strategy may prove to be beneficial to increase the effectiveness of other mPT inhibitory agents. However, further studies are necessary to identify the components and structure of the permeability transition pore in order to design more effective mPT inhibitory compounds to fully exploit the therapeutic potential of this novel drug target.

Keywords: Apoptosis, mitochondria, permeability transition, amiodarone, nitroxide

1. Introduction

Programmed cell death is a genetically conserved mechanism that has crucial implications in developmental processes and in the maintenance of tissue homeostasis. Although development largely relies on cell division and differentiation, carefully orchestrated cell death is also crucial to execute the morphological changes associated with a developing organism. In mature organisms the continuous proliferation of cells, at a variable rate depending on the specificity of the different tissues, is carefully balanced with the elimination of surplus cells in order to maintain the homeostasis of the tissues. As an example, roughly 500 billion lymphocytes are eliminated each day in an average human body to give room for the newly generated white blood cells (1). The theory of a cell death characterized by a sequence of pre-programmed event was formulated in the early 1970s (2). It is also called apoptosis, a word of Greek origin meaning the falling of leaves which suggests that this type of cell death is a natural phase of life.

Apoptosis is also associated with the development of various diseases: the disturbance of the balance between cell proliferation and removal affect the homeostasis of the tissues (3). If the rate of programmed cell death is increased it will lead to degenerative disorders. Diseases such as Parkinson's (4), Alzheimer's (5), and Huntington's disease (6), amyotrophic lateral sclerosis (7) are related to excessive loss of brain cells caused by increased level of apoptosis. Cardiovascular and cerebrovascular diseases such as acute myocardial infarction (8) or stroke (9) will initially result in necrotic cell death at the core area, while cells surrounding this pathological core will undergo apoptosis in due course significantly expanding the size of the damaged tissue. Degenerative joint diseases such as osteoarthritis (10) or rheumatoid arthritis (11) are also characterized by

*Address correspondence to:

Dr. Gabor Varbiro, Institute of Science and Technology in Medicine, School of Pharmacy, 2.26 Hornbeam building, Keele University, Keele, Staffordshire ST5 5BG, UK.

e-mail: g.varbiro@mema.keele.ac.uk

excessive apoptosis.

Apoptosis is characterized by distinct morphological changes, such as the cell shrinkage and condensation due to the disruption of the cytoskeletal structure, condensation of the chromatin and the fragmentation of the nuclear membrane and of the DNA, the blebbing of the cell membrane leading to fragmentation and the formation of apoptotic bodies which are membrane bound cell fragments that are phagocytised by macrophages and neighbouring cells (12).

The components that regulate and execute apoptosis are genetically determined and are readily available in every cell. In order to prevent undesired or accidental activation of the apoptotic program, these components are inactivated and/or securely locked away in various cell compartments (13). Following an apoptotic stimuli, the dormant apoptotic machinery will spring into action to execute the predetermined program of cell death. Depending on whether the apoptotic stimuli arises from the external environment of the cell or from within the cell, two main pathways of the programmed cell death can be distinguished.

2. Apoptotic pathways and the effector machinery

When the programmed cell death is triggered *via* the *extrinsic apoptotic pathway*, the initiating signal derives from cells' external environment (14). In this case apoptosis is activated by the binding of a specific 'death ligand' (*e.g.* FasL, TRAIL, TNF α) to the death receptor (DR) located on the surface of the cell. These receptors belong to the TNF receptor family, and following the binding of the ligand, the internal part of the death receptor will recruit the protein FADD (Fas-associated death domain protein), adaptor proteins and initiator pro-caspases to form the death inducing signalling complex (DISC). This complex will activate the initiator caspases by stimulating their auto-cleavage which in turn will lead to a proteolytic cascade resulting in the activation of the effector caspases. The signal that initiates the extrinsic apoptotic pathway can also be the absence (*e.g.* withdrawal) of various growth or trophic factor (*e.g.* nerve growth factor; NGF) which are required for the normal growth and proliferation of the cells. These ligands stimulate cell survival *via* the PI3K/Akt (protein kinase B) pathway that will phosphorylate and inactivate pro-apoptotic proteins to suppress the apoptotic process (15). The absence of such survival signal the apoptotic effector mechanism maintains its activity and executes the cell death program.

When the programmed cell death is triggered *via* the *intrinsic apoptotic pathway*, the initiating signal derives from cells' internal environment (16). In this case apoptosis is activated by a variety of stimuli such as DNA breaks, deprivation of oxygen or nutrients, accumulation of drugs or increased intracellular Ca²⁺ levels (17). This pathway is also termed as the

mitochondrial apoptotic pathway since its activation is launched by the release of pro-apoptotic proteins from this organelle. Although the main cellular function of mitochondria is to provide chemical fuel for the cell in the form of ATP it also sequesters numerous proteins within its compartments engulfed by a dual-membrane structure that are released in response to stimuli. The most important of these intra-mitochondrial pro-apoptotic proteins include the following:

- **Cyt-c:** a protein that covalently binds its heme group and functions as an electron carrier between mitochondrial respiratory complexes III and IV in the inter-membrane space. When it is released to the cytosol, it facilitates the formation of apoptosome in concert with apoptosis activating factor-1 (Apaf-1), pro-caspase-9 and dATP to produce an active caspase-9 (18,19).
- **Smac/Diablo (second mitochondria-derived activator of caspases/ direct inhibitor of apoptosis-binding protein with low pI):** binds to and inactivates the cytosolic X-linked inhibitor of apoptosis protein (XIAP). XIAP directly interact with caspases in order to inhibit their activity (20). This inhibitory effect of XIAP is suspended by Smac/Diablo.
- **Omi/HtrA2:** is a serine protease with an apoptotic activity similar to Smac/Diablo; when released from mitochondria it also binds and inhibits the action of XIAP. However, unlike Smac/Diablo, Omi/HtrA2 also facilitates apoptosis by utilizing its protease activity in addition to the physical binding to XIAP (21).
- **AIF (apoptosis inducing factor):** is a mitochondrial flavoprotein that carries a NADH-oxidase domain which regulates mitochondrial respiratory complex I and is also indispensable for cell survival and for the integrity of the mitochondria (22). In response to apoptotic stimuli it translocates to the nucleus and induces chromatin condensation and large fragment DNA degradation.
- **Endo G (endonuclease-G):** is a nuclear DNA-encoded nuclease located in the inter-membrane space. Its apoptotic activity is similar to that of the AIF: it translocates to the nucleus and mediates oligonucleosomal DNA fragmentation (23).

Regardless of whether the signal initiating apoptosis arises from the external environment or from within the cell, apoptotic machinery is triggered into action in a predetermined manner, ultimately leading to the activation of effector caspases that execute the program.

The components of the *apoptotic machinery* belong to a family of evolutionary highly conserved proteins, exhibiting structural and functional similarities in various organisms from nematodes to humans. These are cysteine proteases recognizing a specific sequence of

amino acids containing aspartate, hence they are termed as caspases (24). Present in the cells in an inactive form of pro-caspases, they are activated by proteolytic cleavage in an amplifying cascade. The pro-caspases at the initial stage of the cascade form the initiator caspases (caspases 2, 8, 9, 10) while the ones downstream form the effector caspases (caspases 3, 6, 7) that eventually cleave the cellular target proteins. All caspases have specific caspase recruitment domains (CARDs) allowing the binding of adaptor proteins and the formation of activation complexes in response to an apoptotic signal.

Although two different apoptotic pathways are described, in practice there is always cross-talk between them leading to both pathways being simultaneously involved in cell death albeit with the dominance of either one or the other. Intrinsic apoptotic pathway for example can be activated by the extrinsic route *via* the truncation and thus activation of the pro-apoptotic protein Bid (25). Mitochondria, however, play a crucial role in apoptosis: the translocation of the described (and possibly other yet unidentified) pro-apoptotic factors from the mitochondrial compartment to the cytosol marks the point of no return, where commitment to cell death becomes irreversible. Different models are used to describe the mechanism of mitochondrial pro-apoptotic protein release.

3. Mechanism of the mitochondrial pro-apoptotic protein release

The role of B-cell leukaemia (Bcl-2) proteins have been extensively studied (26). They are considered to play a crucial role in controlling the mitochondrial apoptotic pathway. Bcl-proteins are characterized by their BH (Bcl Homology) domains (Figure 1). Pro-apoptotic bcl-

proteins have either 3 BH domains (BH1-3; *e.g.* Bax, Bak) or a single BH domain (BH3; *e.g.* bad, bid, bim, puma, noxa) while anti-apoptotic bcl-proteins have 4 BH domains (BH1-4; *e.g.* Bcl-2, Bcl-X_L). The anti-apoptotic family members form heterodimers with the pro-apoptotic multi-domain family members to prevent the activation of the cell death pathway. Apoptotic signals activate the single BH3 domain regulatory bcl-proteins by various stimuli such as proteolytic cleavage (*e.g.* Bid) or phosphorylation (*e.g.* Bad) causing them to promote the dissociation of the heterodimers. Subsequently, the pro-apoptotic proteins with BH1-3 domains oligomerize and form a pore in the outer membrane of the mitochondria (27), allowing the release of pro-apoptotic mitochondrial proteins from the inter-membrane space (Figure 2). Bcl-proteins can incorporate various signals in the apoptotic pathway. For example p53 can induce apoptosis by increasing the rate of transcription of numerous bcl-related genes, and also by activating BH multi-domain pro-apoptotic bax to bind to the mitochondrial outer membrane (28).

According to another explanation, which also describes the mitochondrial pro-apoptotic protein release, a trans-bi-membrane channel is formed (29). Mitochondria are surrounded by two membranes with the inner mitochondrial membrane having invaginations which form the mitochondrial cristae resulting in a larger overall surface than that of the outer mitochondrial membrane. Apoptotic stimuli leads to a channel formation that spans both mitochondrial inner and outer membranes. This non-selective channel (permeability transition pore; PTP) allows the passage of molecules with a cut-off at 1.5 kDa. Since mitochondria as the metabolic hubs of the cell, contain intermediates at a high concentration with high osmolar activity, it results

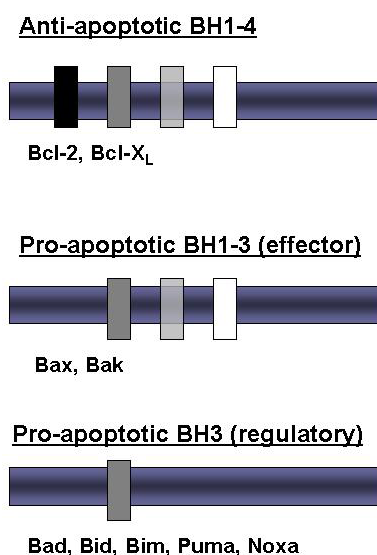


Figure 1. Bcl-proteins can be divided into three major groups depending on the number of bcl homology (BH) domains. Proteins with four BH domains have an anti-apoptotic function while those with one or three BH domains are pro-apoptotic.

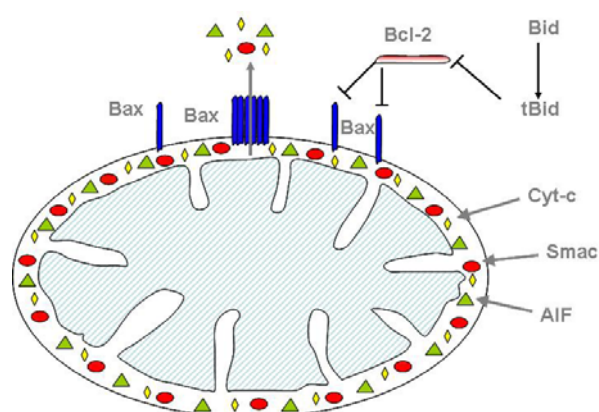


Figure 2. Pro-apoptotic BH1-3 bcl-proteins (Bax) are associated with anti-apoptotic BH1-4 bcl-proteins (Bcl-2). This heterodimer can be disrupted by BH3 pro-apoptotic proteins (tBid) facilitating the homo-oligomerization of the pro-apoptotic BH1-3 bcl-proteins (Bax). This leads to a formation of a pore that transverse the mitochondrial outer membrane, enabling the release of intra-mitochondrial pro-apoptotic proteins (*e.g.* Cyt-c, AIF, Smac/Diablo).

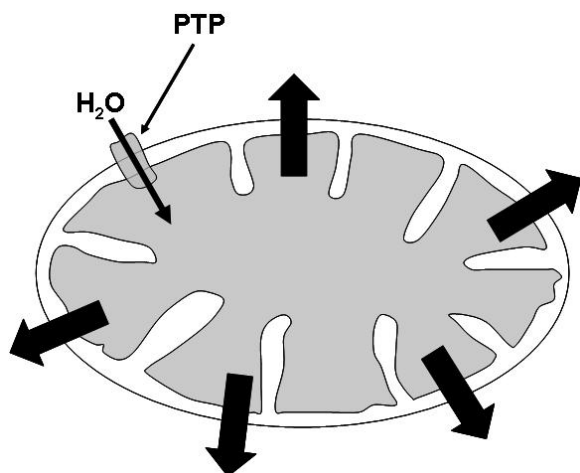


Figure 3. Assemble of a non-specific trans-bimembrane pore spanning both mitochondrial membrane results in H₂O influx due to osmosis. The subsequent mitochondrial swelling will eventually lead to the rupture of the mitochondrial outer membrane enabling the release of intra-mitochondrial pro-apoptotic proteins (e.g. Cyt-c, AIF, Smac/Diablo).

in the influx of water, the swelling of the mitochondria and the rupture of the outer membrane resulting in the release of pro-apoptotic proteins (Figure 3). This process is called the *mitochondrial permeability transition* (mPT). This route of apoptosis is typically characterized by excessive intracellular Ca²⁺ fluxes or the generation of substantial amount of reactive oxygen species (ROS). In a previous study we reported that a heme binding protein with BH3-like domain induced mPT that was sensitive to cyclosporine A (30). The composition of the PTP is not yet fully known, although a wide range of studies indicate that PTP is formed by the dynamic interaction of several molecular components (31). These include the voltage-dependent anion channel (VDAC) located in the outer membrane, the adenine nucleotide translocase (ANT) in the inner membrane and cyclophilin D (CypD) found in the mitochondrial matrix forming the core components of the PTP (32-34). Additional components include the creatine kinase (CK) in the inter-membrane space, the peripheral-type benzodiazepine receptor (PBR) located in the outer membrane and two hexokinase isoforms (HKI and HKII) found in the cytosol (35-37). The mPT, including the assemble of the PTP and the release of Cyt-c, can be demonstrated experimentally in isolated mitochondria (38).

4. Mitochondrial permeability transition pore as novel drug target

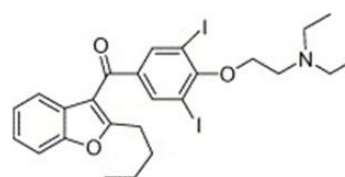
Numerous pharmacological compounds can facilitate the mPT. Our previous studies for example have demonstrated the paclitaxel, an anticancer agent widely used in the clinical practice for the treatment of solid tumors or leukaemias induces mPT in addition to its previously described effect on the microtubular disassembly (39). Similar effect was observed in the

case of cisplatin, another anticancer agents frequently used in practice. In general the activators of mPT may prove to be effective in the treatment of malignancies (40). The administration of mPT inhibitors in combination with conventional anticancer agents can potentiate the effectiveness of these drugs enabling their administration in a lower dose and thus reducing their associated side effects.

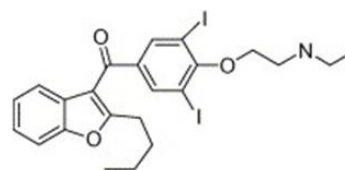
A wide range of pharmacological agent can exert an inhibitory effect on the mPT. One of the first agents proved to have an mPT inhibitory effect was cyclosporine A, an immunosuppressant compound (41). It binds to cyclophilin D in the mitochondrial matrix and inhibits its peptidyl-prolyl cis-trans isomerase activity which in turn prevents the formation of PTP (42). A study conducted to screen more than 1,000 previously established drugs for an effect on the mPT found 28 structurally related compounds including heterocyclic antidepressants and antipsychotic that possesses with inhibitory effect on the mPT (43). Another target for the inhibition of permeability transition is the peripheral-type benzodiazepine receptor (PBR) located in the outer mitochondrial membrane (44). This binds the specific PBR ligand 4'-chlorodiazepam, an agent that protects the myocardium during ischemia reperfusion injuries (45).

5. Amiodarone and structural analogues act as potent inhibitors of mPT

Previous studies have also identified an established pharmacological compound that inhibits mPT and protects the myocardium against oxidative damage sustained during ischemia-reperfusion injuries (46). The antiarrhythmic agent amiodarone (Figure 4) exerts a biphasic effect on the mPT: at lower concentrations it inhibits, while at higher concentrations it induces



Amiodarone



N-desethylamiodarone

Figure 4. Amiodarone, a benzofuran derivate (2-butyl-3-benzofuranyl-4-[2-(diethylamino)-ethoxy]-3,5-diiodophenyl-ketone hydrochloride) is a dominantly class III antiarrhythmic compound. Its main metabolite is N-Desethylamiodarone.

PTP formation as demonstrated in isolated rat liver mitochondria (46). It also had a beneficial effect on the myocardium during ischemia and reperfusion by facilitating the recovery of the level of high energy phosphate metabolites such as ATP and creatine phosphate respectively (47). It also prevented the translocation of apoptosis inducing factor from the mitochondria to the nucleus during ischemia and reperfusion in Langendorff-perfused rat hearts (47). Amiodarone is metabolized in the liver (48) and its major metabolite is the desethyl-amiodarone (Figure 4). This metabolite however does not exert the beneficial effect demonstrated by amiodarone in equimolar concentration. It is particularly noteworthy that it did not have inhibitory effect on the mPT which is a characteristic of amiodarone. Since the difference in the effect on mPT between amiodarone and its major metabolite desethyl-amiodarone is solely due to structural alteration (*e.g.* the absence of the ethyl side chain from the amino group) we designed and developed paramagnetic and diamagnetic amiodarone analogues to evaluate their effect on mPT (49).

Amiodarone is among the most effective antiarrhythmic agents and frequently used in clinical practice to treat various ventricular and supraventricular arrhythmias (50). Its clinical application however is often limited by the severe side effects associated with its long term administration that include pancreas and liver fibrosis, thyroid dysfunction or the potentially life threatening thyrotoxicosis (51). Significant effort has been made in the past to enhance the pharmacokinetic properties of this compound. Amiodarone analogues produced by dealkylation, deiodination or deamination were evaluated to assess their toxic properties (52). Another research group introduced carboxymethoxy side chain to replace the tertiary amine to produce 2-methyl-3-(3,5-diiodo-4-carboxymethoxybenzyl)benzofuran (53), while others evaluated the substitution of the *n*-butyl group with an isobutyl ester. The discovery that amiodarone acts as an inhibitor of mPT (46) provides an explanation on the mechanism by which it reduces mortality after myocardial infarction (54). The ischemia-reperfusion type injury during myocardial infarction is characterized by ROS generation and the release of Ca^{2+} from the intracellular Ca^{2+} -stores and can be an etiological factor in inducing mPT and myocardial cell death during reperfusion. We demonstrated the beneficial effects of amiodarone on Langendorff-perfused rat hearts as well as in isolated mitochondria (46,47). In order to improve the effectiveness of amiodarone to inhibit mPT we produced analogues by varying the diethylaminoethyl side chain of phenol ether and the 2-substituent on the benzofuran ring and evaluated the effect of these modifications in perfused hearts as well as in cultured cells or in isolated mitochondria (49). In the past decades numerous drugs that were modified with

nitroxides or with their precursors exhibited additional beneficial features. This chemical group possesses antioxidant properties and is capable of scavenging ROS and RNS to protect cellular lipids and proteins from damaging oxidative insults (55). It prompted us to modify amiodarone and produce analogues that incorporate 2,2,5,5-tetramethyl-2,5-dihydro-1*H*-pyrrole and 1,2,5,6-tetrahydropyridine nitroxides or their amine precursors to supplement the antiarrhythmic agent with a superoxide dismutase (SOD) mimetic property (49). In order to improve the solubility and the ROS scavenging property of the amiodarone analogues, the nitroxide was reduced to secondary amine (56).

The majority of the amiodarone analogues did not exhibit biphasic effect on the mPT: while they inhibited the swelling in lower concentrations without inducing mPT when administered at higher doses. Those compounds that inhibit mPT with IC_{50} values comparable to that of the amiodarone, which was previously found to be $3.9 \pm 0.8 \mu\text{M}$ (46,47), were selected for further evaluation. Amiodarone has an uncoupling effect on the mitochondria (57) and therefore dissipates the mitochondrial membrane potential ($\Delta\Psi$) with an ED_{50} of $4.2 \pm 0.7 \mu\text{M}$ (46,47). The modified amiodarone analogues exerted uncoupling effect on the mitochondrial oxidative phosphorylation with a higher ED_{50} than that of the amiodarone (49). It should be noted, that a moderate uncoupling effect is believed to be beneficial since it decreases the level of noxious ROS production.

Those amiodarone analogues that exhibited low IC_{50} values in inhibiting mPT and a relatively high ED_{50} value for mitochondrial membrane potential dissipation in comparison to amiodarone were selected to evaluate their toxicological properties in cultured cells. Treating cardiomyocytes and liver cells with amiodarone and the selected analogues in the concentration up to $100 \mu\text{M}$, which is significantly higher than the level in the tissues during prolonged drug administration (47), we were able to identify that specific compound that had the lowest IC_{50} values for mPT inhibition, the highest ED_{50} value for dissipating the mitochondrial membrane potential, and showed the lowest toxicity in cultured cells (49,58). This agent is a 2-methyl-3-(3,5-diiodo-4-{2-[*N*-ethyl, *N*-(1-hydroxy-2,2,5,5-tetramethyl-2,5-dihydro-1*H*-pyrrol-3-ylmethyl)ethyl]}oxybenzoyl)benzofurane containing an additional 1-hydroxy-2,2,5,5-tetramethyl-2,5-dihydro-1*H*-pyrrol-3-ylmethyl component which possesses SOD-mimetic properties (Figure 5). The subcellular localization of this compound was assessed by quantitative HPLC-MS and this demonstrated an increased accumulation in the mitochondria in contrast to its level both in the cytosol and in the nucleus. More than 95% of this benzofuran derivative was taken up in the mitochondria of cultured cardiomyocytes which is similar to the level detected in the mitochondrial fraction of perfused hearts (93.2%). This agent

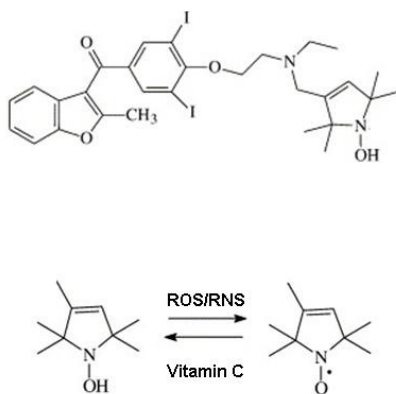


Figure 5. Modifying amiodarone with nitroxides provides antioxidant properties enabling the scavenging of ROS and RNS. An effective compound shown incorporates a 2,2,5,5-tetramethyl-2,5-dihydro-1*H*-pyrrole, 1,2,5,6-tetrahydropyridine nitroxide. ROS induced oxidation of the *N*-hydroxyamine form is reduced by to nitroxide form by natural reducing agents (e.g. GSSG, thiols, ascorbate).

prevented the release of the pro-apoptotic proteins Cyt-*c*, AIF and Endo G from isolated mitochondria, and also decreased the caspase-3 activity in apoptotic cultured cells (49,58). The effect on the myocardial energy metabolism was also assessed in perfused heart by ^{31}P NMR spectroscopy and showed an enhanced recovery of high-energy phosphates in the myocardium following ischemia-reperfusion. Due to the antioxidant properties of the compound, lipid peroxidation as well as protein oxidation was decreased in this experimental model. Furthermore, the infarct size in the myocardium was also reduced (58).

The addition of a nitroxide compound to amiodarone to enhance the mPT inhibitory effect proved to be a successful approach. 2-methyl-3-(3,5-diiodo-4-{2-[*N*-ethyl, *N*-(1-hydroxy-2,2,5,5-tetramethyl-2,5-dihydro-1*H*-pyrrol-3-ylmethyl) ethyl]}oxybenzoyl)benzofurane is the first representatives of a novel class of mPT inhibitors that exerts SOD-mimetic properties as well. These types of agents are capable of inhibiting not only the apoptotic but the necrotic cell death (58). This results in a significantly enhanced cyto-protection and cardio-protection which can be exploited further in the therapeutic practice. Modifying drug with antioxidant compounds may also prove to be a beneficial approach in the case of other classes of pharmacological agents as well (59).

6. Conclusion

Apoptosis is involved in the pathomechanism of numerous diseases. Since mitochondria play a crucial role marking the point of irreversibility by releasing the pro-apoptotic proteins it also presents an excellent opportunity for therapeutic intervention. Some pathological conditions, particularly those involving increased intracellular Ca^{2+} or ROS over-production,

lead to the formation of the permeability transition pore providing a valid therapeutic target. It is also likely, however, that mPT plays a role in necrosis since the aggressive rupture of mitochondria membrane and thus subsequent inactivation of the oxidative phosphorylation will lead to prompt cell death (60). Therefore mPT inhibitors may also be able to influence necrosis. Based on this theory novel hybrid mPT inhibitors were developed, modified with nitroxide structures that have antioxidant properties. Further studies are necessary to identify the components and structure of the PTP in order to design more effective mPT inhibitory compounds. This is however challenging, since PTP formation is believed to be a dynamic and continuously altering interaction of a large number of proteins with each having other important functions in the mitochondrial physiology and it is very likely than some components are yet to be identified (61).

References

- Rathmell JC, Thompson CB. Pathway of apoptosis in lymphocyte development, homeostasis and disease. *Cell*. 2002; 109:S97-S107.
- Kerr JF, Wyllie AH, Currie AR. Apoptosis: a basic biological phenomenon with wide-ranging implications in tissue kinetics. *Br J Cancer*. 1972; 26:239-257.
- Walker NI, Harmon BV, Gobé GC, Kerr JF. Patterns of cell death. *Methods Achiev Exp Pathol*. 1988; 13:18-54.
- Bieler H. Mitochondrial dynamics, cell death and the pathogenesis of Parkinson's disease. *Apoptosis*. (2010; in press)
- Diarra A, Geetha T, Potter P, Babu JR. Signaling of the neurotrophin receptor p75 in relation to Alzheimer's disease. *Biochem Biophys Res Commun*. 2009; 390:352-356.
- Bhattacharyya NP, Banerjee M, Majumder P. Huntington's disease: roles of huntingtin-interacting protein 1 (HIP-1) and its molecular partner HIPPI in the regulation of apoptosis and transcription. *FEBS J*. 2008; 275:4271-4279.
- Brooks BR. Managing amyotrophic lateral sclerosis: slowing disease progression and improving patient quality of life. *Ann Neurol*. 2009; 65 Suppl 1:S17-S23.
- Lee Y, Gustafsson AB. Role of apoptosis in cardiovascular disease. *Apoptosis*. 2009; 14:536-548.
- Candelario-Jalil E. Injury and repair mechanisms in ischemic stroke: considerations for the development of novel neurotherapeutics. *Curr Opin Investig Drugs*. 2009; 10:644-654.
- Johnson EO, Charchandi A, Babis GC, Soucacos PN. Apoptosis in osteoarthritis: morphology, mechanisms, and potential means for therapeutic intervention. *J Surg Orthop Adv*. 2008; 17:147-152.
- Korb A, Pavenstädt H, Pap T. Cell death in rheumatoid arthritis. *Apoptosis*. 2009; 14:447-454.
- Bovellan M, Fritzsche M, Stevens C, Charras G. Death-associated protein kinase (DAPK) and signal transduction: blebbing in programmed cell death. *FEBS J*. 2010; 277:58-65.
- Hengartner MO. The biochemistry of apoptosis. *Nature*.

- 2000; 407:770-776.
14. Lavrik I, Golks A, Krammer PH. Death receptor signalling. *J Cell Sci.* 2005; 118:265-267.
 15. Szanto A, Hellebrand EE, Bognar Z, Tucsek Z, Szabo A, Gallyas F Jr, Sumegi B, Varbiro G. PARP-1 inhibition-induced activation of PI-3-kinase-Akt pathway promotes resistance to Taxol. *Biochem Pharmacol.* 2009; 77:1348-1357.
 16. Green DR, Kroemer G. The pathophysiology of mitochondrial cell death. *Science.* 2004; 305:626-629.
 17. Varbiro G, Veres B, Gallyas F Jr, Sumegi B. Direct effect of Taxol on free radical formation and mitochondrial permeability transition. *Free Rad Biol Med.* 2001; 31:548-558.
 18. Liu X, Kim CN, Yang J, Jemmerson R, Wang X. Induction of apoptotic program in cell-free extracts: requirement for dATP and cytochrome c. *Cell.* 1996; 86:147-157.
 19. Hyun-Eui K, Fenghe D, Fanf M, Wang X. Formation of apoptosome is initiated by cytochrome-c induced dATP hydrolysis and subsequent nucleotide exchange on Apaf-1. *Proc Natl Acad Sci U S A.* 2005; 102:17545-17550.
 20. Verhagen AM, Coulson EJ, Vaux DL. Inhibitor of apoptosis proteins and their relatives: IAPs and other BIRPs. *Genome Biol.* 2001; 2:REVIEWS3009.
 21. Martins LM. The serine protease Omi/HtrA2: a second mammalian protein with a Reaper-like function. *Cell Death Differ.* 2002; 9:699-701.
 22. Hangen E, Blomgren K, Bénil P, Kroemer G, Modjtahedi N. Life with or without AIF. *Trends Biochem Sci.* (2010; in press)
 23. Galluzzi L, Joza N, Tasdemir E, Maiuri MC, Hengartner M, Abrams JM, Tavernarakis N, Penninger J, Madeo F, Kroemer G. No death without life: vital functions of apoptotic effectors. *Cell Death Differ.* 2008; 15:1113-1123.
 24. Boatright KM, Salvesen GS. Mechanisms of caspase activation. *Curr Opin Cell Biol.* 2003; 15:725-731.
 25. Lovell JF, Billen LP, Bindner S, Shamas-Din A, Fradin C, Leber B, Andrews DW. Membrane binding by tBid initiates an ordered series of events culminating in membrane permeabilization by Bax. *Cell.* 2008; 135:1074-1084.
 26. Willis SN, Adams JM. Life in the balance: how BH3-only proteins induce apoptosis. *Curr Opin Cell Biol.* 2005; 17:617-625.
 27. Giam M, Huang DC, Bouillet P. BH3-only proteins and their roles in programmed cell death. *Oncogene.* 2008; 27 Suppl 1:S128-S136.
 28. Vousden KH. Apoptosis. P53 and PUMA: a deadly duo. *Science.* 2005; 309:1685-1686.
 29. Kroemer G, Galluzzi L, Brenner C. Mitochondrial membrane permeabilization in cell death. *Physiol Rev.* 2007; 87:99-163.
 30. Szigeti A, Belyei S, Gasz B, Boronkai A, Hocsak E, Minik O, Bognar Z, Varbiro G, Sumegi B, Gallyas F Jr. Induction of necrotic cell death and mitochondrial permeabilization by heme binding protein 2/SOUL. *FEBS Lett.* 2006; 580:6447-6454.
 31. Brenner C, Grimm S. The permeability transition pore complex in cancer cell death. *Oncogene.* 2006; 25:4744-4756.
 32. Vieira HL, Belzacq AS, Haouzi D, Bernassola F, Cohen I, Jacotot E, Ferri KF, El Hamel C, Bartle LM, Melino G, Brenner C, Goldmacher V, Kroemer G. The adenine nucleotide translocator: a target of nitric oxide, peroxynitrite, and 4-hydroxynonenal. *Oncogene.* 2001; 20:4305-4316.
 33. Baines CP, Kaiser RA, Purcell NH, Blair NS, Osinska H, Hambleton MA, Brunskill EW, Sayen MR, Gottlieb RA, Dorn GW, Robbins J, Molkenin JD. Loss of cyclophilin D reveals a critical role for mitochondrial permeability transition in cell death. *Nature.* 2005; 434:658-662.
 34. Baines CP, Kaiser RA, Sheiko T, Craigen WJ, Molkenin JD. Voltage-dependent anion channels are dispensable for mitochondrial-dependent cell death. *Nat Cell Biol.* 2007; 9:550-555.
 35. Schlattner U, Tokarska-Schlattner M, Wallimann T. Mitochondrial creatine kinase in human health and disease. *Biochim Biophys Acta.* 2006; 1762:164-180.
 36. Papadopoulou V. Peripheral benzodiazepine receptor: structure and function in health and disease. *Ann Pharm Fr.* 2003; 61:30-50.
 37. Wilson JE. Isozymes of mammalian hexokinase: structure, subcellular localization and metabolic function. *J Exp Biol.* 2003; 206:2049-2057.
 38. Cassarino DS, Parks JK, Parker WD Jr, Bennett JP Jr. The parkinsonian neurotoxin MPP⁺ opens the mitochondrial permeability transition pore and releases cytochrome c in isolated mitochondria *via* an oxidative mechanism. *Biochim Biophys Acta.* 1999; 1453:49-62.
 39. Varbiro G, Veres B, Gallyas F Jr, Sumegi B. Direct effect of Taxol on free radical formation and mitochondrial permeability transition. *Free Radic Biol Med.* 2001; 31:548-558.
 40. Hail N Jr, Lotan R. Cancer chemoprevention and mitochondria: targeting apoptosis in transformed cells *via* the disruption of mitochondrial bioenergetics/redox state. *Mol Nutr Food Res.* 2009; 53:49-67.
 41. Halestrap AP, Connern CP, Griffiths EJ, Kerr PM. Cyclosporin A binding to mitochondrial cyclophilin inhibits the permeability transition pore and protects hearts from ischaemia/reperfusion injury. *Mol Cell Biochem.* 1997; 174:167-172.
 42. Gotthel SF, Marahiel MA. Peptidyl-prolyl cis-trans isomerases, a superfamily of ubiquitous folding catalysts. *Cell Mol Life Sci.* 1999; 55:423-436.
 43. Stavrovskaya IG, Narayanan MV, Zhang W, Krasnikov BF, Heemskerk J, Young SS, Blass JP, Brown AM, Beal MF, Friedlander RM, Kristal BS. Clinically approved heterocyclics act on a mitochondrial target and reduce stroke-induced pathology. *J Exp Med.* 2004; 200:211-222.
 44. Obame FN, Zini R, Souktani R, Berdeaux A, Morin D. Peripheral benzodiazepine receptor-induced myocardial protection is mediated by inhibition of mitochondrial membrane permeabilization. *J Pharmacol Exp Ther.* 2007; 323:336-345.
 45. Morin D, Assaly R, Paradis S, Berdeaux A. Inhibition of mitochondrial membrane permeability as a putative pharmacological target for cardioprotection. *Curr Med Chem.* 2009; 16:4382-4398.
 46. Varbiro G, Toth A, Tapodi A, Veres B, Sumegi B, Gallyas F Jr. Concentration dependent mitochondrial effect of amiodarone. *Biochem Pharmacol.* 2003; 65:1115-1128.
 47. Varbiro G, Toth A, Tapodi A, Bognar Z, Veres B, Sumegi B, Gallyas F Jr. Protective effect of amiodarone but not *N*-desethylamiodarone on postischemic hearts through the inhibition of mitochondrial permeability transition. *J Pharmacol Exp Ther.* 2003; 307:615-625.

48. Zipes DP, Prystowsky EN, Heger JJ. Amiodarone: electrophysiologic actions, pharmacokinetics and clinical effects. *J Am Coll Cardiol.* 1984; 3:1059-1071.
49. Kálai T, Várbiro G, Bognár Z, Pálfi A, Hantó K, Bognár B, Osz E, Sümegi B, Hideg K. Synthesis and evaluation of the permeability transition inhibitory characteristics of paramagnetic and diamagnetic amiodarone derivatives. *Bioorg Med Chem.* 2005; 13:2629-2636.
50. Singh SN, Fletcher RD, Fisher SG, Singh BN, Lewis HD, Deedwania PC, Massie BM, Colling C, Lazzeri D. Amiodarone in patients with congestive heart failure and asymptomatic ventricular arrhythmia. Survival trial of antiarrhythmic therapy in congestive heart failure. *N Engl J Med.* 1995; 333:77-82.
51. Amico JA, Richardson V, Alpert B, Klein I. Clinical and chemical assessment of thyroid function during therapy with amiodarone. *Arch Intern Med.* 1984; 144:487-490.
52. Ha HR, Stieger B, Grassi G, Altorfer HR, Follath F. Structure-effect relationships of amiodarone analogues on the inhibition of thyroxine deiodination. *Eur J Clin Pharmacol.* 2000; 55:807-814.
53. Carlsson B, Singh BN, Temciuc M, Nilsson S, Li YL, Mellin C, Malm J. Synthesis and preliminary characterization of a novel antiarrhythmic compound (KB130015) with an improved toxicity profile compared with amiodarone. *J Med Chem.* 2002; 45:623-630.
54. Julian DG, Camm AJ, Frangin G, Janse MJ, Munoz A, Schwartz PJ, Simon P. Randomised trial of effect of amiodarone on mortality in patients with left-ventricular dysfunction after recent myocardial infarction: EMIAT. European Myocardial Infarct Amiodarone Trial Investigators. *Lancet.* 1997; 349:667-674.
55. Krishna MC, DeGraff W, Hankovszky OH, Sar CP, Kalai T, Jeko J, Russo A, Mitchell JB, Hideg K. Studies of structure-activity relationship of nitroxide free radicals and their precursors as modifiers against oxidative damage. *J Med Chem.* 1998; 41:3477-3492.
56. Twomey P, Taira J, DeGraff W, Mitchell JB, Russo A, Krishna MC, Hankovszky OH, Frank L, Hideg K. Direct evidence for *in vivo* nitroxide free radical production from a new antiarrhythmic drug by EPR spectroscopy. *Free Radic Biol Med.* 1997; 22:909-916.
57. Fromenty B, Fisch C, Berson A, Letteron P, Larrey D, Pessayre D. Dual effect of amiodarone on mitochondrial respiration. Initial protonophoric uncoupling effect followed by inhibition of the respiratory chain at the levels of complex I and complex II. *J Pharmacol Exp Ther.* 1990; 255:1377-1384.
58. Bognar Z, Kalai T, Palfi A, Hanto K, Bognar B, Mark L, Szabo Z, Tapodi A, Radnai B, Sarszegi Z, Szanto A, Gallyas F Jr, Hideg K, Sumegi B, Varbiro G. A novel SOD-mimetic permeability transition inhibitor agent protects ischemic heart by inhibiting both apoptotic and necrotic cell death. *Free Rad Biol Med.* 2006; 41:835-848.
59. Radnai B, Veres B, Hanto K, Jakus P, Varbiro G, Bognar Z, Tapodi A, Veto S, Sumegi B. The effect of a novel PARP inhibitor HO-3089 on the LPS stimulated RAW 2647 murine macrophage cells. *FEBS J.* 2005; 272(s1): E1-054P.
60. Kowaltowski AJ, Castilho RF, Vercesi AE. Mitochondrial permeability transition and oxidative stress. *FEBS Lett.* 2001; 495:12-15.
61. Lemasters JJ, Theruvath TP, Zhong Z, Nieminen AL. Mitochondrial calcium and the permeability transition in cell death. *Biochim Biophys Acta.* 2009; 1787:1395-1401.

(Received February 14, 2010; Accepted February 24, 2010)

Review

Uses of single-particle tracking in living cells

Xuan Zhou, Lei Wang*

School of Pharmacy, Shandong University, Ji'nan, Shandong, China.

ABSTRACT: Single-particle tracking (SPT) techniques have been developing rapidly in the field of cellular biology as a means of unravelling the diffusion dynamics of bio-molecules and the function of proteins in the regulation of cellular activity at single molecule sensitivity and nanometer spatial resolution. Suitable probes and technological improvements have made SPT more accessible than it used to be and paved the way for broad applications in cellular biology. This review summarizes the principles of SPT and discusses the main findings yielded by the technique and its contribution to the understanding of proteins in living cells.

Keywords: Single-particle tracking (SPT), living cell, review

1. Introduction

Over the last decade, significant advances in microscopy techniques and the introduction of novel fluorescent probes to label bio-molecules in living cells have changed the field of cell biology. Single-particle tracking (SPT), including real-time single-molecule techniques, has enabled tracking of individual molecules over time and space in living cells. SPT is a general term, and a "particle" refers in a broad sense to any probe selectively attached to a molecule of interest (*I*), such as a receptor, organelle, or virus. The variety of nomenclature in the field (*e.g.* single-virus tracing and single-molecule tracking) presents difficulty when searching the literature (2). SPT uses video microscopy combined with digital computer processing to monitor the motion of single molecules of interest, which are often labeled with submicrometer fluorophores. An SPT experimental system is depicted schematically in Figure 1 (3).

Many cellular processes involve the interaction of

several individual molecules that must come together to transmit information or respond to environmental cues. Hence, importance crucial point is to understand the mechanism by which the motion of related molecules is regulated in the cell. However, molecular behavior is very inhomogeneous, and even molecules of a single species interact stochastically with distinct molecules or cellular structures in a variety of local environments. Furthermore, molecular interactions are by nature stochastic. Therefore, bulk-type observations that report on the tendency of molecular behavior averaged over all molecules under observation may not be able to distinguish various stochastic processes occurring in very inhomogeneous environments. SPT has the advantage of being able to view individual characteristics of a molecule that may be washed out in the ensemble averaging inherent in bulk studies (4). SPT has been used to investigate the movement of receptors or lipids in the plasma membrane (5,6), follow individual viruses along their infection pathway (7,8), or study the motion of individual complexes within living cells (9,10). The current review focuses on the recent progress achieved with SPT techniques, including a summary of the principle of SPT, and it discusses the main findings yielded by this technique and its contribution to the understanding of proteins in living cell.

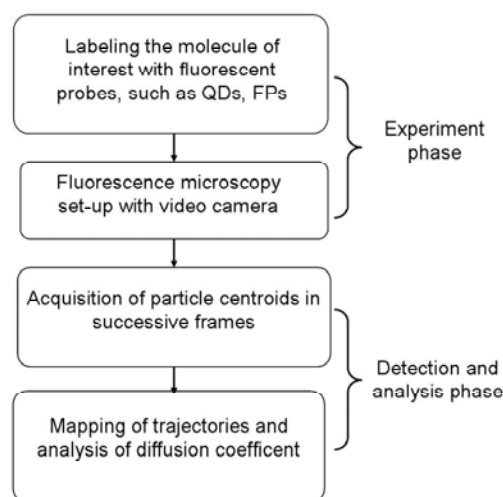


Figure 1. Schematic of an SPT experimental system.

*Address correspondence to:

Dr. Lei Wang, School of Pharmacy, Shandong University, West Cultural Road, No. 44, Ji'nan 250012, Shandong, China.

e-mail: wangl-sdu@sdu.edu.cn

2. Fluorescent probes

The first step toward the realization of SPT in living cells is to label the external and/or internal molecules of interest with fluorophores, allowing imaging using fluorescence microscopy. Fluorescent probes for SPT should have a high quantum yield of fluorescence emission and high photostability. In general, two classes of probes are used for SPT: fluorescent proteins (FPs) and non-genetically encoded probes, such as organic small-molecule fluorophores and quantum dots (QDs) (11). To date, the most popular probe used to study the movement of proteins is QDs (1).

2.1. QDs

Inorganic nanoparticle semiconductor QDs are excellent major fluorescent probes for SPT because of their unique fluorescent properties (12). Their huge one- and two-photon absorption cross sections, tunable emission bands, and excellent photobleaching resistance are stimulating the development of luminescent probes for single-molecule imaging and SPT. The unique wide absorption spectra and narrow emission band that can be tuned from UV to infrared wavelengths distinguish them from conventional organic fluorophores and provide many advantages for multi-color fluorescent imaging. In addition, QDs are orders of magnitude more photostable than organic dyes and FPs, making them attractive candidates for long-term SPT experiments in living cells, where they can provide long tracking trajectories (13). Moreover, the developments in QD surface coating and bio-conjugation schemes have made them the most suitable probes for live cell applications. Over the years, scientists have developed a wide array of surface chemistries for QD modification (14). These surface coatings have not only made QDs retain the advantageous photophysical and size properties of the nanocrystal but also provide additional reactive groups for subsequent conjugation of biomolecular recognition molecules. Finally, a particular property of QDs is their alternation between "on" and "off" states, known as blinking. This adds complexity to the tracking procedure but ensures the identification of single QDs because signals alternate between 0 and 1 and would be fractional in the case of multiple QDs (1).

2.2. Organic small-molecule fluorophores

Organic dyes have diverse structures and photophysical properties that can be designed through organic synthesis. They are usually constructed through either chemical labeling of proteins or physical incorporation into the molecules of interest. Their small size makes them less perturbative than QD. They are, however, less bright and stable, making them suitable only for short trajectories of a few seconds.

2.3. FPs

FPs can be genetically engineered to be incorporated into the molecule interior of cell and they are highly specific with controlled one-to-one stoichiometry. However, they are generally bigger, dimmer, and less photostable than small-molecule fluorophores.

2.4. Gold nanoparticles (GNPs)

Compared to fluorescent dyes and QDs, GNPs (the size from 2 to 100 nm) have unique optical properties such as no photobleaching and absence of blinking, and the small size of the GNPs reduces the potential for probe-related artifacts. Moreover, they show no cytotoxicity under certain experimental conditions (15). Additionally, GNPs show strong light scattering at the plasmon resonance wavelength owing to the collective oscillation of the conduction electrons. Based on this nature of GNPs, a new technique called single nanoparticle photothermal tracking (SNaPT) has been developed to track small probes in live cells. These probes can be detected by local thermal variation after light absorption, allowing tracking experiments over a certain period of time (16).

2.5. Other fluorescent probes

In recent years, there has been enormous interest in the use of nanoparticles as tiny probes to spy on cellular machinery. Useful properties can be incorporated into the design of nanoparticles in order to study cellular functions. For example, single-walled carbon nanotubes (SWNTs) are powerful molecular fluorophores for SPT. SWNTs have interesting photophysical properties. Unlike organic dyes, the conjugated sp^2 carbon bonds in a carbon nanotube are chemically quite stable and the one-dimensional quantum confinement creates an unusual, low energy band gap in the near-infrared (NIR) range. This chemical stability translates into a high degree of photostability. Meanwhile, SWNTs have no significantly irreversible photobleaching threshold at moderate fluence and no intrinsic blinking mechanism (17). Fluorescent nanodiamonds (FNDs) are nontoxic and photostable nanomaterials, ideal for long-term *in vivo* imaging applications (18). Modifying the surfaces of FNDs with different functional groups so that they are treated as pure organic compounds has expanded these materials' applications. One type of FNDs, when exposed to green-yellow light, emits bright-red fluorescence at about 700 nm, which is well away from the spectral region (300-500 nm) where cellular endogenous fluorescence occurs. Moreover, the fluorescence shows no apparent photobleaching, thus allowing long-term probing of FND particles individually in cells (19).

3. Fluorescence microscopy

Labeled particles are visualized in live cells using fluorescence microscopy. Three imaging geometries are most often used, *i.e.*, epifluorescence microscopy, confocal microscopy, and total internal reflection fluorescence microscopy (TIRFM). Of the three, epifluorescence microscopy is the simplest to set up. This method also has the greatest imaging depth and is often used when long-range protein trafficking or transport is being studied. However, owing to the background autofluorescence of cells, epifluorescence is inadequate for SPT involving only a few fluorescent molecules. To reduce the background noise, confocal detection or excitation by total internal reflection (TIR) is used. Confocal microscopy requires a rapid scanning scheme (laser scanning confocal microscopy) or multiplexed detection (spinning disc confocal microscopy) to acquire images of living cells. Using confocal imaging allows the acquisition of 3-dimensional images, but this advantage is mitigated by a relatively severe signal loss. The focus of the laser beam of a laser-scanning confocal microscope is scanned or orbited around the particle. TIRFM, which is a wide-field imaging technique that illuminates only a thin plane of the sample, can also be used for SPT. This is done to greatly reduce the background fluorescence and detect single particles in the cell membrane. However, the excitation depth of an evanescent wave generated by TIR is only 100-200 nm, limiting its use to events that occur close to the cell surface. Therefore, TIRFM imaging is typically used to monitor the mobility of membrane proteins.

In addition to these background-reduction techniques, SPT is performed with specialized video cameras. In a typical SPT system, a video camera is connected to an optical microscope. Video signals from the camera are transmitted to a recording device (3). As a result, the development of charge-coupled device (CCD) cameras with high quantum yields (60-80%) and rapid frame rates (1-500 ms) also represents an important technological advance that has benefited SPT technology (7).

4. Uses of SPT in living cells

4.1. SPT of membrane receptor transport

SPT techniques have offered alternative ways to explore the kinetics of receptor transport and the transport of internalized endosomes on the cell surface. It has been indispensable in understanding the details of the mechanism of cell signaling and particle transport because it eliminates ensemble averaging and provides direct information on heterogeneity and kinetics of the system.

Liang *et al.* (20) used SPT to efficiently explore

the pathway and mechanism for the transport of α_{1A} -Adrenergic receptors (α_{1A} -ARs) in real time in single living cells. In this work, α_{1A} -ARs were specially labeled by primary antibody and Cy3-IgG, and α_{1A} -ARs internalization into cells was triggered by the agonist phenylephrine (PE). They were the first to find that the initial transport of α_{1A} -AR depended on actin filaments at a peak velocity of 0.2 $\mu\text{m}/\text{sec}$ and exhibited discrete 33-nm steps. The step size, the rate constant, and the velocities were broadly in agreement with the character of single myosin molecules *in vitro*. Their results demonstrated that while transporting each endosome myosins did not work in a "tug-of-war" mode and that they did not adopt a strategy of working in coordination to boost transporting speed. These results not only offered some insight into the mode in which myosin works *in vivo* but also provided a model of transportation of internalized G-protein coupled receptors (GPCRs) in living cells. Relevant information on mechanisms of action for other GPCRs has been also obtained with SPT (21,22). Echarte *et al.* (23) investigated the biophysical behavior of retrograde transport of nerve growth factor (NGF) in living cells and in real time using QDs and quantitative SPT technology. They followed NGF trafficking inside neurites of differentiated PC12 cells by tracking trace amounts of streptavidin-coated QDs bound to biotinylated NGF (bNGF). Using this strategy, they visualized NGF binding, internalization, and trafficking and they characterized the kinetics of the NGF trafficking process. They found that a net retrograde transport of QDs-bNGF complexes with a velocity of $0.054 \pm 0.020 \mu\text{m}/\text{sec}$. Individual runs had a mean velocity of approximately 0.15 $\mu\text{m}/\text{sec}$ at room temperature, and the run times were exponentially distributed. Their results demonstrated that the receptor had been internalized, like many cytoplasmic organelles. QDs-bNGF-receptor complexes exhibited bidirectional movement along microtubules after endocytosis. Based on quantitative analysis of the tracking data, they derived the rates and extent of transport in both the retrograde and anterograde directions. The new information gained through SPT is of fundamental importance in understanding normal and pathological processes in the nervous system.

4.2. SPT of exocytosis and endocytosis

Exocytosis and endocytosis are the basic methods of material transport between the cell and its environment. Exocytosis is a process by which the membranes of secretory vesicles fuse with the plasma membrane, releasing the contents of the vesicle into the extracellular medium. This process has been studied in particular depth with regard to the release of neurotransmitters at the synapse (24-26). Import into the cell is possible by the process of receptor-mediated

endocytosis, by which selected plasma membrane proteins are internalized. This not only mediates some signal transduction processes but also allows the cell to maintain or modify its electrolyte balance and control its osmotic properties. Neurons transmit information by the regulated release of neurotransmitters that bind to specific receptors at the target cell. SPT has been used to directly detect the dynamic process of synaptic vesicle trafficking in nerve terminals and to measure the release of neurotransmitters induced experimentally or evoked by normal behavior. Levitan *et al.* (25) used SPT to study neuropeptide vesicle exocytosis and motion at the drosophila larval neuromuscular junction (NMJ). Movement and release of single large dense-core vesicles can be resolved in nerve terminals because green fluorescent protein (GFP)-tagged neuropeptides are highly concentrated in these organelles. Utilization of SPT led to the first detection of vesicle mobilization in nerve terminals and the discoveries of activity-dependent capture of transiting vesicles and post-tetanic potentiation of neuropeptide release. Lemke and Klingauf (26) described a SPT technique using dual fluorescent dye labels to simultaneously visualize the movements of a single vesicle and the respective synaptic bouton during resting conditions and stimulation. They found vesicle mobility to be very low in the absence of stimulation, in accordance with previous studies (27,28). Interestingly, mobility was also found to be low during synaptic activity. They found that vesicles labeled preferentially *via* early, late, and spontaneous endocytotic mechanisms behaved similarly at rest and during stimulation.

Receptor-mediated endocytosis is a complex and dynamic process that is critical to the governing of cellular signaling and subsequent cell function. In order to understand receptor endocytic trafficking at the level of single or small numbers of receptors, Rajan *et al.* (29) developed and tested ligand nerve growth factor-bound quantum dot (NGF-QD) bioconjugates in order to image discrete receptor endocytic events inside live NGF-responsive PC12 cells. Using SPT, they investigated the molecular-scale dynamics of NGF-receptor complexes undergoing endocytic trafficking. The unique value of SPT indicated that NGF trafficking operated with a strikingly high degree of efficiency at the molecular-size scale and that diffusive and active forms of transport inside cells were rapid and efficient.

4.3. SPT of mRNA

SPT is a powerful technique for studying RNA dynamics in living cells. It enables the analysis of the movement of individual RNA molecules in real time and the comparison of the relationship between movement and the subnuclear structure of those molecules. Recently, SPT of mRNA has been performed

in the cytoplasm (30) and in the nucleus (31). Shav-Tal *et al.* (31) used a cellular system for monitoring mRNA expression to characterize the movement in real time of single mRNA-protein complexes (mRNPs) in the nucleus of living mammalian cells. They found that the mobility of mRNA was not directed but governed by simple diffusion. Moreover, half the population of mRNAs diffused freely, with $D = 0.04\text{-}0.05 \mu\text{m}^2/\text{sec}$, and the other half were corralled in the nucleus (31). SPT of mRNA labeled with a molecular beacon was performed in the nucleus by Vargas *et al.* (32). They used small, hairpin-shaped oligonucleotides known as molecular beacons that possessed an internally quenched fluorophore with fluorescence that was restored upon hybridization to the complementary sequence of mRNA. Brownian motion of mRNA with $D = 0.03 \mu\text{m}^2/\text{sec}$ was reported (32). However, these two studies were carried out with a low temporal resolution (300 ms/frame) and mRNAs were only observed over 3 s (33). In 2009, Ishihama and Funatsu (33) successfully observed the movement of individual mRNAs for more than 60 s with a temporal resolution of 30 ms using QDs. mRNA labeled with QDs at a stoichiometric ratio of 1:1 was microinjected into the nuclei of Cos7 cells. They found that almost all mRNA-QDs were in motion, and statistical analyses revealed anomalous diffusion between barriers, with a microscopic diffusion coefficient of $0.12 \mu\text{m}^2/\text{sec}$ and a macroscopic diffusion coefficient of $0.025 \mu\text{m}^2/\text{sec}$. Diffusion of mRNA was observed in interchromatin regions but not in histone2B-GFP-labeled chromatin regions. These results provided direct evidence of channeled mRNA diffusion in interchromatin regions. QD labeling allowed SPT of mRNAs to be carried out with high temporal and spatial resolution over observations of a long duration, a feat that had not been achieved by conventional labeling with a fluorescent dye or fluorescent protein.

In order to study whether these individual mRNA species are specifically sorted into separate or common ribonucleoprotein (RNP) particles before or during transport, Katayama *et al.* (10) analyzed the intracellular movement of individual pairs of localized mRNA in yeast cells. mRNA pairs were tagged with tandem repeats of either bacteriophage MS2 or lambda boxB RNA sequences and fluorescently labeled by fusion protein constructs that bound to the RNA tag sequences. Using SPT with dual-color detection, they tracked the transport of two different localized mRNA species. Their observations indicated that different localized mRNAs were coassembled into common RNP particles and cotransported in a directional manner to the target site. Nonlocalized mRNAs or mutant mRNAs that lack functional localization signals form separate particles that are not transported to the yeast bud. This study revealed a high degree of co-ordination of mRNA trafficking in budding yeast.

4.4. Single-virus tracking

SPT studies of viruses are also known as single-virus tracking. Single-virus tracking (7) uses fluorescence microscopy to monitor individual virus particles or viral components in live cells. It is a powerful tool for investigating viral infection routes and characterizing the dynamic interactions between viruses and target cells. Viral infections are universally acknowledged to be complex processes that include many steps and interactions with different cellular structures. Not only are these interactions dynamic, but often the cellular structures are themselves dynamic. Furthermore, the same virus might infect cells by several different routes and most viral entry events might be futile. Therefore, single-virus tracking enables the possible elucidation of previously unknown but critical steps involved in the penetration of viruses into cells and dissemination of viruses, revealing novel therapeutic opportunities for controlling virus pandemics and pathogenesis.

A number of studies have revealed detailed information about the proteins involved in fusion for many viruses and have elucidated fundamental principles of viral fusion mechanisms, but the dynamics of the process are largely unknown. Koch *et al.* (34) developed a system to study the dynamics of HIV-1 entry using SPT. They generated HIV-1 particles pseudotyped with the envelope (Env) protein of ecotropic murine leukemia virus (eMLV) to study retrovirus entry at the plasma membrane using live-cell microscopy. In their experiment, they established a double labeling strategy in which a fluorescent label in the matrix (MA) domain of HIV-1 Gag was combined with another fluorescent label fused to eMLV Env (Env-YFP). Fusion events were defined as loss of Env signal after virus-cell contact. SPT of > 20,000 individual traces in two color channels recorded 28 events of color separation, indicating that the MA layer dissociated from the surface glycoproteins upon membrane fusion. Forty-five events were detected where both colors were lost simultaneously. Furthermore, they found that virus-cell fusion appeared to be kinetically different from cell-cell fusion. This finding was in line with that from a previous study (35).

Dengue virus (DENV) is a mosquito-transmitted, enveloped RNA virus. DENV causes the most common arthropod-borne infection worldwide, with 50-100 million cases annually. It threatens human health, but there are presently neither vaccines nor antiviral drugs to prevent or treat dengue infection (36). In 2008, van der Schaar *et al.* studied the cell entry, endocytic trafficking, and fusion behavior of DENV, which was achieved using live-cell imaging, single-virus tracking, and real-time multi-color fluorescence microscopy. In the experiment, DENV was labeled with the lipophilic fluorescent probe DiD. The surface density of the DiD dye in the viral membrane allowed clear detection

of single virus particles, and this labeling procedure did not affect the infectious properties of DENV. In order to test whether DENV was internalized through clathrin-mediated endocytosis, BS-C-1 cells were used; these cells stably expressed enhanced yellow fluorescent protein (eYFP) fused to the light chain of clathrin (37). The simultaneous tracking of DENV particles and various endocytic markers revealed that DENV enters cells exclusively *via* clathrin-mediated endocytosis. The virus particles moved along the cell surface in a diffusive manner before being captured by a pre-existing clathrin-coated pit. Following clathrin-mediated uptake, the majority of DENV particles were transported to early endosomes, which subsequently matured into late endosomes, and then fusion of the viral membrane with the endosomal membrane was detected in late endosomal compartments. This is the first report to describe the cell entry process of DENV at the single particle level and therefore provides unique mechanistic and kinetic insights into the route of internalization, endocytic trafficking behavior, and membrane fusion properties of individual DENV particles in living cells. This study has opened up new avenues in flavivirus biology and will lead to a better understanding of the critical determinants in DENV infection (38). In addition, this group studied the transport, acidification, and fusion of single influenza viruses in living cells (39). Influenza is a valuable model system for exploring the cell's constitutive endocytic pathway. The movement of individual viruses revealed a striking three-stage active transport process that preceded viral fusion with endosomes starting with an actin-dependent movement in the cell periphery, followed by a rapid, dynein-directed translocation to the perinuclear region, and finally an intermittent movement involving both plus- and minus-end-directed microtubule-based motilities in the perinuclear region. Surprisingly, the majority of viruses experience their initial acidification in the perinuclear region immediately following the dynein-directed rapid translocation step. This finding suggests a previously undescribed scenario of the endocytic pathway toward late endosomes: endosome maturation, including initial acidification, largely occurs in the perinuclear region.

4.5. SPT of drug delivery

Anticancer therapeutics based on active tumor targeting by conjugating tumor-specific antibodies should help to increase therapeutic efficacy and decrease systemic toxicity. Quantitative investigation of the dynamics of anticancer drug delivery *in vivo* is crucial to enabling the development of more effective drug delivery systems. Recently, SPT has been used to study drug delivery.

Tada *et al.* (40) tracked single-particle QDs conjugated with tumor-targeting antibody in tumors

of living mice using a dorsal skinfold chamber and a high-speed confocal microscope with a highly sensitive camera. They succeeded in capturing the delivery of single QD-antibody complexes in tumor vessels to the perinuclear region of tumor cells in live mice after QD-antibody complexes had been injected into the tail vein of mice with HER2-overexpressing breast cancer. Movement of single complexes of the QD-antibody were clearly observed at 30 frames/sec inside the tumor, and six stages were detected (Figure 2): (1) circulation within a blood vessel, (2) extravasation, (3) movement into the extracellular region, (4) binding to HER2 on the cell membrane, (5) movement from the cell membrane to the perinuclear region after endocytosis, and (6) movement to the perinuclear region. The translational speed of QD-antibody complexes in each process was highly variable, even in vessel circulation. The movement of the complexes at each stage was also found to be "stop-and-go". This indicated that the movement was promoted by a motive power and constrained by both the three-dimensional structure of the complexes and protein-protein interactions. The motive power of the movement was produced by blood circulation, diffusion force driven by thermal energy, and active transport by motor proteins. The cessation of movement is most likely induced by

a structural barricade such as a matrix cage and/or specific interaction between proteins and HER2, motor proteins, and rail filaments such as actin filaments and microtubules. This study provides valuable information on antibody-conjugated therapeutic nanoparticles, which will be of use in analyzing the molecular processes of drug delivery to the tumor and in increasing therapeutic efficacy. SPT has also been used to investigate the potential of magnetic nanoparticles for drug delivery (41).

5. Conclusions

SPT, a very powerful technique, represents the only currently available method to clearly differentiate different types of protein movement without population averaging and will prove indispensable in understanding the details of the mechanism of cell signaling and particle transport (42). Among their major achievements, SPT studies have revealed the molecular details of signaling processes, receptor activation, lateral organization, dynamics of endocytosis and exocytosis, and the mechanisms of entry, trafficking, and egress of various viruses. The next 5 years should see intensive research on the *in vivo* uses of SPT. Although it has made great achievements in the field

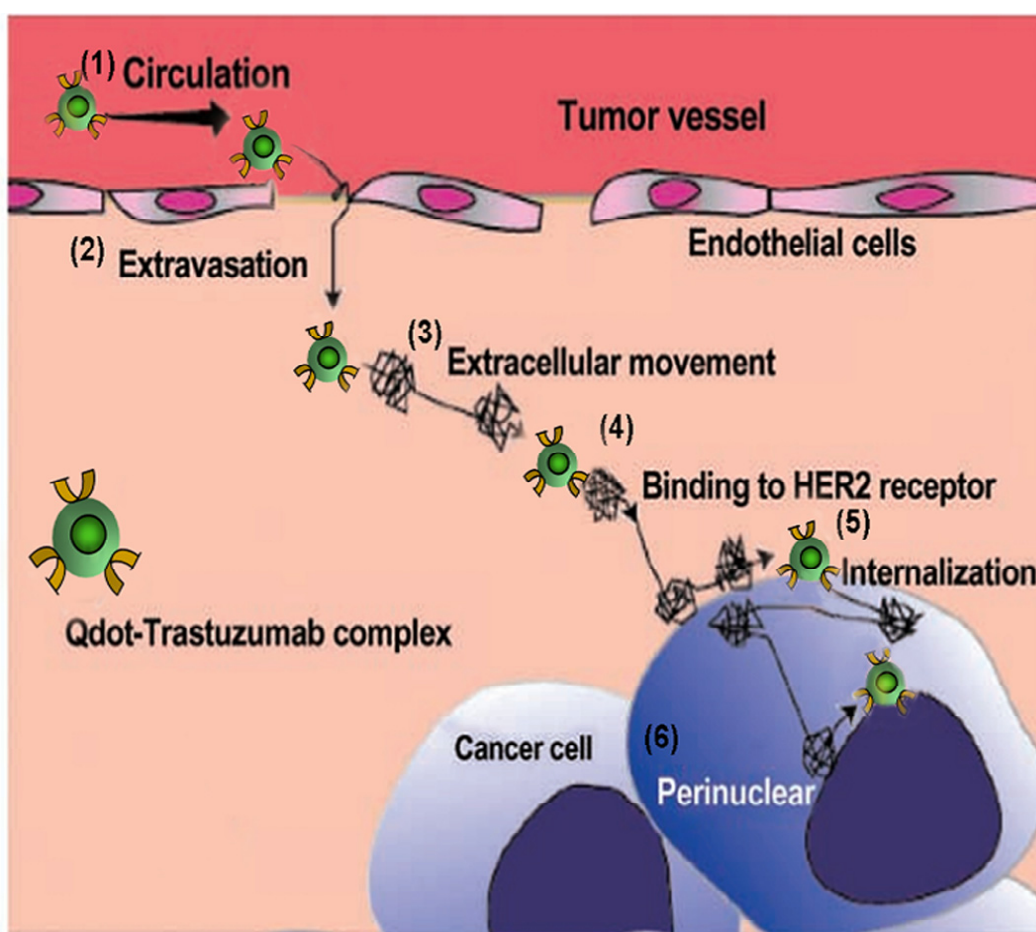


Figure 2. Schematic illustration of the delivery of single QDs-trastuzumab complex in tumor vessels to the perinuclear region of tumor cells.

of life science, many difficulties remain, such as the inconvenient labeling process, the need for a highly sophisticated imaging apparatus, and the limiting of labeling particles to living cells, and continue to represent a hindrance to the more widespread use of SPT.

Acknowledgements

This project was supported by the National Natural Science Foundation of China (Grant No. 20875056) and the Natural Science Foundation of Shandong Province of China (Grant No. Z2008B05).

References

- Alcor D, Gouzer G, Triller A. Single-particle tracking methods for the study of membrane receptors dynamics. *Eur J Neurosci.* 2009; 30:987-997.
- Saxton MJ. Single-particle tracking: connecting the dots. *Nat Methods.* 2008; 5:671-672.
- Chen Y, Lagerholm BC, Yang B, Jacobson K. Methods to measure the lateral diffusion of membrane lipids and proteins. *Methods.* 2006; 39:147-153.
- Ritchie K, Shan XY, Kondo J, Iwasawa K, Fujiwara T, Kusumi A. Detection of non-Brownian diffusion in the cell membrane in single molecule tracking. *Biophys J.* 2005; 88:2266-2277.
- Fujiwara T, Ritchie K, Murakoshi H, Jacobson K, Kusumi A. Phospholipids undergo hop diffusion in compartmentalized cell membrane. *J Cell Biol.* 2002; 157:1071-1081.
- Schutz GJ, Kada G, Pastushenko VP, Schindler H. Properties of lipid microdomains in a muscle cell membrane visualized by single molecule microscopy. *Embo J.* 2000; 19:892-901.
- Brandenburg B, Zhuang X. Virus trafficking - learning from single-virus tracking. *Nat Rev Microbiol.* 2007; 5:197-208.
- Marsh M, Helenius A. Virus entry: open sesame. *Cell.* 2006; 124:729-740.
- Kubitscheck U, Kuckmann O, Kues T, Peters R. Imaging and tracking of single GFP molecules in solution. *Biophys J.* 2000; 78:2170-2179.
- Lange S, Katayama Y, Schmid M, Burkacky O, Brauchle C, Lamb DC, Jansen RP. Simultaneous transport of different localized mRNA species revealed by live-cell imaging. *Traffic.* 2008; 9:1256-1267.
- Fernandez-Suarez M, Ting AY. Fluorescent probes for super-resolution imaging in living cells. *Nat Rev Mol Cell Biol.* 2008; 9:929-943.
- Michalet X, Pinaud FF, Bentolila LA, Tsay JM, Doose S, Li JJ, Sundaresan G, Wu AM, Gambhir SS, Weiss S. Quantum dots for live cells, *in vivo* imaging, and diagnostics. *Science.* 2005; 307:538-544.
- Chang YP, Pinaud F, Antelman J, Weiss S. Tracking bio-molecules in live cells using quantum dots. *J Biophotonics.* 2008; 1:287-298.
- Pinaud F, Michalet X, Bentolila LA, Tsay JM, Doose S, Li JJ, Iyer G, Weiss S. Advances in fluorescence imaging with quantum dot bio-probes. *Biomaterials.* 2006; 27:1679-1687.
- Murphy CJ, Gole AM, Stone JW, Sisco PN, Alkilany AM, Goldsmith EC, Baxter SC. Gold nanoparticles in biology: beyond toxicity to cellular imaging. *Acc Chem Res.* 2008; 41:1721-1730.
- Lasne D, Blab GA, Berciaud S, Heine M, Groc L, Choquet D, Cognet L, Lounis B. Single nanoparticle photothermal tracking (SNaPT) of 5-nm gold beads in live cells. *Biophys J.* 2006; 91:4598-4604.
- Strano MS, Jin H. Where is it heading? Single-particle tracking of single-walled carbon nanotubes. *ACS Nano.* 2008; 2:1749-1752.
- Fu CC, Lee HY, Chen K, Lim TS, Wu HY, Lin PK, Wei PK, Tsao PH, Chang HC, Fann W. Characterization and application of single fluorescent nanodiamonds as cellular biomarkers. *Proc Natl Acad Sci U S A.* 2007; 104:727-732.
- Zhang B, Li Y, Fang CY, Chang CC, Chen CS, Chen YY, Chang HC. Receptor-mediated cellular uptake of folate-conjugated fluorescent nanodiamonds: A combined ensemble and single-particle study. *Small.* 2009; 5:2716-2721.
- Liang ZY, Xu N, Guan YH, Xu M, He QH, Han QD, Zhang YY, Zhao XS. The transport of alpha(1A)-adrenergic receptor with 33-nm step size in live cells. *Biochem Biophys Res Commun.* 2007; 353:231-237.
- Daumas F, Destainville N, Millot C, Lopez A, Dean D, Salome L. Confined diffusion without fences of a g-protein-coupled receptor as revealed by single particle tracking. *Biophys J.* 2003; 84:356-366.
- Guan Y, Xu M, Liang Z, Xu N, Lu Z, Han Q, Zhang Y, Zhao XS. Heterogeneous transportation of alpha1B-adrenoceptor in living cells. *Biophys Chem.* 2007; 127:149-154.
- Echarte MM, Bruno L, Arndt-Jovin DJ, Jovin TM, Pietrasanta LI. Quantitative single particle tracking of NGF-receptor complexes: transport is bidirectional but biased by longer retrograde run lengths. *FEBS Lett.* 2007; 581:2905-2913.
- Yoshina-Ishii C, Chan YH, Johnson JM, Kung LA, Lenz P, Boxer SG. Diffusive dynamics of vesicles tethered to a fluid supported bilayer by single-particle tracking. *Langmuir.* 2006; 22:5682-5689.
- Levitani ES, Lanni F, Shakiryanova D. *In vivo* imaging of vesicle motion and release at the Drosophila neuromuscular junction. *Nat Protoc.* 2007; 2:1117-1125.
- Lemke EA, Klingauf J. Single synaptic vesicle tracking in individual hippocampal boutons at rest and during synaptic activity. *J Neurosci.* 2005; 25:11034-11044.
- Henkel AW, Simpson LL, Ridge RM, Betz WJ. Synaptic vesicle movements monitored by fluorescence recovery after photobleaching in nerve terminals stained with FM1-43. *J Neurosci.* 1996; 16:3960-3967.
- Jordan R, Lemke EA, Klingauf J. Visualization of synaptic vesicle movement in intact synaptic boutons using fluorescence fluctuation spectroscopy. *Biophys J.* 2005; 89:2091-2102.
- Rajan SS, Liu HY, Vu TQ. Ligand-bound quantum dot probes for studying the molecular scale dynamics of receptor endocytic trafficking in live cells. *ACS Nano.* 2008; 2:1153-1166.
- Fusco D, Accornero N, Lavoie B, Shenoy SM, Blanchard JM, Singer RH, Bertrand E. Single mRNA molecules demonstrate probabilistic movement in living mammalian cells. *Curr Biol.* 2003; 13:161-167.
- Shav-Tal Y, Darzacq X, Shenoy SM, Fusco D, Janicki

- SM, Spector DL, Singer RH. Dynamics of single mRNPs in nuclei of living cells. *Science*. 2004; 304:1797-1800.
32. Vargas DY, Raj A, Marras SA, Kramer FR, Tyagi S. Mechanism of mRNA transport in the nucleus. *Proc Natl Acad Sci U S A*. 2005; 102:17008-17013.
33. Ishihama Y, Funatsu T. Single molecule tracking of quantum dot-labeled mRNAs in a cell nucleus. *Biochem Biophys Res Commun*. 2009; 381:33-38.
34. Koch P, Lampe M, Godinez WJ, Muller B, Rohr K, Krausslich HG, Lehmann MJ. Visualizing fusion of pseudotyped HIV-1 particles in real time by live cell microscopy. *Retrovirology*. 2009; 6:84-98.
35. Markosyan RM, Cohen FS, Melikyan GB. Time-resolved imaging of HIV-1 Env-mediated lipid and content mixing between a single virion and cell membrane. *Mol Biol Cell*. 2005; 16:5502-5513.
36. Mackenzie JS, Gubler DJ, Petersen LR. Emerging flaviviruses: the spread and resurgence of Japanese encephalitis, West Nile and dengue viruses. *Nat Med*. 2004; 10:S98-S109.
37. van der Schaar HM, Rust MJ, Waarts BL, van der Ende-Metselaar H, Kuhn RJ, Wilschut J, Zhuang X, Smit JM. Characterization of the early events in dengue virus cell entry by biochemical assays and single-virus tracking. *J Virol*. 2007; 81:12019-12028.
38. van der Schaar HM, Rust MJ, Chen C, van der Ende-Metselaar H, Wilschut J, Zhuang X, Smit JM. Dissecting the cell entry pathway of dengue virus by single-particle tracking in living cells. *PLoS Pathog*. 2008; 4:e1000244.
39. Rust MJ, Lakadamyali M, Zhang F, Zhuang X. Assembly of endocytic machinery around individual influenza viruses during viral entry. *Nat Struct Mol Biol*. 2004; 11:567-573.
40. Tada H, Higuchi H, Wanatabe TM, Ohuchi N. *In vivo* real-time tracking of single quantum dots conjugated with monoclonal anti-HER2 antibody in tumors of mice. *Cancer Res*. 2007; 67:1138-1144.
41. McGill SL, Cuylear CL, Adolphi NL, Osinski M, Smyth HD. Magnetically responsive nanoparticles for drug delivery applications using low magnetic field strengths. *IEEE Trans Nanobioscience*. 2009; 8:33-42.
42. Jaskolski F, Henley JM. Synaptic receptor trafficking: the lateral point of view. *Neuroscience*. 2009; 158:19-24.
- (Received January 14, 2010; Accepted February 24, 2010)

Original Article**Proton magnetic resonance (¹HNMR) spectroscopy and physicochemical studies of zaleplon-hydroxypropyl-β-cyclodextrin inclusion compounds****Manali R. Shah, Pankajkumar P. Sancheti, Vikrant M. Vyas, Poonam S. Karekar, Yogesh V. Pore****Department of Pharmaceutical Chemistry, Government College of Pharmacy, Karad, Maharashtra, India.*

ABSTRACT: Proton magnetic resonance spectroscopy (¹HNMR) studies on inclusion compounds of zaleplon with hydroxypropyl-β-cyclodextrin (HPβCD) were carried out in order to elucidate the strength and binding mode of association. Chemical shift measurements revealed that inclusion complexes of zaleplon and HPβCD were formed by penetration of aromatic rings into the HPβCD cavity from the wider rim side with deep penetration of the amide-substituted ring while inclusion of the cyano-substituted pyrazole ring was shallow. A higher magnitude of ΔδH-3' and ΔδH-5' protons of HPβCD indicated higher stability of the lyophilized product than the kneaded one. Even from the values of ΔδH-5'/ΔδH-3', it could be concluded that zaleplon deeply penetrated inside the HPβCD cavity in the lyophilized product as compared to the kneaded product. The stoichiometry of the inclusion complexes was assessed to be a 1:1 molar ratio with an A_L-type of phase solubility curve and a stability constant of 57.89 ± 1.82 M⁻¹, according to Higuchi and Connors. In the case of dissolution experiments, a lyophilized product displayed a higher release rate of zaleplon (DE₃₀: 77.64 ± 5.74) than the kneaded complex and physical mixture.

Keywords: Zaleplon, hydroxypropyl-β-cyclodextrin, ¹HNMR, inclusion compounds, dissolution

1. Introduction

Molecular encapsulation *via* formation of monomolecular inclusion complexes with cyclodextrins has been extensively used in pharmaceutical research for the

solubility enhancement of poorly soluble aqueous compounds (1). The process of molecular encapsulation involves the spatial entrapment of a single guest molecule in the cavity of the host molecule without any covalent interactions (2,3). Cyclodextrins have been widely employed for this purpose because of their torus shape which gives ability to entrap the hydrophobic portion of properly sized guest molecules, entirely or partially, within their hydrophobic central cavity, both in solution and in the solid state (4). This inclusion decreases the lipophilic character of the drug molecule with simultaneous improvement in its solubility and chemical stability (5-9). While forming an inclusion complex, cyclodextrins do not modify the molecular structure and permeability characteristics of hydrophobic drug molecules but deliver them to the surface of the biological membrane in their original form (10,11).

However, due to toxicological considerations, safety issues, and limited water solubility of parent cyclodextrins (β-cyclodextrin), some modified cyclodextrins such as 2-hydroxypropyl-β-cyclodextrin have been introduced in formulation research (3). 2-Hydroxypropyl-β-cyclodextrin (HPβCD) (Figure 1) is a hydroxyalkyl β-cyclodextrin derivative which is widely used in pharmaceutical formulations owing to its amorphous, non-crystalline nature, high water solubility and low toxicity (12). Toxicological studies revealed that HPβCD is well tolerated by the human body using both intravenous and oral administration (13). Therefore, an inclusion complex with HPβCD could be an effective approach to achieve ideal therapy for drugs with poor aqueous solubility (14).

Zaleplon selected in the current investigation is a GABA_A modulating hypnotic drug belonging to the pyrazolopyrimidine class of fused heterocyclic compounds intended for the management of insomnia (15). However, due to poor aqueous solubility (practically insoluble) and limited dissolution of zaleplon, only 30% of the drug reaches the systemic circulation (16). Because cyclodextrins can improve the solubility/dissolution of hydrophobic substances *via* complex formation (17), which results in improvement

*Address correspondence to:

Dr. Yogesh V. Pore, Department of Pharmaceutical Chemistry, Government College of Pharmacy, Karad, Maharashtra 415 124, India.
e-mail: dryogeshpore@rediffmail.com

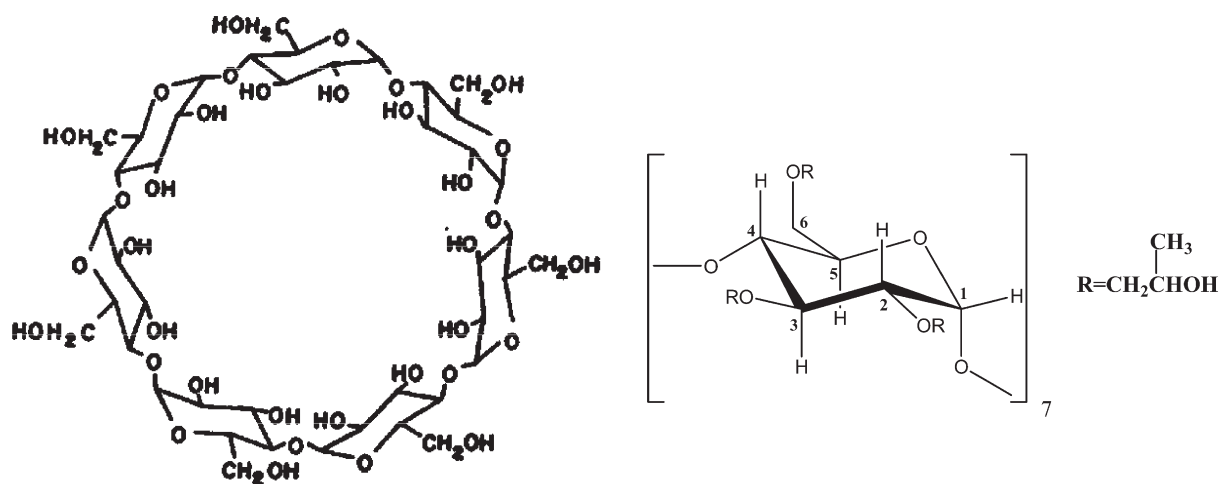


Figure 1. Hydroxypropyl- β -cyclodextrin.

of overall therapeutic effectiveness of such drugs, in this study we have used modified cyclodextrin *viz.* HP β CD to demonstrate the stability, binding mode and dissolution behaviour of zaleplon-HP β CD inclusion compounds prepared by different methods. Further, the chemically modified cyclodextrins may show different modes of arrangement of guest inside the cyclodextrin cavity due to substitution and increased cavity size. Because several papers have reported the use of the NMR technique to study the host-guest interactions during formation of inclusion complexes (18-20), we have employed ^1H NMR chemical shift measurement data to characterize zaleplon-HP β CD binary systems.

The purpose of this work was to investigate the potential of amorphous HP β CD as a solubilizing and complexing agent for zaleplon along with its binding mode with the guest. Phase solubility studies were performed to determine the stoichiometry of the complex formed in aqueous media. The inclusion compounds of zaleplon with HP β CD were prepared by a kneading and lyophilization technique while the physical mixture was prepared by mixing individual components in a mortar. All formulations including pure zaleplon were further evaluated for their dissolution performance in distilled water.

2. Materials and Methods

2.1. Materials

Zaleplon and HP β CD were generously provided by Cipla Ltd., Mumbai, India and Panacea Biotech, Chandigarh, India, respectively. Analytical grade reagents were used for experimental purposes.

2.2. Phase solubility studies

Phase solubility studies in distilled water at room

temperature ($25 \pm 2^\circ\text{C}$) were performed in triplicate according to the method of Higuchi and Connors (21). Excess amounts of zaleplon were added to 20 mL of aqueous solution containing various concentrations of HP β CD (0-0.01 M) in glass flasks. The glass containers were sealed and the suspensions were mechanically shaken on a rotary shaker for 4 days until equilibrium was reached. All suspensions were filtered through a $0.45 \mu\text{m}$ membrane filter and analyzed spectrophotometrically (Shimadzu UV-VIS spectrophotometer 1700, Kyoto, Japan) at 232 nm. The apparent stability constants K_s were estimated from the straight line of the phase solubility diagram according to the equation of Higuchi and Connors (21).

2.3. Preparation of the physical mixture of zaleplon and HP β CD

A physical mixture (PM) of equimolar amounts of zaleplon and HP β CD was prepared by homogeneous blending in a mortar of the individual components which were previously sieved through mesh number $80 \mu\text{m}$.

2.4. Preparation of inclusion complex by kneading method (KN)

Kneaded products were prepared from the PM by adding a small volume of water-ethanol (1:1, v/v) solution followed by vigorously triturating it in a mortar for 45 min to form a homogeneous dispersion. The product was dried at 45°C for 24 h in an oven which was sieved through mesh number $80 \mu\text{m}$.

2.5. Preparation of inclusion complex by lyophilization (freeze-drying) method (LP)

Equimolar amounts of zaleplon and HP β CD were transferred to a beaker containing distilled water and

sonicated for 20 min. The mixture was stirred for 4 days at room temperature, filtered and the resultant clear solution was frozen in a deep freezer at -20°C . The frozen solution was lyophilized in a freeze-dryer (Khera instruments, New Delhi, India) at -40°C until the sample was completely dry.

2.6. Proton nuclear magnetic resonance spectroscopy ($^1\text{H NMR}$)

$^1\text{H NMR}$ spectra of zaleplon, HP β CD, the physical mixture and inclusion complexes were recorded in DMSO (d_6) on a Varian Mercury YH-300 NMR spectrophotometer (Palo Alto, CA, USA) at an operating frequency of 300 MHz.

2.7. Dissolution studies

The dissolution rate studies were performed using a USP Type II dissolution test apparatus (Lab India, Model Disso 2000 Tablet dissolution test apparatus, Mumbai, India). The samples equivalent to 10 mg of zaleplon were placed in a dissolution flask containing 900 mL of distilled water maintained at $37 \pm 0.5^{\circ}\text{C}$ and stirred at 75 rpm (22). Samples were withdrawn at appropriate time intervals and replaced with fresh dissolution medium. After filtration through a $0.45 \mu\text{m}$ membrane filter, the concentration of zaleplon was determined spectrophotometrically at 232 nm. The results were statistically evaluated using ANOVA.

3. Results and Discussion

3.1. Phase solubility studies

Figure 2 shows a phase-solubility curve in aqueous media for the complex formation between zaleplon and HP β CD. It was observed that the aqueous solubility of the drug increases linearly as a function of HP β CD concentration and therefore it could be classified as A_L -

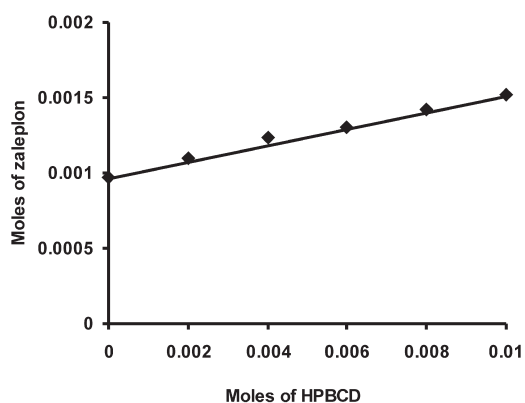


Figure 2. Phase solubility diagram of ZPN-HP β CD system in distilled water.

type. The linear host-guest correlation coefficient $r = 0.9976$ ($r^2 = 0.9952$) with a slope of 0.05420 suggested the formation of a 1:1 complex with respect to HP β CD concentrations as the slope less than unity usually results in first order complexes. The line equation from the linear regression analysis was found to be as follows:

$$y = 0.05420x + 0.0009895 \quad \text{---- Eq. 1}$$

The apparent stability constant, $K_{1:1}$ obtained from the slope of the linear phase solubility diagram was $57.89 \pm 1.82 \text{ M}^{-1}$ (Eq. 1). Thus, the stability constant of the zaleplon-HP β CD complex decreased indicating slightly less affinity of HP β CD toward zaleplon as compared to a zaleplon- β CD complex (17).

3.2. Proton nuclear magnetic resonance spectroscopy ($^1\text{H NMR}$)

Figure 3 displays $^1\text{H NMR}$ spectra of zaleplon (A), HP β CD (B), PM (C), kneaded (D), and lyophilized product (E). $^1\text{H NMR}$ spectra of zaleplon, in the absence of HP β CD, exhibited a quartet and a triplet, each integrating for three and two protons, at 3.79 and 1.15 which were assigned to H-2 and H-3, of methylene and methyl functionalities of the *N*-substituted amide group of the aromatic ring. The signal for H-1 (methyl) of the amide group of the phenyl ring appeared as a singlet at 2.104. Two doublets, each integrating for one proton, at 7.249 and 7.475 could be assigned to H-4 and H-6 protons, respectively, of the aromatic ring whereas a triplet at 7.718 was assigned to the H-5 proton of the same ring. The signals for H-7 of the phenyl ring and H-10 of the pyrazole ring appeared at 7.289 and 8.428, respectively, each as a singlet. The signals for two pyrimidine protons; H-8 and H-9 appeared at 8.006 and 8.801, respectively.

Significant changes in the nature and position of signals for the protons of zaleplon were observed in the presence of HP β CD in PM, kneaded and lyophilized products. The signals for H-1, H-2, H-3, and H-5 protons of the aromatic ring including the amide group, exhibited upfield shifts in all binary systems of zaleplon with HP β CD whereas the signals for H-4, H-6, and H-7 of the aromatic protons exhibited downfield shifts in the PM and kneaded system. Two pyrimidine protons; H-8 and H-9 also experienced downfield shifts in all binary systems of zaleplon while a signal for the H-10 of the pyrazole ring exhibited an upfield shift. The protons H-8 and H-10 were almost diffused in the lyophilized product. However, all aromatic ring protons including protons of the amide group experienced high upfield shifts in the lyophilized system indicating formation of an inclusion complex. The physical mixture and kneaded system displayed a similar shifting pattern of zaleplon protons. The chemical shift change values for

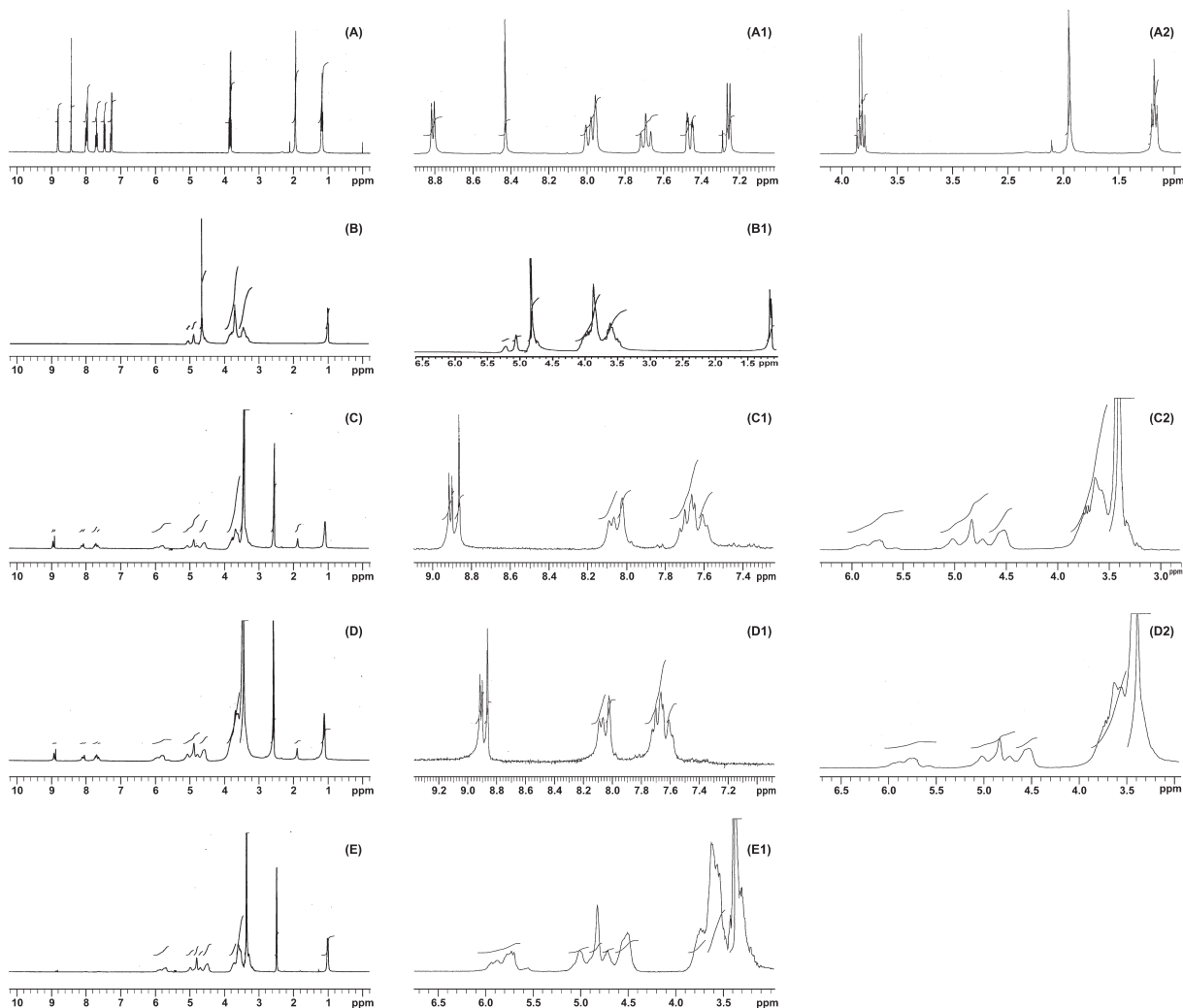


Figure 3. ^1H NMR spectra of ZPN-HP β CD binary systems. A, A1, and A2, ZPN; B and B1, HP β CD; C, C1, and C2, physical mixture; D, D1, and D2, kneaded product; E and E1, lyophilized product.

Table 1. ^1H NMR (300 MHz) chemical shift change ($\Delta\delta$) values for various protons of ZPN in the presence of HP β CD in DMSO

System/Protons	PM	KN	LP
H-1	-0.290	-0.291	-1.076
H-2	-1.290	-1.290	-1.288
H-3	-0.123	-0.122	-0.141
H-4	0.359	0.362	-1.547
H-5	-0.021	-0.020	-1.778
H-6	0.187	0.187	-1.601
H-7	0.357	0.359	-1.558
H-8	0.015	0.015	---
H-9	0.060	0.061	0.063
H-10	-0.365	-0.363	---

Negative values indicate upfield shift. PM, physical mixture; KN, kneaded product; LP, lyophilized product.

various protons of the guest are given in Table 1.

In the NMR spectra of kneaded and lyophilized systems, the signals for H-5' and H-3' protons of HP β CD, situated inside the HP β CD cavity, exhibited high upfield shifts compared to pure HP β CD whereas,

Table 2. ^1H NMR (300 MHz) chemical shift change ($\Delta\delta$) data for HP β CD protons in the presence of ZPN in DMSO

System/Protons	H-3'	H-5'	$\Delta\delta\text{H-5'}/\Delta\delta\text{H-3'}$
KN	-0.098	-0.144	1.50
LP	-0.106	-0.233	2.19

Negative values indicate upfield shift. KN: kneaded product; LP: lyophilized product.

in PM, H-5' and H-3' protons of HP β CD, moved downfield by 0.011 ($\Delta\delta\text{H-5'}$) and 0.004 ($\Delta\delta\text{H-3'}$), respectively. The chemical shift change ($\Delta\delta$) values for HP β CD protons in the kneaded and lyophilized systems are given in Table 2.

The mode of the guest complex into the host cavity of cyclodextrins involves the insertion of the less polar (non-polar) portion of the guest into the CD cavity as reported in earlier papers (4). NMR spectroscopy is an excellent tool for the study of the nature and geometry of the cyclodextrin inclusion complex due to its high sensitivity (23). The penetration of guest usually takes

place from the wider rim side of the cavity. The host-guest interactions are clearly reflected in the form of shifts in NMR signals. The changes in chemical shifts of H-3' and H-5' protons of HP β CD in the presence of the guest molecule indicated that the inclusion in the cavity has taken place in the kneaded and lyophilized systems since these protons are located inside the cavity (24). A deep penetration of guest into the HP β CD cavity results in the chemical shift of both protons H-3' and H-5' of HP β CD whereas the shift in only H-3' protons occurs when the cavity penetration is shallow (25). The ratio for the chemical shift changes for these protons, $\Delta\delta\text{H-5'}/\Delta\delta\text{H-3'}$, gives information about the depth of inclusion of the guest into the HP β CD cavity which was found to be higher in the lyophilized system than the kneaded one (Table 2). On the contrary, in the PM, H-3' and H-5' protons of HP β CD exhibited downfield shifts indicating no formation of an inclusion complex, even though the protons of zaleplon have shown similar behaviour in the PM and kneaded system. These results suggested an existence of a strong physical interaction between zaleplon and HP β CD in the PM. The stability of inclusion complex is related to the magnitude of the chemical shift changes for H-3' and H-5' protons; the higher the value of $\Delta\delta\text{H-3'}$ and $\Delta\delta\text{H-5'}$, the greater is the stability of the complex (26). The protons of the guest molecule located inside the HP β CD cavity in complex, experience upfield shift changes due to the shielding effect by the cavity while, the protons of the guest, which are outside the cavity, show downfield shift changes when complexed (24). Significant high field shifts observed in the NMR signals of H-3' and H-5' of HP β CD in kneaded and lyophilized systems of zaleplon clearly indicated the inclusion of the aromatic part of the guest into the HP β CD cavity due to hydrophobic interactions (27). The higher values of $\Delta\delta\text{H-5'}$ and $\Delta\delta\text{H-3'}$ protons of HP β CD might be attributed to the deep penetration of the zaleplon from the wider rim of HP β CD (28). Further, almost all protons of the aromatic ring, including the protons of the amide group, exhibited significant upfield shifts in kneaded and lyophilized products indicating its penetration inside the HP β CD cavity. However, the H-10 proton of cyano substituted pyrazole ring has also experienced a remarkable upfield shift in kneaded but is diffused in the lyophilized system, which may indicate the possibility of penetration of the cyano substituted pyrazole ring inside the HP β CD cavity. This interpretation has been supported by the loss of intensity and disappearance of the cyanide peak in IR spectra of kneaded and lyophilized products respectively (data not shown). Therefore, two different topologies of complex formation could be possible for each aromatic ring as entry may occur through either the wider or smaller rim of HP β CD, resulting in either shallow or deep penetration of the guest molecule. Figure 4 illustrates possible models of inclusion equilibria of the zaleplon

and HP β CD inclusion complex. The $\Delta\delta\text{H}$ values obtained in NMR signals of kneaded and lyophilized products supports the possible model-1 for the amide-substituted aromatic ring with HP β CD where, the zaleplon enters from the wider rim and penetrates deep so that the amide group protrudes outside the cavity and may interact with 2'-OH of HP β CD at the 6 position. Further evidence was seen in the upfield shift of H-4 and H-5 of zaleplon in the lyophilized product. This might be because of the close proximity of these protons with H-5' while the H-5 and H-6 of zaleplon were in the proximity of both H-3' and H-5' of HP β CD, since these protons have experienced higher upfield shifts than H-4 and H-5 in the lyophilized system. The high upfield shift of H-10 of the cyano substituted pyrazole ring in the kneaded system suggests the possible model-2 indicating the possibility of penetration of the cyano substituted pyrazole ring from the narrow side where only a part of the ring enters the cavity with shallow cavity penetration. Thus ^1H NMR measurements are clearly indicative of formation of inclusion compounds in the solid state.

3.3. Dissolution rate studies

Figure 5 shows dissolution curves of the zaleplon-HP β CD binary systems in distilled water. As shown in Table 3, the values of % drug dissolved at 2 min (DP_2), 15 min (DP_{15}), 30 min (DP_{30}), and dissolution efficiency (29) at 30 min (DE_{30}) were evaluated.

From the results obtained, it was observed that all binary systems of zaleplon with HP β CD show faster dissolution than zaleplon alone. It should be noted that the increase in dissolution rate of zaleplon was 2.04-fold greater from the physical mixture within 2 min whereas, it was 2.96-fold greater from the kneaded system at the

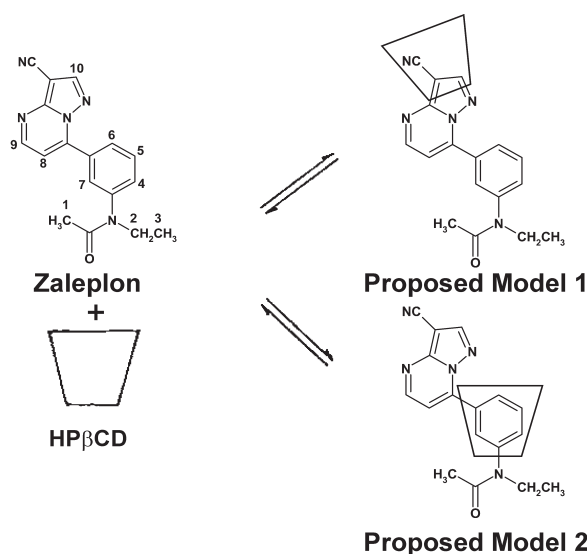


Figure 4. A schematic representation of the inclusion equilibria of ZPN with HP β CD.

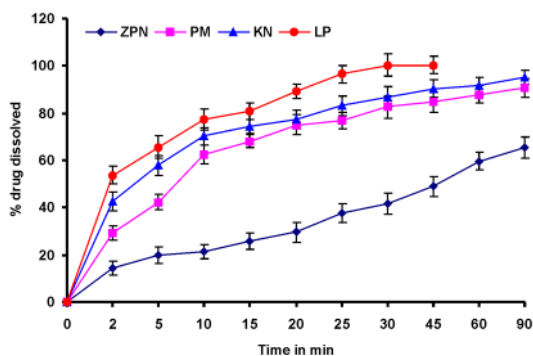


Figure 5. The dissolution curves of ZPN-HP β CD system in distilled water at 37°C \pm 0.5°C. ZPN, zaleplon; PM, physical mixture; KN, kneaded product; LP, lyophilized product.

Table 3. The dissolution data of pure ZPN and its various binary systems with HP β CD in distilled water

System ^a	DP ₂ \pm S.D. ^b	DP ₁₅ \pm S.D. ^b	DP ₃₀ \pm S.D. ^b	DE ₃₀ \pm S.D. ^b
ZPN	14.34 \pm 3.1	25.76 \pm 3.6	41.63 \pm 4.5	26.27 \pm 3.58
PM	29.32 \pm 2.9	68.13 \pm 2.8	82.63 \pm 4.7	62.06 \pm 3.49 ^c
KN	42.55 \pm 3.9	74.25 \pm 2.9	87.02 \pm 4.3	69.08 \pm 3.56 ^c
LP	53.59 \pm 3.7	80.63 \pm 3.5	100.32 \pm 4.6	77.64 \pm 5.74 ^{c,d}

^a ZPN, zaleplon; PM, physical mixture; KN, kneaded product; LP, lyophilized product; ^b DP and DE indicate % drug dissolved and % dissolution efficiency, respectively (mean \pm standard deviation, $n = 3$); ^c p value compared to pure ZPN ($p < 0.001$); *i.e.*, all significant; ^d p value compared to PM ($p < 0.01$); *i.e.*, significant.

same time. The lyophilized product displayed a higher dissolution rate than the physical mixture and kneaded product. The increase in dissolution rate of zaleplon was 3.73-fold greater from lyophilized product within 2 min.

The statistical treatment (ANOVA) of DE₃₀ values of zaleplon and its formulations demonstrated a significant difference between the dissolution profile of pure zaleplon and all of its binary systems with HP β CD ($p < 0.001$). Further, lyophilized product has shown significant improvement in the dissolution profile of zaleplon than the physical mixture ($p < 0.01$). However, no significant difference was observed between the dissolution profiles of physical mixture and kneaded product. Similar results were obtained with the kneaded and lyophilized products. However, the lyophilized product has shown excellent dissolution among all other binary systems of zaleplon studied.

It is noteworthy that the extent of the dissolution enhancing effect was dependent on the method used for the preparation of inclusion complexes. The enhancement in dissolution rate from the physical mixture was possibly due to a local solubilization action and improved wettability by HP β CD and hence dissolution of the drug particles (30,31).

The kneaded product has shown a dissolution rate between the physical mixture and lyophilized product. The higher dissolution rate of kneaded product compared to physical mixture might be because of

reduction in crystals (XRD data not shown) of the drug due to formation of the inclusion complex (kneaded product) in the solid state.

A significant increment in dissolution rate of zaleplon from lyophilized product could be attributed to loss of crystallinity or probably transfer of zaleplon into a higher energetic amorphous state upon complex formation, surfactant-like properties of HP β CD (32-35) and higher stability of inclusion complex in lyophilized product (36).

In conclusion, the dissolution rate of zaleplon could be increased by formation of its inclusion compounds with hydrophilic and amorphous HP β CD by a kneaded and lyophilized process.

4. Conclusion

In the present investigation, ¹HNMR shifts of zaleplon in the presence of HP β CD confirmed the formation of equimolar zaleplon-HP β CD inclusion compounds in the solid state prepared by kneading and lyophilized techniques. Both, the amide-substituted phenyl ring (deep penetration) and cyano-substituted pyrazole ring (shallow penetration) act as guests. In all aspects, a lyophilized product was found to be more stable than a kneaded one. The stoichiometry of complex formation was 1:1 as supported by phase solubility studies. The results obtained from dissolution studies show a high potential for HP β CD as a solubilizing and complexing agent for zaleplon which should be useful for improvement of oral bioavailability of zaleplon.

Acknowledgements

The authors are grateful to Cipla Ltd., Mumbai, India and Panacea Biotech, Chandigarh, India, for providing gift samples of drug and polymer respectively. The authors are thankful to Pune University, Pune, Maharashtra, India for providing NMR facilities. All authors further express their sincere thanks to Principal, Govt. College of Pharmacy, Karad, Maharashtra, India for providing laboratory facilities.

References

1. Ficarra R, Ficarra P, Di Bella MR, Raneri D, Tommasini S, Calabro ML, Villari A, Coppolino S. Study of the inclusion complex of atenolol with β -cyclodextrins. *J Pharm Biomed Anal.* 2000; 23:231-236.
2. Valero M, Rodriguez LJ, Valazquez M. Inclusion of non-steroidal anti-inflammatory agents into aqueous cyclodextrin, A UV-absorption spectroscopic study. *II. Farmaco.* 1996; 51:525-533.
3. Stella VJ, Rajewski RA. Cyclodextrins: Their future in drug formulation and delivery. *Pharm Res.* 1997; 14:556-567.
4. Fernandes CM, Carvalho RA, Pereira da Costa S, Veiga FJ. Multimodal molecular encapsulation of nicardipine

- hydrochloride by β -cyclodextrin, hydroxypropyl- β -cyclodextrin and triacetyl- β -cyclodextrin in solution. Structural studies by ^1H NMR and ROESY experiments. *Eur J Pharm Sci.* 2003; 18:285-296.
5. Szejtli J. Cyclodextrins. In: *Cyclodextrin Technology* (Szejtli J, ed.). Kluwer, Dordrecht, 1988; pp. 1-78.
 6. Uekema K, Hirayama F, Irie T. Cyclodextrin drug carrier system. *Chem Rev.* 1998; 98:2045-2076.
 7. Reddy MN, Rehana T, Ramakrishna S, Chowdary KPR, Diwan PV. β -cyclodextrin complexes of celecoxib: molecular-modeling, characterization, and dissolution studies. *AAPS PharmSci.* 2004; 6:E7.
 8. Figueiras A, Ribeiro L, Vieira MT, Veiga F. Preparation and physicochemical characterization of omeprazole: methyl-beta-cyclodextrin inclusion complex in solid state. *J Incl Phenom Macrocycl Chem.* 2007; 57:173-177.
 9. Peeters J, Neeskens P, Brewster ME. Development of a formulation of pirodavir using 2-hydroxypropyl- β -cyclodextrin. *J Incl Phenom Macrocycl Chem.* 2007; 57:137-139.
 10. Brun H, Paul M, Razzouq N, Binhas M, Gibaud S, Astier A. Cyclodextrin inclusion complexes of the central analgesic drug nefopam. *Drug Dev Ind Pharm.* 2006; 32:1123-1134.
 11. Masson M, Loftsson T, Masson G, Stefanson E. Cyclodextrins as permeation enhancers: some theoretical evaluations and *in vitro* testing. *J Control Release.* 1999; 59:107-118.
 12. Chen C, Chen F, Wu A, Hsu H, Kang I, Cheng H. Effect of hydroxypropyl- β -cyclodextrin on the solubility, photostability and *in vitro* permeability of alkannin/shikonin enantiomers. *Int J Pharm.* 1996; 141:171-178.
 13. Lazaro GS, Ferreira OP, Gimenez IF. Inclusion complexes of pyrimethamine in 2-hydroxypropyl- β -cyclodextrin: Characterization, phase solubility and molecular modeling. *Bioorg Med Chem.* 2007; 15:5752-5759.
 14. Loftsson T, Hreinsdottir D, Masson M. Evaluation of cyclodextrin solubilization of drugs. *Int J Pharm.* 2005; 302:18-28.
 15. Dooley M, Plosker G. Zaleplon a review of its use in the treatment of insomnia. *Drugs.* 2000; 60:413-445.
 16. Hurst M, Noble S. Zaleplon. *CNS Drugs.* 1999; 11:387-392.
 17. Doiphode D, Gaikwad S, Pore Y, Kuchekar B, Late S. Effect of β -cyclodextrin complexation on physicochemical properties of zaleplon. *J Incl Phenom Macrocycl Chem.* 2008; 62:43-50.
 18. Bettinetti G, Melani F, Mura P, Monnanni R, Giordano F. Carbon-13 nuclear magnetic resonance study of naproxen interaction with cyclodextrin in solution. *J Pharm Sci.* 1991; 80:1162-1169.
 19. Mulinacci N, Melani F, Mazzi G, Vincieri F. Molecular modelling and NMR NOE experiments: complementary tools for the investigation of complex ibuprofen- β -cyclodextrin topology. *Int J Pharm* 1993; 90:35-41.
 20. Nishijo J, Ushiroda Y, Ohbori H, Sugiura M, Fujii N. The interaction of 1-naphthalene sulfonate with β -cyclodextrin: studies by calorimetry and proton nuclear magnetic resonance spectroscopy. *Chem Pharm Bull.* 1997; 45:899-903.
 21. Higuchi T, Connors KA. Phase-solubility techniques. *Adv Anal Chem Instr.* 1965; 4:117-212.
 22. U.S. Food and drug administration. Dissolution methods for drug products Website. Available at: http://www.accessdata.fda.gov/scripts/cder/dissolution/dsp_SearchResults_Dissolutions.cfm?PrintAll=1. (Accessed August 14, 2008.)
 23. Schneider HJ, Hacket F, Rudiger V, Ikeda H. NMR studies of cyclodextrins and cyclodextrin complexes. *Chem Rev.* 1998; 98:1755-1786.
 24. Ali SM, Asmat F, Maheshwari A, Koketsu M. Complexation of fluoxetine hydrochloride with β -cyclodextrin. A proton magnetic resonance study in aqueous solution. *Farmaco.* 2005; 60:445-449.
 25. Bergaron RJ, Rowan R. The molecular disposition of sodium *p*-nitrophenolate in the cavities of cycloheptaamylose and cyclohexaamylose in solution. *Bioorg Chem.* 1976; 5:423-436.
 26. Rekharsky MV, Goldberg RN, Schwarz FZ, Tewari YB, Ross PD, Yamashoji Y, Inoue Y. Thermodynamic and nuclear magnetic resonance study of the interactions of α - and β -cyclodextrin with model substances, phenethylamine, ephedrine, and related substances. *J Am Chem Soc.* 1995; 117:8830-8840.
 27. Ali SM, Maheshwari A, Asmat F. Complexation of roxatidine acetate hydrochloride with β -cyclodextrin; NMR spectroscopic study. *Pharmazie.* 2004; 8:653-655.
 28. Nakajima T, Sunagawa M, Hirohashi T, Fujioka K. Studies of cyclodextrin inclusion complexes: I - Complex between cyclodextrin and bencyclane in aqueous solution. *Chem Pharm Bull.* 1984; 32:400-483.
 29. Khan KA. The concept of dissolution efficiency. *J Pharm Pharmacol.* 1975; 27:48-49.
 30. Goldberg AH, Gribaldi M, Kanig JL, Myersohn M. Increasing dissolution rates and gastrointestinal absorption of drugs IV: chloramphenicol-urea system. *J Pharm Sci.* 1966; 55:1205-1211.
 31. Ismail S. Interaction of anti-convulsant drugs with alpha and beta-cyclodextrins I. Methsמיד. *STP Pharma Sci.* 1991; 1:321-325.
 32. Lin S, Kao Y. Solid particulates of drug- β -cyclodextrin inclusion complexes directly prepared by a spray-drying technique. *Int J Pharm.* 1989; 56:249-259.
 33. Moyano J, Arias-Blanco M, Gines J, Giordano F. Solid-state characterization and dissolution characteristics of glioclazide- β -cyclo-dextrin inclusion complexes. *Int J Pharm.* 1997; 148:211-217.
 34. Dollo G, Corre P, Chollet M, Chevanne F, Bertault M, Burgot J, Verge R. Improvement in solubility and dissolution rate of 1,2-dithiole-3-thiones upon complexation with β -cyclodextrin and its hydroxypropyl and sulfobutyl ether-7 derivatives. *J Pharm Sci.* 1999; 88:889-895.
 35. Erden N, Celebi N. A study of inclusion complex of naproxen with β -cyclodextrin. *Int J Pharm.* 1988; 48:83-89.
 36. Shah M, Karekar P, Sancheti P, Vyas V, Pore Y. Effect of PVP K30 and/or L-arginine on stability constant of etoricoxib-HP β CD inclusion complex: Preparation and characterization of etoricoxib-HP β CD binary system. *Drug Dev Ind Pharm.* 2009; 35:118-129.

(Received October 30, 2009; Accepted December 23, 2009)

Original Article

Enhancement of the dissolution profile of allopurinol by a solid dispersion technique

Ahmed M. Samy¹, Maha A. Marzouk², Amal A. Ammar², Maha K. Ahmed^{2,*}

¹ Department of Pharmaceutics, Faculty of Pharmacy (Boys), Al-Azhar University, Cairo, Egypt;

² Department of Pharmaceutics, Faculty of Pharmacy (Girls), Al-Azhar University, Cairo, Egypt.

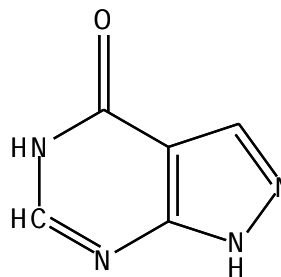
ABSTRACT: The aim of the present study was to improve the solubility, and therefore the dissolution of poorly water-soluble allopurinol. Solid dispersions of allopurinol were prepared with different polymers or carriers such as polyvinylpyrrolidone (PVP K30 and PVP K90), polyethylene glycol (PEG 4000 and PEG 6000), urea and mannitol at two drug : carrier ratios (1:1) and (1:2). Different methods such as melting and solvent evaporation methods were used to improve dissolution characteristics and solubility of allopurinol. The solid dispersions were characterized using a differential scanning calorimeter (DSC) and X-ray diffraction (XRD) while the interactions which took place were identified with fourier transform infrared (FTIR) spectroscopy. Due to formation of hydrogen bonds between allopurinol and urea and mannitol, a transition of allopurinol from the crystalline to amorphous state was achieved. The DSC thermograms of the solid dispersions indicated the potential of heat induced interactions between allopurinol and the carriers used could influence dissolution rate of the drug. The dissolution amount (%) of pure allopurinol was 80% at 45 min. F5, F3, F6, F7, and F1 showed better dissolution percentages of 100, 93, 92.4, 90.6, and 89%, respectively, at 45 min.

Keywords: Allopurinol, solid dispersion, dissolution enhancement, solubility, poorly water soluble

1. Introduction

Allopurinol, chemically known as 1,5-dihydro-4H-pyrazolol (3.4-d) pyrimidin-4-one, is the worldwide mainstay of modern treatment of gout and tumor lysis syndrome. Allopurinol, an isomer of hypoxanthine, and

its active metabolite oxipurinol (alloxanthine) act by inhibiting xanthine oxidase, an enzyme which forms uric acid (urate) from xanthine and hypoxanthine. Allopurinol is a polar compound with strong intramolecular hydrogen bonding and limited solubility in both polar and non polar media (1-3). Allopurinol is very slightly soluble in water and ethanol. It is practically insoluble in chloroform and ether; and is soluble in dimethylformamide and in dilute solutions of alkali hydroxides (4-7).



1,5-dihydro-4H-pyrazolol (3.4-d) pyrimidin-4-one

Solid dispersion techniques have been widely used to improve the dissolution properties and bioavailability of poorly water soluble drugs. Several carrier systems have been used in the preparation of fast release solid dispersions. Polyvinylpyrrolidone (PVP) was used to enhance the dissolution rate of number of drugs such as 5-lipoxygenase inhibitor SB210661 and benidipine HCl (8). Dissolution of prednisolone has been enhanced by polyethylene glycol (PEG) fusion dispersions (9). Increased dissolution rates and extent of absorption were found in rabbits following administration of the sulphathiazole-urea eutectic mixtures (10). In the case of ursodeoxycholic acid the release rate from urea dispersions prepared by the hot melt method was faster than from other carriers studied, including PEG 6000 (11).

2. Materials and Methods

2.1. Materials

Allopurinol (Allo) powder was kindly provided by Alexandria Company for pharmaceutical industries

*Address correspondence to:

Dr. Maha K. Ahmed, Pharmaceutics Department, Faculty of Pharmacy (Girls), Al-Azhar University, Cairo, Egypt.
e-mail: Mahakhalifa_ahmed@hotmail.com

(Alexandria, Egypt). Urea, di-sodium hydrogen phosphate, potassium di-hydrogen ortho phosphate, ethyl alcohol (absolute), and hydrochloric acid were supplied by El-Nasr Pharmaceutical chemicals Co. (Egypt). Mannitol, polyvinylpyrrolidone (PVP) K30 and K90, and PEG 6000 and 4000 were kindly provided by Amoun Company for pharmaceutical industries (Cairo, Egypt).

2.2. Solubility studies

An excess amount of allopurinol was added to 10 mL of aqueous solutions containing different concentrations (2.5, 5, 7.5, and 10%, w/v) of urea, mannitol, PEG (6000 and 4000), PVP (K30 and K90) in capped test tubes. The samples were sonicated for 1 h at room temperature. The capped test tubes were shaken at 37°C for 24 h in a shaking water bath. The suspensions obtained were filtered through a filter paper (double ring, 102), and the filtrate was diluted with distilled water. The diluted solutions were measured spectrophotometrically at a λ_{max} of 250 nm using the same medium as a blank. Each experiment was performed in triplicate. The same technique was used to study the effect of sodium salts of *o*- and *p*-touluc acids on the water solubility of allopurinol (12).

2.3. Preparation of solid dispersions

Solid dispersions of allopurinol with carriers or polymers (urea, mannitol, PEG 6000 and PEG 4000) at weight ratios of 1:1 and 1:2 were prepared by the melting method (Table 1). After the polymer or carrier was completely melted on a thermostatically controlled hot plate, allopurinol was added and then solidified by pouring on a glass petri dish stored on an ice bath. After cooling the solid, it was kept in a desiccator under vacuum at room temperature for 48 h. The mass was then pulverized with a mortar and pestle and was sieved into defined particle size fractions (200-150 μm) (1).

The solvent evaporation method was used to prepare solid dispersions of allopurinol with different polymers

(PVP K30 and PVP K90) at weight ratios of 1:1 and 1:2, drug to carrier (Table 1). A solution of allopurinol in absolute ethanol was mixed with a solution of polymer in ethanol. The solvent was subsequently evaporated under a vacuum, using Rota Vapour apparatus at 70°C and a rotation speed of 100 rpm. The residue was then dried completely in a desiccator for 48 h. The solid mass was then crushed, pulverized, and sieved into defined particle size fractions (200-150 μm) (1).

2.4. Characterization of solid dispersions

2.4.1. Differential scanning calorimetry (DSC) studies

Approximately 5 mg of samples were weighed and hermetically sealed in the aluminium pans. Samples of drug alone, each excipient alone, physical mixtures of allopurinol with the investigated excipients (1:1, w/w) prepared by simple and perfect mixing and solid dispersion (1:1, w/w) were measured with a Shimadzu Model DSC-50 thermal analyzer (Shimadzu, Kyoto, Japan). The DSC thermograms were obtained over a temperature range of 25-400°C using a thermal analyzer equipped with an advanced computer software program at a scanning rate of 10°C/min and a nitrogen gas purge of 40 mL/min. The instrument was calibrated with pure indium as a reference.

2.4.2. X-ray diffraction (XRD) studies

X-ray diffraction (XRD) patterns were obtained using $\text{CuK}\alpha$ radiation, collimated by a 0.08° divergence slit and a 0.2° receiving slit and scanned at a rate of 2.4°/min over the 2 θ range of 5-60°. The diffractometer was a PW 3710 (Philips, Holland).

2.4.3. Fourier transforms infrared spectroscopy (FTIR)

Samples of 1-2 mg of drug alone, each excipient alone, physical mixtures of allopurinol with the investigated excipients (1:1, w/w) prepared by simple and perfect mixing and solid dispersion (1:1, w/w) were mixed with KBr (IR grade) compressed into discs in the compression unit under vacuum and were scanned from 4,000-400 cm^{-1} with an empty pellet holder as a reference. The spectrophotometer was a Perkin-Elmer FTS-1710 (Beaconsfield, UK).

2.4.4. Content uniformity of allopurinol in solid dispersions

An amount equivalent to 10 mg of allopurinol was weighed from each resultant solid dispersion (with different polymers or carriers) and dispersed in 50 mL phosphate buffer pH 7.4 using a 100 mL volumetric flask and then was stirred for 10 min. The volume obtained was completed to 100 mL with phosphate

Table 1. Composition of different allopurinol solid dispersions

Codes	Components	Ratios	Methods
PD	Pure drug	-	-
F1	Allo/urea	1:1	Melting
F2	Allo/urea	1:2	Melting
F3	Allo/mannitol	1:1	Melting
F4	Allo/mannitol	1:2	Melting
F5	Allo/PVP K30	1:1	Solvent evaporation
F6	Allo/PVP K30	1:2	Solvent evaporation
F7	Allo/PVP K90	1:1	Solvent evaporation
F8	Allo/PVP K90	1:2	Solvent evaporation
F9	Allo/PEG 4000	1:1	Melting
F10	Allo/PEG 4000	1:2	Melting
F11	Allo/PEG 6000	1:1	Melting
F12	Allo/PEG 6000	1:2	Melting

buffer pH 7.4 and shaken well. Two mL from the previous solution were taken and were completed to 10 mL with phosphate buffer pH 7.4. The absorbance was measured using a UV spectrophotometer (Model 6405 UV/Vis; Jenway, Ltd., Essex, UK) at 250 nm, using phosphate buffer pH 7.4 as a blank.

2.4.5. *In vitro* dissolution of allopurinol from solid dispersions

The rotating basket dissolution apparatus was used for the determination of dissolution rates of allopurinol solid dispersions. An accurately weighed amount of each solid dispersion equivalent to 100 mg of allopurinol was placed into the basket of the dissolution test apparatus (USP Standards, scientific, DA6D, Bombay-400-069, India). The basket was rotated at 75 rpm in 900 mL of the dissolution medium (0.1 N HCl) and maintained at a constant temperature ($37 \pm 0.5^\circ\text{C}$). Aliquots, each of 5 mL, were withdrawn from the dissolution medium at time intervals of 5, 15, 30, 45, 60, 90, and 120 min. The same volume of 0.1 N HCl was used to replace the withdrawn samples. The samples were suitably filtered, diluted, and measured spectrophotometrically at 250 nm. The concentration of the drug was determined from the previously constructed standard calibration curve. Statistical analysis (ANOVA) was performed for all allopurinol solid dispersion formulas with respect to their percent dissolved at 45 min followed by the Tukey-Kramer multiple comparisons test. Also the kinetic parameters for the *in vitro* dissolution of all allopurinol solid dispersion formulas were determined and analyzed in order to explain the mechanism of drug release.

3. Results and Discussion

3.1. Solubility studies

The solubility of allopurinol in water at 37°C was found to be 0.616 mg/mL. Allopurinol has a limited solubility in both polar and non polar media as it is a polar compound with strong intramolecular hydrogen bonding (1). Addition of urea and mannitol provided an increase in allopurinol solubility. It is evident that, the increased concentration of urea and mannitol was accompanied by a gradual increase in the solubilized amount of allopurinol. Mannitol as well as urea at a 10% concentration caused more than a two fold increase in allopurinol solubility. Figure 1 shows a linear correlation between the concentrations of urea or mannitol and allopurinol solubility in aqueous solutions of urea or mannitol at 37°C . The aqueous solution of PVP K30 was found to increase the solubility of allopurinol much more than PVP K90. Figure 2 shows a linear correlation between the concentrations of PVP K30 or PVP K90 and allopurinol solubility. Figure 3 shows that the drug solubility increased linearly as PEG

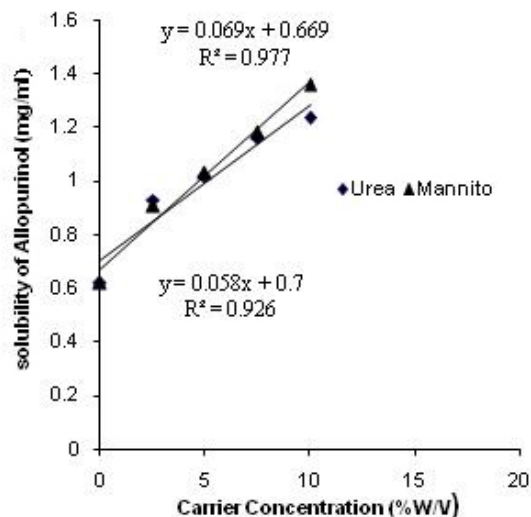


Figure 1. Solubility profiles of allopurinol in aqueous solutions of urea and mannitol at 37°C .

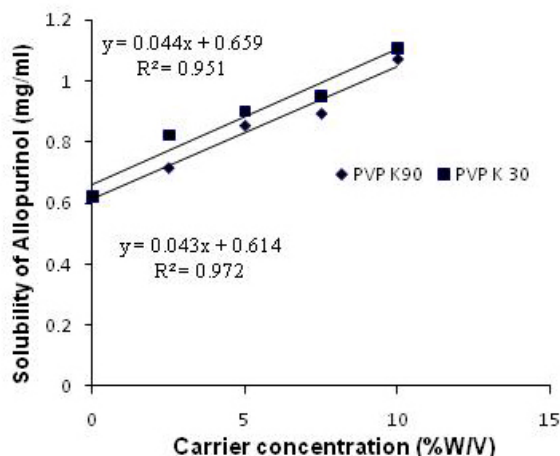


Figure 2. Solubility profiles of allopurinol in aqueous solutions of PVP K90 and K30 at 37°C .

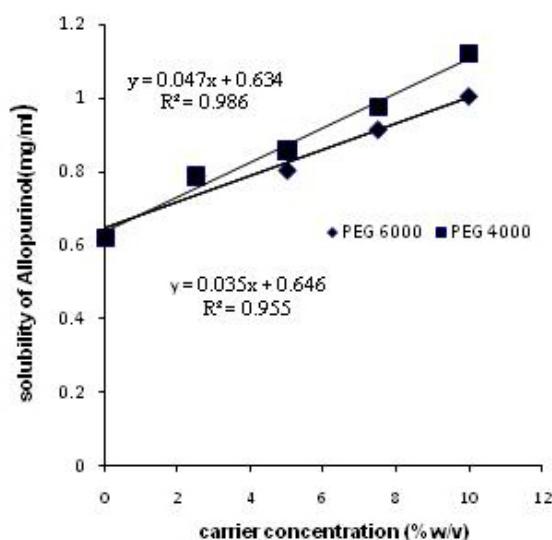


Figure 3. Solubility profiles of allopurinol in aqueous solutions of PEG 6000 and 4000 at 37°C .

concentration increased. PEG 4000 always showed more solubilizing power than PEG 6000.

3.2. Characterization of solid dispersions

3.2.1. DSC studies

The DSC thermogram of allopurinol, carriers, their physical mixtures, and the corresponding solid dispersions are shown in Figure 4. The DSC thermogram of allopurinol alone was characterized by a sharp endothermic peak at 386°C corresponding to its melting point. The DSC thermogram of the solid dispersion containing urea shows that allopurinol lost its shape and distinctive appearance, shifted to a lower melting point and appeared as a broad peak around 250-300°C. It was noticed that there was a change in the characteristic endothermic peaks and the melting points of both allopurinol and urea before and after solid dispersion formation. Also there was a decrease in the melting enthalpy of both allopurinol and urea before and after solid dispersion formation. The more amorphous the product, the lower is the ΔH value (13). It was also suggested that a very small crystalline portion of allopurinol existed in the solid dispersion melted at a lower melting point than of intact allopurinol. The previous results were concluded when studying the DSC of ofloxacin-urea solid dispersions (11). The DSC thermogram of solid dispersions containing mannitol shows that allopurinol lost its shape and distinctive appearance, shifted to a lower melting point than that of intact allopurinol and appears as a shallow broad peak around 328.3°C with a corresponding enthalpy change. As discussed before with urea there was a decrease in the melting point of allopurinol accompanied by a change in the appearance of the endotherm with a corresponding

decrease in the ΔH of both mannitol and allopurinol, which suggest a decrease in the crystalline state. The DSC thermogram of both physical mixtures and solid dispersions containing PVP K30, K90, and PEG 4000 showed the sharp endothermic peak of allopurinol nearly at the same position indicating the absence of strong interactions between the components. The increase in the dissolution rate was thus attributed to an increase in the available surface area of the drug due to improved wettability provided by the polymers used. The DSC thermogram of the solid dispersion containing PEG 6000 showed a broad endothermic peak of allopurinol at 373.8 and 381.8°C, respectively. The melting point of allopurinol in PEG solid dispersions showed a shift to lower values from that of pure drug which revealed a crystalline change.

3.2.2. XRD studies

The XRD of allopurinol, carriers, their physical mixtures and the corresponding solid dispersion is presented in Figure 5. The X-ray diffraction pattern for pure powdered allopurinol alone showed a major sharp peak of 28° at a diffraction angle of 2θ and an intensity of 6,450 (Counts). A comparison X-ray diffraction pattern of allopurinol and its solid dispersion with urea and mannitol showed a significant reduction in the crystalline state of allopurinol in the solid dispersion. This could be attributed to the retardation of allopurinol crystallization by the carrier (11). This also indicates that the drug may be converted to an amorphous form. X-ray diffraction data indicates an interaction between allopurinol and PVP and a much reduced crystallinity extent. The X-ray diffraction study of PEG showed that PEG 6000 is more efficient in the reduction of the crystalline state of allopurinol than PEG 4000 which is comparable to the result of PEG 6000 solid dispersions of nifedipine (13). These results indicate that

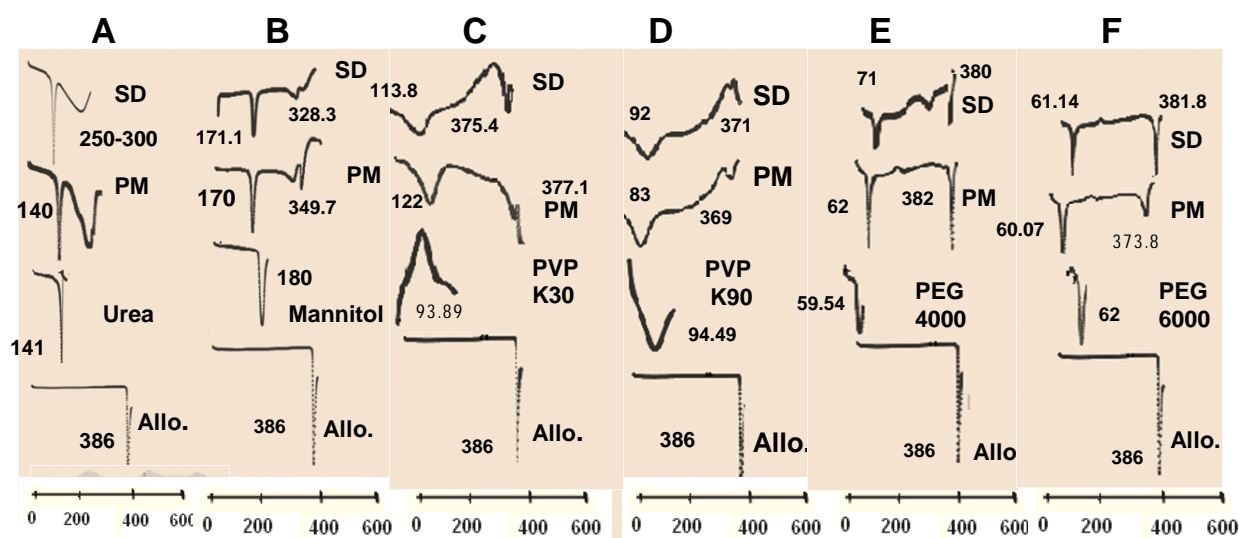


Figure 4. DSC thermograms of allopurinol and various carriers, the physical mixtures, and the corresponding solid dispersions. A, allopurinol and urea; B, allopurinol and mannitol; C, allopurinol and PVP K30; D, PVP K90; E, allopurinol and PEG 4000; F, allopurinol and PEG 6000. Abbreviations: SD, solid dispersion; PM, physical mixture; Allo, allopurinol.

the polymer should have a suitable molecular length and concentration. This enables formation of a polymer net on the crystal surface or among the drug molecules which results in optimum orientation of proton donating and receiving groups and a strong interaction between drug and polymer (14-16).

3.2.3. FTIR spectroscopy

Figure 6 shows FTIR spectra for allopurinol in physical mixtures and solid dispersions with different carriers. The FTIR spectrum of pure allopurinol is characterized by absorption bands at $3,167\text{ cm}^{-1}$ at high frequency, most probably attributed to the N-H stretching band of the secondary amine group, and at $3,034\text{ cm}^{-1}$ denoting a C-H stretching vibration of the

pyrimidine ring. At low frequencies there is a band at $1,693\text{ cm}^{-1}$ indicating a C=O stretching vibration of the keto form of the 4-hydroxy tautomer. Also the bands at $(1,581-1,469.96)\text{ cm}^{-1}$ are attributed predominantly to C-N stretching and C-C ring stretching, respectively. Bands at $1,234.55-698.29\text{ cm}^{-1}$ denote CH in plane deformation. The FTIR spectrum of physical mixtures of allopurinol with both urea and mannitol indicates the absence of any interaction between allopurinol and urea or mannitol upon mixing. While the FTIR spectrum of solid dispersions of allopurinol with urea or mannitol indicates the probability of hydrogen bonding between allopurinol and urea or mannitol in the solid dispersion. The FTIR spectrum of physical mixtures and solid dispersions of allopurinol with PVP K30, PVP K90 and PEG 4000 indicates the absence of any interaction

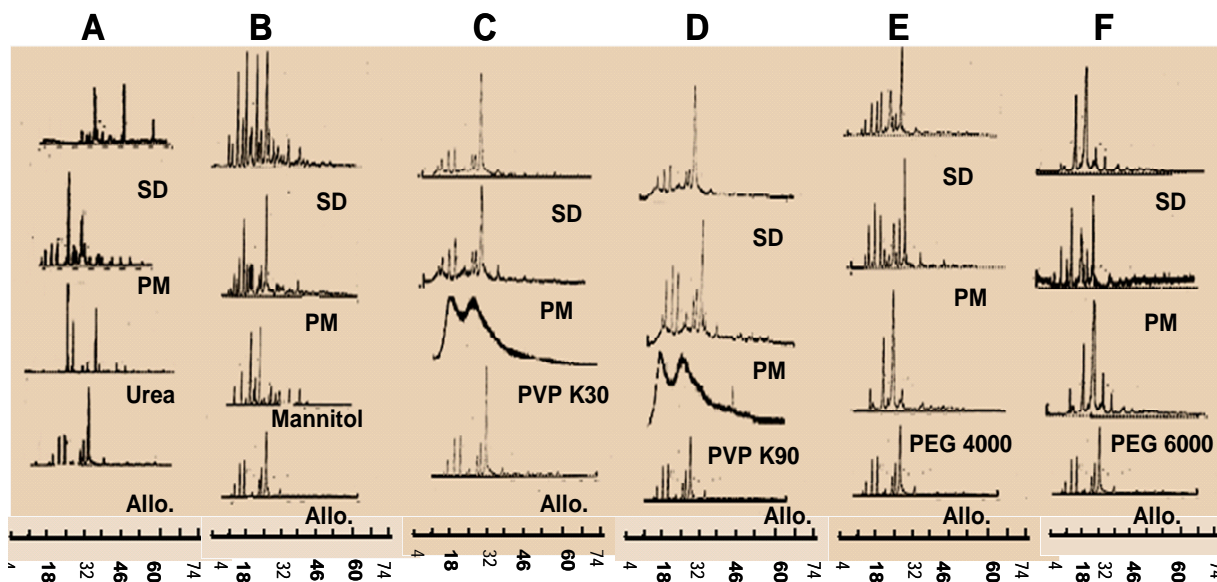


Figure 5. XRD of allopurinol and various carriers, the physical mixtures, and the corresponding solid dispersions. A, allopurinol and urea; B, allopurinol and mannitol; C, allopurinol and PVP K30; D, PVP K90; E, allopurinol and PEG 4000; F, allopurinol and PEG 6000. Abbreviations: SD, solid dispersion; PM, physical mixture; Allo, allopurinol.

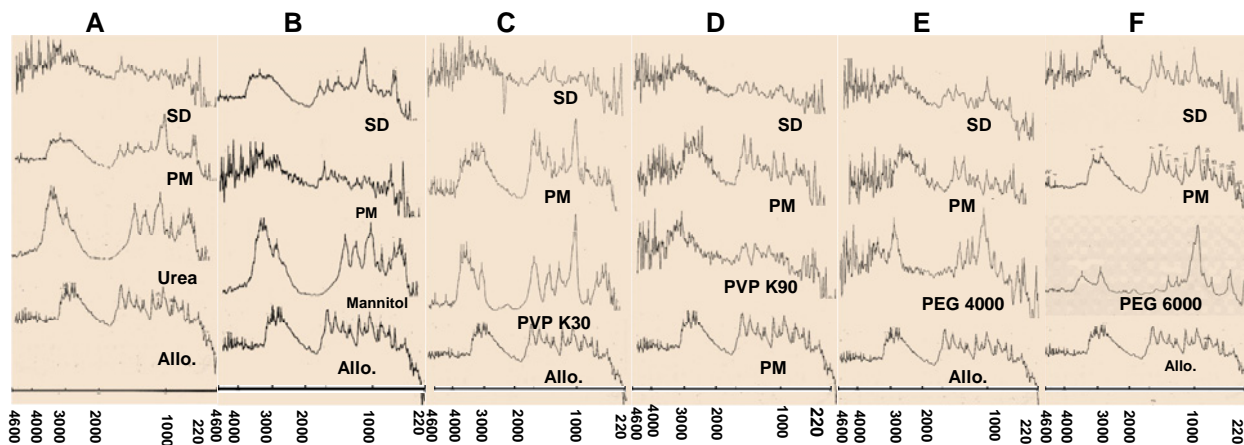


Figure 6. FTIR spectrum of allopurinol and various carriers, the physical mixtures, and the corresponding solid dispersions. A, allopurinol and urea; B, allopurinol and mannitol; C, allopurinol and PVP K30; D, PVP K90; E, allopurinol and PEG 4000; F, allopurinol and PEG 6000. Abbreviations: SD, solid dispersion; PM, physical mixture; Allo, allopurinol.

between allopurinol and PVP K30, PVP K90 or PEG 4000. Addition of such polymers to pure allopurinol resulted in no shift of any of these characteristic bands, indicating no chemical interaction between the drug and the polymers used. Also the FTIR spectrum of physical mixtures of allopurinol with PEG 6000 indicates the absence of any interaction of allopurinol with PEG 6000 upon mixing. While the FTIR spectrum of the solid dispersion indicates the hydrogen bonding interaction between the lone pair of the amino group of allopurinol and the hydrogen atom OH group of PEG 6000. The same result was obtained by studying the IR spectra of diazepam and temazepam-solid dispersions (17).

It was clear that all characteristic bands of allopurinol and its solid dispersions with PVP and PEG appeared nearly in the same regions and at the same ranges and no new bands appeared although the shape of the functional group regions in the spectra of the drug and the polymer used was not identical with that of pure drug alone. This might be indicative of the absence of interactions between allopurinol and the polymers used.

3.3. Content uniformity of allopurinol in solid dispersions

The content of allopurinol in each solid dispersion formula was found to be between 97.41 and 105%. The production yield of allopurinol in each solid dispersion formula was found to be between 97.2 and 99.8%.

3.4. In vitro dissolution of allopurinol from solid dispersions

Dissolution profiles of the pure drug and drug-carrier

binary systems are represented in Figure 7. As is apparent, the solid dispersion technique improved the dissolution rate of allopurinol. The percentages of drug dissolved at 45 min were 100, 93, 92.4, 90.6, and 89 for F5, F3, F6, F7, and F1, respectively. This enhancement can be attributed to the greater hydrophilic character of the systems due to the presence of the carrier, which can reduce interfacial tension between a poorly water-soluble drug and dissolution medium (18). The enhancement of the solubility of allopurinol with carriers or polymers used may be attributed to the wetting effect of the highly water soluble carrier or polymer in intimate contact with it. They solubilized allopurinol by breaking up water clusters surrounding the non polar molecule, increasing the entropy of the system and producing a driving force for the solubilization. These results are in agreement with a result by Lian-Kaun *et al.* (19). Also the improvement in the dissolution rate may be due to the enhancement of the physical amorphism of the drug (20), and this enhancement also might be attributed to the increase in the wettability and solubility of the drug (21).

The kinetic data showed that the *in vitro* release of allopurinol followed different kinetic orders, and no definite kinetic order could express the drug release from different types of solid dispersion formulations (Table 2). One way analysis of variance (ANOVA) of allopurinol solid dispersions was performed with respect to their % released at 45 min followed by the Tukey-Kramer multiple comparisons test (Table 3).

4. Conclusion

Based on the current study, improvement in the

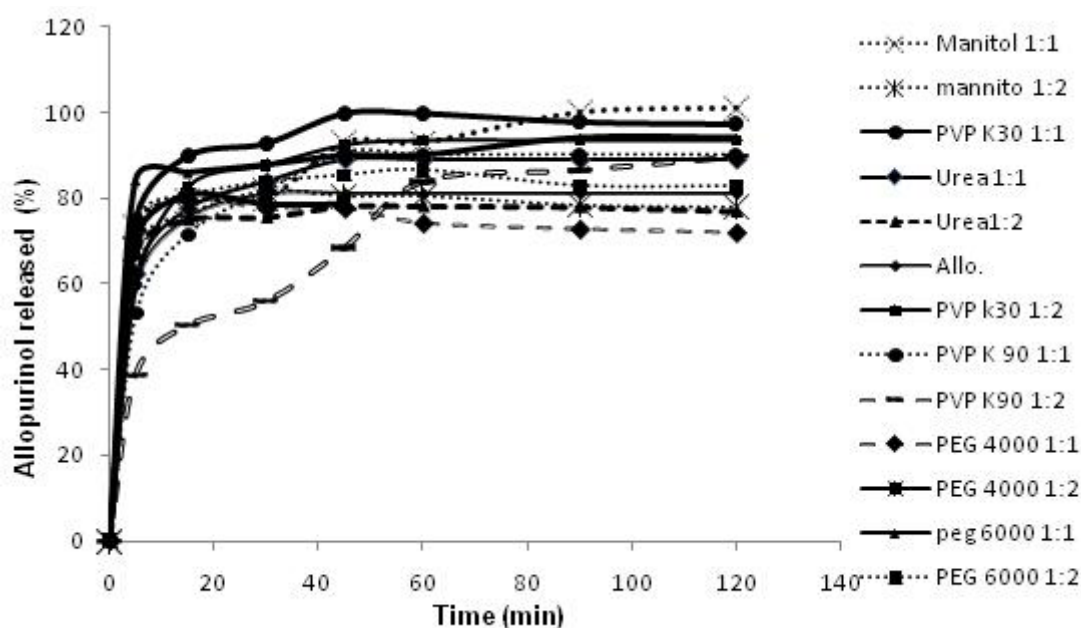


Figure 7. Percentages of drug released from solid dispersions in different ratios compared to pure drug.

Table 2. Kinetic treatments for the *in vitro* release of allopurinol solid dispersions and allopurinol powder

Formula	Correlation coefficient (<i>r</i>)					
	Zero-order	First-order	Second-order	Diffusion-order	Hixcon-Crowell	Baker-Lonsd
F1	0.935365	-0.98277	0.995379	0.974801	0.970108	0.977056
F2	0.871449	-0.89258	0.912432	0.923465	0.885616	0.891134
F3	0.955624	-0.87047	0.772401	0.964457	0.955677	0.97143
F4	0.971244	-0.98702	0.996771	0.992855	0.982369	0.985437
F5	0.926467	-0.88244	0.810008	0.962533	0.953079	0.969205
F6	0.847931	-0.94871	0.990815	0.916509	0.918958	0.927665
F7	0.917021	-0.95681	0.94742	0.966857	0.949169	0.955438
F8	0.931216	-0.96605	0.977153	0.971166	0.956931	0.961161
F9	0.935365	-0.98277	0.995379	0.974801	0.970108	0.977056
F10	0.675845	-0.64575	0.611197	0.759726	0.656281	0.650014
F11	0.921085	-0.95216	0.976206	0.9701	0.942469	0.945657
F12	0.921085	-0.95216	0.976206	0.9701	0.942469	0.945657
Allo. 100	0.891272	-0.94153	0.95288	0.942149	0.928143	0.937529

Table 3. Tukey-Kramer multiple comparisons test of allopurinol solid dispersion formulas and pure drug

Formulae	Significance	Formulae	Significance	Formulae	Significance	Formulae	Significance
F1 vs. F2	***	F2 vs. F9	NS	F4 vs. F9	NS	F7 vs. F8	***
F1 vs. F3	NS	F2 vs. F10	NS	F4 vs. F10	NS	F7 vs. F9	***
F1 vs. F4	***	F2 vs. F11	***	F4 vs. F11	***	F7 vs. F10	***
F1 vs. F5	***	F2 vs. F12	***	F4 vs. F12	**	F7 vs. F11	NS
F1 vs. F6	NS	F2 vs. Allo.100	NS	F4 vs. Allo.100	NS	F7 vs. F12	**
F1 vs. F7	NS	F3 vs. F4	***	F5 vs. F6	***	F7 vs. Allo.100	***
F1 vs. F8	***	F3 vs. F5	***	F5 vs. F7	***	F8 vs. F9	***
F1 vs. F9	***	F3 vs. F6	NS	F5 vs. F8	***	F8 vs. F10	***
F1 vs. F10	***	F3 vs. F7	NS	F5 vs. F9	***	F8 vs. F11	***
F1 vs. F11	NS	F3 vs. F8	***	F5 vs. F10	***	F8 vs. F12	***
F1 vs. F12	NS	F3 vs. F9	***	F5 vs. F11	***	F8 vs. Allo.100	***
F1 vs. Allo.100	***	F3 vs. F10	***	F5 vs. F12	***	F9 vs. F10	NS
F2 vs. F3	***	F3 vs. F11	NS	F5 vs. Allo.100	***	F9 vs. F11	***
F2 vs. F4	NS	F3 vs. F12	***	F6 vs. F7	NS	F9 vs. F12	***
F2 vs. F5	***	F3 vs. Allo.100	***	F6 vs. F8	***	F9 vs. Allo.100	NS
F2 vs. F6	***	F4 vs. F5	***	F6 vs. F9	***	F10 vs. F11	***
F2 vs. F7a	***	F4 vs. F6	***	F6 vs. F10	***	F10 vs. F12	***
F2 vs. F8	***	F4 vs. F7	***	F6 vs. F11	NS	F10 vs. Allo.100	NS
		F4 vs. F8	***	F6 vs. F12	***	F11 vs. F12	*
				F6 vs. Allo.100	***	F11 vs. Allo.100	***
						F12 vs. Allo.100	**

*** Significant at $p < 0.001$; ** Significant at $p < 0.01$; * Significant at $p < 0.05$; NS, not significant.

dissolution of the water-insoluble drug allopurinol was achieved through solid dispersion using different carriers, the best of which was PVP K30 in a drug carrier ratio of 1:1, which exhibited complete drug release in 45 min followed by mannitol in a drug carrier ratio of 1:1.

Acknowledgements

The authors would like to thank Alexandria Company for Pharmaceutical Industries (Alexandria, Egypt) for their donation of allopurinol and Amoun Company for Pharmaceutical Industries (Cairo, Egypt) for providing the other polymers used.

References

1. Samy EM, Hassan MA, Tous SS, Rhodes CT. Improvement of availability of Allopurinol from

- pharmaceutical dosage forms I: suppositories. Eur J Pharm Biopharm. 2000; 49:119-127.
2. Ammar HO, el-Nahhas SA. Improvement of some pharmaceutical properties of drugs by cyclodextrin complexation. 1. Allopurinol. Pharmazie. 1995; 50:49-51.
3. Hamza YE, Kata M. Influence of certain non-ionic surfactants on solubilization and *in-vitro* availability of Allopurinol. Pharm Ind. 1989; 51:1441-1444.
4. Clark's Analysis of Drugs and Poisons in Pharmaceutical Body Fluids and Postmortum Materials, 3rd ed. Pharmaceutical Press, London, UK, 2004; pp. 601-603.
5. Lee DK, Wang DP. Formulation development of Allopurinol suppositories and injectables. Drug Dev Ind Pharm. 1999; 25:1205-1208.
6. Trissel LA, Martinez JF. Compatibility of allopurinol sodium with selected drugs during simulated Y-site administration. Am J Hosp Pharm. 1994; 51:1792-1799.
7. Benzra SA, Bennett TR. In: Analytical Profiles of Drug substances and Excipients. Academic Press, 1978; pp. 1-18.
8. Perng CY, Kearney AS, Patel K, Palepu NR, Zuber G.

- Investigation and formulation approaches to improve the dissolution of SB-210661, a poorly water soluble 5-lipoxygenase inhibitor. *Int J Pharm.* 1998; 176:31-38.
9. Chiou WL, Smith LD. Solid dispersion approach to the formulation of organic liquid drugs using PEG 6000 as a carrier. *J Pharm Sci.* 1971; 60:125-127.
 10. Sekiguchi K, Obi N. Studies on absorption of eutectic mixtures. *Chem Pharm Bull.* 1961; 9:866-872.
 11. Okonogi S, Oguchi T, Yonemochi S, Puttipipatkacharm S, Yamamoto K. Improved dissolution of ofloxacin *via* solid dispersion. *Int J Pharm.* 1997; 156:175-180.
 12. Ammar HO, el-Nahhas SA. Effect of aromatic hydrotropes on the solubility of Allopurinol: Part 3. *Pharmazie.* 1993; 48:751-754.
 13. Emara LH, Badr RM, Abdel-Bary A. Improving the dissolution and bioavailability of nifedipine using solid dispersions and solubilizers. *Drug Dev Ind Pharm.* 2002; 28:795-807.
 14. Sun Y, Rui Y, Wenliang Z, Tang X. Nimodipine semi-solid capsules containing solid dispersion for improving dissolution. *Int J Pharm.* 2008; 359:144-149.
 15. Tantishaiyakul V, Kaewnopparat N, Ingkatawornwong S. Properties of solid dispersions of piroxicam in polyvinylpyrrolidone. *Int J Pharm.* 1999; 181:143-151.
 16. Mura P, Manderioli A, Bramanti G, Ceccarelli L. Properties of solid dispersions of naproxen in various polyethylene glycols. *Drug Dev Ind Pharm.* 1996; 22:909-916.
 17. Verheyen S, Bleton N, Kinget R, Van den Mooter G. Mechanism of increased dissolution of diazepam and temazepam from polyethylene glycol 6000 solid dispersions. *Int J Pharm.* 2002; 249:45-58.
 18. Mura P, Faucci MT, Parrini PL. Effects of grinding with microcrystalline cellulose and cyclodextrins on the ketofen physicochemical properties. *Drug Dev Ind Pharm.* 2001; 27:119-128.
 19. Chen LK, Cadwallader DE, Hung WJ. Nitrofurantoin solubility in aqueous urea and creatinine solutions. *J Pharm Sci.* 1975; 65:868-872.
 20. Pathak D, Dahiya S, Pathak K. Solid dispersion of meloxicam factorially designed dosage form for geriatric population. *Acta Pharm.* 2008; 58:99-110.
 21. Prajapati ST, Gohel MC, Patel LD. Studies to enhance dissolution properties of carbamazepine. *Ind J Pharm Sci.* 2007; 69:427-430.

(Received November 12, 2009; Revised February 3, 2010; Accepted February 6, 2010)

Original Article

Formulation and bioavailability of controlled release salbutamol sulphate tablets using natural additives

Ahmed T. Nouh^{1,*}, Abd El-Gawad H. Abd El-Gawad², Tawhida K. Guda²

¹ *Pharmaceutics Department, Faculty of Pharmacy, Misr International University, Cairo, Egypt;*

² *Pharmaceutics Department, Faculty of Pharmacy, Mansoura University, Cairo, Egypt.*

ABSTRACT: Salbutamol sulphate granules and physical mixtures were prepared using mastic with various natural additives. The prepared granules and physical mixtures were examined using IR and DSC. The obtained results indicate that there is no interaction between salbutamol sulphate and the formulation ingredients used. The physical properties and release behavior of the formulated tablets prepared from granules and physical mixtures were evaluated and showed good physical properties. The rate of drug release from tablets prepared from granules was found to be lower than that prepared from physical mixtures at fixed mastic concentration and the same additive. The rate of drug release decreased with increased mastic concentration in formulated tablets. Pectin and sodium alginate allowed the best controlled release rate of the drug. On the basis of the results obtained from the controlled release studies, selected salbutamol formulations were subjected to an *in vivo* comparison with commercial salbutamol tablets. The pharmacokinetic parameters AUC_{0-24} , C_{max} , and T_{max} of salbutamol from the selected formulation were determined after administration of a single oral dose of 8 mg and compared statistically using an ANOVA test. There was no significant difference in the AUC_{0-24} . On the other hand, there was a significant difference in the C_{max} and T_{max} between the commercial and the formulated tablets. These results demonstrate that the formulated tablets extended the time of the drug effect.

Keywords: Salbutamol sulphate, natural additives, tablets, dissolution rate, *in vivo* studies

*Address correspondence to:

Dr. Ahmed T. Nouh, Pharmaceutics Department, Faculty of Pharmacy, Misr International University (MIU), Cairo-Ismaillia Road, Cairo, Egypt.
e-mail: ahmednouh_8@hotmail.com

1. Introduction

Salbutamol sulphate has a selective action on beta-2 adrenergic receptors. It is used as a bronchodilator in the management of bronchial asthma and in some patients with chronic obstructive pulmonary disease (1). Control of asthma may be achieved using a controlled-release formulation of salbutamol. This also serves to increase patient compliance (2). Several techniques were developed to formulate salbutamol sulphate in controlled release drug delivery systems; microcapsules of salbutamol sulphate were prepared using ethyl cellulose (3), beeswax and carnauba wax (4) as coating materials. Eudragit RS30D-coated controlled-release pellets of salbutamol were prepared using an air suspension technique (5). Prabakaran *et al.* (6) have developed an oral osmotic system to deliver both theophylline and salbutamol sulphate simultaneously. This approach helped to produce extended drug release as well as reduce the problems associated with multi-drug asthma therapy. Hydroxy propyl methyl cellulose hydrophilic-matrix tablets containing encapsulated or unencapsulated salbutamol sulfate were investigated (7). Also, Sirkia *et al.* (8) developed prolonged release press-coated salbutamol sulphate tablets.

Mastic is a natural oleoresin exudate obtained from the stem and main leaves of a cultivated variety of *Pistacia lentiscus* var. (9). Panagopoulou and Georgarakis (10) and Abd El-Aleem (11) used mastic as a binder in tablet production. Also, many authors combined mastic with microcapsule cores in microencapsulation of many substances (12-14). The previous studies have proved that mastic results in larger/compact particles with no pores and a much slower release; and consequently controlled drug release.

The aim of this study was to formulate salbutamol controlled release tablets using mastic as a natural polymer and to find any possible interaction between salbutamol sulphate and mastic. The study was extended to investigate the bioavailability of the formulated tablets compared to commercial brands.

2. Materials and Methods

2.1. Materials

Salbutamol sulphate was kindly supplied by Amriya Pharm. Ind. Co., Alexandria, Egypt. Pectin was obtained from Winlab, a division of Wilfrid Smith, UK. Sodium alginate and lactose monohydrate were from El Nasr Pharmaceutical Chemical Co., Cairo, Egypt. Mastic (commercial grade) was from Chios' Gum Mastic Growers Association. Avicel PH 101 was from Fluka AG, Buchs, Switzerland. Bis-(2-ethylhexyl) phosphate (lot No. 05411ED-107) was from Aldrich.

2.2. Preparation of drug physical mixtures and granules

In a total of 200 mg of powder mixture 8 mg drug in combination with 40 mg mastic and with the rest made up of pectin were mixed thoroughly in a mortar to prepare a physical mixture. Other proportions of mastic (60 and 90 mg) were used to prepare more physical mixtures. Pectin was replaced by sodium alginate, avicel or lactose individually in the same amounts to prepare other formulations. In each of the formulations, the mastic concentration was equivalent to 20, 30, and 40% of tablet weight.

The granules were prepared by wetting the powder mixtures with the smallest possible amount of chloroform to make doughy masses. The obtained masses were converted into granules by forcing them through a sieve with a No. 2 mm mesh. The granules obtained were dried at room temperature for 24 h in open air and further dried at 40°C for 48 h in a hot air oven.

2.3. Infrared (IR) studies

Using an infrared spectrophotometer (UV 150-02, double beam spectrophotometer, Shimadzu, Kyoto, Japan), the IR spectra of each salbutamol sulphate, mastic, pectin, sodium alginate, avicel, and lactose were investigated using a KBr disc method from 4,000-400 cm^{-1} . Also, the IR spectra of the physical mixtures and granules of 1:1 ratio of drug to each of mastic, pectin, sodium alginate, lactose, or avicel were studied.

2.4. DSC studies

Using a differential scanning calorimeter (Model DSC-50, Shimadzu), DSC thermograms of all samples tested by IR were performed at a heating rate of 10°C/min in a nitrogen atmosphere. The sample (5 mg) was placed in the aluminum pan of the instrument and the scanning started up to 500°C against indium in the reference pan.

2.5. Formulation of tablets

Salbutamol sulphate physical mixtures and granules

were mixed with 1% magnesium stearate as a lubricant and compressed into tablets each weighing 200 mg. All batches were prepared using a single punch Eraweka tablet press (G.M.B.H., Germany) at constant pressure.

2.6. Evaluation of tablets

The prepared tablets were tested for uniformity of weight, thickness, content, friability percent, hardness, tensile strength, and disintegration time.

2.7. Release study

Sulbutamol sulphate release from different formulated tablets was performed using the USP basket six jar dissolution apparatus. A round bottom dissolution container containing 250 mL of phosphate buffer, pH 7.4, was immersed in a constant temperature water bath and allowed to equilibrate at $37 \pm 0.2^\circ\text{C}$. A single tablet was placed in the basket and the position of the basket stirrer was kept at a fixed position from the bottom of the dissolution container and rotated at a speed of 50 rpm. Two mL samples were withdrawn at different time intervals. The withdrawn sample was replaced with the same volume of fresh dissolution medium after each sampling. Samples were measured spectrophotometrically at 276 nm. Mean values for six experiments were taken for each batch.

2.8. Analysis of the release data

The release data were analyzed according to zero, first order, a diffusion model, and the Peppas equation.

2.9. Bioavailability study

Tablet formulations containing 40% mastic with pectin (formula **A**) or sodium alginate (formula **B**) which gave acceptable physical characteristics and best controlled drug release behavior, were chosen for the *in vivo* study. These formulations were compared with commercial tablets (2 tablets of Salbovent Forte each contains 4 mg of salbutamol sulphate).

Male albino rabbits weighing 2.0-2.5 kg were randomly selected for the bioavailability study. The animals were divided into three groups and each group was comprised of six rabbits. Each group received one of the tested formulas namely, formula **A**, formula **B**, or the commercial one. The animals were fasted over night before tablet administration and during the experiment and had free access to water. A single dose (8 mg salbutamol) of the tested tablets was given orally to the each rabbit using a balling gun to deliver the tablets to the animal stomach. The ear vein was cannulated with a butter fly scalp No.19 needle and blood samples (2 mL) were withdrawn from the vein before dosing (zero time) and at different intervals after dosing *viz.* 1, 2, 3, 5,

8, 12, and 24 h using heparinized tubes. The collected samples were immediately centrifuged and plasma was separated and stored at -20 °C until analysis.

2.10. Analysis of plasma levels of salbutamol sulphate

The high performance liquid chromatographic method using chloramphenicol as the internal standard (15) was applied in this study. The HPLC system consisted of Series 200 LC pump, sidewinder column heater, Series 200 vacuum degasser, 600 Series LINK interface, Series 200 UV/visible detector (Perkin Elmer, Waltham, MA, USA) and a reversed-phase column Bindapak RP-C18 (5 µm particle size, 300 × 3.9 mm, i.d., Waters, Milford, MA, USA).

To 0.5 mL of plasma sample, 20 µL of internal standard (100 µg/mL) was added. The drug was extracted from plasma using 5 mL chloroform containing 0.1 M bis-(2-ethylhexyl) phosphate. The chloroform layer was subsequently extracted with 1 mL of 0.5 M HCl. The mobile phase was 70:20:10 (v/v) of water, methanol, and acetonitrile, respectively. The pH was adjusted to 2.5 using 10% phosphoric acid and samples were degassed using sonication. Fifty µL of the sample was injected manually. Peaks were monitored using UV absorbance at 276 nm. Quantification of salbutamol sulphate was obtained by plotting salbutamol sulphate to the internal standard peak area ratio as a function of salbutamol sulphate concentration.

2.11. Statistical analysis

The one way analysis of variance (ANOVA) statistical analysis (F-test) at a confidence interval of 5% was applied to estimate any difference between the tested tablets with respect to AUC, C_{max} and T_{max} . A statistics *t*-test was also performed between each pair of the formulations at a confidence interval of 5% (16).

3. Results and Discussion

3.1. Infrared spectroscopy

The IR spectrum of salbutamol sulphate alone (Figure 1, trace A) shows the same characteristic peaks as reported in the literature (17). The IR spectra of physical mixtures (Figure 1, trace C) and granules (Figure 1, trace D) of 1:1 salbutamol sulphate with each of pectin, sodium alginate, mastic, lactose, and avicel (data not shown), respectively, did not provide any difference compared to that of the drug alone. This finding indicated that there was no interaction between salbutamol sulphate and the applied additives.

3.2. DSC study

The DSC thermogram of salbutamol sulphate alone

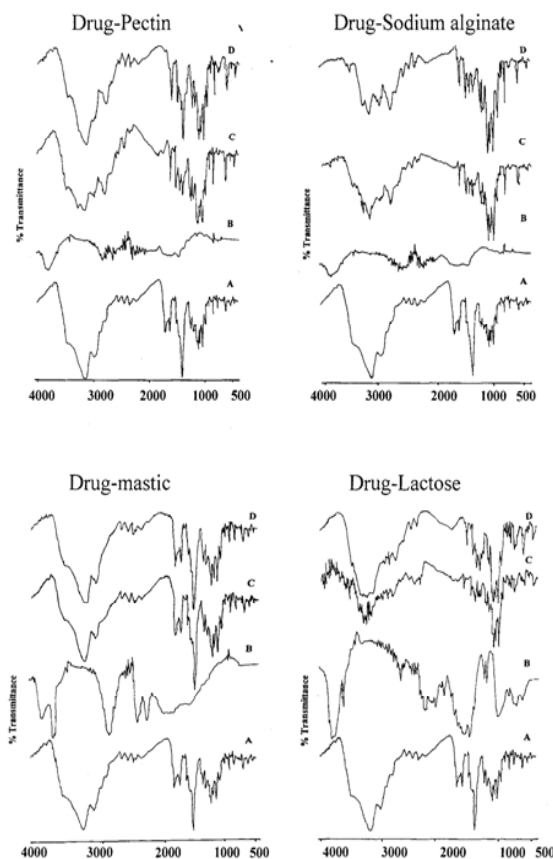


Figure 1. IR spectra of salbutamol sulphate (A), each ingredient alone (B), drug-additive physical mixture (C) and granules (D).

(Figure 2, trace 1) shows an endothermic melting peak with an onset at 190.93°C which reached a maximum peak at 204.58°C. The DSC thermograms of pectin, sodium alginate, mastic, and lactose are shown in trace 2 of Figure 2. The pectin thermal profile demonstrates one broad endothermic peak at 78.41°C (with onset and end set temperatures of 39.54 and 136.26°C, respectively) and an exothermic peak at 258.23°C. This finding is different from that reported by Nurjaya and Wong (18). They stated that the thermogram of unprocessed pectin was characterized by two endothermic peaks at melting temperatures of about 148.4 and 163.7°C and exothermic peak at 233.9 ± 0.4 °C. Sodium alginate showed a broad exothermic peak at 245.54°C indicating the decomposition of the polymer at that particular temperature (19). The thermogram of mastic showed a broad endothermic peak at 71.27°C corresponding to its melting. The lactose thermogram showed two endothermic melting peaks at 145.45 and 219.63°C and agrees very well with literature values (20). The thermogram of avicel (data not shown) illustrates a broad endothermic peak at 336.39°C.

The thermal profiles of the drug-lactose physical mixture and granules exhibited two endothermic

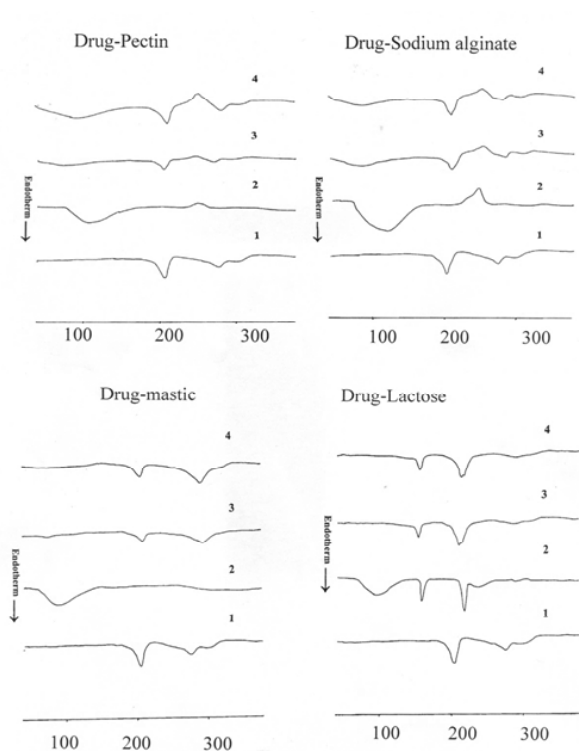


Figure 2. DSC thermograms of salbutamol sulphate (1), each additive alone (2), drug-additive physical mixture (3) and granules (4).

peaks corresponding to the dehydration and fusion of lactose, respectively, and no peak was present associated with the melting of the drug. The thermal behavior of both physical mixture and granules of drug in lactose indicated the ease of dispersion and/or dissolution of the drug into the molten mass of lactose. These findings are similar to that reported in the literature (20,21).

The DSC thermograms of the granules of salbutamol sulphate with each of mastic, pectin, sodium alginate, lactose (Figure 2, trace 4) and avicel (data not shown) are similar to their respective physical mixtures (Figure 2, trace 3). These results demonstrated that salbutamol sulphate did not interact with the chosen additives.

3.3. Physical characteristics of salbutamol sulphate tablets

3.3.1. Uniformity of weight, thickness, and contents

All tablets showed a good weight uniformity with CV ranging from 1.26 to 3.52 (Table 1). The thickness of tablets (the range of CV, 0.75-2.96) correlates well with tablet weight. All the prepared tablets showed a good average content (CV, 2.32-4.59) which complies with the requirements of USP XXVII (22).

Table 1. Physical characteristics of salbutamol sulphate tablets (8 mg) prepared from physical mixture powders and granules containing different concentrations of mastic and additive

Additive Type	Methods of powder preparation	Mastic (%)	Physical parameter of tablets						
			Mean weight (mg)	Mean thickness (mm)	Average drug content (mg)	Friability (%)	Hardness (kg)	Tensile strength (kg/cm ²)	Disintegration time (min)
Pectin	Physical mixture	20	206.5	2.70	7.44	0.77	5.23	13.69	--*
		30	201.4	2.62	7.36	0.67	5.83	15.73	--*
		40	200.6	2.59	7.87	0.64	7.47	20.39	--*
	Granules	20	202.2	2.67	7.44	0.80	5.68	14.90	--*
		30	198.4	2.35	8.03	0.78	6.93	20.84	--*
		40	202.3	2.66	7.78	0.73	8.09	21.50	--*
Sodium alginate	Physical mixture	20	206.1	2.52	7.69	0.94	4.36	12.23	--*
		30	203.4	2.48	8.01	0.88	5.00	14.25	--*
		40	198.4	2.45	7.48	0.85	5.83	16.82	--*
	Granules	20	205.4	2.59	7.74	0.89	5.23	14.27	--*
		30	200.6	2.50	7.44	0.84	5.66	16.00	--*
		40	203.7	2.54	7.58	0.80	6.82	18.98	--*
Lactose	Physical mixture	20	201.0	2.47	7.62	1.12	3.72	10.64	69.54
		30	203.4	2.51	8.37	0.94	4.62	13.01	76.72
		40	197.3	2.45	8.03	0.90	5.77	16.65	98.30
	Granules	20	205.6	2.53	7.58	0.92	5.24	14.64	--*
		30	198.2	2.45	7.49	0.89	5.82	16.79	--*
		40	200.7	2.48	7.84	0.82	6.12	17.44	--*
Avicel	Physical mixture	20	198.9	2.64	7.78	0.64	8.11	21.71	3.53
		30	203.7	2.78	8.42	0.59	8.23	20.93	5.31
		40	198.5	2.72	8.34	0.53	8.94	23.23	7.23
	Granules	20	201.5	2.80	8.19	0.69	7.95	20.07	11.55
		30	196.3	2.71	8.03	0.62	8.50	22.17	20.57
		40	200.6	2.76	8.26	0.50	9.79	25.07	32.64

* Tablets did not disintegrate for 3 h.

3.3.2. Mechanical properties

The obtained results of friability percent and hardness showed that all tablets have friability percents less than 1% and hardness values (Table 1) which comply with USP XXVII (22) requirements except the tablets prepared from the 20% lactose physical mixture which showed a friability % of 1.12 and a hardness of 3.72 kg. The friability percent decreased and hardness increased with an increase of mastic concentration in the tablets. This may be due to the increase in the binding effect of mastic with an increase in its concentration. The highest hardness values obtained were for tablets containing avicel. Both the hardness values and tensile strength increased with an increase of mastic concentration in tablets. Small values of friability percent imply much less friability during transportation, which is important in terms of sustained release of tablets (23).

3.3.3. Disintegration time

The tablets containing pectin and sodium alginate as well as tablets containing lactose prepared by granulation did not disintegrate for 3 h (Table 1). Tablets prepared with pectin and sodium alginate did not disintegrate because they form a hydrophilic non-disintegrated matrix. However, the non-disintegration of the tablets prepared from granules containing lactose may be due to the coating of the particles by the mastic.

In contrast, the tablets prepared from physical mixtures containing lactose disintegrate by erosion and those containing avicel prepared from granules and physical mixtures disintegrated. The disintegration time of tablets containing avicel was longer for those prepared from granules (11.55-32.64 min) compared to those prepared from physical mixtures (3.53-7.23 min). The increased disintegration time with the increase of mastic concentrations in tablets may be attributed to the enhancement of the binding action of mastic (11).

3.3.4. Release studies

The release rate of salbutamol sulphate from tablets made from granules was lower than that of tablets prepared from physical mixtures at fixed mastic concentrations using the same additive such as pectin (Figure 3). The lower release from granules can be explained because mastic solutions act as a binder forming large compact particles which are surrounded by a film of mastic (11). When comparing drug release from tablets containing various mastic concentrations, drug release was retarded by an increase in mastic concentration. This may be attributed to the hydrophobic nature of mastic gum which reduces the penetration of solvent molecules into the tablet matrix and therefore retards the wetting and dissolution of drug (14,24).

The release of salbutamol sulphate from tablets

containing 40% mastic with various additives prepared from physical mixtures and granules is shown in Figure 4. The release rate of drug from tablets containing different additives at constant mastic concentration and the method of preparation can be arranged in the following order: Pectin < Sodium alginate < Lactose < Avicel.

The hydrophilic jelly nature of pectin and sodium alginate is responsible for the sustained release of drug from tablets containing them. These polymers upon contact with aqueous medium start to absorb water and as a consequence the polymers swell forming a gel layer. This layer increases in thickness as time passes creating a considerable barrier for both penetration of solvent into the tablets and drug release from it (25).

The pectin based tablets sustain drug release more than the sodium alginate based tablets due to the difference in viscosity and swelling properties of the

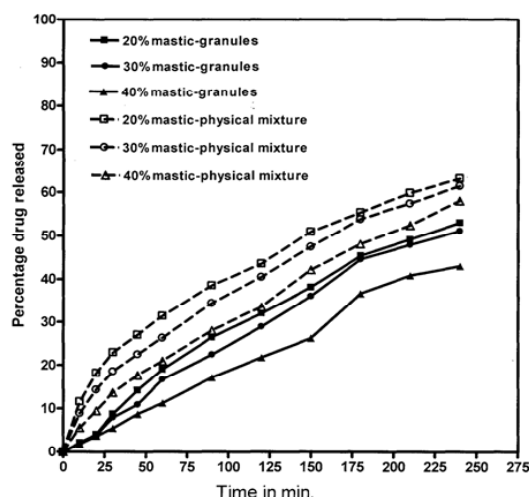


Figure 3. Release profile of salbutamol sulphate tablets prepared from physical mixtures and granules containing pectin as additive and different concentrations of mastic.

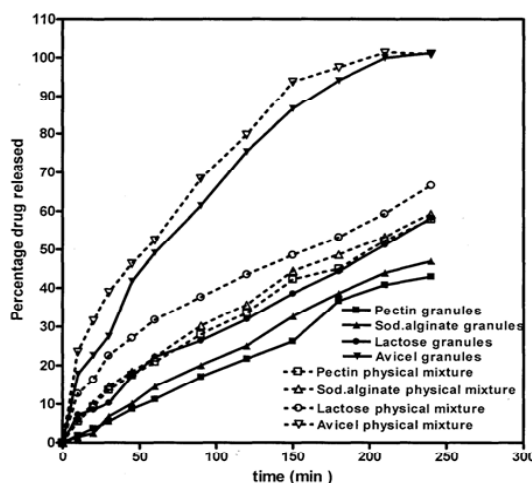


Figure 4. Effect of different additives on the release of salbutamol sulphate from tablets prepared from physical mixtures (---) and granules (—) containing 40% of mastic.

Table 2. Analysis of release data of salbutamol sulphate tablets from tablets containing mastic with different additives using different kinetic models

Additives	Methods of powder preparation	Mastic (%)	Zero order		Diffusion		Peppas equation	
			$K (\%) \times 100$	r^2	$K (\%/\sqrt{\text{min}})$	r^2	n	r^2
Pectin	Physical mixture	20	2.29	0.981	0.416	0.998	0.52	0.997
		30	2.25	0.962	0.415	0.997	0.60	0.998
		40	2.16	0.962	0.339	0.991	0.65	0.997
	Granules	20	2.19	0.933	0.399	0.996	0.84	0.980
		30	2.16	0.989	0.365	0.986	0.92	0.989
		40	1.80	0.992	0.339	0.964	1.00	0.998
Sodium alginate	Physical mixture	20	2.53	0.972	0.456	0.991	0.60	0.994
		30	2.39	0.979	0.434	0.986	0.63	0.993
		40	2.27	0.980	0.416	0.994	0.70	0.998
	Granules	20	2.26	0.979	0.411	0.989	0.88	0.968
		30	2.21	0.993	0.399	0.987	0.97	0.977
		40	1.97	0.993	0.373	0.986	1.00	0.979
Lactose	Physical mixture	20	2.59	0.979	0.470	0.986	0.64	0.998
		30	2.23	0.976	0.405	0.985	0.64	0.981
		40	2.17	0.986	0.397	0.978	0.69	0.978
	Granules	20	2.67	0.892	0.471	0.989	0.53	0.992
		30	2.54	0.941	0.450	0.994	0.48	0.993
		40	2.26	0.945	0.397	0.988	0.51	0.993

polymers (26). On the other hand, the tablets containing lactose gave a relatively lower release rate of drug compared to those containing avicel. This is due to the fact that avicel based tablets disintegrated during release and the lactose based tablets were subjected to erosion due to the dissolution of lactose.

Tablets containing 40% mastic prepared from granules containing pectin or sodium alginate produced the most sustained release compared to other tablets. These tablets are a suitable candidate to control the release of salbutamol sulphate and their bioavailability will be studied.

3.4. Analysis of release data

Table 2 illustrates the analysis of the release data of salbutamol sulphate from the different tablet formulations using zero and first order kinetics (data not shown), diffusion models, and the Peppas equation. The tablets containing avicel prepared from physical mixtures and granules did not follow any kinetic model because of their disintegration (data not shown).

The results of analysis indicate non-Fickian release ($0.5 < n < 1$) for all tablet formulations except those containing 40% mastic and prepared from granules containing pectin or sodium alginate. The non-Fickian release means that the drug release occurred by diffusion and erosion of the tablet matrix (27). However, the tablets containing pectin and sodium alginate prepared from granules at 40% mastic follow zero-order release as indicated by $n = 1$ and high regression coefficients.

3.5. Bioavailability of salbutamol sulphate

Salbutamol mastic tablet formulations that generate

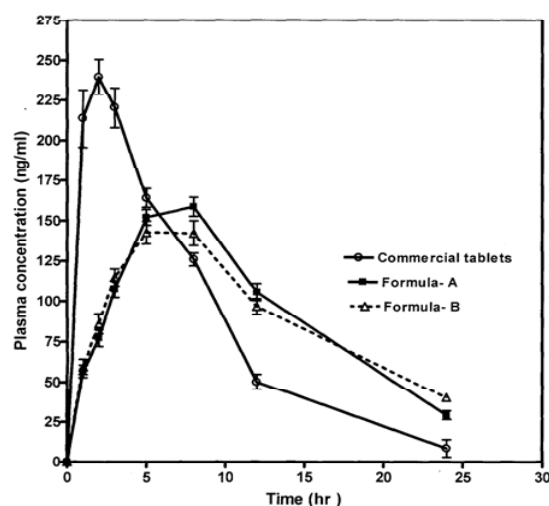


Figure 5. Mean plasma concentration-time curve of salbutamol sulphate after administration of a single dose of formula A, B and two commercial tablets each containing 4 mg.

the best controlled release pattern were selected for this study. These formulas contained 40% mastic and pectin (formula A) or sodium alginate (formula B). The bioavailability of the controlled release tablet formulations was studied by administration of a single dose containing 8 mg drug or two commercial tablets (2×4 mg) to rabbits (4 mg/kg).

The mean plasma concentration curve of salbutamol sulphate after oral administration of formulated tablets A and B was compared with that of the commercial salbutamol tablets (Figure 5). The plasma salbutamol profiles of the two mastic formulated tablets were similar and were nearly superimposed, while these

Table 3. Individual numerical values of T_{max} , C_{max} , and AUC_{0-24} of formulated and commercial tablets of salbutamol sulphate in rabbit plasma

Rabbit	Formula A			Formula B			Commercial tablets		
	T_{max} (h)	C_{max} (ng/mL)	AUC_{0-24} (ng/mL·h)	T_{max} (h)	C_{max} (ng/mL)	AUC_{0-24} (ng/mL·h)	T_{max} (h)	C_{max} (ng/mL)	AUC_{0-24} (ng/mL·h)
I	8.0	158.5	2,203.0	8.0	146.1	1,959.8	1.0	257.8	2,286.6
II	8.0	175.0	2,117.9	5.0	155.5	2,287.9	2.0	264.9	1,981.5
III	8.0	173.0	2,408.8	5.0	148.9	2,137.3	1.0	261.6	1,838.1
IV	5.0	158.3	2,056.8	8.0	161.3	2,352.6	3.0	256.0	2,057.6
V	5.0	172.4	2,261.7	5.0	164.1	2,140.0	2.0	264.6	2,151.6
VI	8.0	160.4	2,442.2	8.0	166.1	2,219.6	1.0	240.2	2,195.2
Mean	7.0	166.2	2,248.4	6.5	157.0	2,182.8	1.66	257.5	2,085.1
S.D.	1.5	7.9	154.4	1.64	8.2	137.7	0.75	9.2	161.0

profiles were completely different from the plasma profile of the commercial tablets (Figure 5).

Pharmacokinetic parameters (C_{max} , T_{max} , and AUC_{0-24}) for each rabbit were calculated on the basis of concentration-time data. From individual pharmacokinetic parameters, their mean values \pm S.D. were obtained and are shown in Table 3 for both the formulated tablets and commercial salbutamol tablets.

The mean salbutamol C_{max} were 166.2 ± 7.9 , 157 ± 8.2 , and 257.5 ± 9.2 ng/mL and occurred at T_{max} 7.0 ± 1.5 , 6.5 ± 1.64 , and 1.66 ± 0.75 h after administration of a single 8 mg dose of formula A, formula B, and commercial tablets, respectively. The results showed that the C_{max} of the commercial tablets was greater than that of formulated tablets. In addition, the T_{max} of the commercial tablets was shorter than that obtained from the formulated tablets. These results demonstrate that the formulated tablets extended the time of drug effect.

The mean AUC_{0-24} of formula A, formula B, and the commercial tablets were $2,248.4 \pm 154.4$, $2,182.8 \pm 137.7$, and $2,085.1 \pm 161$ ng/mL·h, respectively. The ANOVA test of the AUC results ($F_{0.05} = 1.768$) revealed that there is no significant difference in AUC between the different tablets indicating that all tested tablets were equivalent in the extent of drug absorption.

The obtained results revealed that all of the tested salbutamol sulphate formulas are equivalent in the AUC. The formulated tablets A and B have a longer T_{max} and smaller C_{max} compared to the commercial tablets. These results demonstrate prolonged salbutamol sulphate plasma concentrations compared to the commercial tablets. Similar results were reported by Hernández *et al.* (28) who worked on two sustained formulations of salbutamol sulphate, commercial immediate release formulation, and osmotic pump. Also, Sirkia *et al.* (8) found that the bioavailability parameters of salbutamol sulphate prolonged release press-coated tablets and the commercial reference have statistically no difference in AUC but a significant difference in C_{max} values in humans.

4. Conclusion

The incorporation of mastic in the formulation of salbutamol sulphate tablets has a great effect in delaying drug release. Both the method of treatment of powders and type of additives affected the drug release from the tablets. Tablets prepared from granules and containing 40% mastic with pectin or sodium alginate showed the best control of drug release. Formula A (containing pectin and mastic), formula B (containing sodium alginate and mastic) achieved the targets of the present study in controlling drug release and good bioavailability.

References

1. Parfitt K. Martinale: The complete drug reference, 32nd ed. Pharmaceutical Press, Taunton, MA, USA, 1999; pp. 758-761.
2. Mulligan S, Devane J, Martin M. Pharmacokinetic characteristics of a novel controlled-release sprinkle formulation of salbutamol. *Eur J Drug Metab Pharmacokinet.* 1991; 3:312-314.
3. Yazan Y, Demirel M, Guler E. Preparation and *in-vitro* dissolution of salbutamol sulphate microcapsules and tableted microcapsules. *J Microencapsul.* 1995; 12:601-607.
4. Raghuvanshi RS, Tripathi KP, Jayaswal SB, Singh J. Release kinetics of salbutamol sulphate from wax coated microcapsules and tableted microcapsules. *J Microencapsul.* 1992; 9:449-455.
5. Govender T, Dangor CM, Chetty D. Microencapsulated Eudragit RS30D-coated controlled release pellets: the influence of dissolution variables and topographical evaluation. *J Microencapsul.* 1997; 14:1-13.
6. Prabakaran D, Singh P, Kanaujia P, Jaganathan KS, Rawat A, Vyas SP. Modified push-pull osmotic system for simultaneous delivery of theophylline and salbutamol: development and *in-vitro* characterization. *Int J Pharm.* 2004; 284:95-108.
7. Lin SY, Tau J, Wu WH, Chang HN. Biopharmaceutic evaluation of controlled-release hydrophilic-matrix tablets containing encapsulated or unencapsulated salbutamol sulfate. *Current Therapeu Res.* 1992; 2:486-492.
8. Sirkia T, Makimartti M, Liukko-Sipi S, Marvola M.

- Development and biopharmaceutical evaluations of a new press-coated prolonged-release salbutamol sulphate tablet in man. *Eur J Pharm Sci.* 1994; 1:195-201.
9. Martindale: The Extra Pharmacopoeia, 28th ed. The Pharmaceutical Press, London, UK, 1982; p. 315.
 10. Panagopoulou A, Georarakis M. Effect of compression and diluent on drug release from mastic matrix tablets. A statistical analysis. *Drug Dev Ind Pharm.* 1990; 16:637-646.
 11. Abdel-Aleem HM. Formulation and evaluation of mastic in antacid preparations. *Alex J Phar Sci.* 1996; 10:65-68.
 12. Georarakis M, Groning R, Henzler P. Microencapsulation of potassium chloride with mastic. *Pharmazie.* 1987; 42:455-456.
 13. Assimopoulou AN, Papageorgiou VP, Kiparissides C. Synthesis and release studies of shikonin-containing microcapsules prepared by the solvent evaporation method. *J Microencapsul.* 2003; 20:581-596.
 14. Assimopoulou AN, Papageorgiou VP. Preparation and release studies of alkannin containing microcapsules. *J Microencapsul.* 2004; 21:161-173.
 15. Sutariya VB, Mashru RC, Sankalla MG, Sankalla JM. Liquid chromatographic determination and pharmacokinetics study of salbutamol sulphate in rabbit plasma. *Ars Pharm.* 2006; 47:185-197.
 16. Kirkwood BR. *Essential of Medical Statistics.* The Blackwell Science Ltd., UK, 1988; pp. 41-57.
 17. Moffat AC, Osselton MD, Widdop B. *Clarke's Analysis of Drug and Poisons in Pharmaceutical, Body Fluids and Postmortem Material,* 3rd ed. Pharmaceutical Press, London, UK, 2004; pp. 1546-1447.
 18. Nurjaya S, Wong TW. Effects of microwave on drug release properties of matrices pectin. *Carbohydrate Polymers.* 2005; 62:245-257.
 19. Gonzalez-Rodriguez ML, Holgada MA, Sanchez-Lafuente C, Rabasco AM, Fini A. Alginate/chitosan particulate systems for Diclofenac sodium release. *Int J Pharm.* 2002; 232:225-234.
 20. Cavallari C, Albertini B, Rodriguez L, Rabasco AM, Fini A. Release of indomethacin from ultrasound dry granules containing lactose-based excipients. *J Control Rel.* 2005; 102:39-44.
 21. Fini A, Moyano JR, Gines JM, Perez-Martinez JI, Rabasco AM. Diclofenac salts, II. Solid dispersion in PEG 6000 and Gelucire 50/13. *Eur J Pharm Sci.* 2005; 60:99-111.
 22. U.S.P. *The United States Pharmacopoeia,* 27th revision. United States Pharmacopoeial Convention Inc., The Board of Trustees, Washington, USA, 2004; pp. 2396, 2397, 2621, 2622.
 23. Savaser A, Ozkan Y, Isimer A. Preparation and *in-vitro* evaluation of sustained release tablets formulations of diclofenac sodium. *J Pharmaco.* 2005; 60:171-177.
 24. Kuksal A, Tiwary AK, Jain NK, Jain S. Formulation and *in vitro-in vivo* evaluation of extended-release matrix tablets of Zidovudine: Influence of combination of hydrophilic and hydrophobic matrix formers. *AAPS PharmSciTech.* 2006; 7:E1.
 25. Efentakis M, Koligliati S, Vlachou M. Design and evaluation of drug coated drug delivery systems with an impermeable cup, swellable top layer and pulsatile release. *Int J Pharm.* 2006; 311:147-156.
 26. Gursoy A, Cevik S. Sustained release properties of alginate microspheres and tableted microspheres of diclofenac sodium. *J Microencapsul.* 2000; 17:565-575.
 27. Peppas NA. Analysis of fickian and non-fickian drug release from polymers. *Pharm Acta Helv.* 1985; 60:110-111.
 28. Hernández RM, Gascón AR, Calvo MB, Caramella C, Conte U, Domínguez-Gil A, Pedraz JL. Correlation of '*in-vitro*' release and '*in-vivo*' absorption characteristics of four salbutamol sulphate formulations. *Int J Pharm.* 1996; 139:45-52.

(Received December 19, 2009; Revised January 27, 2010; Accepted January 27, 2010)

Original Article

Stability, bioavailability, and ulcerative activity of diclofenac sodium-mastic controlled release tablets

Ahmed T. Nouh^{1,*}, Abd El-Gawad H. Abd El-Gawad², Tawhida K. Guda²

¹ *Pharmaceutics Department, Faculty of Pharmacy, Misr International University, Cairo, Egypt;*

² *Pharmaceutics Department, Faculty of Pharmacy, Mansoura University, Cairo, Egypt.*

ABSTRACT: Controlled release tablets containing 50 mg diclofenac sodium (DS) and 40% mastic with other natural additives were prepared. Drug release was examined and stability was studied using non-isothermal and isothermal thermogravimetric analysis (TGA). The bioavailability of two controlled release tablet formulations was studied and compared to that of commercial tablets, and rabbit stomachs were also histologically examined 24 h after administration of the various tablets.

Additives of pectin and sodium alginate indicated the controlled release profile of the drug. Non-isothermal TG revealed two stages of thermal decomposition for all formulations. Isothermal TG revealed that degradation of the drug in the tablet formulations follows first-order kinetics. The obtained degradation rate constants at various temperatures were plotted according to the Arrhenius equation. The degradation rate constant at 25°C was determined and used in estimation of shelf life. The obtained shelf lives of all formulations ranged from 3.38-4.92 years. In comparative studies with commercial tablets, the bioavailability of the drug from the two formulated tablets had no statistically significant difference in terms of the AUC and produced prolonged blood levels of DS with a delayed peak. The two controlled release tablet formulations resulted in no histological alterations in the stomach in terms of mucous surface cells and glands; in comparison, commercial tablets resulted in a disrupted mucous layer, necrotic ulcerations, hemorrhaging, and inflammatory cell infiltration along the base of the gastric glands.

Keywords: Diclofenac sodium, natural additives, tablets, dissolution rate, ulcerative activity, *in vivo* studies

*Address correspondence to:

Dr. Ahmed T. Nouh, Pharmaceutics Department, Faculty of Pharmacy, Misr International University (MIU), Cairo-Ismailia Road, Cairo, Egypt.
e-mail: ahmednouh_8@hotmail.com

1. Introduction

Stability studies should be conducted to evaluate the physical and chemical degradation of pharmaceutical products. Such products should maintain their identity, strength, quality, and purity within specified limits through their period of storage and use (1).

The use of thermal methods is of great importance in the determination of drug purity, the quantitative and qualitative analysis of drug formulations, tests of stability, and determination of kinetic parameters. Thermogravimetric analysis (TGA) and differential scanning calorimetry (DSC) have been used simultaneously to determine the thermal stability of drugs, excipients, and pharmaceutical products (2-6).

Thermogravimetric methods have been used to determine drug stability either as non-isothermal TG (the temperature is increased at a constant rate) or as isothermal TG (the temperature is set at a predetermined temperature). Non-isothermal TGA with its derivative (thermogravimetry, DTG) were used to study the thermal degradation kinetics of vinyl polyperoxide copolymers (7) and non-isothermal TGA at different heating rates in flowing nitrogen was used to estimate the thermal stability and thermal degradation kinetics of polyimides (8). Isothermal TG was used to study the thermal kinetics and determine the shelf-life of different ampicillin products (9). Both non-isothermal and isothermal TGA have been used to determine the kinetic parameters and shelf-lives of many drugs and drug products, including anti-hypertensive drugs (10), generic hydrochlorothiazide formulations (11), prednisone powder and tablets (2), and metronidazole powder and tablets (12).

The bioavailability of diclofenac sodium (DS) from various drug delivery systems was previously studied in humans (13-15). Different kinds of animals have also been used for bioavailability studies of DS from various drug delivery systems. Yong *et al.* (16) studied the pharmacokinetics of DS delivered by a poloxamer-based suppository in rats. Sarvavanan *et al.* (17) attempted to target DS to its site of action using gelatin magnetic microspheres in rabbits.

The aim of the current study was to determine the

order of decomposition and shelf-lives of DS controlled release tablet formulations using non-isothermal and isothermal TGA. The bioavailability of DS from controlled release tablet formulations was also assessed and compared with that of commercial tablets. The histology of stomach tissues of untreated animals and animals 24 h after administration of a single dose of both formulations of controlled release tablets and commercial tablets was studied.

2. Materials and Methods

2.1. Materials

Diclofenac sodium was obtained from Novartis Pharmaceutical Industry, Cairo, Egypt. Pectin was from Winlab, a division of Wilfrid Smith, UK. Sodium alginate and lactose monohydrate were from El Nasr, Pharmaceutical Chemical Co., Cairo, Egypt. Commercial grade mastic was from Chios' Gum Mastic Growers Association. Avicel PH 101 was from Fluka AG, VH9470, Buchs, Switzerland. Commercial DS tablets (Olfen tablets containing 50 mg drug, Lot No. 060034) were produced by Medical Union Pharmaceuticals Co. Abu Sultan, Ismailia, Egypt, under a license from MEPHA, Basel, Switzerland. Acetonitrile and methanol (CHROMASOLV[®]) were from Sigma-Aldrich Chemie GmbH D-39555, Steinheim, Germany. Mefenamic acid was kindly supplied by the Nile Co. for Pharmaceutical and Chemical Industries (El-Nile), Cairo, Egypt.

2.2. Preparation of DS granules and tablets

Pectin, sodium alginate, avicel PH 101, or lactose monohydrate was individually mixed in a porcelain mortar with DS and mastic using the least amount of chloroform to produce a doughy mass. The mass obtained was converted into granules by forcing it through a 2 mm sieve. The granules obtained were dried at room temperature for 24 h in open air and further dried at 40°C for 48 h in a hot air oven.

Tablet formulations were prepared from the equivalent weight of granules to contain 50 mg drug, 60 mg mastic (40%), and 187 mg of one of the tested additives (pectin, sodium alginate, avicel, or lactose). Magnesium stearate at a concentration of 1% was used as a lubricant. Tablets containing pectin, sodium alginate, avicel, or lactose were designated formulations A, B, C, and D, respectively. All batches were prepared using a single-punch Eraweka tablet press (G.M.B.H., Germany) at a constant pressure.

2.3. Release study

Drug release from different tablets was carried out using a USP dissolution apparatus with six jars (DA-6D,

India). Phosphate buffer adjusted to a pH of 7.4 and temperature of $37 \pm 0.2^\circ\text{C}$ was used as a dissolution medium with a volume of 500 mL. A single tablet was placed in each basket, which was rotated at 50 rpm. Samples were withdrawn at different time intervals and replaced with the same volume of fresh medium. The drug released was measured spectrophotometrically at 276 nm (Spectrophotometer, UV-Visible; JASCO, V-530, Japan). All experiments were conducted in triplicate and the mean values were calculated.

2.4. Non-isothermal and isothermal TG studies

The different tablet formulations were tested with non-isothermal TGA. The data and curves of non-isothermal TGA were obtained with a Shimadzu model TGA-50H thermo-balance (Japan) in an atmosphere of nitrogen with a flow rate of 50 mL/min and a heating rate of $10^\circ\text{C}/\text{min}$ up to 600°C . The sample mass used was 4-6 mg. The isothermal TG data and curves for DS tablet formulations were obtained in the region before the initial temperatures of thermal decomposition of the tablets in non-isothermal curves. The sample mass was in a range of 5-9 mg. The samples were heated at a heating rate of $10^\circ\text{C}/\text{min}$ up to the isothermal temperature, where the temperature was maintained for 120 min (11,12). The isothermal TG curves were measured at 150, 160, 170, and 180°C for 120 min. Isothermal TG data were used to determine the stability of the different tablet formulations to reveal differences (12).

2.5. Analysis of the isothermal data

The degradation order of DS tablet formulations was determined by analysis of the isothermal data using zero, first, and second-order kinetics (18). The kinetic order of thermal decomposition of DS tablet formulations was chosen based on the highest correlation coefficient (r^2) obtained from the statistical data for each reaction order. The rate constants (K) were calculated for the chosen order at each temperature. Then, the natural logarithm (Ln) of the obtained rate constants (K) at different temperatures was plotted with respect to the reciprocal of the corresponding temperature ($1/T$) using the Arrhenius relationship. The degradation rate constant at room temperature (25°C or 298 K) was obtained by extrapolation to that temperature. The degradation rate constant at room temperature was used to calculate the shelf life (t_{90}) by substitution in the first-order equation.

2.6. Bioavailability study

2.6.1. Tested formulations

Formulations A and B were selected for *in vivo* study as

they have acceptable physical characteristics, the best controlled drug release behavior, and good stability. These formulations were compared with commercial tablets (Olfen tablet 50 mg).

2.6.2. Study design

Male Albino rabbits weighing 2.0-2.5 kg were randomly selected for the bioavailability study. The animals were divided into three groups, and each group of six rabbits received one of the tested formulations, namely formulation A, formulation B, and commercial tablets. The animals fasted overnight before tablet administration and during the experiment but were given free access to water. The tablets were given orally to the rabbits using a balling gun to deliver the tablets to the animal's stomach. The ear vein was cannulated with a 19-gauge butterfly (scalp) needle and blood samples (2 mL) were withdrawn from the vein before dosing (zero time) and at different time intervals after dosing, namely 1, 2, 3, 5, 8, 12, and 24 h, using heparinized tubes. The collected samples were immediately centrifuged and plasma was separated and stored at -20°C until analysis.

2.6.3. Analysis of plasma level of diclofenac sodium

High-performance liquid chromatography as reported by Liu *et al.* (13) was performed using mefenamic acid as the internal standard. An HPLC model L-7100 equipped with a Rheodyne injector valve with 20 μL loop and L-7400 UV detector, Merck Hitachi limited, Tokyo, Japan, was used. The plasma protein was precipitated with acetonitrile. Separation was performed on a Nucleosil 100-5 (C_{18}) column (150 \times 4.6 mm). The mobile phase was acetonitrile-0.01 M potassium dihydrogen phosphate (pH 6.3) in a ratio of 35:65 (v/v), and the flow rate was 1 mL/min. A wavelength of 278 nm was used to monitor the drug and the mefenamic acid. The peak area ratio served as the basis for quantification.

2.6.4. Pharmacokinetics calculation

Pharmacokinetics parameters were calculated according to a non-compartmental model. The plasma concentration versus time curves was used to determine the maximum plasma concentration (C_{max}), time to achieve maximum plasma concentration (T_{max}), and the area under the concentration-time curve with respect to the respective sampling AUC_{0-t} .

The maximum concentration (C_{max}) and the time of its occurrence (T_{max}) for each individual animal were determined from the plasma concentration time data. The area under the curve (AUC) for each rabbit was calculated by the trapezoidal rule method using GraphPad Prism Project software.

2.6.5. Statistical analysis

One-way analysis of variance (ANOVA) was used to estimate the difference between the different formulations, namely formulation A, formulation B, and commercial tablets, with regard to the AUC_{0-24} , C_{max} , and T_{max} . A *t*-test was also performed on pairs of formulations at a confidence interval of 5% (19).

2.7. Histological study

Rabbits were sacrificed 24 h after administration of a single dose of A or B formulated tablets or commercial tablets. Control rabbits were also sacrificed and examined. The stomach was isolated from other parts of the gastrointestinal tract, which was opened longitudinally and washed thoroughly with saline. The stomach was sliced into two parts, namely the fundus and the pylorus. The fundus and pylorus were then sliced into small pieces and treated separately by immersion in 10% neutral formalin for two days. They were then dehydrated, cleared, and embedded in paraffin wax. Paraffin sections (6 μm thick) were prepared and stained with hematoxylin and eosin stain (20).

3. Results and Discussion

3.1. Preparation of DS Tablets

The physical characteristics of DS tablets containing mastic and each of the selected additives (formulations A, B, C, and D) were within pharmacopeial limits. With regard to disintegration time, none of the tablet formulations displayed disintegration for 3 h except for formulation C containing avicel, which disintegrated after 37 min.

3.2. Release study

The release rate of DS from tablet formulations (Figure 1) decreased in the following order: formulation C > D > A and B. The highest release rate from formulation C may be due to the disintegrating effect of avicel. Formulation D had an intermediate release rate due to tablet erosion of the water-soluble lactose. That said, formulations A and B provided the best control of drug release. This may be attributed to the hydrophilic gel nature of both pectin and sodium alginate (21).

3.3. Stability study

The non-isothermal TG curve and Dr TGA of formulation D of DS tablets (Figure 2) are shown as a representative example. The results indicate an initial minor % weight loss as the temperature increased up to 200°C . This may be attributed to desorption of moisture as hydrogen bound water to the polysaccharide

structure of the additives (6).

The non-isothermal TG curves and Dr TGA indicate that the onset of thermal decomposition started at 200°C or above for all formulations and the Dr TG peaks were at 241.9, 236.61, 291.52, and 210.44°C for formulations A, B, C, and D, respectively. Li *et al.*

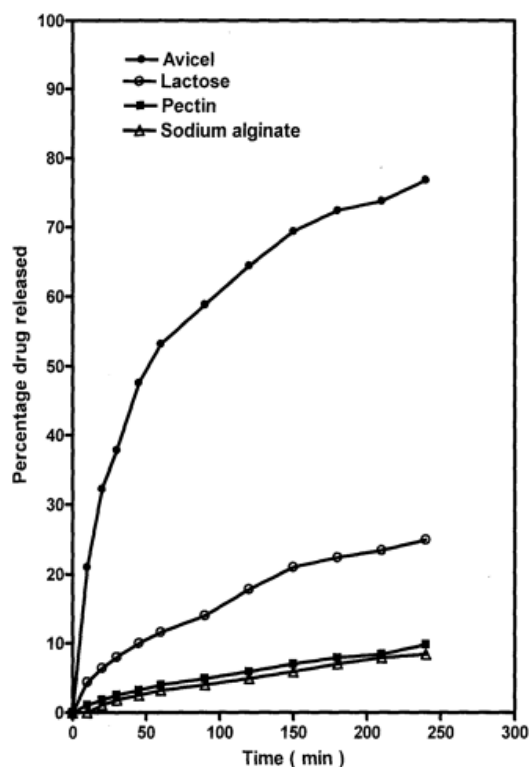


Figure 1. Release profile of DS from tablets containing 50 mg drug, 40% mastic, and various additives.

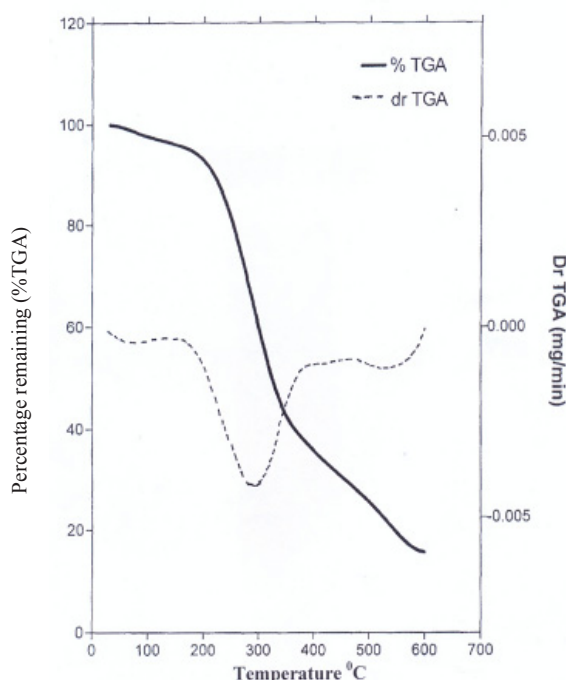


Figure 2. Percentage TGA and the differential TGA for DS tablets containing mastic and avicel.

(7) stated that the lower peak temperature of TG, the higher the thermal decomposition of the material(s). The current results also indicate that after the onset temperature, all formulations exhibited a two-stage decomposition pattern. These intervals are based on the change in the slope of the % weight loss as a function of temperature. The stages of thermal decomposition of different formulations and their onset temperature differ from one formulation to another depending on the melting point of the compound(s) and their stability when exposed to high temperatures (4,10,12).

The isothermal TG data at 150, 160, 170, and 180°C for DS formulations were used to determine the reaction order and the rate constants for thermal decomposition of DS tablet formulations. The decomposition of all formulations followed first-order kinetics. Table 1 shows the first-order rate constant of thermal decomposition for DS tablet formulations containing various additives under isothermal conditions.

The natural logarithm of the rate constants ($\ln K$) of all tablet formulations at different temperatures was plotted as a function of $1/T$ (Kelvin) in Figure 3. A straight line was obtained according to the Arrhenius relationship. The rate constants at 25°C (298 K) for DS formulations were calculated by extrapolation of the line to that temperature (Table 2). The values of the rate constants at 298 K were used to estimate the shelf-lives of DS tablet formulations. The estimated shelf-lives (Table 2) of DS tablet formulations A, B, C, and D were 4.512, 4.046, 4.915, and 3.376 years, respectively. Based on these rate constants, the different formulations had decreasing stability in the following order: formulation C > A > B > D.

Tablets of formulation A containing pectin and formulation B containing sodium alginate achieved the best control of drug release and also had good stability.

Table 1. First-order rate constant and its correlation coefficient for DS tablets containing 40% mastic with different additives

Type of additive	Temperature		r^2 *	Rate constant K (min^{-1})
	°C	K		
Pectin	150	423	0.997	5.210×10^{-4}
	160	433	0.995	8.350×10^{-4}
	170	443	0.989	1.430×10^{-3}
	180	453	0.991	2.232×10^{-3}
Sodium alginate	150	423	0.993	5.460×10^{-4}
	160	433	0.994	9.120×10^{-4}
	170	443	0.991	1.489×10^{-3}
	180	453	0.993	2.377×10^{-3}
Avicel	150	423	0.994	4.830×10^{-4}
	160	433	0.992	7.870×10^{-4}
	170	443	0.988	1.231×10^{-3}
	180	453	0.994	2.155×10^{-3}
Lactose	150	423	0.995	6.050×10^{-4}
	160	433	0.992	1.027×10^{-3}
	170	443	0.995	1.595×10^{-3}
	180	453	0.993	2.640×10^{-3}

* r^2 is the correlation coefficient for the first order.

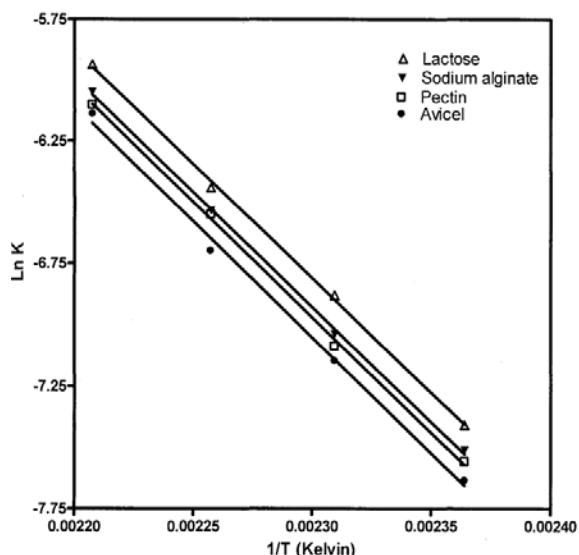


Figure 3. Plot of $\ln K$ versus $1/T$ of the isothermal data of DS tablets containing mastic with pectin, sodium alginate, avicel, or lactose.

Table 2. First-order rate constant at 25°C and shelf life of DS tablets containing mastic and various additives

Type of additives	r^2 values of Arrhenius plot	Rate constant at 25°C (min^{-1})	Shelf-life (year)
Pectin	0.988	4.4276×10^{-8}	4.512
Sodium alginate	0.973	4.9369×10^{-8}	4.046
Avicel	0.990	4.0644×10^{-8}	4.915
Lactose	0.989	5.9166×10^{-8}	3.376

Therefore, they were chosen for the bioavailability study.

3.4. Bioavailability study

Diclofenac sodium-mastic tablets containing pectin and sodium alginate as selected additives (formulations A and B) as well as commercial tablets were administered to rabbits. The plasma concentration of DS in individual rabbits after oral administration of both A and B formulated tablets and the commercial tablets was determined. The mean plasma DS concentration-time profiles following administration of a single oral dose of either the mastic-containing tablets (A and B) or the commercial DS tablets are shown in Figure 4. As is apparent from Figure 4, the two profiles of the formulated tablets are quite comparable and at the same time differ vastly from that of the commercial tablets. Pharmacokinetic parameters (C_{\max} , T_{\max} , and AUC_{0-24}) were calculated individually on the basis of concentration-time data. Mean values \pm S.D. were obtained from individual pharmacokinetic parameters and are shown in Table 3 for both the formulated tablets and commercial DS tablets.

The commercial DS tablets achieved a high C_{\max} value of 18.75 $\mu\text{g/mL}$ in 1.83 h. In contrast, tablets (A and B) containing mastic had lower C_{\max} values of 8.04 and 7.93 $\mu\text{g/mL}$ that occurred at a longer T_{\max} of 6.00

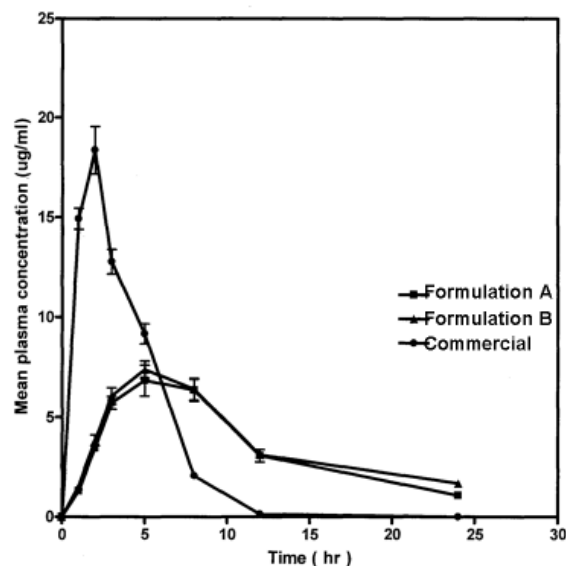


Figure 4. Plasma concentration time curve of DS obtained from formulation A, formulation B, or commercial tablets.

Table 3. The mean pharmacokinetic parameters of DS tablets after administration to rabbits ($n = 6$) of a single dose (50 mg) of either mastic-containing tablets or commercial tablets

Formulation	C_{\max} ($\mu\text{g/mL}$) Mean \pm S.D.	T_{\max} (hr) Mean \pm S.D.	AUC_{0-24} ($\mu\text{g/mL}\cdot\text{h}$) Mean \pm S.D.
Formulation A	8.04 ± 0.43	6 ± 1.54	85.60 ± 7.39
Formulation B	7.93 ± 0.35	6 ± 1.54	90.42 ± 8.36
Commercial tablets	18.75 ± 0.218	1.8 ± 30.4	83.60 ± 5.56

for both. The mean AUC_{0-24} of both formulations A and B and commercial tablets was 85.48, 90.42, and 83.60 $\mu\text{g/mL}\cdot\text{h}$, respectively.

Statistical analysis of the different bioavailability parameters using an ANOVA test (19) revealed no significant difference in the mean AUC_{0-24} values for all of the tested tablets ($p > 0.05$). That said, there was a significant difference in the mean values of C_{\max} and T_{\max} for the tested tablets ($p < 0.05$). Further statistical analysis using a student's t test revealed no significant difference in the C_{\max} and T_{\max} for formulations A and B but it did reveal a significant difference between the commercial tablets and both formulations A and B.

The results obtained indicate that all three formulations are equivalent with regard to the AUC. The A and B formulated tablets have a longer T_{\max} and smaller C_{\max} compared to the commercial tablets. This indicates that a prolonged plasma concentration of DS was obtained from the formulated tablets containing 40% mastic and pectin (formulation A) or sodium alginate (formulation B) in comparison to the commercial tablets. A similar finding was reported by Rani and Mishra (22) working on fabricated controlled release DS tablets. They stated that formulations containing HPMC, ethyl cellulose, or microcrystalline cellulose that they fabricated resulted in prolonged blood levels with a delayed peak in comparison to commercial tablets.

3.5. Histological examination of the rabbit stomach

Figure 5 shows the normal structural features of the stomach fundus of an untreated rabbit; the mucosa is covered by a continuous mucous layer and its surface is lined by healthy surface columnar epithelium. The ducts of fundic glands dip down into the lamina propria and their secretory parts (intact fundic glands) lie perpendicular to the surface. Histological examination of the stomach fundus of rabbits 24 h after administration of commercial tablets (Figure 5) indicated that the mucosa is covered by a disrupted mucous layer and that the surface epithelium displays necrotic ulceration. The lamina propria also displays hemorrhaging and cellular infiltration and the fundic glands are irregularly arranged with wide spaces in between. These results indicated damaged cells and tissues in the stomach fundus of the gastrointestinal tract after administration of the conventional commercial DS tablets. Photomicrographs of rabbit stomachs after administration of formulations A and B show that the mucosa is covered by a mucous layer and that both the surface epithelium and the fundic glands are intact but display mild hyperemia. Comparison to previous results clearly revealed that the administration of DS tablets in the form of formulations A and B reduced the erosion of the mucous membrane of the fundus, hemorrhaging, and cellular infiltration of the lamina propria. In addition, the fundic glands remained intact in comparison to when commercial tablets were administered.

Figure 6 shows the normal pylorus of an untreated rabbit stomach. The mucosa is covered by an intact, continuous epithelium layer and an underlying healthy

lamina propria. Pyloric ducts extend into the lamina propria and the secretory portions of pyloric glands are transversely cut. Histopathological examination of the rabbit stomach pylorus (Figure 6) after administration of commercial tablets revealed that the surface columnar epithelium had necrotic ulceration and both hyperemia and cellular infiltration in the lamina propria. In addition, the underlying pyloric glands were disrupted. Once again, these results indicate damaged cells and tissues in the pyloric portion of the stomach after administration of the conventional commercial DS tablets. Photomicrographs of the rabbit stomach pylorus after administration of formulations A and B (Figure 6) show that the mucosa is covered by healthy, intact epithelium, pyloric ducts, and pyloric glands. That said, the lamina propria displays mild hyperemia with a trace of cellular infiltration. The preceding results demonstrated that the administration of DS in formulations A and B reduces progressive necrotic ulceration and cellular infiltration in the lamina propria of the stomach. Furthermore, disruption of the underlying pyloric glands is absent. However, mild hyperemia is present.

Histological examination of both the fundus and pylorus of rabbit stomachs revealed no histological alterations in mucous surface cells and glands following administration of formulations A and B. In contrast, when the commercial formulation was administered the stomach wall had a disrupted mucous layer, necrotic ulceration, hemorrhaging, and inflammatory cell infiltration along the base of the gastric glands.

This study clearly indicated that formulations A and B did not produce any ulcerative effect where the structural integrity of the stomach was completely intact. These results prove that the presence of pectin and mastic in formulation A or sodium alginate and

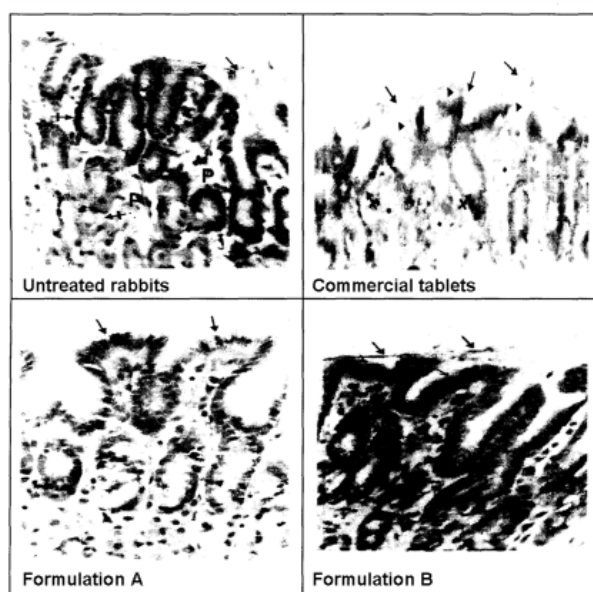


Figure 5. Photomicrographs of rabbit stomach fundus after administration of a signal dose of different formulations.

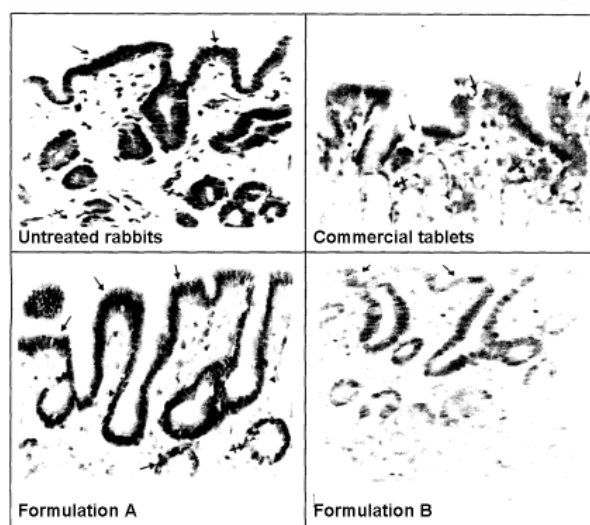


Figure 6. Photomicrographs of rabbit stomach pylorus after administration of a signal dose of different formulations.

mastic in formulation B act to protect the mucous layer of the stomach. This gastroprotective action may be due to the lining of the stomach surface by the gel-forming materials pectin and sodium alginate and/or the oily gum resin of mastic. In addition, mastic has cytoprotective and mild antisecretory properties as evidenced in experimentally induced gastric and duodenal ulcers in rats (23) and both pectin and sodium alginate have gastroprotective action (24-27).

4. Conclusion

In conclusion, formulation A (containing pectin and mastic) and formulation B (containing sodium alginate and mastic) proved satisfactory as evident in their controlled release, acceptable stability, good bioavailability, and prevention of gastric ulcers. These formulations may thus lead to improved patient compliance.

References

- Vadas EB. Stability of pharmaceutical products. In: Remington: The science and Practice of Pharmacy, 20th ed. (Gennaro AR, ed.). Lippincott Williams and Wilkins, Philadelphia, Chapter 52, 2000.
- de Medeiros ACD, de Cervantes NAB, Gomes APB, Macedo RO. Thermal stability of prednisolone drug and tablets. *J Therm Anal Cal.* 2001; 64:745-750.
- Vecchio S, Rodante F, Tomassetti M. Thermal stability of disodium and calcium phosphomycin and the effects of excipients evaluated by thermal analysis. *J Pharm Biomed Anal.* 2001; 24:1111-1123.
- Long GT, Vyazovkin S, Gamble N, Wight A. Hard to swallow dry: kinetics and thermal decomposition of acetylsalicylic acid. *J Pharm Sci.* 2002; 91:800-809.
- Rodante F, Vecchio S, Catalani G, Tomassetti M. Compatibility between active components of a commercial drug. *Farmaco.* 2002; 57:833-843.
- Zohuriaan MJ, Shokrolahi F. Thermal studies on natural and modified gums. *Polym Test.* 2004; 23:575-579.
- Sivalingam G, De P, Parthik R, Madras G. Thermal degradation kinetics of vinyl polperoxide copolymers. *Polym Degrad Stab.* 2004; 84:173-179.
- Li L, Guan C, Zhang A, Chen D, Qing Z. Thermal stabilities and the thermal degradation kinetics of polyimides. *Polym Degrad Stab.* 2004; 84:369-373.
- Barreto Gomes AP, Souza FS, Macedo RO. Thermal and dissolution kinetics of ampicillin drug and capsules. *J Thermal Anal Cal.* 2003; 72:545-548.
- Macedo RO, Do Nascimento TG, Aragao CFS, Gomes APB. Application of thermal analysis in the characterization of anti-hypertensive drugs. *J Thermal Anal Cal.* 2000; 59:657-661.
- Macedo RO, Do Nascimento TG, Veras JWE. Comparison of generic hydrochlorothiazide formulations by means of TG and DSC coupled to photovisual system. *J Thermal Anal Cal.* 2001; 64:757-763.
- de Souza NAB, de Medeiros AC, Basilio Jr ID, Medeiros ACD, Oliveira EJ, Santos AFO, Macwdo RO, Macedo RO. Thermal stability of metronidazole drug and tablets. *J Thermal Anal Cal.* 2003; 72:535-538.
- Liu CH, Kao YH, Chen SC, Sokoloski TD, Sheu MT. *In vitro* and *in vivo* studies of the DS controlled-release matrix tablets. *J Pharm Pharmacol.* 1995; 47:360-364.
- Hasan M, Ootom S, Najib N, Sallam E. A two-way cross-over bioequivalence study of diclofenac sodium suppositories in healthy human volunteers. *Basic Clin Pharmacol Toxicol.* 2004; 95:263-265.
- Mukherjee B, Mahapatra S, Das S, Roy G, Dey S. HPLC detection of plasma concentrations of diclofenac in human volunteers administered with povidone-ethylcellulose-based experimental transdermal matrix-type patches. *Exp Clin Pharmacol.* 2006; 28:301-306.
- Yong CS, Oh Y, Kim YI, Kim JO, Yoo B, Rhee J, Lee KC, Kim D, Park Y, Kim C, Choi H. Physicochemical characterization and *in vivo* evaluation of poloxamer-based solid suppository containing DS in rats. *Int J Pharm.* 2005; 301:54-61.
- Sarvavanan M, Bhaskar K, Maharajan G, Pillai KS. Ultrasonically controlled release and targeted delivery of DS *via* gelatin magnetic microspheres. *Int J Pharm.* 2004; 282:71-82.
- Espenson JH. Chemical Kinetics and Reaction Mechanisms. McGraw-Hill Book Company, New York, USA, Chapter 2, 1981.
- Kirkwood BR. Essential of Medical Statistics. The Blackwell Science Ltd., UK, 1988; pp. 41-57.
- Bancroft JD, Gamble M. Theory and Practice of Histological Techniques, 5th ed.. Churchill Livingstone, London, UK, 2002; p. 130.
- Efentakis M, Koligliati S, Vlachou M. Design and evaluation of drug coated drug delivery systems with an impermeable cup, swellable top layer and pulsatile release. *Int J Pharm.* 2006; 311:147-156.
- Rani M, Mishra B. Comparative *in vitro* and *in vivo* evaluation of matrix, osmotic matrix, and osmotic pump tablets for controlled delivery of DS. *AAPS PharmSciTech.* 2004; 5:e71.
- Al-Said MS, Ageel AM, Parmar NS, Tariq M. Evaluation of mastic, a crude drug obtained from *Pistacia lentiscus* for gastric and duodenal anti-ulcer activity. *J Ethnopharmacol.* 1986; 15:271-278.
- Khotimchenko MY, Zueva EP, Lopatina KA, Khotimchenko YS, Shilova NV. Gastroprotective effect of pectin preparations against indomethacin-induced lesions in rats. *Int J Pharmacol.* 2006; 2:471-476.
- Krylova S, Khotimchenko YS, Zueva E, Amosova E, Razina T, Efimova L, Khotimchenko M, Kovalyov V. Gastroprotective effect of natural non-starch polysaccharides. *Bull Exper Biol Med.* 2006; 142:454-457.
- Galati EM, Monforte MT, Miceli N, Mondello MR, Taviano MF, Galluzzo M, Tripodo MM. *Opuntia ficus indica* (L.) Mill. mucilages show cytoprotective effect on gastric mucosa in rat. *Phytotherap Res.* 2007; 21:344-346.
- Yegin BA, Moulari B, Durlu-Kandilci NT, Korkusuz P, Pelleguer Y, Lamprecht A. Sulindac loaded alginate beads for a mucoprotective and controlled drug release. *J Microencapsul.* 2007; 24:371-382.

(Received January 4, 2010; Accepted February 26, 2010)

Original Article

Biopharmaceutical evaluation of formulated metformin/rosiglitazone tablets

Howida K. Ibrahim^{1,*}, Ahmed M. Attia², Mahmoud M. Ghorab¹

¹ Department of Pharmaceutics and Industrial Pharmacy, Faculty of Pharmacy, Cairo University, Cairo, Egypt;

² Chemical Industrial Development Company (CID), Cairo, Egypt.

ABSTRACT: The study aimed to combine two antidiabetic agents with different mechanisms of action, namely, metformin HCl and rosiglitazone maleate, in a tablet to improve glycemic control in patients with type II diabetes. The preformulation study started with development and validation of an HPLC method for the determination of both drugs in the mixture. The results of visual inspection, TLC, DSC, and FT-IR verified the absence of any physical or chemical interaction between both compounds. Four compatible excipients were selected for the formulation of the tablets by wet granulation according to a 2² factorial design. The prepared tablet blends were acceptable in terms of the modal size of particle distribution, bulk density, Hausner's ratio, Carr's index, and flowability. All formulations fulfilled the pharmacopoeial specifications for weight variation, content uniformity, friability, and hardness. They released 100% of the drug during the first 45 min, displaying higher dissolution efficiency than commercially available Rosiplus tablets. The tablet formulation that passed the physical and chemical stability study for 24 months at ambient conditions was tested *in vivo* on healthy volunteers in a cross-over design. Statistical analysis proved that the prepared tablets were bioequivalent to the commercial ones in terms of both the rate and the extent of absorption.

Keywords: Wet granulation, factorial design, stability study, bioavailability

1. Introduction

Non-insulin-dependent (Type 2) diabetes mellitus is a heterogeneous disorder characterized by an underlying

*Address correspondence to:

Dr. Howida Kamal Ibrahim, Department of Pharmaceutics and Industrial Pharmacy, Faculty of Pharmacy, Cairo University, Kasr El Aini Street, Cairo 11562, Egypt.

e-mail: Howidakamal@gmail.com

insufficiency of insulin. This insufficiency results from defective insulin utilization and can be corrected by diet control, exercise, and administration of one or more of the currently available oral hypoglycemic agents (1).

Metformin (dimethylbiguanide) is an antihyperglycaemic drug used to treat non-insulin-dependent diabetes mellitus. It acts in the presence of insulin to increase glucose utilization and reduce glucose production, thereby counteracting insulin resistance. The effects of metformin include increased glucose uptake, oxidation and glycogenesis by muscle, increased glucose metabolism to lactate by the intestine, reduced hepatic gluconeogenesis, and possibly a reduced rate of intestinal glucose absorption (2,3). Metformin absorption is limited to the upper gastrointestinal (GI) tract, thus requiring suitable delivery systems providing complete release during stomach-to-jejunum transit (4).

Rosiglitazone is a thiazolidinedione. It improves insulin resistance by activating the nuclear peroxisome proliferator activated receptor- γ (PPAR- γ), resulting in increased glucose uptake in muscle and reduced endogenous glucose production. Rosiglitazone has been shown to be active as a monotherapy, in combination therapy with metformin or sulfonylureas, and even in triple therapy (5-7).

A review of the literature revealed a lack of data on the stability of rosiglitazone maleate in combination with metformin-HCl and the compatibility of both drugs with commonly used tablet excipients. Thus, the aim of this work was to combine those two different, yet complementary, oral antidiabetic agents in a single stable and bioavailable tablet form to improve blood sugar control in patients with type 2 diabetes and to ensure patient compliance.

2. Materials and Methods

2.1. Materials

Rosiglitazone maleate and metformin-HCl were obtained from Sri Venkateswara Co., Bollaram, India and Dr. Reddy Ltd., Andhra, India, respectively. PVP-K90, magnesium stearate, and talc were from Prolabo, France. Spray-dried lactose was from Meggle,

Germany. Avicel PH 102 and starch were from FMC, PA, USA. Liquid paraffin was from El-Nasr Pharmaceutical Chemical Co., Cairo, Egypt. Methanol, butanol, and acetic acid were from E. Merck, Germany. HPLC grade solvents (methanol and acetonitrile) were from Sigma-Aldrich Chemical Co., USA. Rosiplus® tablets were obtained from Sabaa Company, Egypt, batch #10651.

2.2. Preformulation studies

2.2.1. Compatibility study of rosiglitazone maleate and metformin-HCl

Thin layer chromatography (TLC) – Five μL samples of test and standard solutions of both drugs were spotted on the loading zone of a silica gel plate at an adequate distance from each other. A solvent system consisting of a 2:4:1 mixture of distilled water:butanol:acetic acid was freshly prepared and allowed to run for 10 cm. The plate was then dried and examined under a UV lamp at a wavelength of 254 nm.

Fourier transform-infrared spectroscopy (FT-IR) – The KBr disc technique was used for sample preparation. Sample spectra were collected in the range of 4,000 and 500 cm^{-1} using a Perkin-Elmer 1600 spectrophotometer (Bruker, Coventry, UK). Collected spectra were smoothed and baseline-corrected.

Differential scanning calorimetry (DSC) – DSC thermograms of samples were recorded using a DSC-7 calorimeter (Perkin-Elmer, Norwalk, USA). Samples of 3-4 mg of the pure drugs and a 1:1 physical mixture of rosiglitazone maleate:metformin-HCl were placed in an aluminium pan and heated to a temperature of 350°C at a rate of 10°C/min, with indium in the reference pan in an atmosphere of nitrogen.

2.2.2. HPLC determination of rosiglitazone and metformin

In vitro determination – Rosiglitazone maleate and metformin-HCl were assayed in a mixture using a method of HPLC as previously reported (8). The assay was carried out using a Waters 2790 HPLC system for extraction and Shimadzu LC-10AD VP pumps for analysis. Samples were eluted on a Nova-pak C₁₈ column using acetonitrile:0.01 M phosphate buffer (50:50, v/v) at a flow rate of 1 mL/min at 40°C, followed by detection at 254 nm. Calibration curves were prepared and assayed in triplicate on three different days to evaluate linearity, precision, and accuracy.

In vivo determination – The metformin content was determined using the aforementioned HPLC method

used *in vitro* after generating a calibration curve using blank plasma. The plasma was spiked with different amounts of metformin-HCl in methanol. The mixture was then centrifuged at 3,000 rpm for 10 min and the supernatant (organic phase) was transferred to another clean tube and evaporated to dryness at 40°C. The residue was then reconstituted in 1 mL of methanol and the concentration of 10 μL of the final solution was determined based on the reported peak areas (9).

2.2.3. Compatibility study of both drugs with different tablet excipients

A physical mixture of rosiglitazone maleate:metformin-HCl in a 2:500 weight ratio was prepared alone and in combination with other tablet excipients in a drug-to-excipient ratio of 1:1. The tested excipients were Avicel PH 102, spray-dried lactose, PVP-K90 magnesium stearate, talc, dicalcium phosphate, and starch. The prepared mixtures were evaluated *via* visual inspection, DSC and FT-IR.

2.3. Formulation of rosiglitazone and metformin tablets

2.3.1. Experimental design

A 2² full factorial design was used to prepare rosiglitazone/metformin tablets using four compatible excipients. Two independent variables were used, namely, the binder type (PVP-K90, starch) and the lubricant type (Mg stearate, talc). Drug concentrations were kept constant at 2.649 mg rosiglitazone maleate (equivalent to 2 mg rosiglitazone base) and 500 mg metformin-HCl per tablet. The composition of the four prepared tablet formulations is shown in Table 1. Statistical analysis of the results was performed using statistical software (Statview Abacus Concept, version 4.57). Analysis of variance (including the sum of squares), subsequent significance tests, and the calculation of average values was done using this software.

2.3.2. Characterization of the blends to be compressed

The formulation blends were mixed in a mortar using the geometrical dilution technique and were characterized in terms of their particle size, %

Table 1. Composition of metformin/rosiglitazone tablets according to the experimental design used

Ingredient/tablet (mg)	Tablet formulation			
	1	a	b	ab
Metformin-HCl	500	500	500	500
Rosiglitazone maleate*	2.649	2.649	2.649	2.649
Starch	–	26	–	26
PVP-K90	26	–	26	–
Mg stearate	–	–	6	6
Talc	6	6	–	–

* 2.649 mg rosiglitazone maleate = 2 mg rosiglitazone base.

compressibility, and flowability. The particle size was determined using a laser diffraction particle size analyzer (Master sizer, Malvern, UK). The volume occupied by 5 g of each blend (bulk volume V_b) and the true volume after tapping in a graduated cylinder (tapped volume V_t) were determined and used to calculate (a) the bulk density by dividing the weight of the powder being tested by V_b , (b) Hausner's ratio given by dividing V_b by V_t , and (c) % compressibility (Carr's index) determined by $(1 - V_t/V_b) \times 100$.

The flowability of the prepared blends was calculated using the fixed height cone method. The angle of repose was calculated from the equation:

$$\tan \theta = 2h/D$$

where, D is the average diameter of the formed cone and h = 2.5 cm.

2.3.3. Tablet compression

Direct compression – Accurately weighed amounts of rosiglitazone and metformin were mixed using a mortar and a pestle for 5 min. The specified binder was then mixed by geometric dilution for an extra 5 min. Talc or magnesium stearate was added and the blends were compressed using a single-punch tablet machine and 20 mm oblong punches and dies (HEYNAU single station press, 5v1m, Germany). The compression force was kept constant at 10 kpsi.

Wet granulation – A mixture of the two drugs was geometrically mixed with the specified amount of the binder and kneaded using 300 mg isopropyl alcohol/tablet. The resultant mass was passed through a 1-cm sieve to produce granules with a particle size of 780 μ m and dried in a hot air oven at 60°C for 20 min. The dried mass was passed through a 1-mm sieve and finally mixed with the specified lubricant. The blend was compressed with a single punch tablet machine using 20 mm oblong punches and dies. The compression force was kept constant at 10 kpsi. A film coating was then applied to the compressed tablets using a simplified BYC-1000 coating machine, JiangSu TaiZhou Medicines Machinery Factory, in order to improve tablet aesthetics. The coat weighed 10 mg and consisted of HPMC, talc, PG, PEG, red iron oxide, and titanium dioxide after dissolution in ethanol.

2.4. Evaluation of compressed tablets

2.4.1. Weight, thickness, and diameter variation

The weight, thickness, and diameter of twenty coated tablets of each formulation were individually measured. The mean value of each measurement was calculated, with the variation serving as the relative standard deviation (% RSD).

2.4.2. Content uniformity

The content uniformity was determined by crushing ten tablets of each formulation. An accurately weighed amount corresponding to the weight of one tablet was dissolved in 100 mL methanol. The solution was then passed through a 0.45- μ m membrane filter, properly diluted, and assayed using the previously described HPLC method.

2.4.3. Friability

Ten tablets of each formulation were accurately weighed and placed in the drum of a friabilator and rotated at 25 rpm for a period of 4 min. The tablets were then brushed and reweighed. The percentage loss in weight was calculated and served as a measure of friability.

2.4.4. Hardness

Ten tablets of each formulation were tested for hardness using a Monsanto tablet hardness tester, USA. The mean hardness in kilograms was then determined.

2.4.5. Disintegration time

The disintegration time for each of six tablets of each formulation was determined using a USP disintegration tester (Pharma Test, Type PTZ2, Germany) in accordance with standard testing procedures.

2.4.6. In vitro dissolution study

The dissolution of the prepared tablets was performed using the USP XXVIII rotating basket, at a speed of 100 rpm in 900 mL N/10 HCl (pH 1.2) and at a temperature of $37 \pm 0.5^\circ\text{C}$. The study was conducted on 6 tablets for 1 h and aliquots, each of 3 mL, were withdrawn at appropriate time intervals from the dissolution medium and replaced with an equivalent amount of the freshly heated medium. The samples were analyzed for metformin and rosiglitazone content using the proposed HPLC method.

For assessment and comparison, the dissolution profiles were evaluated on the basis of the dissolution efficiency parameter at 1 h (DE_{1h}) as described by Khan *et al.* (10) according to the following equation:

$$DE = \int_0^t \frac{y \cdot dt}{y_{100} t} \times 100 \quad (\text{Eq. 1})$$

where the integral in equation 1 is the area under the dissolution curve up to the dissolution time t and y_{100} is the area of the rectangle described by 100% dissolution at the same time.

Kinetic analysis of the dissolution data for all formulations was performed using the linear regression

method. The determination coefficients (r^2) according to zero-order, first-order, Higuchi (11), Hixson-Crowell (12), and Korsmeyer-Peppas (13) models were computed for each formulation.

2.5. Stability study

The four prepared tablet formulations were subjected to a long-term physical and chemical stability study (24 months at ambient temperature and humidity). Tablet samples were collected at time intervals of 2, 6, 12, and 24 months and inspected visually for any changes in colour and/or appearance. The tablets were evaluated for the percent of remaining rosiglitazone and metformin using the proposed HPLC method of analysis as well as for weight variation, thickness, diameter, hardness, and disintegration time and *in vitro* dissolution tests as previously mentioned for the freshly prepared tablets. To detect any significant variations in the dissolution profiles, the similarity factor f_2 (14) was calculated from the mean dissolution data according to the following equation:

$$f_2 = 50 \log \left\{ \left[1 + \frac{1}{n} \sum_{n=1}^n W_i (R_i - T_i)^2 \right]^{-0.5} \times 100 \right\}$$

(Eq. 2)

where n is the number of pull points, W_i is an optional weight factor, and R_i is the reference profile that is considered similar. The value of f_2 should be between 50 and 100. An f_2 of 100 suggests that the test and reference profiles are identical. Conversely, f_2 decreases as the dissimilarity between two release profiles increases.

The formulation of choice was subjected to an accelerated stability study to predict its shelf life. Tablets were stored in ovens at temperatures of 50, 60, and 70°C. Samples were collected after 2, 4, and 6 months for each working temperature and analyzed for both active ingredients. The method of Free and Blythe was used, *i.e.*, the time required for the drug to fall to 90% of its original concentration was determined at the three temperatures by plotting the log percent of drug remaining with respect to time. The log time to $t_{90\%}$ was then plotted with respect to $1/T$ and the shelf life was the time at 25°C.

2.6. In vivo study

The performance of the selected tablet formulation in comparison to the commercial tablet formulation (Rosiplus tablets, batch No. 10651, Sabaa Pharm, Egypt) was evaluated in human volunteers. Comparison was done through the quantification of metformin in plasma. The bioequivalence between both formulations was assessed by calculating individual C_{\max} , $AUC_{(0-24h)}$, $AUC_{(0-\infty)}$, and $C_{\max}/AUC_{(0-24h)}$ ratios (test/reference)

together with their mean and 90% confidence intervals (CIs). The inclusion of the 90% CI for the ratio in the 80 to 125% range was analyzed using ANOVA.

The study involved six healthy male volunteers with ages between 21 and 42 years (mean \pm S.D., 31.3 \pm 3.7 years). The height of the volunteers ranged from 145.0 to 165.0 cm (mean \pm S.D., 156.7 \pm 6.9 cm) and their body weight ranged from 55.1 to 87.8 kg (mean \pm S.D., 71.3 \pm 8.1 kg). The volunteers did not suffer from significant cardiac, hepatic, renal, pulmonary, neurological, gastrointestinal, or hematological diseases. The study protocol was approved by the University Committee for the Protection of Human Subjects and it complies with the Declarations of Helsinki and Tokyo for humans.

The study was conducted in an open, randomized, two-period crossover fashion with a 2-week washout period between doses. Blood samples (10 mL) from a suitable antecubital vein were collected before and 0.5, 1.5, 2, 2.5, 3, 3.5, 6, 8, 12, and 24 h after the administration of each dose. The blood samples were centrifuged at 2,500 \times g for 10 min at room temperature and the plasma was decanted and stored at -20°C until assayed. All samples from a single volunteer were analyzed on the same day to avoid inter-assay variation.

3. Results and Discussion

3.1. Preformulation studies

3.1.1. Compatibility study of rosiglitazone maleate and metformin-HCl

The spots on the TLC plate of the test solutions corresponded to those of standard solutions with the same intensity and R_f , indicating the absence of interaction between the two drugs.

The DSC thermograms of rosiglitazone and metformin showed endothermic peaks at 75.96 and 241.42°C, respectively, corresponding to the melting of both drugs (Figure 1). The two peaks persisted in the DSC thermogram of the 1:1 rosiglitazone:metformin physical mixture. This indicates the absence of physical interactions between the two active ingredients.

The infrared spectra of rosiglitazone, metformin, and their 1:1 physical mixture are shown in Figure 2. The spectrum of the physical mixture exhibited characteristic bands corresponding to the functional groups of both drugs, indicating the absence of any chemical interaction between them.

3.1.2. Determination of rosiglitazone and metformin in combination

The retention time for rosiglitazone and metformin was approximately 2.89 and 5.21 min, respectively.

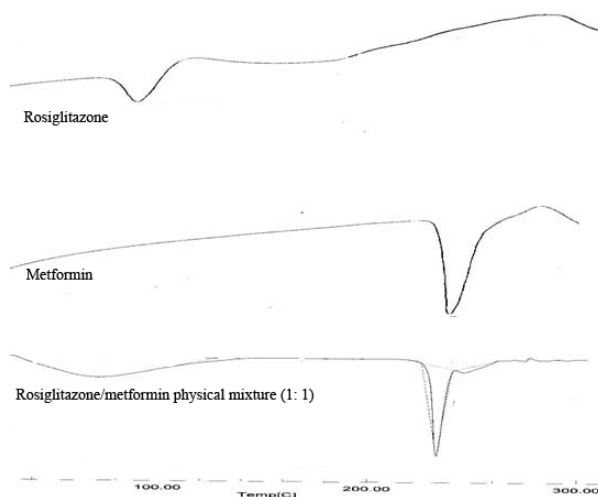


Figure 1. Compatibility study of rosiglitazone and metformin using differential scanning calorimetry.

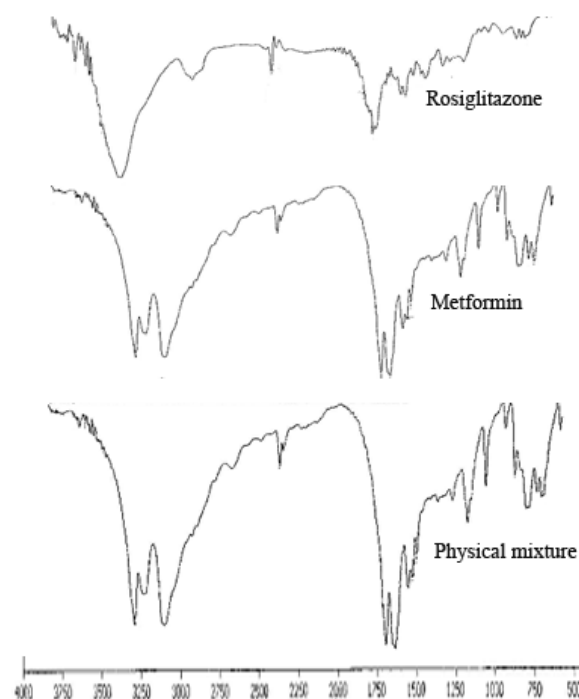


Figure 2. Compatibility study of rosiglitazone and metformin using FT-IR spectroscopy.

The proposed HPLC method was accurate, precise, and rugged, as shown in Table 2.

3.1.3. Compatibility study of both drugs with different tablet excipients

No changes in color or appearance (*e.g.* caking, liquefaction, and formation of clumps) were noted for any of the aforementioned pharmaceutical excipients, indicating good physical stability.

Figure 3 illustrates the DSC thermograms, where the thermal properties of the mixtures of magnesium stearate, starch, talc, and PVP-K90 with drug combination were the sum of the individual components. Few changes in the transition temperatures resulted from the mixing of the two components; the process of mixing was found to reduce the purity of each of the components and thus cause a slight lowering of the melting endotherms.

In contrast, samples of Avicel PH 102, spray-dried lactose and dicalcium phosphate either had additional peaks or the drugs' peaks were masked, so these samples were excluded from further investigations.

Similarly, the infrared spectra indicated the absence of interaction between the combined drugs with all the tested excipients except avicel, anhydrous lactose, and dicalcium phosphate (data not shown).

3.2. Formulation of rosiglitazone and metformin tablets

3.2.1. Characterization of the blends to be compressed

Analysis of random samples of the four prepared blends indicated adequate uniformity of mixing. The evaluation parameters for the four tablet blends are shown in Table 3.

The modal size of particle distribution was 77.78, 32.52, 65.43, and 59.61 μm for tablet formulations 1, a, b, and ab, respectively. PVP-K90 produced blends with markedly larger mean particle sizes than those containing starch (formulations a and ab) due to its larger particle size.

Values for Carr's index ranged from 17.89-21.69%

Table 2. Precision and accuracy of the HPLC method for the determination of rosiglitazone and metformin in a mixture

Concentration ($\mu\text{g/mL}$)	Mean	S.D.	Precision (CV)	Accuracy (%)	Mean	S.D.	Precision (CV)	Accuracy (%)	
Metformin	Intraday (within batch) ($n = 3$)				Interday (between batches) ($n = 3$)				
	10	9.95	0.46	4.62	99.5	9.88	0.53	5.36	98.8
	20	19.71	1.664	8.44	98.55	19.04	1.72	9.03	95.2
	30	31.51	1.80	5.71	105.03	30.9	1.21	3.92	103
Rosiglitazone	Intraday (within batch) ($n = 3$)				Interday (between batches) ($n = 3$)				
	2	1.97	0.14	7.11	98.5	1.92	0.23	11.98	96
	3	3.02	0.36	11.92	100.67	3.12	0.38	12.18	104
	5	4.93	0.27	5.47	98.6	4.76	0.33	6.93	95.2

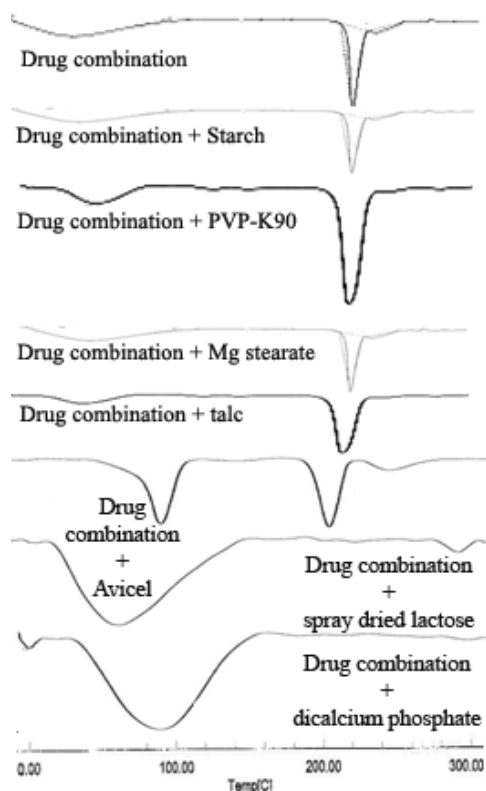


Figure 3. DSC thermograms of rosiglitazone/metformin in combination with different tablet excipients.

Table 3. Evaluation parameters for the prepared tablet blends

Formulation	Modal size of particle distribution	Bulk density (g/mL)	Hausner Ratio	Carr's index	Angle of repose (θ)
1	77.78	0.732	1.220	17.896	34.61
a	32.52	0.469	1.250	20.042	35.03
b	65.43	0.750	1.225	18.367	34.14
ab	59.61	0.461	1.277	21.687	34.45

indicating good flow characteristics. However, Carr's index is a one-point determination and does not reflect the ease or speed with which consolidation occurs. Indeed, some materials have a high index, suggesting a poor flow, but may consolidate rapidly; such a property is essential for uniform filling in a machine. Hausner's ratio relates to interparticle friction and can be used to predict powder flow properties. The recorded values ranged from 1.22 to 1.25, indicating that powders had a low interparticle friction. The tested blends had a similar angle of repose and the range of that angle indicated a reasonable flow (34.14°-35.03°).

Statistical analysis of the aforementioned data is summarized in Table 4. Results showed that the binder type, the lubricant type, and their interaction had a significant effect on both Hausner's ratio and Carr's index. Using PVP-K90 as a binder and talc as a lubricant significantly decreased Carr's index and Hausner's ratio, indicating better flowability and compressibility, respectively. Only the lubricant

Table 4. ANOVA results of factorial experiments

Source	Response (Probability > F)			
	Bulk density	Carr's index	Hausner's ratio	Angle of repose
Binder type	< 0.0001 ^a	0.43	0.0716	< 0.0001 ^a
Lubricant type	0.2005	0.374	0.834	< 0.0001 ^a
Binder type * Lubricant type	0.6727 ^a	0.329	0.1482	< 0.0001 ^a

^a Significant at a level of $p < 0.05$.

type had a significant effect on the bulk density. In comparison to Mg stearate, Talc significantly decreased the bulk density of the tablet blends. None of the tested variables had a significant effect on the angle of repose.

3.2.2. Method of preparation

Direct compression was attempted due to its advantages, like simplicity, but it produced friable tablets regardless of the excipients used and was thus excluded. Wet granulation produced tablets with good physical characteristics.

3.3. Evaluation of the prepared tablets

3.3.1. Physical properties of tablets

Relative standard deviation (% RSD) values for the mean tablet weights ranged from 0.02-0.11% for the four formulations, indicating a high level of weight uniformity. Similarly, the % RSD for the mean tablet thickness and diameter was very low (in the range of 0.04-0.08 and 0.05-0.08%, respectively).

The average drug content for all formulations complied with the pharmacopoeial limits in a range of 85% to 115% of the label claim, and the standard deviation was less than 6%. Similarly, the percent friability of all formulations was less than 0.5%, which conforms to the acceptable range for compressed tablets. All the prepared formulations had a narrow range for both the disintegration time and the hardness ranging from 7.5 to 9.1 kg.

One-way ANOVA was performed to evaluate the effect of the tested factors on the different physical properties of the prepared tablets. The binder type had a significant effect on tablet friability, hardness, and disintegration time. Starch-based tablets showed significantly greater hardness, lower friability, and slower disintegration compared to those containing PVP-K90. This could be attributed to the higher binding properties of starch. The lubricant type and its interaction with the binder type did not have a significant effect on the tested variables (data not shown).

3.3.2. In vitro dissolution study

The dissolution profiles of rosiglitazone and metformin from the prepared tablets and from the commercial

Rosiplus[®] tablets in 0.1 N HCl are illustrated in Figure 4. The dissolution efficiency (DE_{1h}) is listed in Table 5. The four tablet formulations released 100% of their loadings of both drugs in 45 min. The DE_{1h} values are in accordance with the tablets' physical properties; a higher dissolution efficiency was noted for tablets with less hardness and higher % fines (PVP-K90 based tablets).

The dissolution profile of the commercial tablets revealed a lower dissolution efficiency and the tablets did not completely disintegrate by the end of the dissolution test (1 h).

Drug dissolution data for all formulations were evaluated using various mathematical models. According to the highest determination coefficient (r^2), the dissolution of both rosiglitazone and metformin from the prepared tablets generally fits the Korsmeyer-Peppas and Higuchi diffusion models best. Results for the diffusion exponent (n) indicated that the release of both drugs was generally controlled by a non-Fickian transport mechanism that involves both diffusion and dissolution mechanisms. The exponent " n " values ranged 0.765-0.851 for rosiglitazone and 0.609-0.661

for metformin. Formulations containing starch as a binder had higher values of " n ".

3.4. Stability study

All the stored tablets retained the same physical properties as fresh ones except for those containing talc (formulations 1 and a). Those tablets had a marked decrease in tablet hardness and an increase in their disintegration times upon storage, which could be attributed to moisture absorption. The residual drug loadings remained within the accepted official limits. All the dissolution profiles had high levels of similarity at the different time intervals, indicating good stability. The f_2 values ranged between 91.3 and 95 for rosiglitazone and 92 and 97.6 for metformin.

Based on the stability study and the *in vitro* evaluations results, formulations 1 and a were excluded due to their physical instability. Formulation b had a greater extent of dissolution in relation to formulation ab and was selected for *in vivo* evaluation.

Table 6 summarizes the accelerated stability study

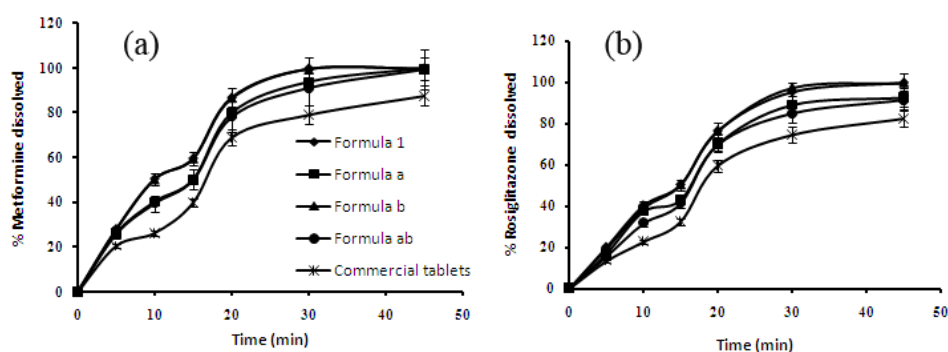


Figure 4. *In vitro* dissolution profiles of metformin (A) and rosiglitazone (B) from the prepared tablets and commercial Rosiplus tablets.

Table 5. *In vitro* evaluation parameters for the prepared rosiglitazone/metformin tablets

Formulation	Friability (% fines)*	Hardness (kg)*	Disintegration time (min)**	DE_{1h} (%)	
				rosiglitazone	metformin
1	0.161 ± 2.01	7.50 ± 0.424	8 ± 0.990	75.96	80.63
a	0.088 ± 1.11	8.95 ± 0.354	11 ± 1.414	71.13	76.69
b	0.136 ± 1.23	8.2 ± 0.707	7.5 ± 2.121	76.25	80.61
ab	0.072 ± 2.1	9.1 ± 0.707	10.1 ± 1.131	69.13	75.84

* Values are mean ± S.D., $n = 10$, ** $n = 6$.

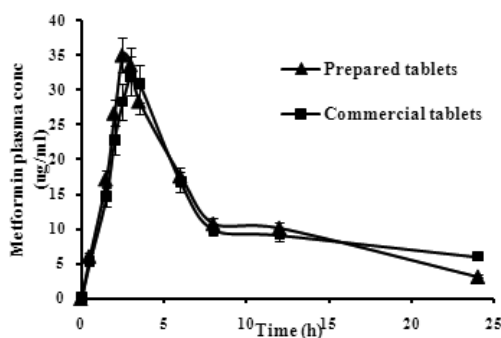
DE_{1h} for the commercial tablets = 60.55 for rosiglitazone and 66.23 for metformin.

Table 6. Results of an accelerated stability study

Storage temperature (°C)	% drug remaining at the following time intervals			$t_{90\%}$	Shelf life (months)
	2 months	4 months	6 months		
Metformin					
50	97.2 ± 1.45	95.5 ± 2.51	93.32 ± 1.77	7.413	51.28
60	95.5 ± 2.06	89.1 ± 2.99	85.12 ± 2.43	3.98	
70	87.1 ± 2.51	79.4 ± 1.87	69.2 ± 2.55	1.86	
Rosiglitazone maleate					
50	97.7 ± 1.67	94.4 ± 1.55	91.2 ± 2.66	7.079	39.8
60	94.4 ± 2.07	88.1 ± 2.54	83.17 ± 1.67	3.65	
70	87 ± 2.66	75.8 ± 1.52	66.8 ± 2.11	1.78	

Table 7. Summary of metformin pharmacokinetic parameters and the results of statistical analysis

Parameter	Means \pm S.D.		Ratio of means	
	Prepared tablets	Commercial tablets	Point estimate	90% CI
C_{max} ($\mu\text{g/mL}$)	36.535 \pm 5.385	32.322 \pm 4.529	113.054	111.29, 114.817
$AUC_{(0-24)}$ ($\mu\text{g}\cdot\text{h/mL}$)	282.515 \pm 4.940	261.335 \pm 4.345	106.584	104.701, 108.466
$AUC_{(0-\infty)}$ ($\mu\text{g}\cdot\text{h/mL}$)	287.870 \pm 7.012	269.940 \pm 6.057	–	–
t_{max} (h)	2.667 \pm 0.258	3.250 \pm 0.274	–	–
$t_{1/2}$ (h)	2.725 \pm 0.389	2.625 \pm 0.530	–	–
k (h^{-1})	0.257 \pm 1.036	0.267 \pm 1.058	–	–

**Figure 5. Mean plasma concentration-time profiles of metformin after the administration of a single dose.** Error bars indicate S.D., $n = 4$.

results. The data showed that the estimated $t_{90\%}$ values at 25°C were 51.28 and 39.8 months for metformin and rosiglitazone maleate, respectively. Therefore, the shelf life for formulation b is about three years.

3.5. *In vivo* study

The calibration curve of metformin-HCl in plasma was linear in the range of (5-55 $\mu\text{g/mL}$) with $r^2 = 0.9983$. Mean values of metformin plasma concentrations are shown in Figure 5 and the pharmacokinetic parameters are listed in Table 7.

The maximum concentration reached (C_{max}) and the areas under the curve ($AUC_{(0-24h)}$) were compared. The geometric mean and 90% confidence intervals of prepared tablets/commercial tablets ratios are summarized in Table 7. Since the 90% CI for both C_{max} and $AUC_{(0-24h)}$ ratio (test/reference) was inside the 80-125% interval proposed by the US Food and Drug Administration (15,16), the prepared tablets were concluded to be bioequivalent to commercial tablets in terms of both the rate and the extent of absorption.

4. Conclusion

A tablet formulation containing 500 mg metformin-HCl, 2.649 mg rosiglitazone maleate, 26 mg PVP-K90, and 6 mg Mg stearate succeeded both *in vitro* and *in vivo* as a conventional stable and bioavailable tablet for the delivery of both drugs. The formulation can be easily prepared and the excipients used are cheap and

available, indicating its potential for use on a larger scale.

Acknowledgements

Special thanks are extended to the CID Company for providing the metformin and rosiglitazone maleate used in the study.

References

1. Thomas CR, Turner SL, Jefferson WH, Bailey CJ. Prevention of dexamethasone-induced insulin resistance by metformin. *Biochem Pharmacol.* 1998; 56:1145-1150.
2. Bailey CJ. Metformin--an update. *Gen Pharmacol.* 1993; 24:1299-1309.
3. Sirtori CR, Pasik C. Re-evaluation of a biguanide, metformin: mechanism of action and tolerability. *Pharmacol Res.* 1994; 30:187-228.
4. Corti G, Cirri M, Maestrelli F, Mennini N, Mura P. Sustained-release matrix tablets of metformin hydrochloride in combination with triacetyl- β -cyclodextrin. *Eur J Pharm Biopharm.* 2008; 68:303-309.
5. Elte JW, Blicklé JF. Thiazolidinediones for the treatment of type 2 diabetes. *Eur J Intern Med.* 2007; 18:18-25.
6. Ovalle F, Bell DS. Clinical evidence of thiazolidinedione-induced improvement of pancreatic β -cell function in patients with type 2 diabetes mellitus. *Diabetes Obes Metab.* 2002; 4:56-59.
7. Dailey GE, Noor MA, Park JS, Bruce S, Fiedorek FT. Glycemic control with Glyburide/Metformin tablets in combination with rosiglitazone in patients with type 2 diabetes: a randomized, double-blind trial. *Am J Med.* 2004; 116:223-229.
8. Onal A. Spectrophotometric and HPLC determinations of anti-diabetic drugs, rosiglitazone maleate and metformin hydrochloride, in pure form and in pharmaceutical preparations. *Eur J Med Chem.* 2009; 44:4998-5005.
9. Sambol NC, Chiang J, O'Conner M, Liu CY, Lin ET, Goodman AM, Benet LZ, Karam JH. Pharmacokinetics and pharmacodynamics of metformin in healthy subjects and patients with noninsulin-dependent diabetes mellitus. *J Clin Pharmacol.* 1996; 36:1012-1021.
10. Khan KA. The concept of dissolution efficiency. *J Pharm Pharmacol.* 1975; 27:48-49.
11. Higuchi T. Rate of release of medicaments from ointment bases containing drugs in suspensions. *J Pharm Sci.* 1961; 50:874-875.
12. Hixson AW, Crowell JH. Dependence of reaction velocity upon surface and agitation. *Ind Engng Chem.*

- 1931; 23:923-931.
13. Korsmeyer RW, Gurny R, Doelker E, Buri P, Peppas NA. Mechanisms of solute release from porous hydrophilic polymers. *Int J Pharm.* 1983; 15:25-35.
 14. U.S. Department of Health and Human Services, Food and Drug Administration, Center for Drug Evaluation and Research. Guidelines for Industry: Dissolution Testing of Immediate Release Solid Dosage Forms, August 1997.
 15. FDA Guidance for Industry, Bioavailability and Bioequivalence Studies for Orally Administered Drug Products-General Considerations, US Department of Health and Human Services, Food and Drug Administration, Center for Drug Evaluation and Research (CDER), 2000.
 16. FDA Guidance for Industry, Statistical Approaches to Establishing Bioequivalence, US Department of Health and Human Services, Food and Drug Administration, Center for Drug Evaluation and Research (CDER), 2001.
- (Received January 29, 2010; Revised February 25, 2010; Accepted March 2, 2010)*

Original Article**Calcium alginate cross-linked polymeric microbeads for oral sustained drug delivery in arthritis****K. M. Manjanna^{1,*}, T. M. Pramod Kumar², B. Shivakumar³**¹ Department of Pharmaceutics, T. V. M. College of Pharmacy, Bellary Karnataka, India;² Department of Pharmaceutics, J.S.S. College of Pharmacy, JSS University, Mysore, Karnataka, India;³ Department of Pharmaceutical Chemistry, S. C. S. College of Pharmacy, Harapanahalli, Karnataka, India.

ABSTRACT: After the successful optimization and development of a drug entity, design of dosage form then plays an important role. Hence, research continuously keeps on searching for ways to deliver drugs over an extended period of time. With aceclofenac, a novel NSAID used in the treatment of rheumatoid arthritis, frequency of administration may cause certain GI-adverse effects. The objective of the present research work was to develop a microparticulate oral sustained release dosage form, to reduce dosing frequency, to eliminate the dose related adverse effects and to ultimately improve compliance in the pharmacotherapy of arthritis. The microbeads were prepared by an ionotropic external gelation technique, by using sodium alginate as the hydrophilic carrier and calcium chloride as the cross-linking agent. The shape and surface characteristics were determined by scanning electron microscopy (SEM). Particle size distribution was determined by an optical microscope. The physical state of the drug in the formulation was determined by differential scanning calorimetry (DSC). While increasing the concentration of sodium alginate dispersion increased flow properties, mean particle size, swelling ratio and drug entrapment efficiency. The mean particle sizes of drug-loaded microbeads were found to be in the range 596.45 ± 1.04 to $880.10 \pm 0.13 \mu\text{m}$. The drug entrapment efficiency was obtained in the range of 63.24-98.90% (w/v). The release of drug from the microbeads at pH 1.2 is negligible. Under neutral conditions, the beads will swell and the drug release depends on swelling and the erosion process resulting in an optimum level of drug released in a sustained manner which exhibits zero-order kinetics.

Keywords: Oral sustained release, sodium alginate, aceclofenac sodium, ionotropic external gelation, zero-order kinetics

*Address correspondence to:

Dr. K. M. Manjanna, T. V. M. College of Pharmacy, Department of Pharmaceutics, Gandhinagar, Bellary 583103, Karnataka, India.

e-mail: kmhuruli@rediffmail.com

1. Introduction

Arthritis is a term that includes a group of disorders that affect joints and muscles. Arthritis symptoms include joint pain, inflammation and limited movement of joints. When a joint is inflamed it may be swollen, tender, warm to the touch or red. Surrounding each joint is a protective capsule holding a lubricating fluid to aid in motion. Cartilage, a slippery smooth substance, covers most joints to assure an even, fluid motion of the joint. With joint arthritis, the cartilage may be damaged, narrowed and lost by a degenerative process or by inflammation making movement painful (1). Most of the conventional NSAIDs are used in the treatment of arthritis but have short biological half-lives and hence require repeated administration 3 to 4 times a day. This leads to patient non-compliance and also fluctuation in blood level drug concentration.

The design of effective drug delivery systems has recently become an integral part of the development of new medicines. Hence, research continuously keeps on searching for ways to deliver drugs over an extended period of time, with a well-controlled release profile. The oral administration of pharmaceutical dosage forms is the more usual, convenient and comfortable route for active drug delivery to the body. An oral modified release drug-delivery system should be able to achieve optimum therapeutic drug concentration in the blood with minimum fluctuation, to predict and reproduce release rates for extended duration, to enhance pharmacotherapy of short half life drugs, to reduce frequent dosing, to minimize/or eliminate dose related adverse effects, and to improve therapy, safety, efficacy and better patient compliance (2). The use of hydrogel systems for controlling the release of drugs has been increasingly well known to respond to surrounding conditions such as pH, ionic strength, temperature, and frequent changes of environment in the GI-tract, which has a variation of pH from the stomach to intestine. Hydrogels from natural polymers, especially polysaccharides, have been widely used because of their advantageous properties over synthetic polymers such as non-toxicity, biocompatibility, biodegradability, ability

to modify the properties of aqueous environments, and capacity to thicken, emulsify, stabilize, encapsulate, swell, and form gels and films (3). Alginate is one of the natural polysaccharides that has been widely used in numerous biomedical applications. Sodium alginate is a salt of alginic acid, a natural polysaccharide found in all species of brown algae and certain species of bacteria. It is a linear polymer of β -(1 \rightarrow 4) mannuronic acid (M) and α -(1 \rightarrow 4) L-guluronic acid (G) residues in varying proportions and arrangements. It has been shown that the G and M units are joined together in blocks, and as such, the following 3 types of blocks may be found: homo-polymeric G blocks (GG), homo-polymeric M blocks (MM), and hetero-polymeric sequentially alternating blocks (MG). The reactivity with calcium and the subsequent gel formation capacity is a direct function of the average chain length of the G-blocks. Hence, alginates containing the highest GG fractions possess the strongest ability to form gels. This initially arises from the ability of the divalent calcium cation to fit into the guluronate structures like eggs in an "egg box junction". Consequently, this binds the alginate chains together by forming junction zones, sequentially leading to gelling of the solution mixture and bead formation. When aqueous solutions of sodium alginate are added drop wise to an aqueous solution of calcium chloride, it forms a spherical gel with regular shape and size, also known as an "alginate bead". Alginate microbeads have the advantages of being nontoxic orally, have high biocompatibility, and inability to reswell in an acidic environment, whereas they easily reswell in an alkaline environment. Therefore, acid sensitive drugs incorporated into the beads would be protected from gastric juice (4).

Aceclofenac sodium is non-steroidal anti-inflammatory drug used extensively in the treatment of rheumatoid arthritis, osteoarthritis and ankylosing spondylitis. It is rapidly and completely absorbed after oral administration, and peak plasma concentrations are reached 1 to 3 h after oral dose. The plasma elimination half-life of the drug is approximately 4 h and dosing frequency is 2-3 times daily with a dose range of 100-200 mg (5). An adverse gastrointestinal reaction has been observed and due to its short biological half-life aceclofenac requires multiple dosing. This leads to fluctuation in the drug blood levels and dose related adverse effects. Multiple dosing also fails to release the drug at the desired rate and in the desired amount which often results in poor patient compliance and inefficient therapy (6).

Microencapsulation is a well accepted technique for development of homogeneous, monolithic particles in a range of about 0.1-1,000 μ m and is employed to sustain drug release. Among the microparticulate systems, microbeads have special interest as carriers for NSAIDs, mainly to reduce and/or eliminate gastrointestinal irritation, dose intake and ultimately

to improve compliance in the pharmacotherapy of arthritis, inflammation and pain. In the proposed method of ionotropic gelation we drop the mixture of drug and polymer dispersion into aqueous calcium chloride solution and gelation occurs instantaneously resulting in the formation of spherical micro-scale sized beads, with narrow particle size. Calcium induced alginate beads have been developed in recent years as a unique vehicle for modified drug delivery systems. Their preparation is quite easy and is usually based on the gelling properties of the polysaccharide in the presence of several divalent ions (7).

The aim of the present study was to develop sustained release oral microbeads of aceclofenac sodium using sodium alginate as the hydrophilic carrier and calcium chloride as the cross-linking agent and to examine the effects of various process parameters on the physicochemical properties and drug release potential of the product.

2. Materials and Methods

2.1. Materials

Aceclofenac sodium was obtained as a gift sample from Microlabs, Bangalore, Karnataka, India. Sodium alginate was a gift sample from F. M. C. International Biopolymers, Willingtown, Ireland, through Signet Chemical Corporation Pvt. Ltd., Mumbai, India. Calcium chloride (fused) was purchased from S. B. Fine Chemicals Ltd., Mumbai, India. All other reagents and solvents used were of analytical grade satisfying pharmacopoeias specifications.

2.2. Preformulation studies

2.2.1. Saturation solubility study

The saturation solubility of aceclofenac sodium was determined with various concentrations of surfactants *i.e.*, 0.5, 1.0, 1.5, and 2% (w/v) of sodium lauryl sulfate (SLS) in double distilled water, 0.1 N HCl, pH 4.5 acetate buffer, pH 6.8, and pH 7.4 phosphate buffers at 37°C. An excess quantity of aceclofenac sodium was added to 100 mL of dissolution medium in a conical flask and agitated continuously at room temperature for 8 h on a shaker. The solutions were kept aside for 6 h until equilibrium was achieved. The solutions were then filtered through No. 41 Whatman filter paper, and the filtrate suitably diluted and analyzed spectrophotometrically at 275 nm (8). The results of the solubility study are summarized in Table 1.

2.2.2. Solubility of aceclofenac sodium in calcium chloride solution

The solubility of drug in a calcium chloride (1%, w/v)

Table 1. Solubility of the aceclofenac sodium in different dissolution media

Dissolution media	Concentration of SLS (% w/v)	Solubility (mg/mL)
Double-Distilled water	--	0.067 ± 0.12
	0.5	0.126 ± 0.56
	1.0	0.455 ± 0.23
	1.5	0.643 ± 0.55
	2.0	0.924 ± 0.68
0.1 N HCl	--	0.016 ± 0.87
	0.5	0.098 ± 0.77
	1.0	0.208 ± 0.87
	1.5	0.389 ± 0.65
	2.0	0.487 ± 0.08
Acetate buffer, pH 4.5	--	0.996 ± 0.76
Phosphate buffer, pH 6.8	--	3.963 ± 1.06
Phosphate buffer, pH 7.4	--	5.567 ± 0.98
Calcium chloride solution (1%, w/v)	--	0.096 ± 1.54

was determined by adding an excess of drug into the medium containing vials and shaking at constant temperature 37°C in a water bath for 12 h. The samples were filtered and diluted with distilled water, and then assayed spectrophotometrically at 275 nm (9). The results are summarized in Table 1.

2.3. Drug polymer compatibility studies

2.3.1. Thin layer chromatography (TLC)

Silica gel 60 g plates activated by heating at 105°C for 1 h were used. The mixture of methanol/acetonitrile/buffer solution (pH 6.8) in a ratio of 45:45:10 was used as a solvent system. The drug extracted from different microbeads was spotted on the plates. The R_f values were determined for comparison of pure drug and extracted drug by examining spots under UV-light.

2.3.2. Fourier transform-infrared (FT-IR) spectroscopic analysis

Drug polymer interactions were studied using FT-IR spectroscopy. One to 2 mg of aceclofenac sodium alone, and a mixture of drug and polymer were weighed and mixed properly with potassium bromide uniformly. A small quantity of the powder was compressed into a thin semitransparent pellet by applying pressure. The IR-spectrum of the pellet from 450-4,000 cm^{-1} was recorded taking air as the reference and compared to study interference.

2.3.3. Differential scanning calorimetry (DSC)

Differential scanning calorimetry (DSC) was performed using a DSC-60 (Shimadzu, Kyoto, Japan) calorimeter to study the thermal behavior of drug alone and mixtures of drug and polymer. The instrument was comprised of calorimeter (DSC-60), flow controller

(FCL-60), thermal analyzer (TA-60) and operating software (TA-60). The samples were heated in sealed aluminum pans under nitrogen flow (30 mL/min) at a scanning rate of 5°C/min from 24 ± 1 to 250°C. An empty aluminum pan was used as reference. The heat flow as a function of temperature was measured for the drug and drug-polymer mixture (10).

2.4. Preparation of aceclofenac sodium-loaded microbeads

The microbeads were prepared by the ionotropic external gelation technique. Sodium alginate was dissolved in deionized water at a concentration of 1-3% (w/v) by gentle heat at 40°C on a magnetic stirrer. An accurately weighed 200 mg of aceclofenac sodium was added and dispersed uniformly. The dispersion was sonicated for 30 min to remove any air bubbles that may have been formed during the stirring process. The bubble free sodium alginate-drug dispersions (50 mL) were added drop wise *via* an 18-gauge hypodermic needle fitted with a 10 mL glass-syringe into 50 mL of calcium chloride solution (1-5%, w/v) and stirred at 200 rpm for 30 min. The droplets from the dispersion instantaneously gelled into discrete matrices upon contact with the solution of gelling agent. The drug-loaded microbeads were further stirred in the solution of gelling agent for an additional 2,000 rpm up to 1-3 h. After the specified stirring time and stirring speed gelled beads were separated by filtration, washed with 3×50 mL volumes of deionized water and finally dried at 80°C for 2 h in a hot air oven (10).

Fifteen batches of drug-loaded microbeads were prepared by the ionotropic gelation method to investigate the effect of certain formulation and process variables, such as drug to polymer ratio, concentration of cross-linking agent, cross-linking time and stirring time on the mean particle size, yield, distribution pattern, drug entrapment efficiency and *in vitro* drug release. To study the effect of these variables, each time one variable was varied, the other variables were kept constant and optimized to get small, discrete, uniform, and smooth surface spherical microbeads. The detailed composition of the various formulations is stated in Table 2.

2.5. Characterization and evaluation of microbeads

2.5.1. Granulometric study

Particle size has a significant effect on the release profile of microbeads. Size and size distribution, determined by sieve analysis, was carried out on mechanical sieve shaker. The drug-loaded microbeads were separated into different size fractions by sieving for 5 min using standard sieves having nominal mesh apertures of 1.4 mm, 1.2 mm, 1.0 mm, 0.85 mm, and 0.71 mm (sieve

Table 2. Composition and physical characteristics of various formulations

Batch code	D/P ratio (%, w/w) ^a	Calcium chloride (%, w/v)	Stirring time (h)	Yield (%)	Drug loading capacity (mg/100 mg)	Drug entrapment efficiency (%)
F1	1:5	4	2	88.30	56.20 ± 0.50	63.24 ± 0.66
F2	1:7.5	4	2	80.60	60.80 ± 0.75	75.43 ± 0.42
F4	1:12.5	4	2	74.80	70.20 ± 0.74	93.85 ± 0.50
F5	1:15	4	2	73.40	72.60 ± 1.20	98.90 ± 0.86
F6	1:10	1	2	72.40	60.30 ± 0.67	83.30 ± 0.75
F7	1:10	2	2	74.60	64.20 ± 1.10	86.05 ± 0.96
F8	1:10	3	2	75.10	66.80 ± 0.97	88.94 ± 0.84
F9	1:10	4	2	76.40	68.70 ± 0.60	89.95 ± 0.25
F10	1:10	5	2	77.60	72.30 ± 0.35	93.30 ± 0.23
F11	1:10	4	0.5	75.65	72.80 ± 0.55	96.23 ± 0.30
F12	1:10	4	1.0	76.15	70.15 ± 0.58	92.15 ± 0.48
F13	1:10	4	1.5	76.30	69.50 ± 0.95	91.08 ± 0.87
F14	1:10	4	2.0	76.40	68.70 ± 0.60	89.95 ± 0.25
F15	1:10	4	2.5	77.70	66.35 ± 1.45	85.40 ± 0.55

^a Drug/polymer ratio (aceclofenac/sodium alginate). Each formulation contains 200 mg of aceclofenac sodium. Data are expressed as mean ± S.D. ($n = 3$).

No. 12, 14, 16, 18, and 22, respectively). Particles that passed through one sieve but were retained on the next sieve were collected and weighed and the distribution was analyzed based on the weight fraction on each sieve. The particle size distribution and mean particle size of microbeads were calculated using the following formula (11):

$$\text{Mean particle size} = \frac{\sum(\text{particle size of the fraction} \times \text{weight fraction})}{\sum(\text{weight fraction})}$$

2.5.2. Measurement of micromeritic properties

The flow properties were investigated by measuring the angle of repose of drug-loaded microbeads using the fixed-base cone method. Microbeads were allowed to fall freely through a funnel fixed 1 cm above the horizontal flat surface until the apex of the conical pile just touches the tip of the funnel. The height and diameter of the cone was measured and angle of repose was calculated by using the following formula (11). Each experiment was carried out in triplicate ($n = 3$).

$$\text{Angle of repose } (\theta) = \tan^{-1}(h/r)$$

(h = cone height, r = radius of circular base formed by the microbeads on the ground.)

The bulk and tapped densities were measured in a 10 mL graduated cylinder as a measure of packability of the microbeads. The sample contained in the measuring cylinder was tapped mechanically by means of a constant velocity rotating cam. The initial bulk volume and final tapped volume were noted from which their respective densities were calculated (11).

Compressibility index or Carr's index value of microbeads was computed according to the following equation:

$$\text{Carr's index } (\%) = \frac{[(\text{Tapped density} - \text{Bulk density}) / \text{Tapped density}] \times 100}{}$$

Hausner's ratio of microbeads was determined by comparing the tapped density to the bulk density by using the equation:

$$\text{Hausner's ratio} = \text{Tapped density} / \text{Bulk density}$$

2.5.3. Mechanical strength study

To precisely measure mechanical strength of the alginate gel beads, large beads were prepared with sodium alginate polymer dispersion dropped through a 1 mL pipette into calcium chloride solution. The fully formed beads were collected, washed with distilled water and subsequently dried at 80°C for 2 h. Compression testing was performed with an Instron (4460). Ten beads of identical size were selected, crosshead speed and probe diameter were set at 1 mm/min and 3.5 cm, respectively (12).

2.5.4. Water uptake determination

Weighed drug-loaded microbeads were placed in a small basket, soaked in pH 6.8 phosphate buffer or distilled water and shaken occasionally at room temperature. After a predetermined time to remove excess water, beads were immediately weighed on an analytical balance. The water uptake can be calculated from the following equation (13):

$$\text{Water uptake } (\%) = [(W_t - W_0) / W_0] \times 100$$

where W_t and W_0 are the wet and initial mass of beads, respectively.

2.5.5. Determination of calcium content in the beads

Alginate drug-loaded microbeads (250 mg) were dissolved in 10 mL by boiling in concentrated nitric acid. Samples were diluted with 1% (w/v) of nitric acid solution and calcium content was determined spectrophotometrically (14).

2.5.6. Disintegration test of drug-loaded microbeads

Disintegration studies were carried out in 50 mL of buffer media pH 1.2 and pH 7.2 in 100 mL conical flasks. A maximum of 5 pellets were used in each trial and stirred on a magnetic stirrer maintained at 37°C, at 25 rpm. Each batch of microbeads was run in triplicate and the time taken for all 5 pellets to disintegrate leaving behind polymer in the soluble form and drug in the insoluble form was noted as the disintegration time.

2.5.7. Particle size analysis

The particle sizes of both placebo and drug-loaded formulations were measured using an optical microscope fitted with an ocular and stage micrometer to calculate particle size distribution. The Olympus model (SZX-12) having a resolution of 30 μ m was used for this purpose. The instrument was calibrated at 1 unit of eyepiece micrometer equal to 1/30 mm (33.33 μ m). In all measurements at least 100 particles in five different fields were examined (15). Each experiment was carried out in triplicate.

2.5.8. Scanning electron microscopy (SEM) analysis

The shape and surface characteristics were determined by scanning electron microscopy (model-JSM, 35CF, Jeol, Japan) using a gold sputter technique. The particles were vacuum dried and coated to 200 Å thicknesses with gold palladium prior to microscopy. A working distance of 20 nm, a tilt of zero-degrees and an accelerating voltage of 15 kV were the operating parameters. Photographs were taken within a range of 50-500 magnification.

2.5.9. Determination of entrapment efficiency

Aceclofenac sodium content in the microbeads was estimated using a UV-spectrophotometric method. Accurately weighed 50 mg of microbeads were suspended in 100 mL of phosphate buffer pH 7.2 \pm 0.1. The resulting solution was kept for 24 h. The next day it was stirred for 15 min. The solution was filtered, after suitable dilution. Aceclofenac sodium content in the filtrate was analyzed at 275 nm using a Shimadzu 1201 UV-Visible spectrophotometer. The absorbance obtained was plotted on a standard curve to get the exact concentration of the entrapped drug. Calculating this concentration with the dilution factor the percentage of actual drug encapsulated in microbeads

was obtained (16). The drug entrapment efficiency was determined using the following relationship:

$$\% \text{ Drug entrapment efficiency} = \left[\frac{\text{Actual drug content}}{\text{Theoretical drug content}} \right] \times 100$$

2.5.10. Loose surface crystal (LSC) study

This study was conducted to estimate the amount of drug present on the surface of the microbeads which showed immediate release in dissolution media. A hundred mg of microbeads were suspended in 100 mL of phosphate buffer (pH 7.2), simulating the dissolution media. The samples were shaken vigorously for 15 min in a mechanical shaker. The amount of drug leached out from the surface was analyzed spectrophotometrically at 275 nm (16). The percentage of drug released with respect to entrapped drug in the sample was recorded.

2.5.11. Swelling properties

Swelling properties of drug-loaded microbeads were determined in various pH ranges (*i.e.*, 1.2, 4.8, and 6.8 buffer solutions), thirty dried beads were placed in a small beaker to which 100 mL of buffer solutions was added and then allowed to swell at 37°C. After a 2 h interval, the equilibrium swollen beads were observed and measured by optical microscopy (Olympus model SZX-12). The magnitude of swelling was presented as the ratio of the mean diameter of swelling beads to the mean diameter of the dried beads before the test (17). Swelling ratio was determined from the following relation:

$$\text{Swelling ratio} = \left[\frac{\text{Mean diameter at time } t\text{-initial diameter}}{\text{Initial diameter of beads}} \right] \times 100\%$$

2.6. In vitro drug release studies

The release profiles of aceclofenac sodium from microbeads were examined in three different buffer solutions to mimic the various physiological GI-tracts. The media of pH 1.2 represented the gastric condition; pH 6.8 was a compromise condition between the gastric pH and the small intestine and pH 7.2, which is phosphate buffer solution. The dissolution process was carried out using a USP XIII rotating basket apparatus (Microlabs, Mumbai, India). The drug-loaded microbeads (equivalent to 200 mg of aceclofenac sodium) filled in empty capsule shells were put into the basket, rotated at a constant speed of 75 rpm and a temperature of 37°C. The 900 mL of dissolution medium, pH 1.2, containing 2% (w/v) sodium lauryl sulfate (SLS) and the test was conducted for 2 h. At the end of 2 h the test was continued changing the dissolution media with pH 6.8 buffer solution up to 6 h and pH 7.2 phosphate buffer up to the end of 12 h. At

scheduled time intervals, a 5 mL sample was withdrawn and replaced with the same volume of fresh medium. The samples were filtered through a 0.45 μm membrane filter and after appropriate dilution, aceclofenac sodium concentration was estimated spectrophotometrically at 275 nm (Shimadzu 1201, Japan). Finally, the corresponding drug content in the samples was calculated from the calibration curve of aceclofenac sodium to determine the drug release pattern (18).

2.7. Kinetics of drug release

In order to understand the mechanism and kinetics of drug release, the drug release data of the *in vitro* dissolution study was analyzed with various kinetic equations like zero-order (% release v/s time), first-order (Log% retained v/s time) and korsmeyer and peppas equations. Correlation coefficients (*r*) values were calculated for the linear curves obtained by regression analysis of the above plots.

2.8. Stability studies of microbeads

After determining the drug content, the optimized drug-loaded microbeads were charged for the accelerated stability studies according to ICH guidelines. To assess long-term stability, accurately weighed drug-loaded microbeads equivalent to 200 mg of aceclofenac sodium were filled into hard gelatin capsules manually and sealed in aluminum packaging coated inside with polyethylene. The studies were performed at $25 \pm 2^\circ\text{C}$, $40 \pm 2^\circ\text{C}$ with $60 \pm 5\%$, and $75 \pm 5\%$ relative humidity (RH) in desiccators with saturated salt solution for up to 6 months (19). A visual inspection for drug content was conducted every month for the entire period of the stability study.

3. Results and Discussion

Side effects, mainly at the gastric level are well known, following oral administration of NSAIDs. Therefore the efforts of many researchers have been concerned to solve these problems, through a variety of techniques of protection of the gastric mucosa or alternatively to prevent the NSAIDs release in this gastric region. In this paper we evaluate the potential utility of natural material such as sodium alginate to inhibit the release of aceclofenac sodium in the gastric environment. Among microparticulate systems, microbeads have special interest as carriers for NSAIDs, mainly to extend the duration of the dosage form.

Aceclofenac sodium loaded microbeads formulated with 0.5% sodium alginate which were cured for 2 h at 2,000 rpm in 0.5% calcium chloride solution were not spherical and had a flattened base at the points of contact with the drying vessel. However, an increase in the concentration of sodium alginate tended to make

the particles more spherical. This indicates that at low alginate concentrations the particles were composed of a loose networks structure which collapsed during drying. On the other hand, higher sodium alginate concentrations formed a dense matrix structure which prevented collapse of microbeads. However, forming a highly viscous polymer dispersion did not pass easily in the needle during the manufacturing process. Moreover, we found a small tail at one end of the beads which significantly affected the flow properties and particle size distribution. It was found that optimum concentration of sodium alginate (1:10), calcium chloride (4%), and cross-linking time (2 h), could influence the microbead size, average diameter, recovery, encapsulation efficiency, and size distribution swelling behavior.

3.1. Preformulation studies (saturation solubility studies)

The available data on the solubility profile of aceclofenac sodium indicated that the drug is freely soluble in acetone and practically insoluble in water. The results of the solubility study and the influence of sink conditions are summarized in Table 1. The results showed, that there was a significant increase in solubility with increasing pH. The addition of different concentrations of SLS in 0.1 N HCl significantly increased solubility up to 0.487 mg/mL. A dissolution study of dosage forms necessitates modifications in the dissolution medium to increase the solubility of practically insoluble drugs. Aceclofenac sodium is a weak acid; the solubility of aceclofenac sodium in HCl was much less compared to distilled water. However, the addition of surfactant is a reasonable approach for solubilizing such drugs, because various surfactants are present in the GI-fluid. Saturation solubility of aceclofenac sodium in different media increased with an increase in buffer pH as well as with an increase in surfactant concentration. The significant increase is attributed to the micellar solubilization by SLS. Aceclofenac sodium showed sufficient solubility in 0.1 N HCl with 2% (w/v) of SLS which was adequate to maintain sink condition and was selected as the dissolution medium for *in vitro* drug release studies.

The solubility of aceclofenac sodium in calcium chloride was found to be 0.96 ± 1.54 mg/mL. The solubility of aceclofenac sodium was more in 1% (w/v) calcium chloride solution than in double-distilled water, which induces a certain amount of drug release, when there is prolonged exposure of the beads in curing medium during the manufacturing process.

3.2. Drug/polymer compatibility studies

3.2.1. Thin layer chromatography (TLC)

In results from TLC studies the R_f value of aceclofenac

sodium pure drug was 22, and linearity was between 700-2,400 ng/zone. The R_f value of extracted drug from microbeads was 21.40, and linearity was in the range between 2,350 ng/zone. In images of spots observed on the TLC plates, there is no overlap of spots; this indicates that the drug did not contain any extraneous matter. Moreover, extracted drug R_f values obtained from microbeads are almost equal to that of the standard drug. This indicates there is no deformation during the process.

3.2.2. Fourier transform-infrared (FT-IR) spectroscopic analysis

IR-spectra of pure aceclofenac sodium, sodium alginate and the physical mixture of drug and polymer are shown in Figure 1. The characteristic absorption peaks were obtained at 2966.36, 2915.5, 1716.5, 1589.3, 1479.6, and 665.4 cm^{-1} for pure aceclofenac sodium, 2814.98, 1603.34, 1519.3, 1359.60, and 674.05 cm^{-1} for sodium alginate, 2820.28, 1591.72, 1384.91, 1102.03, and 666.4 cm^{-1} for physical mixture of drug and polymer (Figure 1). The compatibility of aceclofenac sodium with polymer was investigated by an IR-spectroscopy study. The IR spectra of the drug and polymer combination were compared with the spectra of the pure drug and individual polymer spectra. There were no considerable changes in the IR peaks of aceclofenac in the physical mixture, thereby indicating the absence of any interaction.

3.2.3. Differential scanning calorimetry (DSC)

Differential scanning calorimetry thermo grams of pure drug and drug-loaded sodium alginate microbeads was observed, calcium chloride shows two endotherm peaks in the temperature range 180-200°C; while sodium alginate decomposes at about 240°C with a broad exotherm. Pure drug aceclofenac sodium showed a sharp endotherm at 154.50°C corresponding to its melting point. There was no appreciable change in the melting endotherm of the physical mixture as compared to pure drug. The peak of the drug did not appear in the thermogram of any type of the prepared microbeads containing the drug. This may indicate that the drug was uniformly dispersed at the molecular level of polymers.

3.3. Characterization and evaluation of microbeads

The total percentage yields of drug-loaded microbeads obtained were in the range between 72.40 to 88.30% (w/w). It was observed that increasing the polymer ratio in the formulation significantly lowered the product yield due to the formation of a highly viscous polymer dispersion which may be lost during the manufacturing process. A further observation, when the drug/polymer ratio was constant, an increase in the concentration of

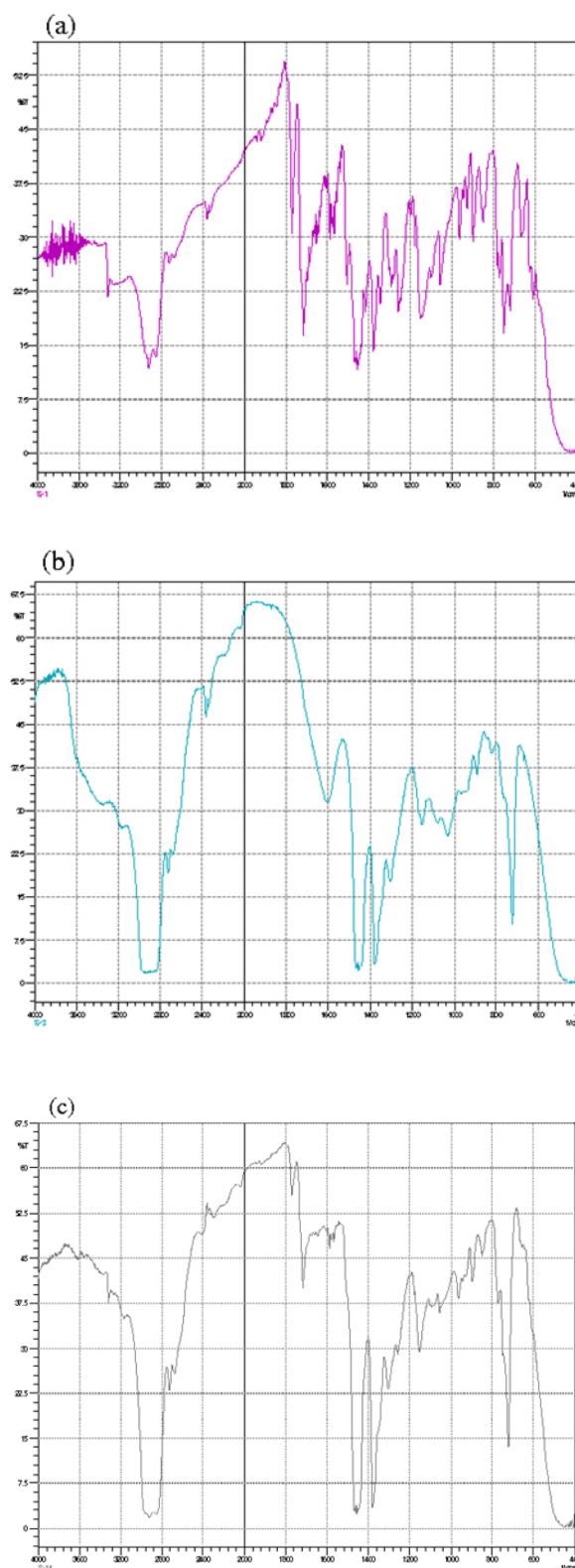


Figure 1. IR-spectra. (a) Aceclofenac sodium pure drug. (b) Sodium alginate. (c) Physical mixture.

calcium chloride and curing time slightly increased the percent yield. Actual drug concentration in the microbeads was evaluated and found to be in the range of 56.20 ± 0.50 to 72.80 ± 0.55 mg/100 mg. The polymer concentration consequently makes the actual drug loading higher due to the increase

in hydrophobicity, leading to better precipitation of polymer at the boundary phase of the droplets.

3.3.1. Granulometric study

The effects of various processes and formulation parameters on the micromeritic properties of drug-loaded microbeads were evaluated, and the size distribution of the microbeads in different sieves was observed and showed 32.46% to 89.50% of microbeads retained \neq 22 sieve. The size distribution of microbeads was observed and that an increase in the concentration of sodium alginate and calcium chloride solutions tends to form more spherical particles and more uniform size spheres. On the other hand, an increase in cross-linking time and stirring speed are also favorable for the formation of more spherical beads and distribution of particle size slightly shifts to the lower pore size.

3.3.2. Measurement of micromeritic properties

The rheological parameters like angle of repose, bulk density and tapped density of all microbeads confirms better flow and packaging properties. All the formulations showed excellent flowability represented in terms of angle of repose ($< 40^\circ$) (20). Here, the sodium alginate concentration also has a significant positive effect on the angle of repose (Table 3). Particle size increased with an increase in the concentration of sodium alginate and resulted in a decreased angle. However, higher calcium chloride concentration, cross-linking time and high stirring speed influenced the formation of smaller beads because of shrinkage and showed an increased angle of repose (Table 3). Bulk and tapped density of beads showed an acceptably good range which indicates that the beads have good packability. The density of the beads increases as the concentration of the polymer increases suggesting that

the beads formed at high polymer concentration are more compact and less porous than those prepared at low polymer contents (Table 3). Carr's index and Hausner's ratio explain that the formulated microbeads had excellent compressibility and good flow properties. The improvement of flow properties suggest that the microbeads can be easily handled during processing. Mechanical testing was performed in order to study the effect of concentration of calcium chloride and cross-linking time. The results show increasing the concentration of calcium chloride and cross-linking time significantly increases the mechanical strength due to formation of a dense matrix between sodium and Ca^{2+} divalent ions.

3.3.3. Water uptake determination

The % water uptake of the aceclofenac sodium loaded microbeads in distilled water was significantly lower than that in pH 6.8 phosphate buffer. The equilibrium time of water uptake in distilled water of the beads was between 0.5-2 h. In the case of phosphate buffer pH 6.8 the equilibrium time of water uptake reaches 1 h because calcium ions cross-linked with alginate were rapidly exchanged with sodium ions in phosphate buffer with a prolonged cross-linking time. Moreover, calcium alginate gels could be solubilized by the addition of phosphate ion, which acted as a complexing agent for calcium ions at a pH above 5.5 (20). The sodium alginate concentration increased water uptake of the beads ultimately increases the swelling behavior of the beads at higher pH levels which would significantly delay drug release.

3.3.4. Determination of calcium content in the beads

Calcium content in the drug-loaded microbeads was performed and obtained in the range 0.346 ± 0.116

Table 3. Micromeritic properties of drug-loaded microbeads

Batch code	Mean particle size (μm)	Angle of repose (θ)	Bulk density (g/mL)	Tapped density (g/mL)	Carr's index (CI) (%)	Hausner's ratio
F1	596.45 \pm 1.04	32.20 \pm 1.96	0.475 \pm 0.07	0.593 \pm 0.03	19.89	1.24 \pm 0.20
F2	624.86 \pm 0.98	28.16 \pm 0.62	0.566 \pm 0.92	0.675 \pm 0.06	16.14	1.19 \pm 0.30
F3	703.55 \pm 0.75	22.65 \pm 0.55	0.665 \pm 0.75	0.782 \pm 0.05	14.96	1.17 \pm 0.58
F4	844.75 \pm 1.10	20.55 \pm 1.07	0.695 \pm 0.05	0.807 \pm 0.87	13.87	1.16 \pm 0.15
F5	880.10 \pm 1.23	19.85 \pm 0.54	0.745 \pm 0.08	0.855 \pm 0.16	12.86	1.14 \pm 0.78
F6	746.60 \pm 0.73	30.65 \pm 0.85	0.515 \pm 0.16	0.665 \pm 0.22	22.55	1.29 \pm 0.12
F7	734.10 \pm 0.54	27.75 \pm 0.96	0.565 \pm 0.25	0.697 \pm 0.45	18.95	1.23 \pm 0.45
F8	724.40 \pm 0.34	26.25 \pm 0.55	0.635 \pm 0.35	0.753 \pm 0.96	15.70	1.18 \pm 0.68
F9	703.55 \pm 0.75	22.65 \pm 0.55	0.665 \pm 0.75	0.782 \pm 0.05	14.96	1.17 \pm 0.58
F10	688.56 \pm 1.25	19.10 \pm 1.23	0.712 \pm 0.15	0.810 \pm 0.46	12.10	1.13 \pm 0.77
F11	804.35 \pm 1.43	25.75 \pm 0.64	0.555 \pm 0.77	0.695 \pm 0.55	20.14	1.25 \pm 0.84
F12	764.45 \pm 1.05	24.66 \pm 0.77	0.588 \pm 0.93	0.724 \pm 0.15	18.80	1.24 \pm 0.56
F13	724.64 \pm 1.54	23.15 \pm 0.87	0.625 \pm 0.66	0.758 \pm 0.35	17.62	1.20 \pm 0.34
F14	703.55 \pm 0.75	22.65 \pm 0.55	0.665 \pm 0.75	0.782 \pm 0.05	14.96	1.17 \pm 0.58
F15	708.10 \pm 0.86	18.85 \pm 1.15	0.695 \pm 0.82	0.805 \pm 0.77	13.65	1.15 \pm 0.55

Data are expressed as mean \pm S.D. of at least triplicate.

to $0.676 \pm 0.232\%$ (w/w) in 10 mg beads. Results are known that calcium chloride concentration affects the amount of Ca^{2+} ions in alginate beads. Formulations prepared with 5% (w/v), have higher Ca^{2+} contents than those of the formulations prepared with low concentrations of calcium chloride. On the other hand, sodium alginate concentration and cross-linking time increases the calcium content in the beads.

3.3.5. Disintegration test of drug-loaded microbeads

In all formulations the disintegration time was found in the range between 116 to 185 min. The disintegration times of the drug-loaded microbeads increased with increased sodium alginate concentrations because it leads to increased viscosity of the polymeric matrix and increased cross-linking in turn to form stronger beads which take longer times for disintegration.

3.3.6. Particle size analysis

The mean particle size of drug-loaded microbeads were performed using optical microscopy, and mean particle size of the various formulations (F1-F15) of microbeads were obtained in the range between 596.45 ± 1.04 to 880 ± 1.23 (μm) (Table 3). It was found that the particle size distribution of each formulation was within a narrow size but the mean particle size was different among the formulations. The results indicated that the proportional increase in the mean particle size of microbeads increased with the amount of sodium alginate in the formulations. This could be attributed to an increase in relative viscosity at higher concentrations of sodium alginate and formation of large droplets during addition of polymer solution to the gelling agent. On the other hand, the mean particle size of microbeads was found to decrease with an increase in the concentration of calcium chloride. It has been stated that when a drop of alginate solution comes in contact

with calcium ions, gelation occurs instantaneously. As Ca^{2+} ions penetrate into the interior of droplets, water is squeezed out of the droplets resulting in contraction of beads (Table 3). The size of the spherical matrix could be easily controlled by varying the stirring speed of the system. The mean particle size of microbeads was tremendously decreased with an increase of rotational speed. At a stirring speed of 500 rpm, the mean particle diameter and the size distribution of the beads increased significantly. This low stirring speed might have decreased the uniformity of the mixing force throughout the emulsion mixture, and the particles were found to settle at the bottom of the vessel resulting in a wider diameter for the final beads. Consequently, at a higher stirring speed, a vigorous, uniform, increased mechanical shear might have influenced the formation of lesser diameter beads. A higher mixing rate did not further reduce the mean diameter, because high turbulence caused frothing and adhesion to the container wall. The effect of cross-linking time at a particular stirring speed was also observed, and it was recorded that cross-linking time influenced the shape as well as the size distribution of microbeads, possibly because of the variable shear force experienced by the particulate system.

3.3.7. Scanning electron microscopy analysis (SEM)

The SEM photomicrographs of the dried drug-loaded microbeads and their surface morphology are shown in Figure 2. Morphology of the various formulations of drug-loaded microbeads was discrete and spherical in shape with a rough outer surface and visible large wrinkles with a sandy appearance because of the surface-associated crystals of drug.

3.3.8. Determination of entrapment efficiency

The effect of various process and formulation

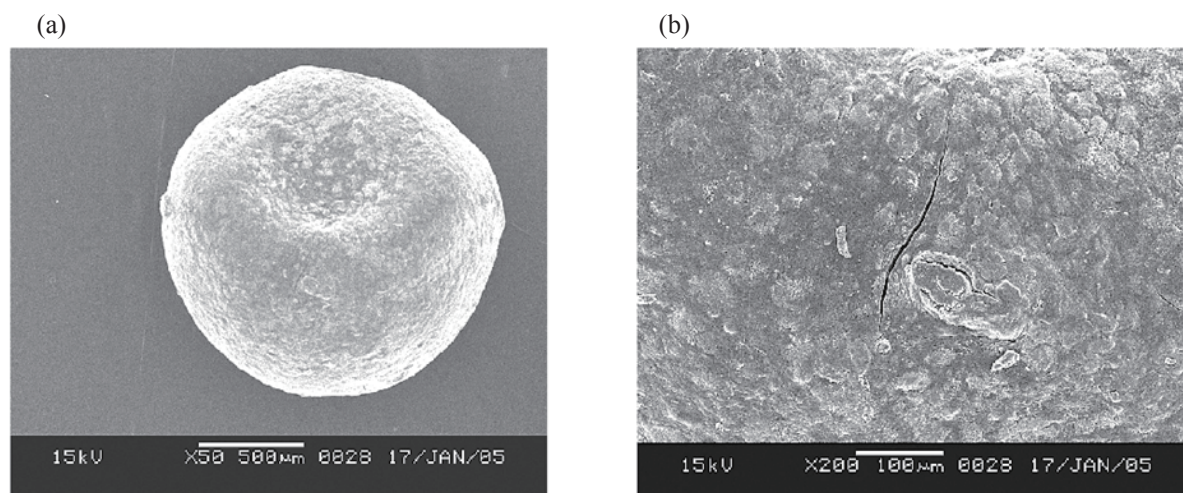


Figure 2. Scanning electron micrographs of aceclofenac sodium microbeads at 15 kV. (a) Overall. (b) Surface.

parameters on the drug entrapment efficiency of microbeads were investigated, keeping the concentration of calcium chloride, stirring speed, and cross-linking time fixed at 4% (w/v), 2,000 rpm, and 2 h, respectively. By increasing the drug/polymer ratio concentration from 1:5 to 1:15 (w/w), the drug entrapment efficiencies were found to be in the range of 63.24 ± 0.66 to $98.90 \pm 0.86\%$ (w/w). It was observed that the drug entrapment efficiencies increased progressively with increased concentration of sodium alginate resulting in the formation of larger beads entrapping a greater amount of drug. This may be attributed to the greater availability of active calcium binding sites in the polymeric chains and, consequently, a greater degree of cross-linking as the amount of sodium alginate increased. Alginate concentration increases may also reduce loss of drug in the curing medium due to the formation of a dense matrix structure.

When the concentration of drug/polymer ratio, stirring speed, and cross-linking time were fixed at 1:10, 2,000 rpm, and 2 h, respectively, increasing calcium chloride concentration from 1-5% (w/v) the drug entrapment efficiencies were found to be in the range 83.30 ± 0.75 to $93.30 \pm 0.2\%$ (w/w). From the results, it is obvious that increasing calcium chloride concentration produced beads with higher levels of Ca^{2+} ions. Consequently, the cross-linking of the polymer and compactness of the formed insoluble dense matrices also increased, which resulted in more drug entrapment in the microbeads (Table 2). On the other hand, further increase in the concentration of calcium chloride above 5% (w/v) did not enhance drug loading. This could be due to possible saturation of calcium binding sites in the guluronic acid chain, which prevented further Ca^{2+} ion entrapment and, hence, cross-linking was not altered with higher concentrations of calcium chloride solution.

Drug entrapment efficiencies were evaluated while keeping the drug/polymer ratio, concentration of calcium chloride, and stirring speed constant at 1:10 (w/w), 4% (w/v), and 2,000 rpm, respectively. Increasing cross-linking time from 0.5 to 2.5 h, the drug entrapment efficiencies were found to be in the range 85.40 ± 0.55 to $96.77 \pm 0.30\%$ (w/w). The cross-linking time also effects the drug entrapment efficiencies of formulated drug-loaded microbeads. Increasing the cross-linking time resulted in a decrease in the drug entrapment efficiencies (Table 2), since the solubility of aceclofenac sodium was slightly higher in calcium chloride than in distilled water. Prolonged exposure in the curing medium caused greater loss of drug through weakly cross-linked alginate beads. However, constant drug loading was achieved at 2 h, with no further decrease after 4 and 5 h of curing time. This could be due to the formation of a tight junction between calcium ions and the active sites on the guluronic acid chain. Consequently, the drug was entrapped in the

highly bound calcium alginate matrix which resulted in no further diffusion of drug in the curing medium.

3.3.9. Loose surface crystal study (LSC)

The loose surface crystal (LSC) study was an important parameter giving an indication of the amount of drug on the surface of the microbeads without proper entrapment. With increased concentration of sodium alginate and calcium chloride solutions, the LSC decreased significantly due to high entrapment of drug in the dense matrix structure.

3.3.10. Swelling properties

The "Swelling-Dissolution-Erosion" process is highly complex. In systems based on sodium alginate cross-linked with calcium chloride, the osmotic pressure gradient that exists between the alginate gel and the environment comprises an important factor in the swelling process. The swelling ratio of the beads was dependent on the pH of the solution. Under acidic conditions, swelling of calcium alginate beads occurs scarcely. Under neutral conditions, the beads will swell and the drug release depends on the swelling and erosion process. Being a polyelectrolyte, alginate can exhibit swelling properties that are sensitive to pH, ionic strength, and ionic composition of the medium (21). Optical microscopy was used to investigate the hydration and swelling of microbeads at pH 1.2, 4.8, and 6.8 up to 4 h (Figures 3a-3c). The equilibrium swelling studies showed that, with an increase in the polymer concentration, swelling of beads was significantly increased. The low swelling in acidic media at pH 1.2 was probably due to proton-calcium ion exchange forming insoluble alginic acid regions followed by solvent penetration into the gel network. The swelling of beads was ultimately increased at pH 4.8 and pH 6.8 at the end of 4 h. This was due to increased solubility of the polymer in basic pH leading to relaxation of the cross-linked polymeric network. It has been reported that the swelling can be enhanced by the presence of phosphate ions at higher pH which displaces the Ca^{2+} ions within the beads (Figure 3a). Increasing the concentration of calcium chloride produces beads with higher levels of Ca^{2+} ions that could reduce the swelling of beads in acidic medium. However, the amount of calcium in swollen gel films after 4 h in the medium was about 10-30%, which apparently prevented total breakdown of the gel structures. The swelling behavior of beads at pH 4.8 and 6.8 was observed as a result of slight increases of swelling ratio due to ionic exchange between the phosphate ions in the buffer and a higher level of Ca^{2+} ions within the beads (Figure 3b). When we compared the swelling ratio with a prolonged cross-linking time while maintaining the same drug/polymer ratio

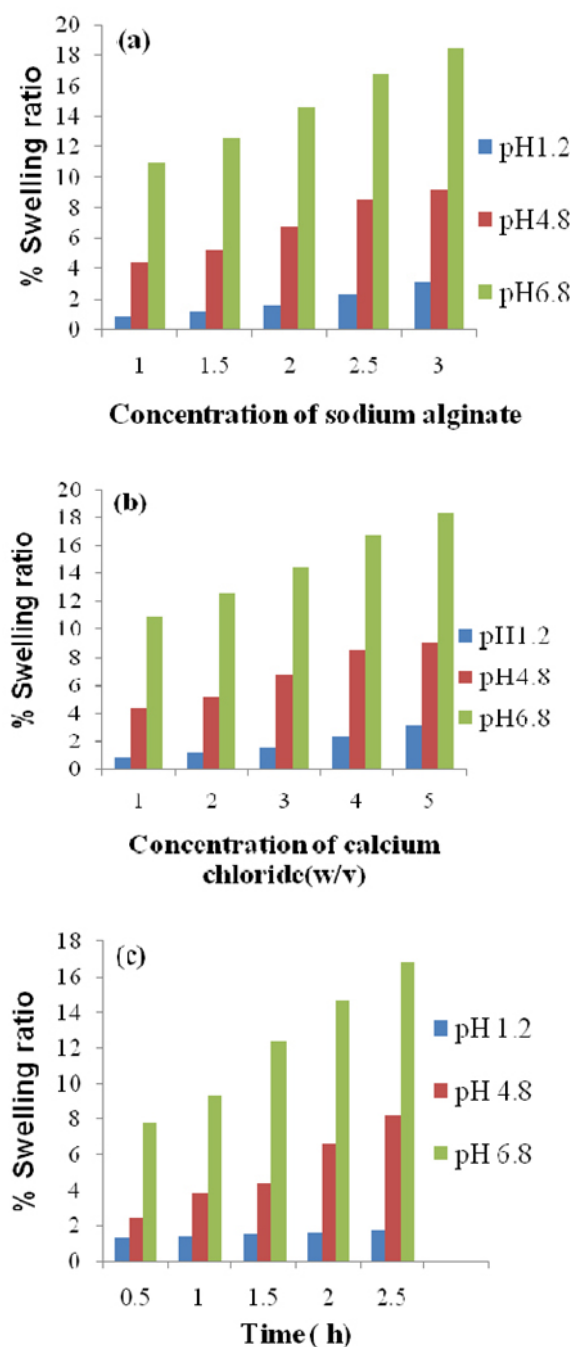


Figure 3. Effect of various parameters on the swelling behavior of drug-loaded microbeads. (a) Polymer concentration. (b) Calcium chloride concentration. (c) Cross-linking time.

and concentration of calcium chloride in the system, appreciable maximum swelling was shown with increased pH levels. These results may be due to the maximum extent of cross-linking that yielded compact beads, which might have rehydrated to a greater extent. The sequestering action of phosphate ions in higher pH media on Ca^{2+} ions may have contributed to the swelling of cross-linked beads. The lower rehydration of beads that were prepared at shorter cross-linking times may be correlated with incomplete cross-linking of sodium alginate (Figure 3c). We further observed that

the swelling ratio of microbeads prepared at various stirring speeds could not affect much of the swelling equilibrium of the beads. When we compared the overall results of the swelling ratio of all formulations, the slowest swelling ratio was obtained at pH 1.2, whereas the highest was at increased pH levels of the medium, initially. Further they were broken after 2 h. The overall results suggest that the dried beads swell slightly in the stomach. When they are subsequently transferred to the upper intestine, the particles begin to swell and they behave as matrices for sustained release of incorporated drug but they are subjected to erosion in the lower intestine.

3.4. *In vitro* drug release studies

Acetoclofenac sodium release from formulated microbeads have been performed in different media, either in simulated gastric fluid (SGF) at pH 1.2 for an initial 2 h, and mixed phosphate buffer at pH 6.8 for a period up to 6 h and pH 7.2 at the end of 12 h studies. When we changed the pH from 1.2 to 6.8 by mixing with the phosphate buffer, the drug release rate was slightly increased and found to be in the range of 37.80 ± 0.32 to 64.80 ± 0.12 (%). On further changing the pH from 6.8 to 7.2 (SIF) till 12 h, the maximum drug released at a constant rate was found to be in the range of 78.60 ± 0.67 to 97.20 ± 0.36 (%) (Table 4).

The acetoclofenac sodium was slightly soluble in water and showed very poor solubility in the acidic buffer media as a result of which we had to use 2.0% (w/v) SLS in the media to aid the dissolution of the drug. It is generally seen that when microbeads formulated with hydrophilic polymer are immersed in water, they swell and form a gel diffusion layer that hinders the outward transport of the drug, hence producing a sustained release effect. However, the drug release from alginate beads was pH dependent, and all of the formulations showed negligible drug release in acidic pH 1.2 ($< 5\%$, w/w) which may be due to the stability of alginate at lower pHs and conversion of Ca-alginate from the insoluble alginic acid to a formed tightening of the gel mesh work. On the other hand, the polymer is eroded at alkaline pH and the contents are released in a sustained manner by both diffusion and slow erosion of polymer matrix. However, the swelling behavior of drug-loaded Ca-alginate beads at higher pH could be explained by the ionotropic effect that occurs between the Ca^{2+} ion of alginate and Na^+ ions present in phosphate buffer and consequently, capturing of the Ca^{2+} by phosphate ions (22). The ion exchange with phosphate buffer which resulted in swelling and erosion of the beads and formation of the solute Ca-phosphate all have an influence on the increase of drug release rate at higher pH. This might be due to the lower number of Na^+ ions present in that buffer and consequently a slower rate of

Table 4. *In vitro* drug release and various kinetic data of drug-loaded microbeads

Batch code	Cumulative % drug release			Various Kinetic models				
	pH 1.2 ^a	pH 6.8 ^b	pH 7.2 ^c	Zero-order (r) ^d	First-order (r) ^d	Higuchi-matrix (r) ^d	Korsmeyer-peppas (r) ^d	'n'- values ^e
F1	4.32 ± 0.05	64.80 ± 0.12	93.70 ± 0.19	0.9980	0.9515	0.9737	0.9984	0.8806
F2	3.80 ± 0.06	60.40 ± 0.44	88.80 ± 0.43	0.9960	0.9076	0.9694	0.9932	0.9160
F3	3.06 ± 0.12	54.60 ± 0.32	86.40 ± 0.36	0.9981	0.9098	0.9674	0.9955	1.0745
F4	2.60 ± 0.23	57.40 ± 0.56	83.90 ± 0.88	0.9942	0.9854	0.9951	0.9937	1.0682
F5	2.06 ± 0.44	45.80 ± 0.32	78.60 ± 0.67	0.9988	0.9887	0.9940	0.9969	1.1304
F6	4.04 ± 0.03	58.20 ± 0.16	95.40 ± 0.90	0.9756	0.9143	0.9675	0.9855	1.0791
F7	3.42 ± 0.02	56.40 ± 0.66	90.20 ± 0.15	0.9866	0.9843	0.9910	0.9834	1.2962
F8	3.24 ± 0.08	55.80 ± 0.74	88.80 ± 0.19	0.9955	0.9784	0.9870	0.9904	1.2304
F9	3.06 ± 0.07	54.60 ± 0.65	86.40 ± 0.36	0.9978	0.9865	0.9943	0.9967	1.0745
F10	2.44 ± 0.04	47.80 ± 0.45	81.50 ± 0.55	0.9993	0.9877	0.9930	0.9987	1.4023
F11	3.96 ± 0.06	58.70 ± 0.43	97.20 ± 0.36	0.9786	0.9712	0.9890	0.9915	0.9406
F12	3.10 ± 0.07	56.10 ± 0.55	94.30 ± 0.56	0.9852	0.9087	0.9648	0.9833	1.3720
F13	3.20 ± 0.05	55.60 ± 0.36	90.50 ± 0.84	0.9844	0.9765	0.9908	0.9867	1.2882
F14	3.06 ± 0.04	54.60 ± 0.48	86.40 ± 0.36	0.9976	0.9863	0.9917	0.9877	1.0745
F15	2.43 ± 0.15	48.30 ± 0.90	82.30 ± 0.64	0.9991	0.9923	0.9912	0.9886	0.9684

All the results shows S.D. ($n = 3$). ^a Values expressed at the end of 2 h; ^b Values at the end of 6 h; ^c Values expressed at the end of 12 h; ^d Correlation coefficient; ^e Diffusion exponent related to mechanism of drug release, according to equation of $Mt/M = Kt^n$.

ion exchange and swelling of the polymer at this pH. The present results revealed that swelling is the main parameter controlling the release rate of aceclofenac sodium from alginate matrices, which is modulated by a "swelling-dissolution-erosion" process.

3.4.1. Effect of drug/polymer ratio on drug release

The effect of drug/polymer ratio on aceclofenac sodium release from different batches of microbeads is shown in Figure 4a. As the drug/polymer ratio increased, the release rate of aceclofenac sodium from the microbeads decreased. The slower release rate can be explained by the increase in the extent of swelling and the gel layer thickness that acted as a barrier for the penetration medium, thereby retarding the diffusion of drug from the swollen alginate beads. However, the steady state release was achieved after an initial lag time and it was directly proportional to the concentration of sodium alginate. The first phase might be due to the negligible dissociation of alginate beads in phosphate buffer mainly based on drug diffusion through the small pores and cracks. The second phase exhibited a burst-like release pattern, which was accompanied by alginate disintegration. The sodium alginate concentration in the formulation greatly influenced the steady state release of drug from the microbeads.

3.4.2. Effect of calcium chloride concentration on drug release

The effect of cross-linking agent on aceclofenac sodium release from different batches of microbeads is shown in Figure 4c. The results indicate that rate and extent of drug release decreased significantly with increase

of calcium chloride concentration. This is because sodium alginate is a linear copolymer consisting of β -(1 \rightarrow 4) mannuronic acid and α -(1 \rightarrow 4) L-guluronic acid residues and a tight junction is formed between the residues of alginate with calcium ions. However, higher calcium chloride concentrations, increased surface roughness and porosity (Figure 2) and also poor entry of dissolution medium into the polymer matrix may delay drug release.

3.4.3. Effect of stirring time on drug release

Variation in cross-linking time was also studied for selecting the most optimized formulation. The effect of stirring time on aceclofenac sodium release from different batches of microbeads is shown in Figure 4d. An increase in the cross-linking time from 0.5-2.5 h significantly decreased drug release due to penetration of calcium into the interior of the beads. Faster drug release was observed with 0.5-1 h, which can be attributed to the poor binding of drug within the polymer matrix and also incomplete gelling of sodium alginate. Increasing the cross-linking time to more than 2 h, however, caused no significant change in the amount of drug release.

3.5. Kinetics of drug release

The *in vitro* dissolution data were analyzed using different kinetic models in order to find out the n -value, which describes the drug release mechanism (Table 4). Correlation values (r) were calculated and were found to be more linear for first-order drug release compared to zero-order. Cumulative % drug release was analyzed using PRISM software. Kinetic data was a reasonable best fit to Korsmeyer and Peppas's model and a good

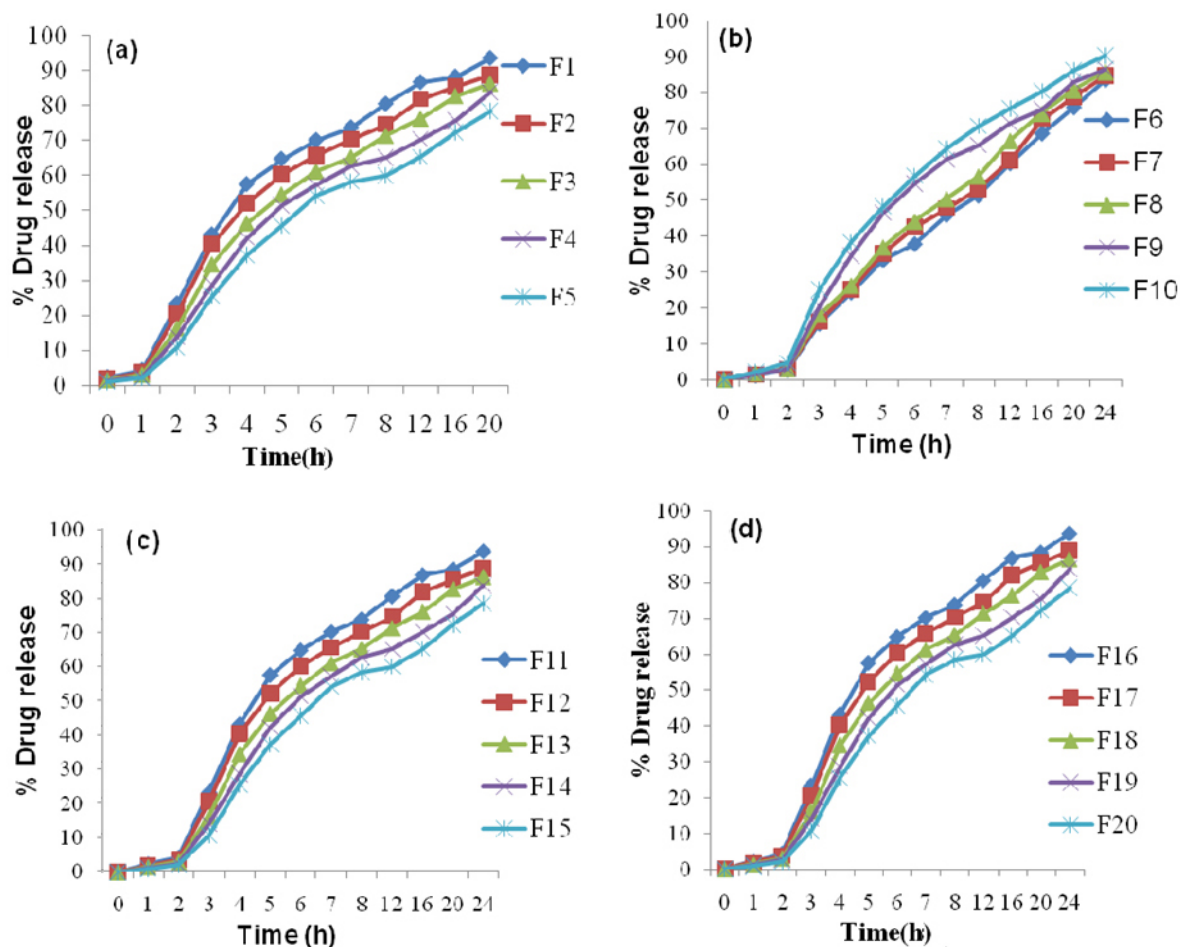


Figure 4. Effect of various parameters on the drug release rate of microbeads. (a) Sodium alginate concentration. (b) Stirring rate. (c) Calcium chloride concentration. (d) Cross-linking time.

Table 5. Stability data for aceclofenac sodium drug-loaded microbeads

Serial No.	Sampling interval (months)	Drug-content of microbeads			Physical characteristics		
		5°C %, w/w	25°C/60%RH %, w/w	40°C/75%RH %, w/w	5°C	25°C/60%RH	40°C/75%RH
0	0	100	100	100	*	*	*
1	1	100	100	99.56	*	*	*
2	2	100	99.89	98.67	*	*	*
3	3	100	98.76	97.45	*	*	*
4	4	100	97.90	96.16	*	*	*
5	5	100	97.32	95.55	*	*	*
6	6	100	96.87	94.64	*	*	*

* No change.

regression coefficient was observed. The values of the diffusion coefficient ranged between $n = 0.8806$ and 1.4503 indicating that the drug released from microbeads followed Zero-order kinetics controlled by swelling and relaxation of polymer chains.

3.6. Stability studies

The developed optimum formulations were subjected to stability studies at 25°C/60%RH, and 40°C/75%RH for up to 6 months. The dissolution profiles, and capsule

potency results for all of the stability conditions were within 90% to 110% of the label claim. Overall, results from the stability studies indicated that capsules were physically stable but the drug content at 40°C/75%RH was slightly reduced to 94.64% (w/w) after 6 months (Table 5). Good stability was observed at the lower temperature for more than 6 months.

4. Conclusion

It can be concluded from the above investigation

that the proper selection of optimized formulation conditions is very important to achieve high encapsulation efficiency and to control the release of aceclofenac sodium from the alginate microbeads. The alginate drug-loaded microbeads swelled at pH 1.2 predominantly very slowly but underwent increases at pH 6.8. The drug release from the microbeads was affected by the pH of the dissolution medium and results in a more sustained effect in alkaline medium. The ionotropic gelation technique is very easy to prepare, is free from any organic solvents and has a low manufacturing cost that can be successfully used for preparation of aceclofenac sodium microbeads using sodium alginate as drug release modifier. Therefore, one can assume that the aceclofenac sodium microbeads are a promising pharmaceutical dosage form that provides a sustained release drug delivery system. This system reduces the dosing frequency, eliminates the dose related adverse effects in the entire physiological region and ultimately improves compliance in the pharmacotherapy of arthritis, inflammation and pain. The entire process is feasible on an industrial scale and demands a pilot study.

Acknowledgements

Authors thank Micro Labs Pharmaceuticals, Ltd., Bangalore, India, for a gift sample of aceclofenac sodium and Signet Chemical Corporation Pvt., Ltd., Mumbai, India, for providing a gift sample of sodium alginate.

References

- Naik SR, Chatterjee NR. Non-steroidal anti-inflammatory drugs (NSAIDs) genesis and present status. *Ind Drugs*. 1993; 1:1-9.
- Chein YW. Oral drug delivery and delivery systems. In: *Novel Drug Delivery Systems*, 2nd ed., Marcel Dekker Inc., New York, USA, 1992; p. 139.
- Covelo T, Matricardi P. Polysaccharide hydrogels for modified release formulations. *J Control Release*. 2007; 119:5-24.
- Deasy PB. Microencapsulation and related drug process. In: *Drugs and Pharmaceutical Science*, 2nd ed., Marcel Dekker Inc, New York, USA, 1984; pp. 1-22.
- Grant GT, Morris ER, Rees DA, Smith PJC, Thom D. Biological interactions between polysaccharides and divalent cations: The egg-box model. *FEBS Lett*. 1973; 32:195-198.
- Martindale: The Complete Drug Reference. 32nd ed. (Parfitt K, ed.). Part-I. Analgesics, Anti-inflammatory Drugs, and Antipyretics, Philadelphia Pharmaceutical Press, 1996; pp. 1-11.
- Edith M, Mark RK. Microencapsulation. In: *Encyclopedia of Controlled Release*, 1st ed., Vol II. John Wiley and Sons Inc., London, UK, 1999; pp. 520-538.
- Soni T, Nagada C, Gandhi T, Chotal NP. Development of Discriminating method for dissolution of aceclofenac marketed formulation. *Dissol Technol*. 2008; 15:31-35.
- Bodmeier R, Paeratkul O. Spherical agglomerates of water insoluble drugs. *J Pharm Sci*. 1989; 78:964-970.
- Das MK, Senapat PC. Evaluation of furosemide loaded alginate microspheres prepared by ionotropic external gelation technique. *Acta Pharm Drug Res*. 2007; 64:253-262.
- Alfred M, Swarbrick J, Cammarata A. Micromeritics. In: *Physical Pharmacy*, 4th ed., B. I. Waverly Pvt., Ltd., Newdelhi, India, 1991; p. 760.
- Choi BY, Park HJ, Hwang SJ, Park JB. Preparation of alginate beads for floating drug delivery system: effects of CO₂ gas-forming agents. *Int J Pharm*. 2002; 239:81-91.
- Pongjanyakul T, Puttipipatkachorn S. Xanthan-alginate composite gel beads: Molecular interaction and *in-vitro* characterization. *Int J Pharm*. 2007; 331:61-71.
- Takka S, Ocak OH, Acarturk F. Formulation and investigation of nicardipine HCl-alginate gel beads with factorial design-based studies. *Eur J Pharm Sci*. 1998; 6:241-246.
- Dandagi PM. Microencapsulation of verapamil hydrochloride by ionotropic gelation technique. *Ind J Pharm Sci*. 2004; 66:631-663.
- Rajesh KS, Khanrah A, Sa B. Release of ketoprofen from alginate microparticles containing film forming polymers. *J Sci Ind Res*. 2004; 62:965-989.
- Sriamornsak P, Kennedy RA. Development of polysaccharide coated pellets for oral administration: Swelling and release behavior of calcium pectinate gel. *AAPS PharmSciTech*. 2007; 8:1-8.
- Mutalik S, Anju P, Manoj K, Usha AN. Enhancement of dissolution rate and bioavailability of aceclofenac: A chitosan based solvent change approach. *Int J Pharm*. 2008; 350:279-290
- Tayade PT, Kale RD. Encapsulation of water-insoluble drug by a cross-linking technique: effect of process and formulation variables on encapsulation efficiency, particle size, and *in vitro* dissolution rate. *AAPS Pharm Sci*. 2004; 6:E12.
- González-Rodríguez ML, Holgado MA, Sánchez-Lafuente C, Rabasco AM, Fini A. Alginate/chitosan particulate systems for sodium diclofenac release. *Int J Pharm*. 2002; 232:225-234.
- Tqnnesen HH, Karisen J. Alginate in drug delivery systems. *Dug Dev Ind Pharm*. 2002; 28:621-630.
- Raida S. Controlling of systemic absorption of gliclazide through incorporation into alginate beads. *Int J pharm*. 2007; 341:230-237.

(Received September 4, 2009; Revised November 17, 2009; Accepted November 25, 2009)

Original Article

Effects of lubricants on binary direct compression mixtures

Timuçin Uğurlu, Mekin Doğa Halaçoğlu, Murat Türkoğlu*

Marmara University, Faculty of Pharmacy, Department of Pharmaceutical Technology, Haydarpaşa, Istanbul, Turkey.

ABSTRACT: The objective of this study was to investigate the effects of conventional lubricants including a new candidate lubricant on binary direct compression mixtures. Magnesium stearate (MGST), stearic acid (STAC), glyceryl behenate (COMP) and hexagonal boron nitride (HBN) were tested. The binary mixtures were 1:1 combinations of spray dried lactose (FlowLac 100), dicalcium phosphate dihydrate (Emcompress), and modified starch (Starch 1500) with microcrystalline cellulose (Avicel PH 102). Tablets were manufactured on a single-station instrumented tablet press with and without lubricants. In the case of unlubricated granules, the modified starch-microcrystalline cellulose mixture provided the highest percent compressibility value at 8.25%, spray dried lactose-microcrystalline cellulose mixture was 7.33%, and the dicalcium phosphate dihydrate-microcrystalline cellulose mixture was 5.79%. Their corresponding tablet crushing strength values were: 104 N, 117 N, and 61 N, respectively. The lubricant concentrations studied were 0.5, 1, 2, and 4%. Effects of lubricant type and lubricant concentration on crushing strength were analyzed using a factorial ANOVA model. It was found that the Avicel PH 102-Starch 1500 mixture showed the highest lubricant sensitivity (110 N vs. 9 N), the least affected formulation was FlowLac-Avicel PH 102 mixture (118 N vs. 62 N). The crushing strength vs. concentration curve for MGST showed a typical biphasic profile, a fast drop up to 1% and a slower decline between 1 and 4%. The STAC, COMP, and HBN for all formulations showed a shallow linear decline of tablet crushing strength with increasing lubricant concentration. The HBN was as effective as MGST as a lubricant, and did not show a significant negative effect on the crushing strength of the tablets. The COMP and STAC also did not interfere with the crushing strength, however, they were not as effective lubricants as MGST or HBN.

Keywords: Lubricants, direct compression, hexagonal boron nitride, tablet crushing strength, magnesium stearate

1. Introduction

For a wide range of drugs, tablets are the preferred form of delivery. There are many reasons for this preference. Tablets have a high level of patient acceptability and compliance, they provide an accurate dosage and are easy to swallow. The form is distinctive and identifiable as tablets come in a variety of shapes and colors. Tablets taste bland, are less prone to tampering than other dosage forms and they offer advantages in manufacturing speed and cost (1,2). Before the 1960s, tablet manufacturing often required a wet granulation process to convert the active ingredients into flowable and compressible granules. With the introduction of carriers such as microcrystalline cellulose, tablet manufacturing *via* direct compression has become a convenient option (2,3). In contrast to wet granulation, direct compression methods are rather simple. In fact, the three step process, involving screening and/or milling, final mixing and compression, can often save labor, time, equipment and space (4,5). Although direct compression may seem to be a simple method for making tablets, the selection of appropriate excipients and their levels in the formulation are crucial for successful manufacturing (6,7). The compressibility and flowability of an excipient must be considered when developing a direct compression formula. The lubricants are pharmaceutical excipients that decrease friction at the interface between a tablet and the die wall during ejection. Without external lubricant addition the modern tableting operations can not be carried out. Inadequate lubrication due to friction and adhesion among powder particles leads to troubles in the manufacturing process and deterioration of productivity (8,9). Friction will damage the machine and tablet during the ejection phase. Moreover, high temperature generated during compression can affect drug stability (10). Because of the aforementioned reasons, determining the type and level of lubricants are among the critical parameters in direct compression. If the concentration of a lubricant is too high, or the mixing time is too long, the potential problem will be a decrease

*Address correspondence to:

Dr. Murat Turkoglu, Marmara University, Faculty of Pharmacy, Department of Pharmaceutical Technology, 34668, Haydarpaşa, Istanbul, Turkey.
e-mail: turkoglu@marmara.edu.tr

in tablet hardness, inability to compress into tablets, increase in tablet disintegration time, and a decrease in dissolution rate (11-14). In our previous studies (9,15), we reported that magnesium stearate (MGST), and a newly introduced lubricant, hexagonal boron nitride (HBN) provided the smallest lower punch ejection forces (LPEF) during tableting for a wet granulation process. While stearic acid (STAC) and glyceryl behenate (COMP) resulted in a much higher LPEF. This study was designed based on that information. In this study, selected binary direct compression mixtures spray dried lactose-microcrystalline cellulose (DC1), dicalcium phosphate dihydrate-microcrystalline cellulose (DC2), and modified starch-microcrystalline cellulose (DC3) were used to assess the effect of lubricant type and concentration on directly compressed tablets' mechanical properties. A two-way ANOVA design was used to evaluate these effects.

2. Materials and Methods

2.1. Materials

Microcrystalline cellulose (Avicel PH 102) was donated by FMC, Brussels, Belgium. Spray dried Lactose (FlowLac 100) was obtained from Meggle AG, Wasserburg, Germany. Dibasic calcium phosphate dihydrate (Emcompress), and Starch 1500 were donated by Select Chemie AG, and Colorcon Ltd., Istanbul, Turkey. MGST (0.43 m²/g), STAC (0.03 m²/g), COMP (0.23 m²/g), and HBN (1.13 m²/g) were obtained from Mallinckrodt, St. Louis, MO, USA, Sherex, Dublin, OH, USA, Gattefose, Cedex, France, and ITU, High Technology Ceramics and Composites Research Center, Istanbul, Turkey, respectively.

2.2. Powder mixtures

A 1:1 mixture of Avicel PH 102-FlowLac 100, Avicel

PH 102-Emcompress, and Avicel PH 102-Starch 1500 were used as the master mixtures without a drug. Binary mixtures were mixed for 20 min in a laboratory size V-blender. All lubricants were added to those binary mixtures depending on their studied concentrations and mixed further for 3 min.

2.3. Bulk and tapped densities

Twenty grams of binary mixtures DC1, DC2, and DC3 were mixed separately in a V-blender for 10 min, the mixtures were poured into a 100 mL graduated cylinder. Their bulk volumes were recorded. The cylinder was directly mounted onto a tapping machine which had a tapping speed of 100 taps/min. After 3 min tapped volumes were recorded. Measurements were made in triplicate. Average d_b and d_t were calculated from M/V_b and M/V_t where M was the weight of the binary mixture, V_b was the bulk volume and V_t was the tapped volume. The bulk density was d_b and d_t was the tapped density. Percent compressibility (Carr Index) was calculated for each mixture as: $1 - d_b/d_t \times 100$.

2.4. Tablet preparation

For lubrication performance, 48 batches (B1-B48) of tablets were manufactured using a single-station instrumented tablet press (Korsch EK0, Berlin, Germany) with a 9 mm flat faced punch set. Study design is given in Table 1. A 250 mg direct compression mass was filled into the die cavity and 6 perpetual compressions were made. Tablet weight and the upper punch compression pressure were kept constant for each binary mixture for 0.5, 1, 2, and 4% lubricant concentrations. However, when the tableting operation was changed to the next formulation (*i.e.*, DC2), the tablet weight was kept constant but the compression pressure was adjusted to obtain approximately 110-120 N crushing strength for the

Table 1. Study design

Formulation DC 1 [Spray dried lactose/Avicel PH 102 (1:1)]			Formulation DC 2 [Emcompress/Avicel PH 102 (1:1)]			Formulation DC 3 [Starch 1500/Avicel PH 102 (1:1)]		
Batches	Lubricant type	Lubricant concentration (%)	Batches	Lubricant type	Lubricant concentration (%)	Batches	Lubricant type	Lubricant concentration (%)
B1	MGST	0.5	B17	MGST	0.5	B33	MGST	0.5
B2	MGST	1	B18	MGST	1	B34	MGST	1
B3	MGST	2	B19	MGST	2	B35	MGST	2
B4	MGST	4	B20	MGST	4	B36	MGST	4
B5	HBN	0.5	B21	HBN	0.5	B37	HBN	0.5
B6	HBN	1	B22	HBN	1	B38	HBN	1
B7	HBN	2	B23	HBN	2	B39	HBN	2
B8	HBN	4	B24	HBN	4	B40	HBN	4
B9	COMP	0.5	B25	COMP	0.5	B41	COMP	0.5
B10	COMP	1	B26	COMP	1	B42	COMP	1
B11	COMP	2	B27	COMP	2	B43	COMP	2
B12	COMP	4	B28	COMP	4	B44	COMP	4
B13	STAC	0.5	B29	STAC	0.5	B45	STAC	0.5
B14	STAC	1	B30	STAC	1	B46	STAC	1
B15	STAC	2	B31	STAC	2	B47	STAC	2
B16	STAC	4	B32	STAC	4	B48	STAC	4

Mixing time: 3 min in V-blender.

manufactured tablets at 0.5% lubricant concentration to be able to observe the decline of crushing strength with increasing lubricant level from the same starting point.

2.5. Tablets of unlubricated powder mixtures

The compression pressure and tablet weight adjustment were made once for DC1 and no further change was made during the compaction of the DC2 and DC3. An

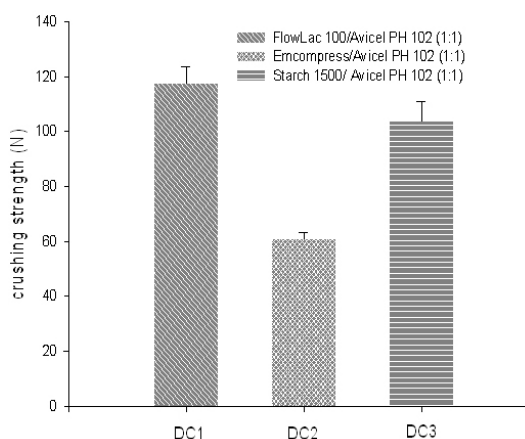


Figure 1. The case of no lubricant. Average tablet crushing strengths for DC1, DC2, and DC3 (250 mg tablet weight, 1,000 kg.f compression force).

Table 2. Bulk/tapped densities and compressibility of binary mixtures

	d-Bulk (g/mL)	d-Tapped (g/mL)	% Compressibility (CI)
DC1	0.43 ± 0.03	0.46	7.33
DC2	0.52 ± 0.03	0.55	5.79
DC3	0.47 ± 0.05	0.51	8.25

CI = Carr Index.

unlubricated, 250 mg binary powder was filled into the die cavity and 6 perpetual compressions were made for each batch and the average of the data was calculated.

2.6. Measurement of tablet properties

The weight variation of tablets was determined according to the USP 24. The diametrical tablet crushing strength was evaluated using a tablet hardness tester (Model C 50, I-Holland, Ltd., Nottingham, UK).

2.7. Statistical analysis

The effect of lubricant type and lubricant concentration on the crushing strength of tablets were tested using a factorial ANOVA model, specifically, a two-way analysis of variance (two-way ANOVA) procedure for the main effects (SPSS 13.0 for windows).

3. Results and Discussion

Study design is summarized in Table 1. Trials were made with four levels (0.5, 1, 2, and 4%) of MGST, HBN, COMP, and STAC for all direct compression formulations (Batches 1 to 48). Figure 1 presents the crushing strength values of unlubricated binary mixtures (DC1, DC2, and DC3), the crushing strength values were found to be 117 N for DC1, 61 N for DC2, and 104 N for DC3, respectively (Figure 1). These values correlated well with the bulk densities of the binary powders. The values were 0.43 g/mL for DC1, 0.52 g/mL for DC2, and 0.47 g/mL for DC3, respectively (Table 2). In the case of unlubricated granules, DC3 showed the highest compressibility value of 8.25%, DC1 was 7.33%, and DC2 provided a value of 5.79% (Table 2). Table 3 and Figures 2-4, show

Table 3. Weight and crushing strength variation of tablets including different lubricants

Lubricant type	Lubricant amount (%)	Formulation DC1 [FlowLac/Avicel PH 102 (1:1)] Batches (B1 to B16)		Formulation DC2 [Emcompress/Avicel PH 102 (1:1)] Batches (B17 to B32)		Formulation DC3 [Starch 1500/Avicel PH 102 (1:1)] Batches (B33 to B48)	
		Weight (mg)	Crushing Strength (N)	Weight (mg)	Crushing Strength (N)	Weight (mg)	Crushing Strength (N)
MGST	0.5	245.17 ± 2.64	101.53 ± 9.71	247.65 ± 0.87	71.61 ± 3.53	243.75 ± 1.77	59.65 ± 4.31
	1	247 ± 1.79	78.38 ± 4.70	247.53 ± 2.08	54.74 ± 3.13	241.38 ± 1.35	49.84 ± 6.86
	2	246.17 ± 2.64	70.14 ± 5.98	248.48 ± 1.64	48.65 ± 2.94	244.33 ± 3.27	27.76 ± 2.84
	4	245 ± 2.68	62.19 ± 3.92	248 ± 2.63	40.02 ± 3.33	245.72 ± 2.26	8.93 ± 1.66
HBN	0.5	246.67 ± 1.64	117.32 ± 6.37	246.65 ± 0.35	102.61 ± 7.75	241.77 ± 3.21	104.18 ± 7.75
	1	245.33 ± 1.41	114.18 ± 6.27	250.33 ± 1.48	100.55 ± 3.72	242.97 ± 2.49	99.76 ± 4.51
	2	245.23 ± 2.7	113.20 ± 11.77	247.53 ± 3.06	88.68 ± 7.84	244.65 ± 1.91	98.88 ± 5.49
	4	246.65 ± 3.49	102.02 ± 6.47	247.97 ± 2.9	79.95 ± 3.23	242.82 ± 3.78	89.17 ± 10.20
COMP	0.5	245.42 ± 0.28	118.40 ± 4.70	245.6 ± 2.75	90.84 ± 7.75	243.6 ± 3.58	103.10 ± 12.65
	1	245.75 ± 0.56	117.03 ± 3.63	245.7 ± 1.12	89.27 ± 5.59	243.15 ± 1.78	92.01 ± 7.45
	2	244.83 ± 1.73	109.48 ± 5.98	245.23 ± 2.05	89.07 ± 2.74	244.4 ± 3.07	80.34 ± 3.23
	4	243.35 ± 1.42	96.04 ± 4.12	246.6 ± 1.61	86.52 ± 4.90	243.27 ± 3.17	68.57 ± 5.98
STAC	0.5	241.63 ± 2.4	111.83 ± 7.25	247.12 ± 2.99	97.41 ± 6.96	246.43 ± 2.2	109.57 ± 5.10
	1	243.37 ± 2.43	108.30 ± 4.12	246.83 ± 3.55	96.62 ± 7.25	243.55 ± 5.37	100.94 ± 6.37
	2	243.72 ± 1.74	105.35 ± 8.63	247.08 ± 1.44	95.942 ± 6.57	245.02 ± 4.22	86.62 ± 8.92
	4	244.72 ± 2.01	97.41 ± 4.70	247.08 ± 1.6	92.99 ± 1.86	245.33 ± 2.74	69.55 ± 3.92

lubricant concentration vs. crushing strength profiles. MGST resulted in a biphasic curve, up to 1% lubricant concentration and a fast drop in crushing strength was observed for DC1, DC2, and DC3. From 1% to 4% lubricant concentration the curve was shallow (Figures 2-3) except for DC3 where the mechanical strength of tablets fell drastically (Figure 4). It was well known

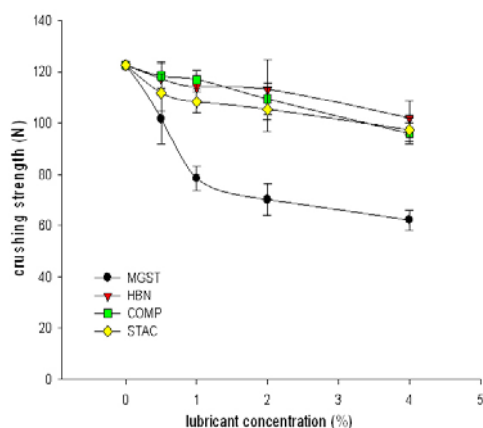


Figure 2. Effect of lubricant concentration on tablet crushing strength for DC1 [FlowLac 100/Avicel PH 102 (1:1)].

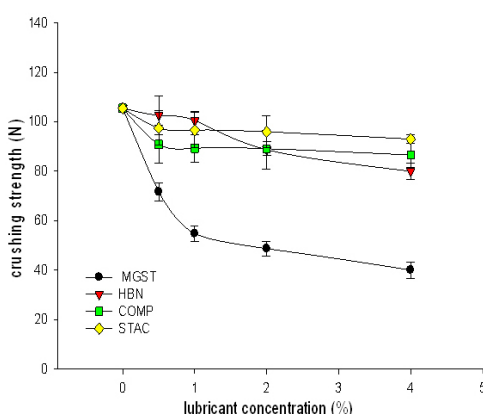


Figure 3. Effect of lubricant concentration on tablet crushing strength for DC2 [Emcompress/Avicel PH 102 (1:1)].

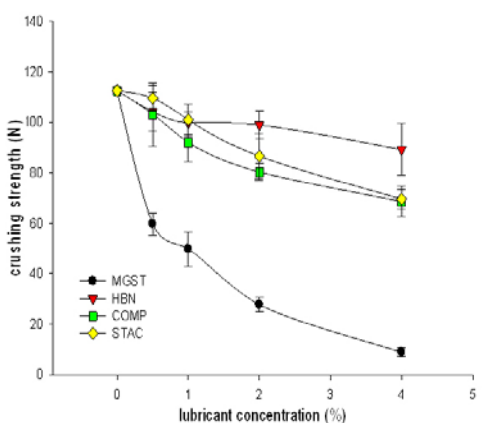


Figure 4. Effect of lubricant concentration on tablet crushing strength for DC3 [Starch 1500/Avicel PH 102 (1:1)].

from the literature that surface covering properties of lubricants are more drastic in the case of plastically deformed particles that are unable to create new clean surfaces during compression (16). The other three lubricants, HBN, COMP, and STAC showed a shallow linear decline in tablet crushing strength vs. lubricant concentration curves. The binary mixture Starch 1500/Avicel PH 102 showed a steeper decline when compared to DC1 and DC2. This observation correlates well with less effective lubricant behavior. However, in one of our previous reports (9) it was found that hexagonal boron nitride was as effective as MGST in terms of lower punch ejection force. In the same study, COMP and STAC were much inferior in lowering the ejection forces (9). Based on the data obtained from Figures 2-4, 0.5% MGST addition as a lubricant with 3 min mixing time was not appropriate for mechanically acceptable tablets regardless of binary combination in direct compression. Either less MGST should be used, or another effective lubricant such as HBN could be considered. It can be concluded that STAC or COMP will not be satisfactory lubricants at those concentrations. For the statistical analysis, a two-way analysis of variance (Two-way ANOVA) was separately performed for spray dried lactose-microcrystalline cellulose (DC1), dicalcium phosphate dihydrate-microcrystalline cellulose (DC2), and modified starch-microcrystalline cellulose (DC3). The crushing strength was the dependent variable. Lubricant type and lubricant concentration were selected as the fixed factors. The general linear model/univariate analysis of variance, main effects were evaluated. The Bonferroni method was chosen for the post hoc test. It was found that for all cases (DC1, DC2, and DC3) there was a significant difference among the lubricants ($p < 0.0001$). In terms of lubricant concentration the most significant case was DC3 ($p < 0.0001$) and the least significant case was DC2 ($p < 0.033$) with DC1 in between ($p < 0.003$) (Tables 4-7). Therefore, it seemed that the dicalcium phosphate dihydrate-microcrystalline cellulose binary mixture showed the least lubricant sensitivity, and modified starch-microcrystalline cellulose binary mixture showed the highest lubricant sensitivity. The effect of MGST on tablet crushing strength was significantly different than the other lubricants, the difference among the other three lubricants (STAC,

Table 4. Factors and their levels for ANOVA.

		N
Lubricant	1	4
	2	4
	3	4
	4	4
Concentration	0.5	4
	1.0	4
	2.0	4
	4.0	4

Table 5. Effects of factors on dependent variable (DC1) [Spray dried lactose/Avicel PH 102 (1:1)]

Source	Type III Sum of Squares	df	Mean Square	F	Sig.
Corrected Model	42.480 ^a	6	7.080	18.664	0.000
Intercept	1,710.443	1	1,710.443	4,508.936	0.000
Lubricant	31.061	3	10.354	27.293	0.000
Concentration	11.419	3	3.806	10.034	0.003
Error	3.414	9	0.379		
Total	1,756.337	16			
Corrected Total	45.894	15			

Dependent Variable: Crushing strength. ^a R Squared = 0.926 (Adjusted R Squared = 0.876).

Table 6. Effects of factors on dependent variable (DC2) [Emcompress/Avicel PH 102 (1:1)]

Source	Type III Sum of Squares	df	Mean Square	F	Sig.
Corrected Model	53.477 ^a	6	8.913	21.861	0.000
Intercept	1,141.088	1	1,141.088	2,798.805	0.000
Lubricant	47.863	3	15.954	39.132	0.000
Concentration	5.614	3	1.871	4.590	0.033
Error	3.699	9	0.408		
Total	1,198.235	16			
Corrected Total	57.174	15			

Dependent Variable: Crushing strength. ^a R Squared = 0.936 (Adjusted R Squared = 0.893).

Table 7. Effects of factors on dependent variable (DC3) [Starch 1500/Avicel PH 102 (1:1)]

Source	Type III Sum of Squares	df	Mean Square	F	Sig.
Corrected Model	127.536 ^a	6	21.256	39.836	0.000
Intercept	1,012.990	1	1,012.990	1,898.444	0.000
Lubricant	29.031	3	9.677	18.136	0.000
Concentration	98.505	3	32.835	61.536	0.000
Error	4.802	9	0.534		
Total	1,145.328	16			
Corrected Total	132.339	15			

Dependent Variable: Crushing strength. ^a R Squared = 0.964 (Adjusted R Squared = 0.940).

Table 8. Multiple comparison of lubricant types among each other as a post hoc test/ Bonferroni

(I) Lubricant	(J) Lubricant	Mean Difference (I-J)	Std. Error	Sig.
MGST	STAC	-3.4275*	0.43551	0.000
	COMP	-3.2800*	0.43551	0.000
	HBN	-2.8200*	0.43551	0.000

Dependent variable: Crushing strength. Based on observed means.

* The mean difference is significant at the 0.05 level.

HBN, COMP) was not significant (Table 8). The FlowLac-Avicel binary mixture (DC1) was found to be the best candidate for further evaluation as a direct compression formula based on lubricant sensitivity and tablet mechanical strength. However, the DC3 mixture gave the highest compressibility value. Furthermore, a lubricant concentration lower than 0.5% for MGST and more preferably selecting HBN between 0.5-1% would result in mechanically acceptable tablets.

References

- Pharma Ingredients & Services. Dry binder used in direct compression. 2006; 20:1-5. (http://www.pharma-ingredients.basf.com/PDF/.../ExAct_20_May2008.pdf)
- Sheth BB, Bandelin FJ, Shangraw RF. Compressed Tablets. In: Pharmaceutical Dosage Forms: Vol. 1 Tablets (Lieberman HA, Lachman L, eds.). Marcel Dekker Inc., New York, USA, 1980; pp. 109-184.
- Yuan J, Wu SHW. Sustained release tablets *via* direct compression: A feasibility study using cellulose acetate and cellulose acetate butyrate. *Pharm Dev Technol.* 2008; 24:92-106.
- Gohel MC. A review of co-processed directly compressible excipients. *J Pharm Pharm Sci.* 2003; 8:76-93.
- Turkoglu M, Sakr A. Tablet Dosage Forms. In: Modern Pharmaceutics: Vol. 1 Basic Principles and Systems (Florence AT, Siepmann J, eds.). PharmaceuTech, Inc., Pinehurst, North Carolina, USA, 2009; pp. 481-497.
- Bolhuis GK, Eissens AC, Adrichem TP, Wessenlingh JA, Frijlink HW. Hollow filler-binders as excipients for direct compression. *Pharm Res.* 2003; 20:515-518.
- Armstrong NA. Tablet manufacture by direct compression. In: Encyclopedia of Pharmaceutical Technology, 3rd ed. (Swarbrick J, ed.). Informa Healthcare Inc., New York, USA, 2007; pp. 3673-3685.
- Aoshima H, Miyagisnima A, Nozawa Y, Saduka Y, Sonobe T. Glycerin fatty acid esters as a new lubricant of tablets. *Int J Pharm.* 2005; 293:25-34.
- Ugurlu T, Turkoglu M. Hexagonal boron nitride as a

- tablet lubricant and a comparison with conventional lubricants. *Int J Pharm.* 2008; 353:45-51.
10. Kara A, Tobyn MJ, Stevens R. An application for zirconia as a pharmaceutical die set. *J Eur Ceram Soc.* 2004; 24:3091-3101.
 11. Otsuka M, Yamane I, Matsuda Y. Effects of lubricant mixing on compression properties of various kinds of direct compression excipients and physical properties of the tablets. *Adv Powder Technol.* 2004; 15:477-493.
 12. Flores LE, Arellano RL, Díaz Esquivel JJ. Lubricant susceptibility cellactose and Avicel pH-200: a quantitative relationship. *Drug Dev Ind Pharm.* 2000; 26:297-305.
 13. Mollan MJ, Celik M. The effects of lubrication on the compaction and post compaction properties of directly compressible maltodextrins. *Int J Pharm.* 1996; 144:1-9.
 14. Shah AC, Mlodozieniec AR. Mechanism of surface lubrication: Influence of duration of lubricant excipient mixing on processing characteristics of powders and properties of compressed tablets. *J Pharm Sci.* 1977; 66:1377-1382.
 15. Turkoglu M, Sahin I, San T. Evaluation of hexagonal boron nitride as a new tablet lubricant. *Pharm Dev Technol.* 2005; 10:381-388.
 16. De Boer AH, Bolhuis GK, Lerck CF. Bonding characteristics by scanning electron microscopy of powders mixed with magnesium stearate. *Powder Technol.* 1978; 20:75-82.

(Received October 27, 2009; Accepted November 22, 2009)

Original Article

Effects of the herbal medicine Hachimi-jio-gan (Ba-Wei-Di-Huang-Wan) on insulin secretion and glucose tolerance in type 2 diabetic Goto-Kakizaki rats

Yoshihiko Hirotsu*, Kenji Ikeda, Michiaki Myotoku

Laboratory of Clinical Pharmaceutics, Faculty of Pharmacy, Osaka Ohtani University, Tondabayashi, Osaka, Japan.

ABSTRACT: Hachimi-jio-gan (HJ) is a Chinese medicine that has been widely used for the treatment of nephrotic syndromes, hypertension, and diabetes mellitus. We reported that HJ lowers plasma glucose in type 1 diabetic rats. We investigated the effects of HJ on diabetic hyperglycemia and insulin secretion in type 2 diabetic Goto-Kakizaki (GK) rats. Eight-week-old diabetic GK rats were given free access to pellets containing 1% HJ extract powder for 14 weeks. HJ consumption increased the food intake and body weight of these rats in comparison to control rats. HJ may control the body weight loss observed in GK rats. HJ also reduced hyperglycemia in diabetic GK rats, and it significantly increased insulin secretion in non-fasting GK rats over the experimental period. In oral glucose tolerance tests, HJ significantly improved the insulin response at 30 min and reduced the plasma glucose level at 60 min after glucose administration ($p < 0.05$). Ten weeks after administration, the plasma leptin levels significantly increased in the HJ group rats. These results demonstrate that in diabetic GK rats, HJ decreased the level of postprandial glucose via enhanced insulin secretion coupled with the regulation of food intake by leptin.

Keywords: Hachimi-jio-gan (HJ), hyperglycemia, insulin, body weight, Goto-Kakizaki rat

1. Introduction

The herbal medicine Hachimi-jio-gan (HJ) (Ba-Wei-Di-Huang-Wan) has been widely used for the treatment of hypertension, nephrotic syndromes, glomerulonephritis, and diabetes mellitus since the late middle ages. In Japan, the medicinal uses of HJ are provided in the

package insert of the HJ extract. Animal studies have shown that *Rehmanniae radix*, *Corni fructus*, and *Hoelen* lower blood sugar (1). However, HJ does not contain ginseng, which is frequently used to treat diabetes in the clinical setting. Various human and animal studies have been conducted on the therapeutic effects of HJ (2-5). Most of these studies have investigated the effects of HJ on renal damage, including diabetic nephropathy, and the mechanism underlying these effects (6-8). We have reported the antidiabetic effects of HJ in rats in which various symptoms, including persistent hyperglycemia, were induced by streptozotocin (STZ) administration (9-11). HJ is used in the treatment of diabetes-associated symptoms such as dry mouth, thirst, and polyuria (12). However, despite the fact that clinical and experimental studies have provided evidence for the various beneficial effects of HJ, to date, only a few scientific studies have presented corroborating evidence on such subjective symptoms.

In the present study, we used spontaneously diabetic Goto-Kakizaki (GK) rats as animal models of genetic predisposition to non-insulin-dependent diabetes mellitus (NIDDM) (13). In GK rats, glucose-stimulated insulin secretion is reduced, and glucose tolerance is impaired. Moreover, GK rats with impaired insulin secretion do not become obese and do not develop hyperlipidemia (14). These characteristics of GK rats are similar to those observed in NIDDM patients (15-17). The GK rat is thus considered a suitable model for the investigation of the effects of HJ on insulin secretion and glucose tolerance. In this study, we investigated the effects of HJ on diabetes symptoms, including hyperglycemia, in diabetic GK rats. We also examined the effect of HJ administration on the food intake and body weight of GK rats.

2. Materials and Methods

2.1. Animals

Male GK and Wistar rats (Japan SLC Inc., Shizuoka, Japan) weighing 180-190 g were used in this study. The rats were maintained for 1 week on a standard pellet

*Address correspondence to:

Dr. Yoshihiko Hirotsu, Laboratory of Clinical Pharmaceutics, Faculty of Pharmacy, Osaka Ohtani University, 3-11-1 Nishikiorikita, Tondabayashi, Osaka 584-8540, Japan.
e-mail: hirotsu@osaka-ohtani.ac.jp

diet (MF diet; Oriental Yeast, Tokyo, Japan). They were kept in a room maintained at $22 \pm 2^\circ\text{C}$ with a 12 h/12h light/dark cycle (diurnal time, 8:00-20:00) and had free access to rat chow and water. All experimental procedures were conducted in accordance with the Osaka Ohtani University Guidelines for the Care and Use of Laboratory Animals.

2.2. Drugs

The HJ extract was obtained from Tsumura & Co. Ltd. (Tokyo, Japan). The composition of HJ is as follows: Rehmanniae Radix (*Rehmannia glutinosa* Libosch), 6 g; Corni Fructus (*Cornus officinalis* Sieb et Zucc.), 3 g; Dioscoreae Rhizome (*Dioscorea japonica* Thunb.), 3 g; Alismatis Rhizome (*Alisma orientale* Juzep.), 3 g; Hoelen (*Poria cocos* Wolf), 3 g; Moutan Cortex (*Paeonia suffruticosa* Andrews), 2.5 g; Cinnamomi Cortex (*Cinnamomum cassia* Blume), 1 g; and Aconiti Tuber (*Aconitum carmichaeli* Debx), 0.5 g. Aqueous extracts were prepared from the crude drugs and spray dried to obtain the extract powder. The three-dimensional HPLC profile of HJ provided by Tsumura Inc. is shown in Figure 1.

2.3. Treatment of animals and preparation of sample

The GK rats were randomly divided into 2 groups of 5 animals each. The control group was given pellet chow without HJ, while the HJ group was given pellet chow containing 1% HJ extract powder. The pellets and tap water were provided *ad libitum*. The food intake and body weight of the rats were measured every week. Every week for the next 14 weeks, non-fasting blood samples were collected from the jugular vein at 10:00 A.M. and stored in chilled tubes containing EDTA-2Na (at a final concentration of 0.03 mM) and dipeptidyl peptide IV (DPP-IV) inhibitor (10 $\mu\text{L}/\text{mL}$ blood) (Millipore, MO, USA). At the end of the 14-week period, blood samples were collected from the inferior vena cava under ether anesthesia, and the plasma was immediately separated by centrifugation.

2.4. Assay of plasma glucose levels

Plasma glucose levels were determined by using a commercial reagent (Glucose CII-Test Wako; Wako Pure Chemical Industries Ltd., Osaka, Japan).

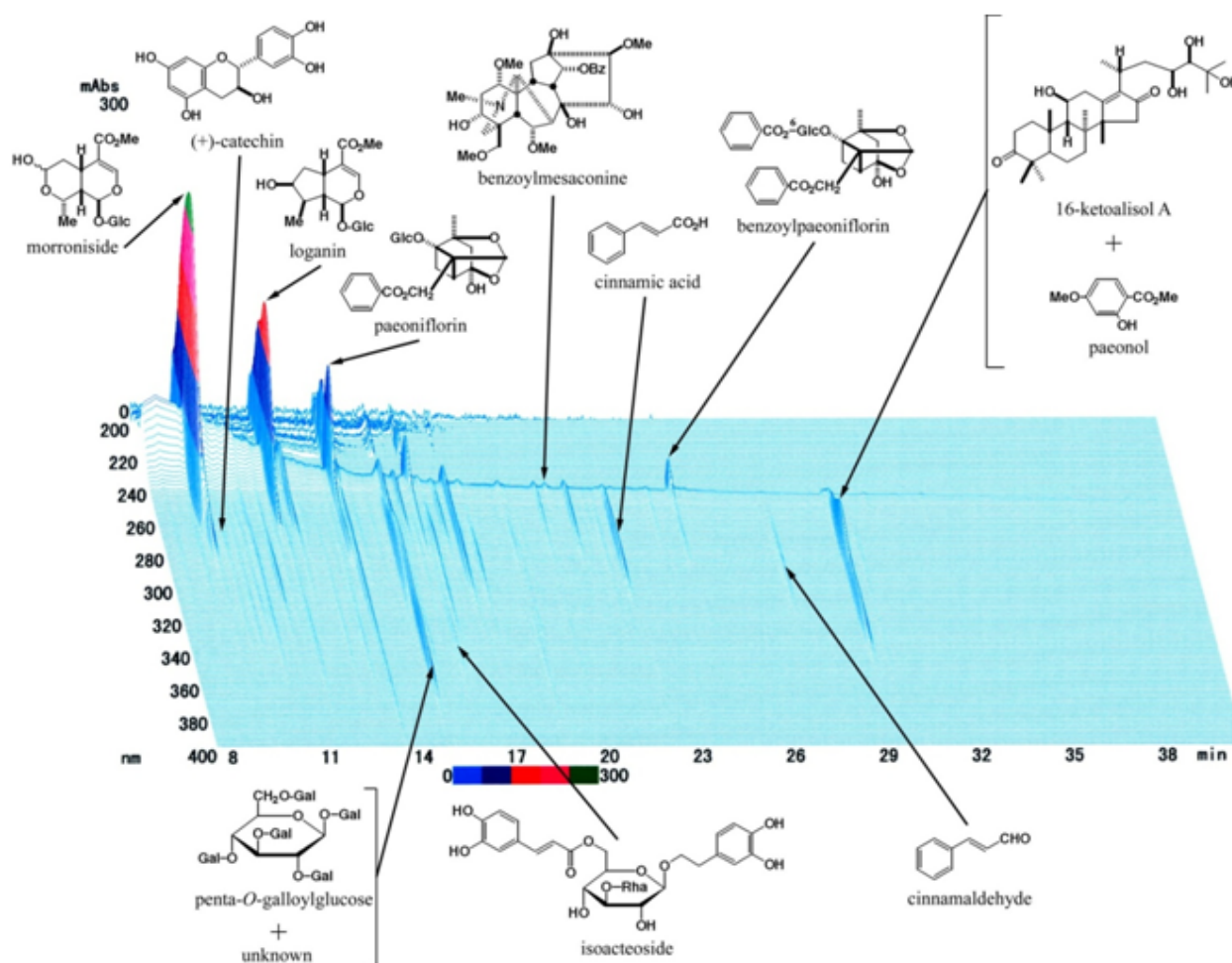


Figure 1. Three-dimensional HPLC profile of HJ.

2.5. Immunoassay of plasma hormone levels

Plasma immunoreactive insulin levels were measured by using a commercial radioimmunoassay kit (Insulin Eiken RIA kit; Eiken Chemical Co. Ltd., Tokyo, Japan). In each assay tube, 25 μ L of standard insulin or the unknown sample, 50 μ L of guinea pig anti-insulin plasma, and 50 μ L of 125 I-labeled insulin were mixed, and the mixture was incubated at 2-8°C for 24 h. To the mixture, 50 μ L of goat anti-guinea pig γ -globulin plasma was added; this was followed by further incubation at 2-8°C for 30 min and centrifugation at 3,000 rpm at 4°C for 30 min. The supernatant was aspirated, and the radioactivity of the precipitate was counted in a gamma counter. Plasma leptin levels were measured by using the Rat Leptin-HS ELISA Kit (YK051; Yanaihara Institute Inc., Shizuoka, Japan).

2.6. Oral glucose tolerance test

In the final week of treatment, an oral glucose tolerance test (OGTT) was performed on the GK (age, 23 weeks) rats after 16 h of starvation. The control blood sample was collected from the jugular vein at 0 min and stored in chilled tubes containing EDTA-2Na. Glucose (2 g glucose/kg body weight) was administered orally *via* a stomach tube, and blood was collected from the jugular vein at 0, 30, 60, and 120 min. The plasma glucose and insulin levels were determined for each time point by using the same reagents.

2.7. Data analysis

Except for the amount of food intake, all experimental data are expressed as mean \pm standard deviation (S.D.). The differences between the mean values were statistically analyzed by using Tukey-Kramer test and Student's unpaired *t*-test with a significance level of $p < 0.05$.

3. Results

3.1. Food intake and body weight

The changes in the food intake and body weights are showed in Figure 2. The body weights of rats from the HJ group significantly increased after the fifth week compared with the control group ($p < 0.05$). The mean daily food consumption and body weights of the HJ-administered rats were higher than those of the control rats, but were not beyond those of the normal rats.

3.2. Non-fasting plasma glucose levels

Figure 3 shows the changes in non-fasting plasma glucose levels during the period of HJ administration. The plasma glucose level for the HJ group rats had a tendency to lower than that for the control group rats

except weeks 1 and 12. This tendency was particularly marked in weeks 5, 7, 8, 9, and 13 ($p < 0.05$).

3.3. Plasma insulin levels

Figure 4 shows the changes of plasma insulin levels observed during the study period. In the HJ group rats, the non-fasting plasma insulin level significantly

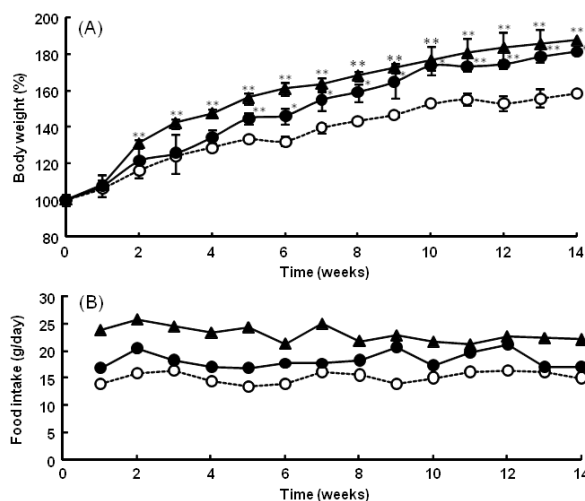


Figure 2. Effects of 14-week treatment with HJ on body weight (A) and mean food intake amount per cage (g/day) (B) in GK rats. \blacktriangle , normal rats treated vehicle (Normal group); \circ , GK rats treated with vehicle (Control group); \bullet , GK rats treated with HJ (HJ group). * $p < 0.05$, ** $p < 0.01$ compared with the control group. Data are mean \pm S.D. ($n = 5$).

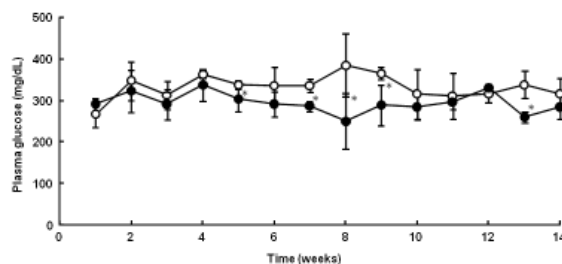


Figure 3. Effects of HJ on non-fasting plasma glucose levels during 14 weeks of treatment in GK rats with or without HJ. \circ , GK rats treated with vehicle (Control group); \bullet , GK rats treated with HJ (HJ group). * $p < 0.05$ compared with the control group. Data are mean \pm S.D. ($n = 5$).

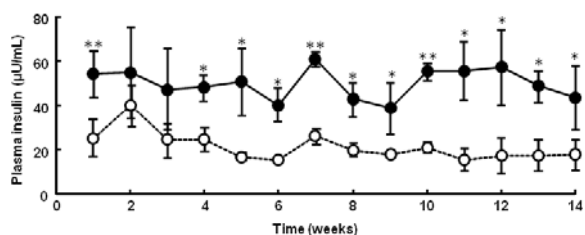


Figure 4. Effect of HJ on non-fasting plasma insulin levels during 14 weeks of treatment in GK rats with or without HJ. \circ , GK rats treated with vehicle (Control group); \bullet , GK rats treated with HJ (HJ group). * $p < 0.05$, ** $p < 0.01$ compared with the control rats. Data are mean \pm S.D. ($n = 5$).

increased throughout the experiment except for the second and third weeks. The plasma insulin level of the HJ group rats was approximately twice as high as that of the control group rats.

3.4. Oral glucose tolerance test

Figure 5 shows the changes in OGTTs performed 14 weeks after treatment. The control group exhibited the typical pattern observed in diabetes: glucose administration caused a quick increase in the plasma glucose, and it remained high. However, at 60 min, the plasma glucose was found to be significantly lower in the HJ group rats than in the control group rats (459 ± 19 vs. 413 ± 10 mg/dL, $p < 0.05$). In contrast, the plasma insulin levels of the HJ group rats increased markedly at 30 min (7.4 ± 0.2 vs. 14.5 ± 1.1 μ U/mL, $p < 0.05$) and returned to the control levels after 120 min (Figure 5B).

3.5. Plasma leptin levels

Figure 6 shows the changes in the non-fasting plasma leptin levels during the study period. In the control

group rats, these levels did not change significantly during the study period. In the HJ group rats, however, they increased gradually along with HJ administration, and in the 10th, 12th, and 14th weeks, they were significantly higher than those of the control group rats (10th and 14th week, $p < 0.05$; 12th week, $p < 0.01$).

4. Discussion

Diabetic GK rats have been reported to have i) decreased insulin secretory response of the pancreatic β cells to glucose and ii) insulin resistance – the 2 main characteristics of NIDDM (18). In contrast to many other rodent models of NIDDM, GK rats do not become obese and do not develop hyperlipidemia. These characteristics are similar to the typical Asian-type diabetes (17,19). The GK rat is thus considered to be a suitable model for the investigation of the effect of HJ on insulin secretion and glucose tolerance.

HJ is a Chinese medicine that has been widely used in the treatment of diabetes for a long period of time. Although few clinical studies have developed the herbal formula to lower blood glucose levels, HJ is administered to diabetic patients. It has been

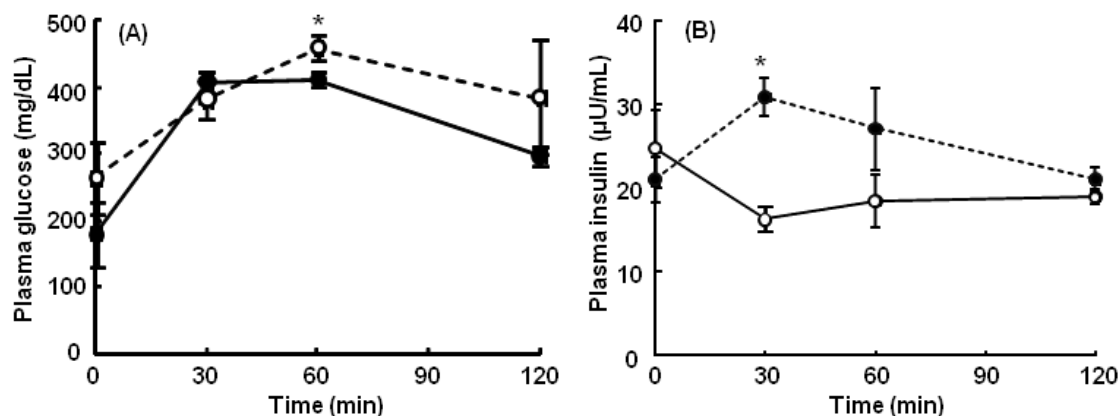


Figure 5. Effects of HJ on plasma glucose (A) and insulin (B) levels in oral glucose tolerance test after 14 weeks of treatment in GK rats with or without HJ. \circ , GK rats treated with vehicle (Control group); \bullet , GK rats treated with HJ (HJ group). * $p < 0.05$ compared with the control rats. Data are mean \pm S.D. ($n = 5$).

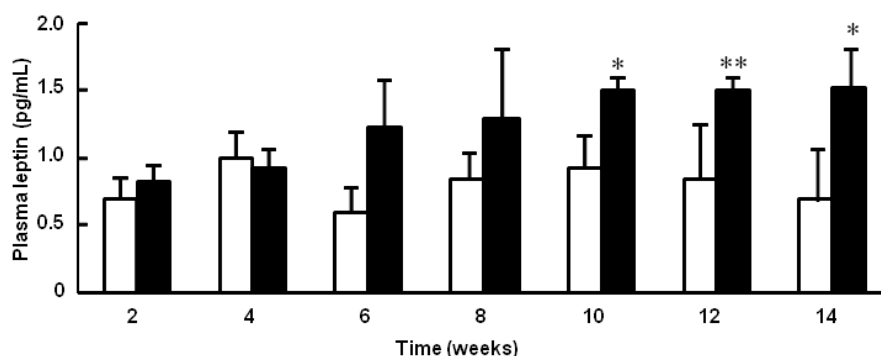


Figure 6. Effects of HJ on plasma leptin levels during 14 weeks of treatment in GK rats with or without HJ. \square , GK rats treated with vehicle (Control group); \blacksquare , GK rats treated with HJ (HJ group). * $p < 0.05$, ** $p < 0.01$ compared with the control rats. Data are mean \pm S.D. ($n = 5$).

clinically established that while HJ does not improve hyperglycemia, it can abate diabetes-related subjective symptoms such as dry mouth, frequent thirst, frequent urination, and fatigue. Moreover, in recent years, many studies have been conducted on the prevention and treatment of diabetic complications (20,21), and HJ has been found to be effective in some patients who do not respond to modern medicine. However, these studies are not sufficient to support these therapeutic effects of HJ.

We have previously reported the antidiabetic effects of HJ in STZ-induced diabetic rats as a model of insulin-dependent diabetes mellitus (IDDM) (9). HJ significantly increased the plasma and pancreatic insulin levels in these rats. Although there was no increase in the number of pancreatic β cells in the islets of Langerhans, HJ induced an increase in insulin production and secretion by the residual pancreas and also significantly reduced the synthesis of glucose transporter-2 protein, which is involved in glucose uptake and its release, in the liver. Hence, these results suggest that HJ affects not only the production and secretion of insulin but also the release of glucose from the liver. Further, it alleviates subjective symptoms and prevents complications of diabetes mellitus (8,10,22). In these our reports, the administration of 1% HJ contents to the animals substantially exhibited the anti-diabetic effects.

We used GK rats as a model of human NIDDM to ascertain the effects of HJ on hyperglycemia. In order to examine the effect of HJ in glycemic control, we studied its effects on insulin secretion in diabetic GK rats. HJ administration in GK rats lowered the non-fasting plasma glucose levels throughout the study period and significantly suppressed it in weeks 5, 7, 8, and 13 (Figure 3). The increasing of leptin levels after weeks 10 may directly influence an antihyperglycemic action by insulin. However, HJ also significantly increased plasma insulin levels over the experimental period in these rats (Figure 4).

The OGTTs revealed that the tolerance to glucose had improved in the HJ group rats compared to the control group rats. The plasma glucose levels at 60 min also decreased significantly ($p < 0.05$) in the HJ group rats (Figure 5A). The plasma insulin levels at 30 min were significantly higher in the HJ group rats than in the control group rats (Figure 5B). In addition, the HJ group showed a rapid increase at 30 min in the plasma insulin levels that returned to the control levels after 120 min and HJ restored the impaired insulin secretion in GK rats. HJ improved glucose tolerance at 14 weeks after HJ administration in GK rats. And also, the HOMA-R score (index of insulin resistance) in the HJ group rats at 14 weeks was significantly lower than that in the control rats (shown not data), indicating that insulin resistance was ameliorated in HJ-treated rats.

In the present study, the body weights and food

intake increased in the HJ group (Figure 2). We found that the body weights of the HJ group rats increased significantly after the fifth week ($p < 0.05$), and these weights were similar to those of normal rats (Wistar rats). HJ normalized the body weight of GK rats. Thus, HJ administration resulted in an increase in the body weight and food consumption, in addition to an improvement in insulin secretion. We thus investigated the effects of HJ on plasma leptin levels, since leptin is involved in food intake. The plasma leptin levels increased in the HJ group rats compared to the control group rats. We think that the HJ group rats did not become obese due to this involvement of leptin. However, further studies are required to clarify this issue. The body weights of the genetically diabetic GK rats were reduced as compared to that of normal (Wistar) rats of the same age. But the HJ group rats exhibited a moderate increase in body weight when the plasma insulin and leptin levels increased. Plasma leptin levels were lower in GK rats than in Wistar rats and plasma leptin levels in the HJ group rats were nearly the same as those in Wistar rats reported by Huang *et al.* (23). However, it remains to be elucidated whether leptin sensitivity is altered by HJ administration.

In conclusion, HJ is a useful antidiabetic agent which shows improvement of glucose tolerance by glucose stimulated insulin secretion, and body weight loss in spontaneously diabetic GK rats.

Acknowledgement

The authors thank Tsumura Inc. for the courtesy of providing the HJ extracted powder.

References

1. Suzuki J, Kimura M. Hypoglycemic effects of the blended Chinese traditional medicines in genetically and chemically diabetic mice. *Folia pharmacol Japon.* 1984; 83:1-10.
2. Yamahara J, Mibu H, Sawada T, Fujimura H, Takino S, Yoshikawa M, Kitagawa I. Biologically active principles of crude drugs: Antidiabetic principles of corni fructus in experimental diabetes induced by streptozotocin. *Yakugaku Zasshi.* 1981; 101:86-90.
3. Luo WQ, Kanno T, Winarto A, Iwanaga T, Jun L, Futai Y, Yanaihara C, Yanaihara N. An experimental analysis of a therapeutic effect of a Chinese herbal prescription in streptozotocin-treated rats. *Biomed Res.* 1988; 190:127-133.
4. Yoshimura K, Terai A, Arai Y. Two-week administration of low-dose Hachimi-jio-gan (Ba-Wei Di-Huang-Wan) for patients with benign prostatic hyperplasia. *Hinyokika Kiyo.* 2003; 49:509-514.
5. Kim HY, Yokozawa T, Cho EJ, Yamabe N. Protective effects of the Chinese prescription Hachimi-jio-gan against diabetic oxidative stress. *J Pharm Pharmacol.* 2004; 56:1299-1305.
6. Nakagawa T, Yokozawa T, Terasawa K. A study of

- Kampo medicines in a diabetic nephropathy model. *J Trad Med.* 2001; 18:161-168.
7. Yokozawa T, Yamabe N, Cho EJ, Nakagawa T, Oowada S. A study on the effects to diabetic nephropathy of Hachimi-jio-gan in rats. *Nephron Exp Nephrol.* 2004; 97:e38-e48.
 8. Yamabe N, Yokozawa T. Activity of the Chinese prescription Hachimi-jio-gan against renal damage in the Otsuka Long-Evans Tokushima fatty rat: a model of human type 2 diabetes mellitus. *J Pharm Pharmacol.* 2006; 58:535-545.
 9. Hirotani Y, Ikeda T, Yamamoto K, Kurokawa N. Effects of Hachimi-jio-gan (Ba-Wei-Di-Huang-Wan) on hyperglycemia in streptozotocin-induced diabetic rats. *Biol Pharm Bull.* 2007; 30:1015-1020.
 10. Hirotani Y, Ikeda T, Yamamoto K, Kurokawa N. Effects of Hachimijiogon (Ba-Wei-Di-Huang-Wan) on renal aldose reductase activity in streptozotocin-induced diabetic rats. *J Trad Med.* 2007; 24:144-148.
 11. Hirotani Y, Ikeda T, Yamamoto K, Kurokawa N. Effects of Hachimi-jio-gan (Ba-Wei-Di-Huang-Wan) on intestinal function in streptozotocin-induced diabetic rats. *Yakugaku Zasshi.* 2007; 127:1509-1513.
 12. Hukuzawa M. Dry mouth and polyposia. *Modern Physician.* 2001; 21:765-767.
 13. Goto Y, Kakizaki M. The spontaneous-diabetic rat: a model of non-insulin-dependent diabetes mellitus. *Proc Jpn Acad.* 1981; 57:381-384.
 14. Ohta T, Furukawa N, Komuro G, Yonemori F, Wakitani K. JTT-608 restores impaired early insulin secretion in diabetic Goto-Kakizaki rats. *Br J Pharmacol.* 1999; 126:1674-1680.
 15. Portha B, Serradas P, Bailbé D, Suzuki K, Goto Y, Giroix MH. Beta-cell insensitivity to glucose in the GK rat, a spontaneous nonobese model for type II diabetes. *Diabetes.* 1991; 40:486-491.
 16. Bisbis S, Bailbe D, Tormo MA, Picarel-Blanchot F, Derouet M, Simon J, Portha B. Insulin resistance in the GK rat: decreased receptor number but normal kinase activity in liver. *Am J Physiol.* 1993; 265:E807-E813.
 17. O'Rourke CM, Davis JA, Saltiel AR, Cornicelli JA. Metabolic effects of troglitazone in the Goto-Kakizaki rat, a non-obese and normolipidemic rodent model of non-insulin-dependent diabetes mellitus. *Metabolism.* 1997; 46:192-198.
 18. Picarel-Blanchot F, Berthelie C, Bailbe D, Portha B. Impaired insulin secretion and excessive hepatic glucose production are both early events in the diabetic GK rat. *Am J Physiol.* 1996; 271:E755-E762.
 19. Zhou YP, Ostenson CG, Ling ZC, Grill V, Zhou YP, Ostenson CG, Ling ZC, Grill V. Deficiency of pyruvate dehydrogenase activity in pancreatic islets of diabetic GK rats. *Endocrinology.* 1995; 136:3546-3551.
 20. Goto H, Shimada Y, Sekiya N, Yang Q, Kogure T, Mantani N, Hikiami H, Shibahara N, Terasawa K. Effects of Keishi-bukuryo-gan on vascular function and hemorheological factors in spontaneously diabetic (WBN/kob) rats. *Phytomedicine.* 2004; 11:188-195.
 21. Goto H, Shimada Y, Tanikawa K, Sato S, Hikiami H, Sekiya N, Terasawa K. Clinical evaluation of the effect of daio (rhei rhizoma) on the progression of diabetic nephropathy with overt proteinuria. *Am J Chin Med.* 2003; 31:267-275.
 22. Goto M, Hayashi M, Todoroki T, Seyama Y, Yamashita S. Effects of traditional Chinese medicines (dai-saikoto, sho-saikoto and hachimi-zio-gan) on spontaneously diabetic rat (WBN/Kob) with experimentally induced lipid and mineral disorders. *Yakurigaku Zasshi.* 1992; 100:353-358.
 23. Huang W, Dedousis N, O'Doherty RM. Hepatic steatosis and plasma dyslipidemia induced by a high-sucrose diet are corrected by an acute leptin infusion. *J Appl Physiol.* 2007; 102:2260-2265.

(Received December 3, 2009; Revised December 24, 2009; Accepted December 24, 2009)

Original Article**Phagocytosis plays a dual role in activating dendritic cells; digestive production of active Toll-like receptor ligands and cooperation with Toll-like receptor signaling****Masanori Miyauchi^{1,*}, Masashi Murata¹, Keiko Shibuya¹, Erina Koga-Yamakawa¹, Yoshiki Yanagawa², Ichiro Azuma³, Yasuo Kashiwazaki¹**¹ Pharmacology Research Laboratories, Drug Research Division, Dainippon Sumitomo Pharma Co., Ltd., Suita, Osaka, Japan;² Department of Pharmacology, Faculty of Pharmaceutical Science, Health Sciences University of Hokkaido, Ishikari-Tobetsu, Hokkaido, Japan;³ Hokkaido Pharmaceutical University School of Pharmacy, Otaru, Hokkaido, Japan.

ABSTRACT: Phagocytosis is an initial step in innate immunity, which is also stimulated by signals *via* Toll-like receptors (TLRs); however, the cooperation of phagocytosis with signals through TLRs to establish acquired immunity is unknown. We found that phagocytosis is an essential process to induce an immune reaction against an insoluble TLR ligand. Cell-wall skeleton prepared from *Mycobacterium bovis* BCG (BCG-CWS), an insoluble TLR2 ligand, activated and matured murine splenic dendritic cell (DC) line BC-1 as well as a soluble TLR2 ligand, Pam3CSK4. Surprisingly, BC-1 maturation with BCG-CWS was completely suppressed by inhibiting phagocytosis, while that with Pam3CSK4 was not affected. Moreover, BCG-CWS induced intense delayed-type hypersensitivity (DTH) reactions against mitomycin C-inactivated Lewis lung carcinoma cells but Pam3CSK4 did not. These results suggested that the phagocytosis process enables the insoluble TLR2 ligand to activate DCs *via* TLR2 comparable to a soluble TLR2 ligand *in vitro*, and stimulating TLR2 alone is not sufficient to establish T cell-mediated immunity *in vivo*. It is therefore conceivable that the process of phagocytosis induces additional effects on TLR2-stimulated DCs to activate cell-mediated immunity *in vivo*.

Keywords: Adjuvant, phagocytosis, TLR2, BCG-CWS, SMP-105

*Address correspondence to:

Dr. Masanori Miyauchi, Pharmacology Research Laboratories, Drug Research Division, Dainippon Sumitomo Pharma Co., Ltd., 33-94, Enoki-cho, Suita, Osaka 564-0053, Japan.

e-mail: masanori-miyauchi@ds-pharma.co.jp

1. Introduction

Phagocytosis is the process of endocytosis involving the vesicular internalization of solid particles, such as bacteria, and is therefore an essential step for eliciting effective innate immunity in mammals. Macrophages and DCs make use of a variety of surface receptors to internalize microbes, including direct pattern-recognition receptors and receptors for opsonins (1). TLRs are pathogen-associated molecular pattern recognition receptors (PRRs), and assume an important role in induction of the immune response *via* activation of innate immunity (2,3). Recent studies have demonstrated that signaling by TLRs can modulate phagocytosis (4) and moreover a complex interaction between phagocytosis and TLR signaling. Phagocytosis comprises the processes of recognition of particles by phagocytic receptors, phagosome formation, phagosome maturation and transcriptional responses in phagocytosis. Although many reports suggest TLRs do not act directly as phagocytic receptors (5-8), some reports insist that TLRs regulate phagocytosis (1,9-14).

BCG-CWS, cell-wall skeleton prepared from *Mycobacterium bovis* BCG as an insoluble fraction, is known to be an activator of innate immunity (15) and has been examined in several clinical studies (16-19). We originally prepared CWS from *M. bovis* BCG Tokyo 172 strain with purity of more than 97% (SMP-105) and investigated. SMP-105 is an insoluble TLR2 ligand and elicited immune reactions such as inducing interferon- γ -producing cells and cytotoxic T lymphocytes (CTL) and prevented the growth of tumors through TLR2 (20). SMP-105 was observed at the draining lymph nodes phagocytosed by macrophages and DCs (21). We therefore hypothesize that SMP-105 requires phagocytosis by macrophages or DCs for immune activation and it shows different effects from Pam3CSK4, a soluble TLR2 ligand, *in vivo*.

In this report, we investigated the maturation and activation of BC-1, a mouse immature DC line, by analyzing surface antigens and measuring cytokines *in vitro*. We found that cytocharasin B, an inhibitor of phagocytosis, suppressed BC-1 maturation by BCG-CWS, but a soluble TLR2 ligand, Pam3CSK4, did not. Acquired immunity established by BCG-CWS or Pam3CSK4 was also addressed as DTH reactions and is discussed in the context of the contribution of phagocytosis to immune reactions in this paper.

2. Materials and Methods

2.1. Preparation of SMP-105

SMP-105 was prepared as described previously (17,22). Contaminated endotoxin was less than 0.005 endotoxin units/mg. For *in vitro* experiments, SMP-105 was suspended in saline containing 0.01% polysorbate 80. SMP-105 labeled with fluorescein 5-isothiocyanate (FITC; Sigma) was prepared by incubating the mixture of FITC (0.5 mM) and SMP-105 suspension (2 mg/mL). For *in vivo* experiments, an oil-in-water emulsion of SMP-105 was prepared with the following formulation: 0.6 mg/mL SMP-105, 1.6% squalane, 1.0% polysorbate 80, and 5.0% mannitol (21,23). Vehicle preparation used the same formulation, except for SMP-105.

2.2. Reagent

Pam3CSK4 was purchased from Calbiochem (Merck, Tokyo, Japan). *Escherichia coli* J5 lipopolysaccharide (LPS) was purchased from LIST Biological Laboratories (Campbell, CA, USA). LPS was further purified using phenol extraction methods (24-26). Cytochalasin B and cytochalasin E were purchased from Wako Pure Chemical Industries, Ltd. (Osaka, Japan). Muramyl dipeptide (MDP-Lys (L18)) was purchased from Sigma-Aldrich Japan (Tokyo, Japan). CpG1826 (27) was synthesized by Hokkaido System Science Co., Ltd. (Hokkaido, Japan).

2.3. Cells

BC-1, a mouse immature DC line (28,29), was kindly provided by Drs. Onoe and Yanagawa from the Institute for Genetic Medicine, Hokkaido University, Japan. The BC-1 cell line was maintained as described previously (28,29). In brief, BC-1 cells were maintained in Iscove's Modified Dulbecco's Medium (IMDM) supplemented with 10% fetal calf serum (FCS), 30% NIH/3T3 supernatant, mouse recombinant GM-CSF, 4 mM L-glutamine, 50 µg/mL streptomycin, 50 U/mL penicillin, and 50 µM 2-mercaptoethanol. Lewis lung carcinoma 3LL was obtained from the Cancer Institute for the Japanese Foundation for Cancer Research (Tokyo, Japan). 3LL cells were maintained in RPMI-1640 medium

supplemented with 10% FCS, 50 µg/mL streptomycin, and 50 U/mL penicillin. To prepare inactivated 3LL, cells were incubated for 20 min at 37°C in culture medium containing 200 µg/mL mitomycin C (Kyowa Hakko Kogyo, Tokyo, Japan), followed by repeated washing with sufficient culture medium.

2.4. Animals

C57BL/6J female mice were purchased from Charles River Japan (Kanagawa, Japan). BALB/c-[Tg]DO11.10-[KO]Rag2 mice (30) were obtained from Taconic (NY, USA). Mice were maintained under specific pathogen-free conditions. All animal experiments were conducted according to the guidelines of the Animal Care and Use Committee at Dainippon Sumitomo Pharma.

2.5. IL-12 p40 induction assay

BC-1 cells were cultured with SMP-105, Pam3CSK4 or MDP-Lys (L18) overnight. The concentrations of IL-12 p40 in the supernatants were determined by enzyme-linked immunosorbent assay (ELISA) (BIOSource). In order to examine the effect of phagocytosis inhibitor, BC-1 cells were pretreated for 1 h in the presence of cytochalasin B (1, 10 µg/mL) or cytochalasin E (0.1, 1 µg/mL).

2.6. Flow cytometry

BC-1 cells were cultured with SMP-105 (10 µg/mL), CpG1826 (10 µg/mL), LPS (1 µg/mL), or Pam3CSK4 (1 µg/mL) overnight. Cells were collected and stained with FITC-conjugated anti-mouse CD11c, CD40, CD80, CD86, I-A^d, H-2K^d supplied by BD PharMingen (San Diego, CA) for 30 min in the dark at 4°C. After washing with PBS, samples were analyzed on a Coulter Epics XL (Beckman Coulter, Tokyo, Japan). Data were analyzed and presented using FlowJo Ver. 8.8.4 (Tree Star, Inc., Ashland, Oregon, USA).

2.7. DO11.10 T-cell activation by BC-1 cells

BC-1 cells were treated with 100 nM ovalbumin peptide, OVA323-339 (ISQAVHAAHAEINEAGR; Bachem), along with SMP-105, Pam3CSK4 or CpG1826 overnight. DO11.10 T cells were enriched from spleen cell suspensions prepared from BALB/c-[Tg]DO11.10-[KO]Rag2 by AutoMACS (Miltenyi Biotech K.K., Tokyo, Japan) with CD90 (Thy1.2) Microbeads (Miltenyi Biotech K.K.). DO11.10 T cells were co-cultured with pre-treated BC-1 cells overnight. The concentrations of IL-2 and IL-12 p40 in the supernatants were determined by ELISA (BIOSource).

2.8. Fluorescence microscope

BC-1 cells were cultured with 20 µg/mL FITC-

labeled SMP-105 for 1 h and fixed with 4% (w/v) paraformaldehyde/PBS. Lysosomes were labeled with Lyso Tracker Red DND-99 (Molecular Probes, Leiden, The Netherlands) as recommended by the manufacturer. BC-1 cells were analyzed by confocal microscopy (Leica TCS NT, Leica).

2.9. Delayed-type hypersensitivity (DTH) reaction

A mixture of inactivated 3LL cells (3×10^4 cells) and vehicle, SMP-105 (12.5 μ g) or Pam3CSK4 (12.5 μ g) were administered into the left flank region of C57BL/6J mice twice intradermally with a 7-day interval. Seven days after the second administration, inactivated 3LL cells were inoculated at 10^5 cells in 50 μ L HBSS into the left footpads. Just before and 24 h after inoculation, the thickness of the left footpad was measured by dial gauge (Mitsutoyo Co., Kanagawa, Japan). The percentage of swelling was calculated according to the following equation:

$$\begin{aligned} \text{Footpad swelling (\%)} \\ = & (\text{thickness of post-injected footpad (mm)} \\ & - \text{thickness of pre-injected footpad (mm)}) / \\ & \text{thickness of pre-injected footpad (mm)} \times 100 \end{aligned}$$

3. Results

3.1. SMP-105 induces BC-1 maturation

BC-1 is a phenotypically and functionally immature myeloid DC line (29). Exposure of BC-1 cells to various soluble ligands to TLRs, such as FSL-1, Poly(I:C), LPS and CpG1826, up-regulates the expression of CD86, a co-stimulatory molecule, and induces IL-12 p40 production (31). SMP-105 stimulated TLR2 (20) and we investigated whether SMP-105 matures BC-1 cells and induces IL-12 p40 protein.

BC-1 cells were incubated with SMP-105 or other TLRs ligands (Pam3CSK4, LPS or CpG1826) and expression levels of co-stimulatory and MHC molecules were analyzed by flow cytometry (Figure 1). SMP-105 up-regulated the expressions of CD40, CD80, CD86, I-A^d and H-2K^d on BC-1 to the same level as Pam3CSK4 and LPS. TNF- α induced IL-12 p40 production slightly in BC-1, as previously reported (Figure 2a) and SMP-105 induced a significant amount of IL-12 p40 dose-dependently (Figure 2b), as also observed by treatment with Pam3CSK4 and MDP-Lys (L18) (Figures 2c and 2d). It was shown that SMP-105 induces DC maturation and activation, such as TLRs ligands and NOD2 ligand.

3.2. SMP-105 activates DCs as antigen-presenting cells

We tested whether SMP-105 activates DCs as antigen-presenting cells. BC-1 cells were treated with SMP-105

or TLR ligands along with OVA peptide (OVA 323-339) before incubation with CD4⁺ T cells from DO11.10 mice. These T cells express a transgenic T-cell receptor that recognizes the OVA peptide in the context of BALB/c MHC class II (I-A^d) (32). DO11.10 T cells did not produce IL-2 when co-cultured with BC-1 cells without the OVA peptide, or in the presence of SMP-105 alone (data not shown), but a small quantity was observed in the culture of T cells with OVA-peptide pulsed BC-1. When BC-1 cells were pre-treated with SMP-105, IL-2 production was increased similar to pre-treatment with soluble TLRs ligands (Figure 3a). Moreover, we confirmed BC-1 activation under this condition by measuring IL-12 p40 (Figure 3b). These data suggested that DCs activated by SMP-105 function as antigen-presenting cells.

3.3. SMP-105 is localized in lysosomes after phagocytosis

Previously, we observed SMP-105 engulfed in phagocytes in regional lymph nodes when SMP-105 was injected intradermally (21,23). SMP-105 might be phagocytosed by macrophages or DC to elicit tumor immunity in the regional lymph nodes. We therefore investigated the uptake of SMP-105 by DCs employing BC-1. To observe SMP-105 localization in cells, fluorescent imaging was performed using FITC-labeled SMP-105 by confocal microscope (Figure 4). SMP-105 was localized in the intracellular region, especially in lysosomes, which prompted us to investigate the effect of inhibiting phagocytosis. Pre-treatment with cytochalasin B completely blocked the capture of SMP-105 by BC-1 and there was no SMP-105 in the cytoplasm or lysosomes of BC-1.

3.4. Activation of BC-1 by SMP105 requires phagocytosis

We investigated whether SMP-105 needs to be phagocytosed to activate BC-1 cells by pre-treatment with cytochalasin B. Cytochalasin B completely inhibited the production of IL-12 p40 by SMP-105, while stimulation by Pam3CSK4 and MDP-Lys (L18) was not affected (Figure 5a). Moreover, cytochalasin E, which also inhibits phagocytosis, abolished the production of IL-12 p40 by SMP-105, but not by other reagents (Figure 5b). These data suggested that phagocytosis is an indispensable step for activating BC-1 by SMP-105, different from the soluble TLR2 ligand and NOD2 ligand.

3.5. SMP-105, but not Pam3CSK4, significantly induces delayed-type hypersensitivity (DTH) reactions against 3LL

To investigate the activation and maturation of DCs by

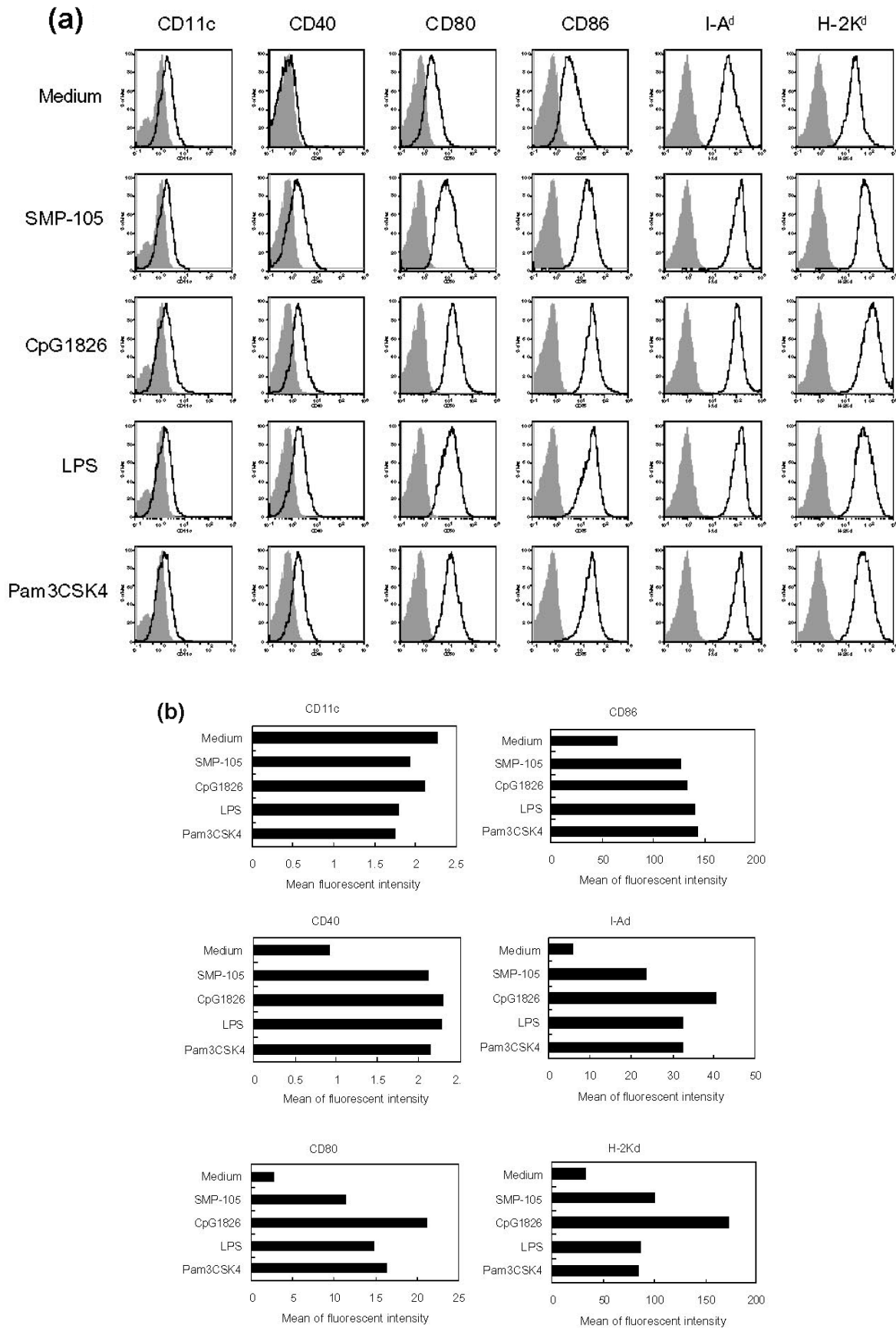


Figure 1. SMP-105 up-regulated CD40, CD80, CD86, I-A^d, and H-2K^d in BC-1. BC-1 cells were stimulated with medium, SMP-105 (10 $\mu\text{g}/\text{mL}$), CpG1826 (10 $\mu\text{g}/\text{mL}$), LPS (1 $\mu\text{g}/\text{mL}$), or Pam3CSK4 (1 $\mu\text{g}/\text{mL}$) overnight. **(a)** Histogram of expression intensities analyzed by flow cytometry are shown concerning CD11c, CD40, CD80, CD86, I-A^d, or H-2K^d (thick lines) or isotype control antibodies (shaded area). **(b)** Mean expression levels were demonstrated in graphs. The experiments were performed twice and the same results were obtained.

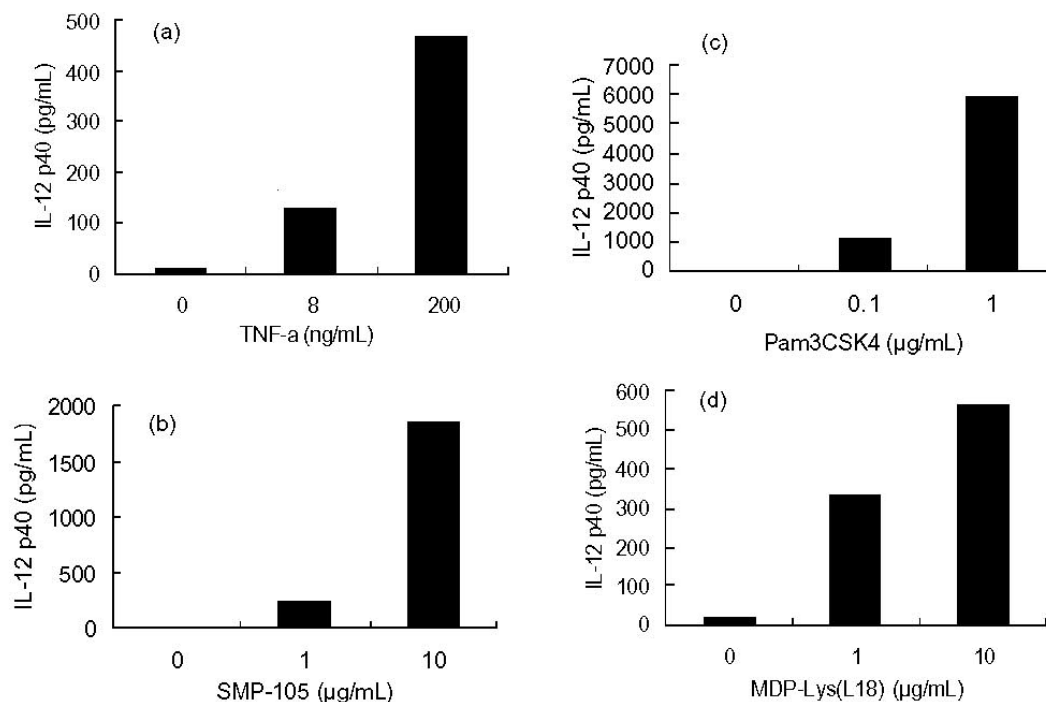


Figure 2. SMP-105 induced IL-12 p40 production by BC-1. BC-1 cells were stimulated with (a) TNF- α (8, 200 ng/mL), (b) SMP-105 (1, 10 μ g/mL), (c) Pam3CSK4 (0.1, 1 μ g/mL), (d) MDP-Lys (L18) (1, 10 μ g/mL) or medium alone overnight. IL-12 p40 in the supernatants was measured by ELISA. Shown are representative data of more than four experiments.

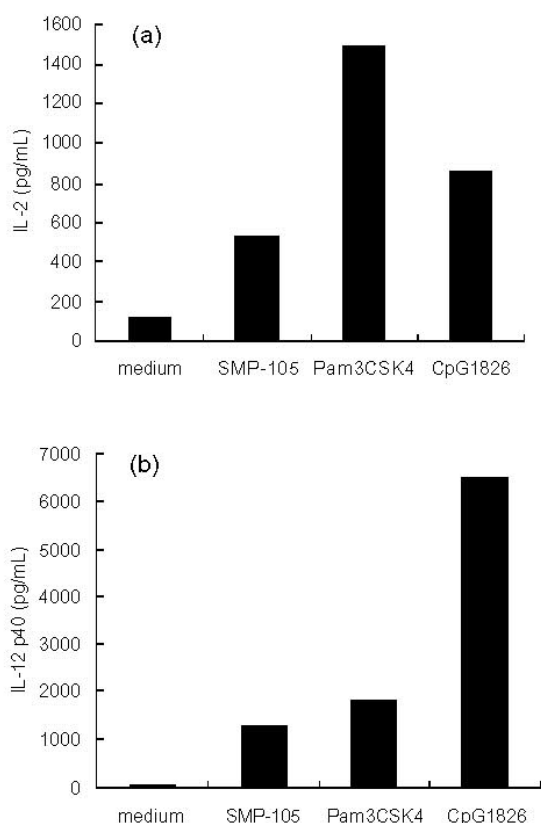


Figure 3. SMP-105 promoted (a) IL-2 and (b) IL-12 p40 secretion in DO11.10 T cells co-cultured with antigen-presenting BC-1 cells. BC-1 cells were pre-treated with SMP-105, Pam3CSK4 or CpG1826 at 10 μ g/mL, 1 μ g/mL, 1 μ g/mL, respectively, and pulsed with 100 nM OVA peptide (OVA 323-339). The cells were co-incubated with T cells derived from DO11.10 mice overnight. IL-2 and IL-12 p40 in the supernatant were assessed by ELISA. The experiments were performed twice and the same results were obtained.

SMP-105 and Pam3CSK4 *in vivo*, we evaluated DTH reactions elicited when injected with an antigen at immunization. Mice were immunized with inactivated 3LL cell suspension admixed with each emulsified reagent, before injecting inactivated 3LL alone in the hind footpad, and edema was measured (Figure 6). SMP-105 evoked footpad swelling clearly when immunized with 3LL cells, whereas Pam3CSK4 exhibited no effect. The lack of an *in vivo* effect of Pam3CSK4, which is a potent TLR2 ligand that strongly activated BC-1 *in vitro*, suggested that activities other than TLR2 stimulation are required to establish strong acquired immunity to elicit DTH reactions.

4. Discussion

TLRs are important and major PRRs and recognize distinct microbial components and directly activate immune cells. Various PRR ligands, such as LPS, and peptidoglycan, stimulated immune systems (2,3). SMP-105 activates TLR2 and enhances immune responses, such as the number of interferon- γ -producing cells and CTL (20). We investigated the activation of DCs by SMP-105 employing BC-1, a mouse immature DC line and investigated the maturation and activation of BC-1 cells by measuring the expression intensity of co-stimulatory and MHC molecules and the production of IL-12 p40, respectively. As expected, SMP-105 up-regulated the expression of surface antigens (Figure 1) and induced IL-12 p40 production dose-dependently (Figure

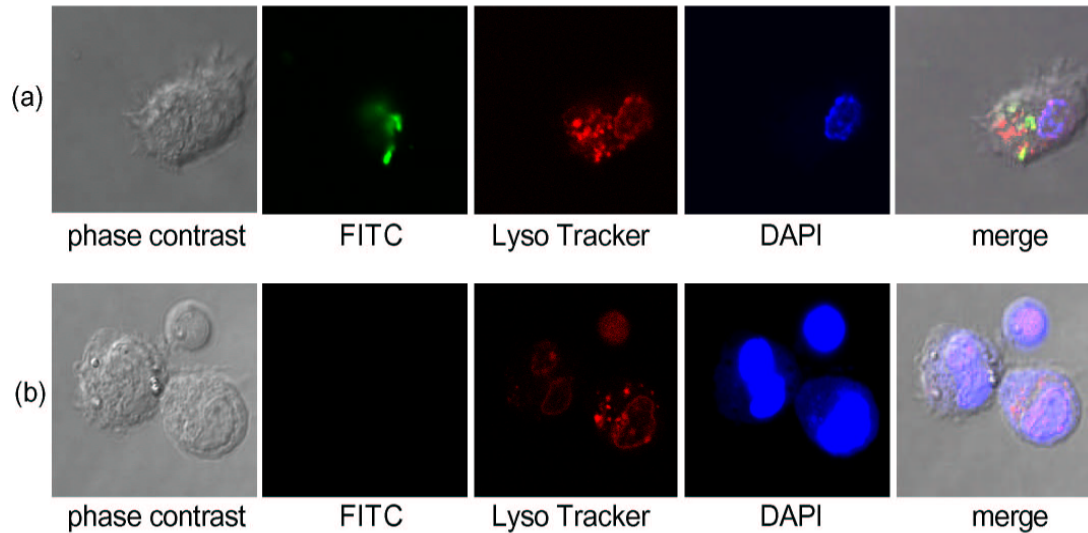


Figure 4. Cytochalasin B, an actin polymerization inhibitor, inhibited phagocytosis of SMP-105 by BC-1. BC-1 cells were pre-treated with (a) medium alone or (b) cytochalasin B for 1 h and then further incubated with FITC-labeled SMP-105 (10 $\mu\text{g}/\text{mL}$) overnight. BC-1 cells were examined with a fluorescence microscope (Leica TCS NT, Leica) for the distribution. Panels from left: phase contrast, SMP-105: FITC, lysosome: Lyso Tracker, DNA: DAPI, merge.

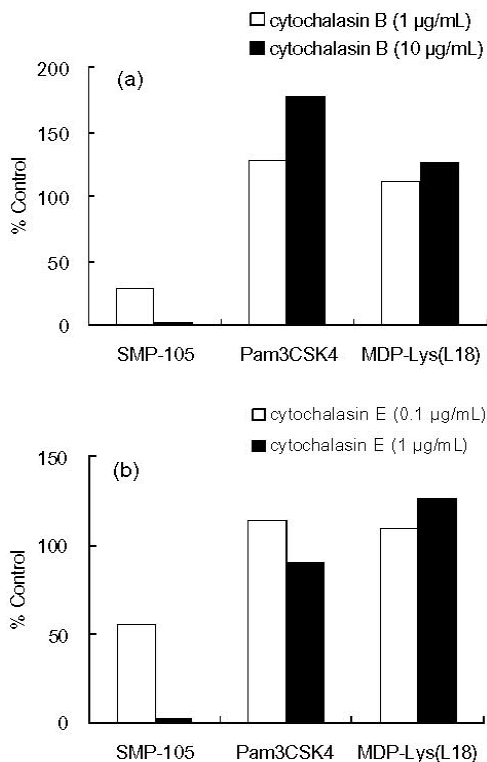


Figure 5. Cytochalasin B inhibits cytokine production of BC-1 by SMP-105, but not by Pam3CSK4 and MDP-Lys (L18). BC-1 cells were pre-treated with cytochalasin B (1, 10 $\mu\text{g}/\text{mL}$) (a) or cytochalasin E (0.1, 1 $\mu\text{g}/\text{mL}$) (b) for 1 h, and then stimulated with SMP-105 (10 $\mu\text{g}/\text{mL}$), Pam3CSK4 (0.1 $\mu\text{g}/\text{mL}$) or MDP-Lys (L18) (10 $\mu\text{g}/\text{mL}$) overnight. IL-12 p40 in the supernatants were measured by ELISA. Relative production is shown in the figure. Cytochalasin B or E treatment did not affect cell viability at the concentration used. Shown are representative data of five experiments.

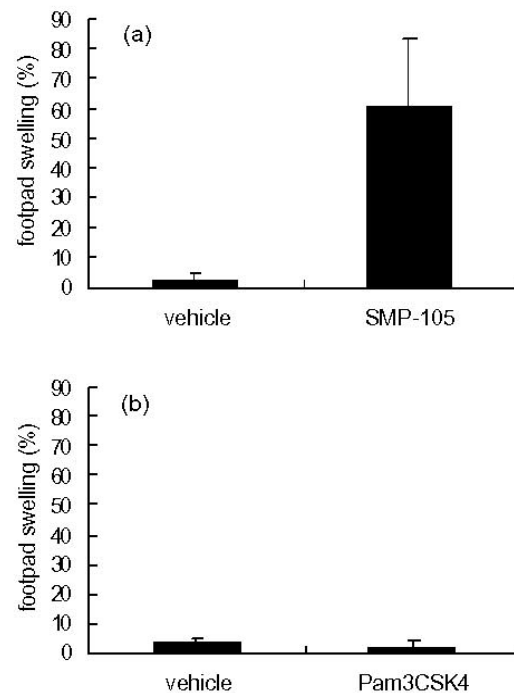


Figure 6. SMP-105, but not Pam3CSK4, induced strong delayed-type hypersensitivity reactions. A mixture of inactivated 3LL cells (3×10^4 cells) and SMP-105 (12.5 μg) (a) or Pam3CSK4 (12.5 μg) (b) was administered intradermally into the left flank region of C57BL/6J mice twice at a 7-day interval. Seven days after the second administration, inactivated 3LL cells were inoculated into the left footpads and swelling was monitored by measuring the thickness 24 h after inoculation, and the relative swelling was calculated. Means \pm S.D. of six mice are shown.

2). Moreover, we confirmed the antigen-presenting function of BC-1 cells matured by SMP-105 by analyzing OVA-specific IL-2 production from T cells derived from DO11.10 mice (Figure 3).

The effects of SMP-105 on the maturation and activation of BC-1 cells were completely abolished by cytochalasin B, whereas those of Pam3CSK4 and MDP-Lys (L18) were not affected (Figure 5), indicating that cytochalasin B did not inhibit the TLR2/MyD88/NF- κ B/IL-12 p40 pathway or the NOD2/NF- κ B/IL-12 p40 pathway *per se*. SMP-105 might need to be phagocytosed before exhibiting its activity. Analysis with a fluorescence microscope demonstrated the localization of SMP-105 in lysosomes (Figure 4), which suggested that SMP-105 might be converted to active ligands by digestive enzymes in the acidic organelle. SMP-105 has a gigantic molecular structure composed of a peptidoglycan linked to arabinogalactan and mycolic acids. Mycoloyl-arabinans, parts of SMP-105, showed potent TNF- α -inducing activities *in vitro* in almost the same order as CWS itself (33). Moreover, SMP-105 in physiological saline takes a double-folded sheet form, resulting in a mycolic acid layer on the inner side (34). It is conceivable that the digestion of SMP-105 following phagocytosis produces some immunoactive fragments. Okamoto reported that OK-432 activates TLR4 mediated by phagocytosis (35). The intact form of OK-432 is not able to stimulate TLR4, but after capture and digested by DCs or macrophages, it is converted to a soluble ligand for TLR4, OK-PSA, and shows antitumor effects accordingly (35,36). Our results concerning BCG-CWS additionally support that phagocytosis is an important step in activating the immune system *via* PRRs. Mycoloyl-arabinans are suggested as more direct ligand structures for TLR2, but further analysis is required.

It is well-known that preexisting immune T cells cause DTH reactions. We therefore investigated the establishment of antigen-specific T cell immunity *in vivo* by analyzing DTH reactions. Pam3CSK4 matured and activated BC-1 cells *in vitro* and induced the migration of a significant number of DCs and macrophages into a draining lymph node, which is dependent on TLR2 stimulation (20); however, although SMP-105 induced strong DTH reactions, surprisingly, Pam3CSK4 failed (Figure 6). These results prompted us to consider that it is not sufficient to stimulate TLR2 alone to establish T cell-mediated immunity *in vivo*. Comparing Pam3CSK4 with SMP-105 as to the effect of cytochalasin B to activate BC-1 cells, it is likely that the process of phagocytosis induces additional effects on TLR2-stimulated DCs to activate cell-mediated immunity *in vivo*. Actually, TLR2 and other signaling act synergistically (37,38). In addition, we reported in the previous paper that SMP-105 resided for a long time at the inoculation

site and activated T cells in guinea pigs (23). As probable insoluble particles resistant to digestion, SMP-105 is retained in the skin and activates DCs for a long period, whereas Pam3CSK4 is soluble and probably easily excreted from the body, having only a transient effect on DCs. We think that the difference in retention at the inoculation site explains the strong activity of SMP-105 for the DTH reactions but not a lack of activity of Pam3CSK4, because rather a larger number of DCs were accumulated in the draining lymph node by Pam3CSK4 than SMP-105 (20).

We showed previously that SMP-105 induces an immune response against tumors dependent on TLR2/MyD88, but other mechanisms are not known. In this paper we newly showed that phagocytosis is an indispensable process for SMP-105 to activate TLR2. In addition, phagocytosis may also be important to mature and activate immature DCs together with TLR2 signaling to establish T cell immunity *in vivo*. The study of phagocytosis in the context of activating DCs will be necessary.

Acknowledgements

The mouse line was obtained through the NIAID Exchange Program, NIH: BALB/c-[Tg]DO11.10-[KO]Rag2 mice (NIAID Transgenic Exchange #4219). We thank Dr. Nobuyoshi Chiba for helpful discussion, and Ms. Yukari Ishitsubo for assistance with experiments.

References

1. Underhill DM, Ozinsky A. Phagocytosis of microbes: complexity in action. *Annu Rev Immunol.* 2002; 20:825-852.
2. Takeda K, Akira S. Toll-like receptors in innate immunity. *Int Immunol.* 2005; 17:1-14.
3. Takeda K, Kaisho T, Akira S. Toll-like receptors. *Annu Rev Immunol.* 2003; 21:335-376.
4. Underhill DM, Ozinsky A. Toll-like receptors: key mediators of microbe detection. *Curr Opin Immunol.* 2002; 14:103-110.
5. Underhill DM, Ozinsky A, Hajjar AM, Stevens A, Wilson CB, Bassetti M, Aderem A. The Toll-like receptor 2 is recruited to macrophage phagosomes and discriminates between pathogens. *Nature.* 1999; 401:811-815.
6. Gantner BN, Simmons RM, Canavera SJ, Akira S, Underhill DM. Collaborative induction of inflammatory responses by dectin-1 and Toll-like receptor 2. *J Exp Med.* 2003; 197:1107-1117.
7. Peiser L, De Winther MP, Makepeace K, Hollinshead M, Coull P, Plested J, Kodama T, Moxon ER, Gordon S. The class A macrophage scavenger receptor is a major pattern recognition receptor for *Neisseria meningitidis* which is independent of lipopolysaccharide and not required for secretory responses. *Infect Immun.* 2002; 70:5346-5354.
8. Reiling N, Ehlers S, Holscher C. MyDths and un-TOLled truths: sensor, instructive and effector immunity to tuberculosis. *Immunol Lett.* 2008; 116:15-23.

9. Amiel E, Alonso A, Uematsu S, Akira S, Poynter ME, Berwin B. Pivotal Advance: Toll-like receptor regulation of scavenger receptor-A-mediated phagocytosis. *J Leukoc Biol.* 2009; 85:595-605.
10. Lennon-Dumenil AM, Bakker AH, Maehr R, Fiebiger E, Overkleeft HS, Roseblatt M, Ploegh HL, Lagaudriere-Gesbert C. Analysis of protease activity in live antigen-presenting cells shows regulation of the phagosomal proteolytic contents during dendritic cell activation. *J Exp Med.* 2002; 196:529-540.
11. Peiser L, Mukhopadhyay S, Gordon S. Scavenger receptors in innate immunity. *Curr Opin Immunol.* 2002; 14:123-128.
12. Shi S, Nathan C, Schnappinger D, Drenkow J, Fuortes M, Block E, Ding A, Gingeras TR, Schoolnik G, Akira S, Takeda K, Ehrt S. MyD88 primes macrophages for full-scale activation by interferon-gamma yet mediates few responses to *Mycobacterium tuberculosis*. *J Exp Med.* 2003; 198:987-997.
13. Ravetch JV, Bolland S. IgG Fc receptors. *Annu Rev Immunol.* 2001; 19:275-290.
14. Willment JA, Lin HH, Reid DM, Taylor PR, Williams DL, Wong SY, Gordon S, Brown GD. Dectin-1 expression and function are enhanced on alternatively activated and GM-CSF-treated macrophages and are negatively regulated by IL-10, dexamethasone, and lipopolysaccharide. *J Immunol.* 2003; 171:4569-4573.
15. Begum NA, Ishii K, Kurita-Taniguchi M, Tanabe M, Kobayashi M, Moriwaki Y, Matsumoto M, Fukumori Y, Azuma I, Toyoshima K, Seya T. *Mycobacterium bovis* BCG cell wall-specific differentially expressed genes identified by differential display and cDNA subtraction in human macrophages. *Infect Immun.* 2004; 72:937-948.
16. Kodama K, Higashiyama M, Takami K, Oda K, Okami J, Maeda J, Akazawa T, Matsumoto M, Seya T, Wada M, Toyoshima K. Innate immune therapy with a *Bacillus Calmette-Guerin* cell wall skeleton after radical surgery for non-small cell lung cancer: a case-control study. *Surg Today.* 2009; 39:194-200.
17. Azuma I, Ribi EE, Meyer TJ, Zbar B. Biologically active components from mycobacterial cell walls. I. Isolation and composition of cell wall skeleton and component P3. *J Natl Cancer Inst.* 1974; 52:95-101.
18. Matsumoto M, Seya T, Kikkawa S, *et al.* Interferon gamma-producing ability in blood lymphocytes of patients with lung cancer through activation of the innate immune system by BCG cell wall skeleton. *Int Immunopharmacol.* 2001; 1:1559-1569.
19. Hayashi D, Takii T, Fujiwara N, Fujita Y, Yano I, Yamamoto S, Kondo M, Yasuda E, Inagaki E, Kanai K, Fujiwara A, Kawarazaki A, Chiba T, Onozaki K. Comparable studies of immunostimulating activities *in vitro* among *Mycobacterium bovis* bacillus Calmette-Guerin (BCG) substrains. *FEMS Immunol Med Microbiol.* 2009; 56:116-128.
20. Murata M. Activation of Toll-like receptor 2 by a novel preparation of cell wall skeleton from *Mycobacterium bovis* BCG Tokyo (SMP-105) sufficiently enhances immune responses against tumors. *Cancer Sci.* 2008; 99:1435-1440.
21. Kashiwazaki Y, Murata M, Sato T, Miyauchi M, Nakagawa M, Fukushima A, Chiba N, Azuma I, Yamaoka T. Injection of cell-wall skeleton of *Mycobacterium bovis* BCG draining to a sentinel lymph node eliminates both lymph node metastases and the primary transplanted tumor. *Drug Discov Ther.* 2008; 2:168-177.
22. Uenishi Y, Okada T, Okabe S, Sunagawa M. Study on the cell wall skeleton derived from *Mycobacterium bovis* BCG Tokyo 172 (SMP-105): establishment of preparation and analytical methods. *Chem Pharm Bull (Tokyo).* 2007; 55:843-852.
23. Kashiwazaki Y, Murata M, Fujii T, Nakagawa M, Fukushima A, Chiba N, Azuma I, Yamaoka T. Immune response against cell-wall skeleton of *Mycobacterium bovis* BCG at the inoculation site and peripheral lymphoid organs. *Drug Discov Ther.* 2008; 2:178-187.
24. Hirschfeld M, Ma Y, Weis JH, Vogel SN, Weis JJ. Cutting edge: repurification of lipopolysaccharide eliminates signaling through both human and murine toll-like receptor 2. *J Immunol.* 2000; 165:618-622.
25. Manthey CL, Perera PY, Henricson BE, Hamilton TA, Qureshi N, Vogel SN. Endotoxin-induced early gene expression in C3H/HeJ (Lpsd) macrophages. *J Immunol.* 1994; 153:2653-2663.
26. Manthey C, Vogel S. Elimination of trace endotoxin protein from rough chemotype LPS. *J Endotoxin Res.* 1994; 1:84-91.
27. Ballas ZK, Krieg AM, Warren T, Rasmussen W, Davis HL, Waldschmidt M, Weiner GJ. Divergent therapeutic and immunologic effects of oligodeoxynucleotides with distinct CpG motifs. *J Immunol.* 2001; 167:4878-4886.
28. Winzler C, Rovere P, Rescigno M, Granucci F, Penna G, Adorini L, Zimmermann VS, Davoust J, Ricciardi-Castagnoli P. Maturation stages of mouse dendritic cells in growth factor-dependent long-term cultures. *J Exp Med.* 1997; 185:317-328.
29. Yanagawa Y, Iijima N, Iwabuchi K, Onoe K. Activation of extracellular signal-related kinase by TNF-alpha controls the maturation and function of murine dendritic cells. *J Leukoc Biol.* 2002; 71:125-132.
30. Murphy KM, Heimberger AB, Loh DY. Induction by antigen of intrathymic apoptosis of CD4⁺CD8⁺TCRlo thymocytes *in vivo*. *Science.* 1990; 250:1720-1723.
31. Chan RC, Wang M, Li N, Yanagawa Y, Onoe K, Lee JJ, Nel AE. Pro-oxidative diesel exhaust particle chemicals inhibit LPS-induced dendritic cell responses involved in T-helper differentiation. *J Allergy Clin Immunol.* 2006; 118:455-465.
32. Chapman TJ, Castrucci MR, Padrick RC, Bradley LM, Topham DJ. Antigen-specific and non-specific CD4⁺ T cell recruitment and proliferation during influenza infection. *Virology.* 2005; 340:296-306.
33. Ishiwata A, Akao H, Ito Y, Sunagawa M, Kusunose N, Kashiwazaki Y. Synthesis and TNF-alpha inducing activities of mycoloyl-arabinan motif of mycobacterial cell wall components. *Bioorg Med Chem.* 2006; 14:3049-3061.
34. Uenishi Y, Kawabe K, Nomura T, Nakai M, Sunagawa M. Morphological study on *Mycobacterium bovis* BCG Tokyo 172 cell wall skeleton (SMP-105). *J Microbiol Methods.* 2009; 77:139-144.
35. Okamoto M, Oshikawa T, Tano T, Ahmed SU, Kan S, Sasai A, Akashi S, Miyake K, Moriya Y, Ryoma Y, Saito M, Sato M. Mechanism of anticancer host response induced by OK-432, a streptococcal preparation, mediated by phagocytosis and Toll-like receptor 4 signaling. *J Immunother.* 2006; 29:78-86.
36. Katano M, Morisaki T. The past, the present and future

- of the OK-432 therapy for patients with malignant effusions. *Anticancer Res.* 1998; 18:3917-3925.
37. Yang S, Tamai R, Akashi S, Takeuchi O, Akira S, Sugawara S, Takada H. Synergistic effect of muramyl dipeptide with lipopolysaccharide or lipoteichoic acid to induce inflammatory cytokines in human monocytic cells in culture. *Infect Immun.* 2001; 69:2045-2053.
38. Uehara A, Yang S, Fujimoto Y, Fukase K, Kusumoto S, Shibata K, Sugawara S, Takada H. Muramyl dipeptide and diaminopimelic acid-containing desmuramylpeptides in combination with chemically synthesized Toll-like receptor agonists synergistically induced production of interleukin-8 in a NOD2- and NOD1-dependent manner, respectively, in human monocytic cells in culture. *Cell Microbiol.* 2005; 7:53-61.

(Received December 17, 2009; Revised February 9, 2010; Accepted February 12, 2010)

Drug Discoveries & Therapeutics

Guide for Authors

1. Scope of Articles

Drug Discoveries & Therapeutics mainly publishes articles related to basic and clinical pharmaceutical research such as pharmaceutical and therapeutical chemistry, pharmacology, pharmacy, pharmacokinetics, industrial pharmacy, pharmaceutical manufacturing, pharmaceutical technology, drug delivery, toxicology, and traditional herb medicine. Studies on drug-related fields such as biology, biochemistry, physiology, microbiology, and immunology are also within the scope of this journal.

2. Submission Types

Original Articles should be reports new, significant, innovative, and original findings. An Article should contain the following sections: Title page, Abstract, Introduction, Materials and Methods, Results, Discussion, Acknowledgments, References, Figure legends, and Tables. There are no specific length restrictions for the overall manuscript or individual sections. However, we expect authors to present and discuss their findings concisely.

Brief Reports should be short and clear reports on new original findings and not exceed 4000 words with no more than two display items. *Drug Discoveries & Therapeutics* encourages younger researchers and doctors to report their research findings. Case reports are included in this category. A Brief Report contains the same sections as an Original Article, but Results and Discussion sections must be combined.

Reviews should include educational overviews for general researchers and doctors, and review articles for more specialized readers.

Policy Forum presents issues in science policy, including public health, the medical care system, and social science. Policy Forum essays should not exceed 2,000 words.

News articles should not exceed 500 words including one display item. These articles should function as an international news source with regard to topics in the life and social sciences and medicine. Submissions are not restricted to journal staff - anyone can submit news articles on subjects that would be of interest to *Drug Discoveries & Therapeutics'* readers.

Letters discuss material published in *Drug Discoveries & Therapeutics* in the last 6 months or issues of general interest. Letters should not exceed 800 words and 6 references.

3. Manuscript Preparation

Preparation of text. Manuscripts should be written in correct American English and submitted as a Microsoft Word (.doc) file in a single-column format. Manuscripts must be paginated and double-spaced throughout. Use Symbol font for all Greek characters. Do not import the figures into the text file but indicate their approximate locations directly on the manuscript. The manuscript file should be smaller than 5 MB in size.

Title page. The title page must include 1) the title of the paper, 2) name(s) and affiliation(s) of the author(s), 3) a statement indicating to whom correspondence and proofs should be sent along with a complete mailing address, telephone/fax numbers, and e-mail address, and 4) up to five key words or phrases.

Abstract. A one-paragraph abstract consisting of no more than 250 words must be included. It should state the purpose of the study, basic procedures used, main findings, and conclusions.

Abbreviations. All nonstandard abbreviations must be listed in alphabetical order, giving each abbreviation followed by its spelled-out version. Spell out the term upon first mention and follow it with the abbreviated form in parentheses. Thereafter, use the abbreviated form.

Introduction. The introduction should be a concise statement of the basis for the study and its scientific context.

Materials and Methods. Subsections under this heading should include sufficient instruction to replicate experiments, but well-established protocols may be simply referenced. *Drug Discoveries & Therapeutics* endorses the principles of the Declaration of Helsinki and expects that all research involving humans will have been conducted in accordance with these principles. All laboratory animal studies must be approved by the authors' Institutional Review Board(s).

Results. The results section should provide details of all of the experiments that are required to support the conclusions of the paper. If necessary, subheadings may be used for an orderly presentation. All figures, tables, and photographs must be referred in the text.

Discussion. The discussion should include conclusions derived from the study and supported by the data. Consideration should be given to the impact that these conclusions have on the body of knowledge in which context the experiments were conducted. In Brief Reports, Results and Discussion sections must be combined.

Acknowledgments. All funding sources should be credited in the Acknowledgments section. In addition, people who contributed to the work but who do not fit the criteria for authors should be listed along with their contributions.

References. References should be numbered in the order in which they appear in the text. Cite references in text using a number in parentheses. Citing of unpublished results and personal communications in the reference list is not recommended but these sources may be mentioned in the text. For all references, list all authors, but if there are more than fifteen authors, list the first three authors and add "*et al.*" Abbreviate journal names as they appear in PubMed. Web references can be included in the reference list.

Example 1:

Hamamoto H, Akimitsu N, Arimitsu N, Sekimizu K. Roles of the Duffy antigen and glycoprotein A in malaria infection and erythrocyte. *Drug Discov Ther.* 2008; 2:58-63.

Example 2:

Zhao X, Jing ZP, Xiong J, Jiang SJ. Suppression of experimental abdominal aortic aneurysm by tetracycline: a preliminary study. *Chin J Gen Surg*. 2002; 17:663-665. (in Chinese)

Example 3:

Mizuochi T. Microscale sequencing of *N*-linked oligosaccharides of glycoproteins using hydrazinolysis, Bio-Gel P-4, and sequential exoglycosidase digestion. In: *Methods in Molecular Biology: Vol. 14 Glycoprotein analysis in biomedicine* (Hounsell T, ed.). Humana Press, Totowa, NJ, USA, 1993; pp. 55-68.

Example 4:

Drug Discoveries & Therapeutics. Hot topics & news: China-Japan Medical Workshop on Drug Discoveries and Therapeutics 2007. <http://www.ddtjournal.com/hotnews.php> (accessed July 1, 2007).

Figure legends. Include a short title and a short explanation. Methods described in detail in the Materials and methods section should not be repeated in the legend. Symbols used in the figure must be explained. The number of data points represented in a graph must be indicated.

Tables. All tables should have a concise title and be typed double-spaced on pages separate from the text. Do not use vertical rules. Tables should be numbered with Arabic numerals consecutively in accordance with their appearance in the text. Place footnotes to tables below the table body and indicate them with lowercase superscript letters.

Language editing. Manuscripts submitted by authors whose primary language is not English should have their work proofread by a native English speaker before submission. The Editing Support Organization can provide English proofreading, Japanese-English translation, and Chinese-English translation services to authors who want to publish in *Drug Discoveries & Therapeutics* and need assistance before submitting an article. Authors can contact this organization directly at <http://www.iacmhr.com/iac-eso>.

IAC-ESO was established in order to facilitate manuscript preparation by researchers whose native language is not English and to help edit work intended for international academic journals. Quality revision, translation, and editing services are offered by our staff, who are native speakers of particular languages and who are familiar with academic writing and journal editing in English.

4. Figure Preparation

All figures should be clear and cited in numerical order in the text. Figures must fit a one- or two-column format on the journal page: 8.3 cm (3.3 in.) wide for a single column; 17.3 cm (6.8 in.) wide for a double column; maximum height: 24.0 cm (9.5 in.). Only use the following fonts in the figure: Arial and Helvetica. Provide all figures as separate files. Acceptable file formats are JPEG and TIFF. Please note that files saved in JPEG or TIFF format in PowerPoint lack sufficient resolution for publication. Each Figure file should be smaller than 10 MB in size. Do not compress files. A fee is charged for a color illustration or photograph.

5. Online Submission

Manuscripts should be submitted to *Drug Discoveries & Therapeutics* online at <http://www.ddtjournal.com>. The manuscript file should be smaller than 10 MB in size. If for any reason you are unable to submit a file online, please contact the Editorial Office by e-mail: office@ddtjournal.com

Editorial and Head Office

Wei TANG, MD PhD
Executive Editor
Drug Discoveries & Therapeutics
TSUIN-IKIZAKA 410,
2-17-5 Hongo, Bunkyo-ku,
Tokyo 113-0033, Japan.
Tel: 03-5840-9697
Fax: 03-5840-9698
E-mail: office@ddtjournal.com

Cover letter. A cover letter from the corresponding author including the following information must accompany the submission: name, address, phone and fax numbers, and e-mail address of the corresponding author. This should include a statement affirming that all authors concur with the

submission and that the material submitted for publication has not been previously published and is not under consideration for publication elsewhere and a statement regarding conflicting financial interests.

Authors may recommend up to three qualified reviewers other than members of Editorial board. Authors may also request that certain (but not more than three) reviewers not be chosen.

The cover letter should be submitted as a Microsoft Word (.doc) file (smaller than 1 MB) at the same time the work is submitted online.

6. Accepted Manuscripts

Proofs. Rough galley proofs in PDF format are supplied to the corresponding author *via* e-mail. Corrections must be returned within 4 working days of receipt of the proofs. Subsequent corrections will not be possible, so please ensure all desired corrections are indicated. Note that we may proceed with publication of the article if no response is received.

Transfer of copyrights. Upon acceptance of an article, authors will be asked to agree to a transfer of copyright. This transfer will ensure the widest possible dissemination of information. A letter will be sent to the corresponding author confirming receipt of the manuscript. A form facilitating transfer of copyright will be provided. If excerpts from other copyrighted works are included, the author(s) must obtain written permission from the copyright owners and credit the source(s) in the article.

Cover submissions. Authors whose manuscripts are accepted for publication in *Drug Discoveries & Therapeutics* may submit cover images. Color submission is welcome. A brief cover legend should be submitted with the image.

Revised April 20, 2009



Drug Discoveries & Therapeutics



Editorial Office

TSUIN-IKIZAKA 410,
2-17-5 Hongo, Bunkyo-ku,
Tokyo 113-0033, Japan

Tel: 03-5840-9697

Fax: 03-5840-9698

E-mail: office@ddtjournal.com

URL: www.ddtjournal.com

JOURNAL PUBLISHING AGREEMENT

Ms No:

Article entitled:

Corresponding author:

To be published in Drug Discoveries & Therapeutics

Assignment of publishing rights:

I hereby assign to International Advancement Center for Medicine & Health Research Co., Ltd. (IACMHR Co., Ltd.) publishing Drug Discoveries & Therapeutics the copyright in the manuscript identified above and any supplemental tables and illustrations (the articles) in all forms and media, throughout the world, in all languages, for the full term of copyright, effective when and if the article is accepted for publication. This transfer includes the rights to provide the article in electronic and online forms and systems.

I understand that I retain or am hereby granted (without the need to obtain further permission) rights to use certain versions of the article for certain scholarly purpose and that no rights in patent, trademarks or other intellectual property rights are transferred to the journal. Rights to use the articles for personal use, internal institutional use and scholarly posting are retained.

Author warranties:

I affirm the author warranties noted below.

- 1) The article I have submitted to the journal is original and has not been published elsewhere.
- 2) The article is not currently being considered for publication by any other journal. If accepted, it will not be submitted elsewhere.
- 3) The article contains no libelous or other unlawful statements and does not contain any materials that invade individual privacy or proprietary rights or any statutory copyright.
- 4) I have obtained written permission from copyright owners for any excerpts from copyrighted works that are included and have credited the sources in my article.
- 5) I confirm that all commercial affiliations, stock or equity interests, or patent-licensing arrangements that could be considered to pose a financial conflict of interest regarding the article have been disclosed.
- 6) If the article was prepared jointly with other authors, I have informed the co-authors(s) of the terms of this publishing agreement and that I am signing on their behalf as their agents.

Your Status:

I am the sole author of the manuscript.

I am one author signing on behalf of all co-authors of the manuscript.

Please tick one of the above boxes (as appropriate) and then sign and date the document in black ink.

Signature:

Date:

Name printed:

Please return the completed and signed original of this form by express mail or fax, or by e-mailing a scanned copy of the signed original to:

Drug Discoveries & Therapeutics office
TSUIN-IKIZAKA 410, 2-17-5 Hongo,
Bunkyo-ku, Tokyo 113-0033, Japan
e-mail: proof-editing@ddtjournal.com
Fax: +81-3-5840-9698

